State-to-State Chemistry

In State-to-State Chemistry; Brooks, P., et al.;
ACS Symposium Series; American Chemical Society: Washington, DC, 1977.

State-to-State Chemistry

Philip R. Brooks and
Edward F. Hayes, EDITORS
Rice University

A symposium sponsored by
the Division of Physical Chemistry
at the 173rd Meeting of the
American Chemical Society,
New Orleans, La.,
Mar. 21–23, 1977.

ACS SYMPOSIUM SERIES 56

AMERICAN CHEMICAL SOCIETY
WASHINGTON, D. C. 1977

Library of Congress CIP Data

State-to-state chemistry.
(ACS symposium series; 56 ISSN 0097-6156)

Includes bibliographical references and index.

1. Quantum chemistry—Congresses.
I. Brooks, Philip R., 1938– . II. Hayes, Edward F., 1941– . III. American Chemical Society. Division of Physical Chemistry. IV. Series: American Chemical Society. ACS symposium series; 56.

QD462.A1S7 541'.28 77-14164
ISBN 0-8412-0386-5 ACSMC8 56 1–259

PRINTED IN THE UNITED STATES OF AMERICA

ACS Symposium Series

Robert F. Gould, *Editor*

In State-to-State Chemistry; Brooks, P., et al.;
ACS Symposium Series; American Chemical Society: Washington, DC, 1977.

FOREWORD

The ACS SYMPOSIUM SERIES was founded in 1974 to provide a medium for publishing symposia quickly in book form. The format of the SERIES parallels that of the continuing ADVANCES IN CHEMISTRY SERIES except that in order to save time the papers are not typeset but are reproduced as they are submitted by the authors in camera-ready form. As a further means of saving time, the papers are not edited or reviewed except by the symposium chairman, who becomes editor of the book. Papers published in the ACS SYMPOSIUM SERIES are original contributions not published elsewhere in whole or major part and include reports of research as well as reviews since symposia may embrace both types of presentation.

In State-to-State Chemistry; Brooks, P., et al.;
ACS Symposium Series; American Chemical Society: Washington, DC, 1977.

PREFACE

One of the main goals of chemistry is to understand and predict chemical changes. Toward this end chemists have attempted to characterize reactive intermediates and to study the rates of various elementary chemical processes. A complete understanding of a chemical reaction requires knowledge of the microscopic rate constant for evolution of a system in a single reagent "quantum state" (translation, rotation, vibration, and electronic state) to a single product "quantum state." Conventional bulk rate studies are incapable of resolving these states and merely provide average rates. Although much has been learned from these average rates, further understanding demands less averaging. Fortunately, technological developments—such as molecular beams and lasers —are providing us with the tools necessary to probe these states, and the direct measurement of some of these fundamental microscopic "state-to-state" reaction rates has begun to be feasible.

The papers assembled in this volume represent the proceedings of a symposium held at the 173rd ACS National Meeting, March 21–23, 1977, in New Orleans. The purpose of the symposium and this book is to present a snapshot of the exciting and rapidly developing field of state-to-state chemistry. The papers represent early attempts to answer such questions as: "Which quantum states are most likely to react?" and "Which quantum states are most likely to be formed?" Few papers actually represent studies of the evolution of one quantum state into another (except some of the theoretical papers), attesting to the present difficulties in performing such experiments. Instead, collision processes (both chemical reactions and energy transfer collisions) are studied with varying groups of quantum states specified.

In the area of state-to-state chemistry the interaction between theory and experiment is strong, with theory suggesting new experiments and new approaches and experiment providing calibration for the theory. This marriage has been very productive in the generation of chemical "scope" or understanding, but some practical children have also been born. One past example of this is the infrared chemiluminescence experiments of Polanyi (1961) showing that HCl was preferentially formed in vibrationally excited states in the reaction of H atoms with Cl_2. These results were essential to Kasper and Pimentel in their development of the first HCl chemical laser (1965). While other studies have led to still other lasers, the emphasis has recently been reversed: lasers are being

In State-to-State Chemistry; Brooks, P., et al.;
ACS Symposium Series; American Chemical Society: Washington, DC, 1977.

used to alter the course of reactions. This raises the tantalizing possibilities of laser chemistry where lasers are used to choose a quantum state of the reagents which may react faster or form different products from the ground state. Currently there is considerable interest in the possibility that laser-induced chemistry may be attractive for large-scale chemical processing.

The papers in this volume have been grouped under three main headings: Reactive Collisions, Energy Transfer Collisions, and Theory. In addition, Reactive Collisions has beeen further divided into Beam Studies and Bulk Studies. The assignment of a paper to a particular group in many cases was somewhat arbitrary. It should be recognized that there are strong complementary interactions between research activities in each of these areas.

The editors hope that this book will help the reader share in the exciting developments in state-to-state chemistry. It is a pleasure to thank the contributors and publishers for their excellent cooperation, without which this volume would not have been possible. A special note of thanks goes to Dorothy D. Butler for her assistance in assembling the manuscripts.

July 1977

PHILIP R. BROOKS
EDWARD F. HAYES

1

State-to-State Cross Sections and Rate Constants for Reactions of Neutral Molecules

RICHARD B. BERNSTEIN

Chemistry Department, The University of Texas, Austin, TX 78712

Recent experimental and theoretical advances have led to the development of a new field known as "state-to-state" chemistry. It is now becoming possible to measure directly (and interpret, on a sound theoretical basis) the relative probabilities of formation of nascent reaction products in specified internal states from reagents in selected states.

In addition to a number of important practical applications (e.g., the discovery of new laser-induced reactions and the development of improved chemical lasers) there are many fundamental implications for the field of gas-phase chemical kinetics. The basic components of the reaction rate constant are the state-to-state rate coefficients, say $k_{i\to f}(T)$, or, at a more fundamental level, the state-to-state reaction cross sections, $\sigma_{i\to f}(E)$. Here i and f denote initial (reagent) and final (product) states, respectively, T the translational temperature, and E the total energy.

The theoretical framework for dealing with state-to-state kinetics was laid down by Eliason and Hirschfelder (1) in 1959, who established the relationship between the transition probabilities, the detailed differential state-to-state cross sections, the reaction cross sections, state-to-state rate coefficients and the thermal rate constant. A number of subsequent fundamental papers have advanced the understanding of state-to-state reactions (2-4).

Reviewing briefly (5), the gas-phase bimolecular thermal rate constant can be expressed

$$k(T) = \sum_i P_i(T) k_i(T), \qquad (1)$$

where $P_i(T)$ represents the relative population of

In State-to-State Chemistry; Brooks, P., et al.;
ACS Symposium Series; American Chemical Society: Washington, DC, 1977.

reagent state i at the given temperature T, and $k_i(T)$ is the total rate constant out of state i,

$$k_i(T) = \sum_f k_{i\to f}(T), \tag{2}$$

summing over all final states f.

Consider an experiment at a given translational energy distribution characterized by a certain value of the average relative translational energy $\bar{E}_{tr}$. The state-to-state rate constant is the expectation value of the product of the relative speed times the cross section, i.e.

$$k_{i\to f}(\bar{E}_{tr}) = \left\langle v_r \sigma_{i\to f}(v_r) \right\rangle_{\bar{E}_{tr}} \tag{3}$$

where $v_r = (2E_{tr}/\mu)^{\frac{1}{2}}$. Thus

$$k_{i\to f}(\bar{E}_{tr}) = \int v_r \sigma_{i\to f}(v_r) p(v_r|\bar{E}_{tr}) dv_r \tag{4a}$$

$$= (2/\mu)^{\frac{1}{2}} \int \sigma_{i\to f}(E_{tr}) E_{tr}^{\frac{1}{2}} P(E_{tr}|\bar{E}_{tr}) dE_{tr} \tag{4b}$$

where p and P represent the normalized probability density functions (pdf's) for v_r and E_{tr}, respectively.

Considering the total rate constant out of state i,

$$k_i(\bar{E}) = (2/\mu)^{\frac{1}{2}} \int E^{\frac{1}{2}} \sigma_i(E) P(E|\bar{E}) dE \tag{5}$$

where $$\sigma_i(E) = \sum_f \sigma_{i\to f}(E) \tag{6}$$

(dropping the subscript tr).

For the special case of a Maxwellian translation energy distribution (for which $\bar{E} = 3\underline{k}T/2$),

$$P(E|3\underline{k}T/2) = 2(E/\pi)^{\frac{1}{2}} (\underline{k}T)^{-3/2} \exp(-E/\underline{k}T) \tag{7}$$

so $$k_i(T) = (\pi\mu)^{-\frac{1}{2}} (2/\underline{k}T)^{3/2} \int E \sigma_i(E) \exp(-E/\underline{k}T) dE \tag{8}$$

from which k(T) is obtained via Eq. (1). For the limiting case of a line-of-centers cross section (rising from threshold at $E=E_o$, to a limiting value of πd^2), and assuming no state dependence, Eq. (8) yields the usual Arrhenius-like temperature dependence for the rate constant

$$k(T) = (8\underline{k}T/\pi\mu)^{\frac{1}{2}} \pi d^2 \exp(-E_o/\underline{k}T). \tag{9}$$

In State-to-State Chemistry; Brooks, P., et al.;
ACS Symposium Series; American Chemical Society: Washington, DC, 1977.

Eq. (9) is not applicable to reactions of excited-state reagents and non-Maxwellian translational distributions; one must use Eq. (1), which requires a knowledge of P_i, together with Eq. (5), which requires both $P(E)$ and $\sigma_i(E)$ for all populated reagent states i. As will be seen later, for reactions with an energy barrier σ_i is extremely sensitive to the state of internal excitation of the reagent, and therefore so is k_i. For many practical situations involving laser excitation the translational distribution can be taken to be essentially Maxwellian and so Eq. (8) may be used.

In 1969 Parker and Pimentel (6) made a significant advance in connection with their chemical laser study dealing with the exothermic $F + H_2 \rightarrow HF^\dagger + H$ reaction, which gives rise to a vibrational population inversion in the HF product. (The dagger denotes internal excitation.) From the ratios of the rate constants for the formation of the various vibrational states of the $HF^\dagger$ (see Fig. 1), they deduced (via detailed balance) that the rate of the reverse, endothermic reaction would be strongly enhanced by vibrational excitation of the HF reagent. The possibility of preferential utilization of reactant internal excitation energy (vs. relative translational energy) had already been suggested on dynamical grounds by Polanyi (7) in 1959 (and, on the basis of trajectory calculations a decade later by Polanyi et al (8, 9) and Raff et al (10)).

In 1969 Anlauf et al (11) showed how to make use of microscopic reversibility to predict the vibrotational selectivity in endoergic reactions from the population-inversion data for the inverse (exoergic reaction), usually obtained from infrared chemiluminescence data (12).

Consider the state-to-state atom–diatomic exchange reaction, written in the exoergic direction:

$$A + BC\ (v,J) \underset{r}{\overset{f}{\rightleftharpoons}} AB(v',J') + C; \qquad \Delta E_o < 0. \qquad (I)$$

At a given value of the total energy E, microscopic reversibility yields (2, 3, 11):

$$\frac{\sigma_f(vJ \rightarrow v'J' \mid E)}{\sigma_r(v'J' \rightarrow vJ \mid E)} = \left(\frac{\mu'}{\mu}\right) X \left(\frac{E'_{tr}}{E_{tr}}\right) X \left(\frac{2J'+1}{2J+1}\right) \qquad (10)$$

In State-to-State Chemistry; Brooks, P., et al.;
ACS Symposium Series; American Chemical Society: Washington, DC, 1977.

$$\text{so } \frac{k_f(vJ \to v'J' \mid E)}{k_r(v'J' \to vJ \mid E)} = \left(\frac{\mu'}{\mu}\right)^{3/2} X \left(\frac{E'_{tr}}{E_{tr}}\right)^{\frac{1}{2}} X \left(\frac{2J'+1}{2J+1}\right) . \qquad (11)$$

Several valuable reviews have been published (5, 13-16) dealing with experimental and theoretical-computational studies of nascent product state distributions for exoergic reactions (which are found to be almost always non-Boltzmann).

Recently, Levine et al (17-20) presented a theoretical analysis of the effect of reagent energy on reaction rates. They employed the information-theoretic method (21-25) to deal with the problem of the selectivity of energy requirements. In the course of their work they considered also the implication of detailed balance.

Kaplan et al (19) showed that for a Maxwellian translational distribution, detailed balance yields

$$\frac{k_f(vJ \to v'J' \mid T)}{k_r(v'J' \to vJ \mid T)} = \left(\frac{\mu'}{\mu}\right)^{3/2} X \left(\frac{2J'+1}{2J+1}\right) X \exp(-\delta_1 E/\underline{k}T) \qquad (12)$$

$$\text{where} \quad \delta_1 E \equiv \Delta E_o + G_{v'j'} - G_{vJ}; \qquad (13)$$

here G_{vJ} is the vibrotational energy of the reagent vJ state, $G_{v'J'}$ that for the product v'J' state.

In the special case for which the rotational states of both reagent and product molecules are Boltzmannized, Eq. (12) leads to the detailed-balance result:

$$\frac{k_f(v \to v' \mid T)}{k_r(v' \to v \mid T)} = \frac{\sum_{J'}(2J'+1)\exp(-G_{J'}/\underline{k}T)}{\sum_{J}(2J+1)\exp(-G_J/\underline{k}T)} X \left(\frac{\mu'}{\mu}\right)^{3/2} X \exp(-\delta_2 E/\underline{k}T) \qquad (14)$$

$$\text{where} \quad \delta_2 E \equiv \Delta E_o + G_{v'} - G_v; \qquad (15)$$

here G_v is the vibrational energy of the reagent in its rotationless state and $G_{v'}$ that of the product. Eq. (14) is essentially that used by Parker and Pimentel (6) in their analysis of the vibrational dependence of the "reverse rate constant", mentioned above.

On the experimental side, an early yet elegant experiment in the ion-molecule field played an important role in stimulating research involving excited neutral reagent molecules. This "textbook example" is the work

In State-to-State Chemistry; Brooks, P., et al.;
ACS Symposium Series; American Chemical Society: Washington, DC, 1977.

of Chupka et al (26) in 1969 on the endoergic ion-molecule reaction $H_2^+(v) + He \rightarrow HeH^+ + H$, from which a direct comparison could be made (27), at constant total energy, of the comparative effect of reagent vibrational energy vs. relative translational energy upon the reaction cross section. Enhancements of more than two orders of magnitude were observed, which have been the subject of considerable theoretical attention (17, 28).

A number of other ion-molecule studies showed important vibrational energy effects, but in the field of neutral-neutral kinetics results on selectivity of energy requirements (14) were forthcoming with more difficulty. These are the subject of the review which follows. Not to be discussed are the closely related but well-reviewed (13-16) subjects of vibrotational and translational energy disposal in exoergic reactions, nor the large body of computer-simulation studies.

Early "bulk" experiments involving vibrationally excited reagents.

In 1970 Stedman et al (29) produced evidence from a discharge-flow experiment that the rate of the reaction Cl + H_2 is enhanced by H_2 vibrational excitation. In 1972 Heidner and Kasper (30) reported that the rate constant for the process (predominately reactive) H + $H_2(v=1) \rightarrow H_2(v=0)$ + H exceeded that of the H-exchange reaction with ground-state H_2 by a factor of ca.10^3. They attributed this to the efficient utilization of the 12 kcal mol^{-1} excitation energy in overcoming the barrier (corresponding to a 7.5 kcal mol^{-1} activation energy). On the other hand, Birely et al (31) in 1975 found in a similar discharge-flow experiment that vibrational excitation of the H_2 was ineffective in overcoming the barrier corresponding to the 10 kcal mol^{-1} activation energy for the reaction of H_2 with oxygen atoms.

Bauer et al (32) in 1973 reported observations of a laser-induced exchange reaction: $H_2 + D_2 \rightarrow 2HD$, interpreted in terms of a vibrational enhancement mechanism. They deduced from a computer analysis of their experimental data that the exchange reaction proceeds with a measureable rate for $H_2(v \geq 4)$. However, there is some doubt about the interpretation of the experi-

In State-to-State Chemistry; Brooks, P., et al.;
ACS Symposium Series; American Chemical Society: Washington, DC, 1977.

ments, since the barrier for the four-center reaction is generally believed to be significantly higher than the internal energy of H_2 in the state v=4. Further work is needed to clarify the situation for this important elementary reaction.

Sims et al (33) in 1975 reported indirect evidence (also from discharge flow experiments) of a vibrational rate enhancement of ca.7×10^3 for the reaction $Br + H_2 \rightarrow HBr + H$, comparing $H_2(v=1)$ vs. $H_2(v=0)$.

In 1973 Gordon and Lin (34) reported a significant enhancement in the rate of the reaction of NO with vibrationally excited O_3, i.e., $NO + O_3^{\dagger}(010) \rightarrow NO_2^{\dagger} + O_2$. The ratio of rate constants for the reaction with $O_3(\nu_2=1)$ vs. $O_3(\nu_2=0)$ was found to be about 20. This reaction, involving O_3 excited in specific modes, has been the subject of considerable further experimental work (35, 36).

Arnoldi and Wolfrum (37) in 1974 used a pulsed chemical laser to excite HCl and found an enhancement of the rate of the nearly thermoneutral reaction $O + HCl \rightarrow OH + Cl$ by ca.4×10^3, and $H + HCl \rightarrow H_2 + Cl$ by more than 1 order of magnitude. Karny et al (38) in 1975 studied the O + HCl reaction in a similar way and reported the vibrational enhancement of the reactive process to be 3×10^2.

These experiments constitute the body of the early, mainly qualitative, bulk gas phase experiments on vibrational enhancement (39-41). In the following section the more quantitative, detailed studies will be discussed.

Quantitative experiments involving vibrationally excited diatomics.

A quantitative study of the rates of the reactions:

$$O(^3P) + HCl(v=1 \text{ vs. } 0) \begin{cases} \xrightarrow{a} OH + Cl \\ \xrightarrow{b} O + HCl(v=0) \end{cases}$$

and the DCl analogue has been reported by Brown et al (42) over a temperature range from 196 to 400K. However, the relative contribution of the rate of the reactive path (a) vs. that of the nonreactive relaxation process (b), an electronically non-adiabatic

In State-to-State Chemistry; Brooks, P., et al.;
ACS Symposium Series; American Chemical Society: Washington, DC, 1977.

vibronic transition, could not be determined, so the large vibrational relaxation rates found here and in Ref. (38) cannot be clearly attributed to a true vibrational enhancement for the reaction $O + HCl^{\dagger} \rightarrow OH + Cl$.

Several series of significant experiments have been carried out by Polanyi and co-workers. In 1972 Kirsch and Polanyi (43) studied the reaction $F + HCl \rightarrow HF + Cl$ for which $E_{act} \simeq 1$ kcal mol^{-1}, and found that excited HCl (v=1) [E_{vib}=8.2 kcal mol^{-1}] gave rise to an enhancement of the overall rate [relative to HCl (v=0)] by a factor between 3 and 9, and also produced a much higher degree of vibrational excitation of the HF product. A more detailed and accurate study (including theoretical interpretation) followed (44).

For the endoergic reaction (ΔE_o=16.5 kcal mol^{-1}) $Br + HCl \rightarrow HBr + Cl$, Douglas et al (45) showed (using a "pre-reactor" producing HCl in states v=1,2,3,4) that when HCl is excited to $v \geq 2$ ($E_{vib} \geq 16$ kcal mol^{-1}) the reaction proceeds with near gas-kinetic rates at thermal collision energies. They were thus able to measure a "vibrational energy threshold" for the reaction (which turned out to be essentially the endoergicity).

Following a study by Leone et al (46), Arnoldi and Wolfrum (47) reported a detailed investigation of the influence of selective vibrational excitation (via a pulsed chemical laser) of HCl (v=2 vs 1, 0) on the rate of reaction with several atomic species. The most interesting results were in the reaction with Br, mentioned above. Fig. 2 shows the relevant energy level diagram. At 298°K, the rate constant for HCl(v=2) was *ca.* 10^9 $M^{-1}sec^{-1}$, vs.k for HCl(v=0) of *ca.* $10^{-2}M^{-1}sec^{-1}$, some 11 orders of magnitude of enhancement! (48). The table below combines the rate constant results of Wolfrum et al with the relative rate data of Polanyi's experiments (scaled for best accord with the Wolfrum results).

$$Br + HCl(v) \xrightarrow{k(v)} HBr + Cl$$

v	0	1	2	3	4
k(v), $M^{-1}sec^{-1}$	$1x10^{-2}$	$2x10^{4}$	$1x10^{9}$	$7x10^{9}$	$1x10^{10}$

In State-to-State Chemistry; Brooks, P., et al.;
ACS Symposium Series; American Chemical Society: Washington, DC, 1977.

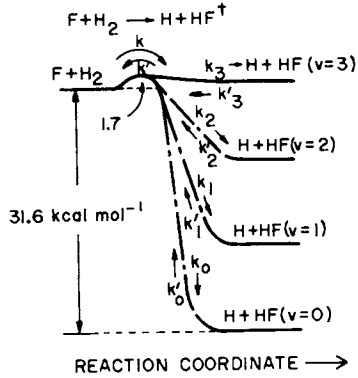

Figure 1. Energy levels, activation barrier, and specific rate constants for the F + H_2 reaction. Adapted from Parker and Pimentel (6).

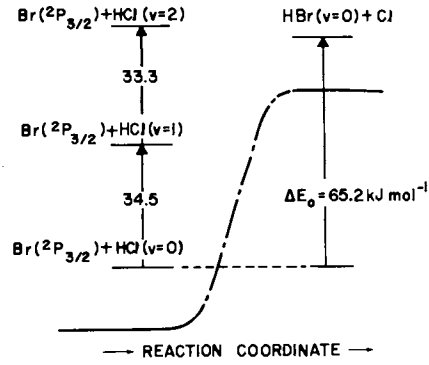

Figure 2. Energy levels for the HCl(v) + Br reaction. Adapted from Arnoldi and Wolfrum (47).

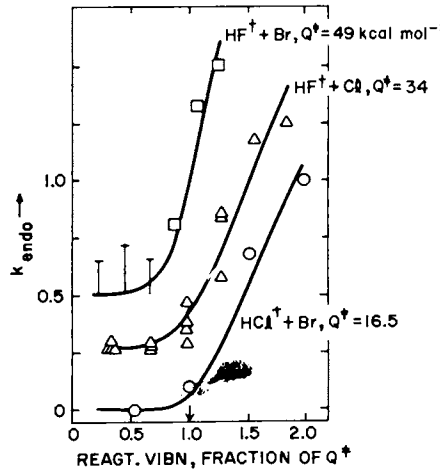

Figure 3. Specific rate constants for the endothermic reactions of HF with Br, Cl and HCl with Br, as a function of the vibrational excitation of the reagent molecule (expressed as a fraction of the barrier height, $Q^{\ddagger}$. Successive ordinate scales displaced as indicated. Adapted from Douglas, Polanyi and Sloan (49).

In State-to-State Chemistry; Brooks, P., et al.;
ACS Symposium Series; American Chemical Society: Washington, DC, 1977.

The strong vibrational state dependence of the rate constant k(v) is in qualitative accord with prior expectation, as will be seen in the next section.

A thorough study of the v-dependence of the rate constant for three endothermic atom-molecule reactions has recently been reported by Douglas et al (49). Their results are displayed in Fig. 3, for the reaction $HF^{\dagger}$ + Br, Cl and $HCl^{\dagger}$ + Br. There is clear evidence for a "vibrational threshold" in each case.

All of the foregoing results were obtained from "bulk" gas phase experiments in flow systems. (For recent reviews see Refs. 16, 50 and 51.) Relatively few experiments have been carried out under single collision conditions.

The first crossed beam experiment was that of Odiorne et al (52) in 1971, involving the reaction HCl (v=1 vs.0) + K → KCl + H. Using a pulsed HCl chemical laser they found that the cross section (i.e., the scattered intensity) for the HCl(v=1) reaction was considerably greater (by a factor of 10-100) then that for the reaction of ground state HCl. This experiment was of a pioneering nature and as such provided only qualitative information on the vibrational enhancement. The translational energy dependence of the ground-state reaction has also been measured (53).

A tour-de-force experiment was recently carried out by Pruett and Zare (54) on the reaction Ba + HF (v=1 vs.0) → $BaF^{\dagger}$ + H. Ca.1% of the HF molecules were excited to the v=1 state by a CW HF laser, and clear evidence for the formation of higher excited states of BaF arising from the excited HF reagent molecules was presented.

Table 1 is a summary of these and other experiments dealing with the reaction of vibrationally excited, neutral diatomic reagents.

Theoretical considerations regarding vibrational enhancement effect.

On the basis of the most primitive argument one would expect that for a reaction whose thermal rate constant follows an Arrhenius temperature dependence (cf. Eq. 9), vibrational excitation of a reagent by an amount E_{vib} would reduce the activation energy E_a by some fraction, say α, of that amount (50). Thus

$$k(v)/k(0) \cong \exp[-(E_a - \alpha E_{vib})/kT], \qquad (16)$$

In State-to-State Chemistry; Brooks, P., et al.;
ACS Symposium Series; American Chemical Society: Washington, DC, 1977.

Table 1. Experiments with vibrationally excited, neutral diatomic reagents.

Reaction	Reference
$H_2^\dagger + Cl \rightarrow HCl + Cl$	Stedman et al (1970) (29)
$H_2^\dagger + D_2 \rightarrow 2HD$; $D_2^\dagger + H_2 \rightarrow 2HD$	Bauer et al (1973) (32)
$H_2^\dagger + O \rightarrow OH + H$	Birely et al (1975) (31)
$H_2^\dagger + Br \rightarrow HBr + H$	Sims et al (1975) (33)
$Cl_2^\dagger + H \rightarrow HCl + Cl$	Ding et al (1973) (44)
$HF^\dagger + D_2 \rightarrow HD + DF$	Wolga, Chang (1976) (55)
$HF(v=1) + O \rightarrow OH + F$	Quigley, Wolga (1974) (40)
$HF(v=1) + Ba \rightarrow BaF + H$	Pruett, Zare (1976) (54)
$HF(v=1\text{-}5) + Na \rightarrow NaF + F$	Blackwell et al (1976) (56)
$HF(v=1\text{-}6) + Br, Cl \rightarrow HBr, HCl + F$	Douglas et al (1976) (49)
$HCl(v=1) + K \rightarrow KCl + H$	Odiorne et al (1971) (52)
$HCl(v=1) + F \rightarrow HF + Cl$	Kirsch, Polanyi (1972) (43) Ding et al (1973) (44)
$HCl(v=1\text{-}4) + Br \rightarrow HBr + Cl$	Douglas et al (1973, 1976) (45, 49)
$HCl(v=1,2) + Br \rightarrow HBr + Cl$	Arnoldi et al (1975) (48) Leone et al (1975) (46) Arnoldi, Wolfrum (1976) (47)
$HCl(v=1) + H \rightarrow H_2 + Cl$	Arnoldi, Wolfrum (1976) (37)
$HCl(v=1\text{-}4) + Na \rightarrow NaCl + H$	Blackwell et al (1976) (57)
$HCl(v=1) + O \rightarrow OH + Cl$	Arnoldi, Wolfrum (1974) (37) Karny et al (1975) (38) Brown et al (1975) (42) [also DCl]
$OH(v=1\text{-}9) + Cl \rightarrow HCl + O$	Blackwell et al (1977) (56)
$NO(v=1) + O_3 \rightarrow NO_2 + O$	Stephenson, Freund (1976) (58)
$CN(v=1\text{-}8) + O \rightarrow CO + N$	Schmatjko, Wolfrum (1977) (59).

In State-to-State Chemistry; Brooks, P., et al.;
ACS Symposium Series; American Chemical Society: Washington, DC, 1977.

so that vibrational dependence per se at a given temperature could be exhibited as a nearly linear semilogarithmic plot [ln k(v) vs E_{vib}] with a slope

$$[\partial \ln k(v)/\partial E_{vib}]_T = \alpha/\underline{k}T. \quad (17)$$

Birely and Lyman (50) have summarized and analyzed the early experimental results in terms of this parameter α, the "conversion efficiency". For most reactions of vibrationally excited H_2, OH, HCl (and O_3) they found α to be less than unity, and uncorrelated with E_a, ΔE_o, or E_{vib}; presumably certain key topological features of the potential energy surface played a dominant role in determining α, but they were not obvious.

Levine and Manz (17), hereafter LM, have considered this problem from the viewpoint of the information-theoretic approach (21-25), in which one first evaluates the prior expectation of the rate constant, i.e., $k^\circ(v|T)$, on the basis of a well-defined statistical (density of states) model. Then the deviation from k° is expressed in terms of a surprisal, in the usual way (22). The surprisal is then examined as a function of the degree of reagent excitation.

For the simple case of an atom-diatomic system (i.e., reaction I), assuming the rigid rotor-harmonic oscillator (RRHO) energy level scheme (3), and taking rotational distributions to be statistical, LM obtained a closed-form expression for the "prior" rate constant $k^\circ(v|T)$ as a function of the dimensionless variable $(G_v-\Delta E_o)/\underline{k}T$ (where G_v is the vibrational energy of the reagent diatomic). This function is plotted (semilogarithmically) in Fig. 4.

LM pointed out that in the "strongly endothermic limit", i.e., $G_v-\Delta E_o \ll 0$, their expression reduces to the simple form

$$k^\circ(v|T) \cong C(T)\exp[(G_v-\Delta E_o)/\underline{k}T] \quad (18)$$

where C(T) is weakly dependent upon temperature. Thus a plot of ln $k^\circ(v)$ vs $(G_v-\Delta E_o)/\underline{k}T$ should approach unit slope; in this limit the vibrational dependence would be

$$[\partial \ln k^\circ(v)/\partial G_v]_T = 1/\underline{k}T \quad (19)$$

(cf. Eq. 17).

However, with additional vibrational excitation the prior-expectation vibrational enhancement effect

In State-to-State Chemistry; Brooks, P., et al.;
ACS Symposium Series; American Chemical Society: Washington, DC, 1977.

becomes much smaller (see Fig. 4). In the "exothermic limit", LM show that

$$k^{\circ}(v|T) \propto [(G_v - \Delta E_o)/\underline{k}T]^{5/2}. \quad (20)$$

It should be pointed out that the LM prior rate is independent of the intrinsic activation barrier or the threshold energy E_o, being a function only of the endoergicity via the reduced variable $(G_v - \Delta E_o)/kT$.

The surprisal (22) of the rate constant is defined in the usual way:

$$I(G_v|T) \equiv -\ln[k(v|T)/k^{\circ}(v|T)], \quad (21)$$

and plotted vs G_v at given T. In most cases the surprisal is essentially linear, and it can be expressed

$$I_v = I_o + \lambda_v G_v/\underline{k}T. \quad (22)$$

Eq. 22 serves to define the parameter $\lambda_v = \underline{k}T(\partial I_v/\partial G_v)_T$. Thus in the case of a linear surprisal, and in the "strongly endothermic" limit, the rate constant can be expressed approximately by

$$k(v|T) \cong A \exp\{-[\Delta E_o - (1-\lambda_v)G_v]/\underline{k}T\} \quad (23)$$

(cf. Eq. 16). Then by analogy with Eq. (17),

$$[\partial \ln k(v)/\partial G_v]_T = (1-\lambda_v)/\underline{k}T, \quad (24)$$

so α is identified with $1-\lambda_v$ in this limit. For most of the examples studied, LM found λ_v to be negative, lying in the range $-0.25 \leq \lambda_v < 0$, implying an "extra" effectiveness of vibrational excitation in promoting reaction (cf. Ref. 6).

This is, of course, consistent (via microreversibility) with the frequent observation of vibrational population inversion in the reverse, exothermic reactions. The advantage of the information-theoretic approach (the surprisal with respect to a statistical "prior") over the purely empirical one (e.g., forcing a fit to Eq. 16) is that the main effect of G_v, i.e., the vibrational enhancement (which comes from the prior itself) is removed. Then one deals only with the deviance. Also, one can rigorously relate the selectivity

In State-to-State Chemistry; Brooks, P., et al.;
ACS Symposium Series; American Chemical Society: Washington, DC, 1977.

of the endothermic reaction with the specificity of the exothermic reaction (14, 19, 20). Normally the latter is obtained more easily experimentally (and computationally, via trajectory simulations). Of course, even in the case of a linear surprisal, one has not yet ascertained the relation between the value of the λ_v parameter and the topology of the potential surface.

Influence of reagent's rotational energy upon reactivity

The rotational energy effect upon molecular reactivity has received considerably less experimental attention than the analogous vibrational effect. Just as in the latter case, of course, microscopic reversibility can be exploited (2, 3, 11, 14, 19, 20) to relate the specificity of the product's rotational state distribution in an exoergic reaction with the selectivity of the reactant's rotational state utilization in the inverse, endoergic reaction. The information-theoretic methodology (24) for the analysis of rotational state distributions (60 - 65) has been extended (17) to deal with reagent's rotational selectivity. However, experimental data on the rotational effect is quite sparse, so the method has not yet been well tested.

The existing experiments deal with three classes of reactions: H_2, HCl + F; HF, HCl + Na; and CsF + K.

The first to be studied was the F + H_2 reaction (66-69):

$$H_2(J=1 \text{ vs. } 0) + F \rightarrow HF + H$$

Measurements were made by Klein and Persky (67) of the rate constant ratio for normal H_2 (25% para) vs. a parahydrogen-enriched (75% para) reagent. The ratio $k[H_2 75\%p]/k[H_2 25\% \text{ para}]$ differed from unity only for the lowest temperature experiment (175°K), at which it was $1.02_5 \pm 0.01$ (from which $k_{para}/k_{ortho} = 1.05 \pm 0.02$). This result implied a slight decrease in reactivity for the J=1 state (vs. J=0). Coombe and Pimentel (66) had already studied the same reaction by the chemical laser technique, comparing product (HF) vibrational state distributions for normal and 85% parahydrogen. Substantial effects were noted, over a wide temperature range, but subsequent chemiluminescence experiments (68) cast doubt upon certain of these results. The most definitive study of this effect is that of Douglas and Polanyi (69), which provides quantitative data on

In State-to-State Chemistry; Brooks, P., et al.;
ACS Symposium Series; American Chemical Society: Washington, DC, 1977.

k(J) for this reaction. They also evaluated the average fraction of the available energy appearing in HF vibration, $\bar{f}_{v'}$; it was found to be slightly J-dependent.

Experiments on the rotational energy effect upon the reaction

$$HCl(J=0\text{-}10) + F \rightarrow HF + Cl$$

were reported by Polanyi and coworkers (44) in 1973. Recently, Blackwell et al (70) have observed the rotational effect for hydrogen halide-alkali reactions:

$$HF(J=0\text{-}12) + Na \rightarrow NaF + H$$
$$HCl(J=0\text{-}12) + Na \rightarrow NaCl + H.$$

All of these studies involved flowing gas systems and would be characterized as "bulk experiments". The only single-collision experiments (i.e., using crossed beams) on the rotational energy effect are those of Stolte et al (71, 72) on the alkali halide-alkali exchange reaction:

$$CsF(J) + K \rightarrow Cs + KF .$$

The influence of the rotational energy of the CsF molecule upon its reactivity with K was measured by the crossed molecular beam technique over a range of relative translational energy $\bar{E}_{tr}$ from 3-6 kcal mol^{-1}. The experiments involved the endoergic reaction [known to proceed via a long-lived complex (73)]: $CsF + K \rightleftarrows [CsFK] \rightarrow Cs + KF - 1.8$ kcal mol^{-1}. The reactive branching fraction F_R had been previously measured (46) using velocity-selected but otherwise "thermal" (Boltzmann) CsF. Beams of low rotational states of CsF were prepared by means of a quadrupole state selector-focusing field placed beyond the velocity selector. This arrangement provided "low-J" beams of CsF, with known speed distributions, which were then crossed with a well-characterized K beam. The measurements consisted of angular distributions of reactive (i.e., Cs) and nonreactive (i.e., CsF) scattering for the "low-J" beam compared to the "thermal" reactant beam at essentially the same $\bar{E}_{tr}$. The reactive yield and thus the reactive branching fraction was found to be significantly smaller for the "low-J" beam than for the "thermal" beam of CsF.

In State-to-State Chemistry; Brooks, P., et al.;
ACS Symposium Series; American Chemical Society: Washington, DC, 1977.

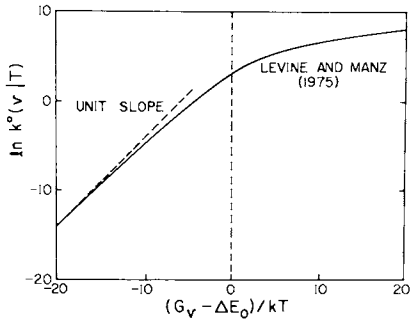

Figure 4. Semilog plot of the prior expectation rate constant, k°(v|T) vs. the reduced available energy, for the RRHO model. Adapted from Levine and Manz (17).

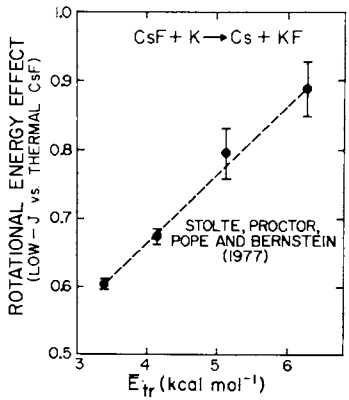

Figure 5. Observed rotational energy effect for the CsF + K reaction as a function of the average translational energy $\bar{E}_{tr}$. The ordinate is the ratio of the reactivity of "low-J" CsF, for which $\bar{E}_{rot} \cong 0.1$ kcal mol^{-1}, to that of the "thermal" reagent, $\bar{E}_{rot} = 2.5$ kcal mol^{-1}. Adapted from Stolte et al. (72).

In State-to-State Chemistry; Brooks, P., et al.;
ACS Symposium Series; American Chemical Society: Washington, DC, 1977.

The average rotational energy $\bar{E}_{rot}$ of the reactant molecules was known at each $\bar{E}_{tr}$. $\bar{E}_{rot}$ ranged from 0.13 to 0.04 kcal mol^{-1} for $\bar{E}_{tr}$ in the range 3 to 6 kcal mol^{-1}, whereas $\bar{E}_{rot}$ for the "thermal" CsF beam was 2.52 kcal mol^{-1}. (Thus the effect of applying the rod voltage to the quadrupoles was to "switch off" some 2.4 kcal mol^{-1} of CsF rotational energy.) The results are shown in Fig. 5.

By combining the data on the $\bar{E}_{tr}$-dependence of F_R for the rotationally cold CsF beams with the previous results for thermal beams it was possible to compare the relative importance of rotational vs. translational energy at a given total energy. It was found that rotational energy of the CsF is significantly less effective than relative translational energy in promoting the reaction, in semiquantitative accord with theory (74).

Concluding remarks

This paper has been a review and an introduction to the subject matter of this symposium on state-to-state chemistry. The topic of state-to-state cross sections and rate constants has considerable theoretical and practical significance (27, 75-77). As evidenced by the scope of the program, the subject encompasses the entire field of molecular reaction dynamics, ranging from ab initio quantum chemistry and potential energy surfaces to scattering theory (quantal and classical), molecular and ion beam scattering, kinetic spectroscopy, gas phase and photochemical kinetics, chemical lasers and laser-induced chemical reactions.

Literature Cited

1. Eliason, M.A. and Hirschfelder, J.O., J. Chem. Phys. (1959) 30, 1426.
2. Ross, J., Light, J.C. and Shuler, K.E., "Kinetic Processes in Gases and Plasmas", p. 281, ed. A.R. Hochstim, Academic, New York, 1965.
3. Kinsey, J.L., J. Chem. Phys. (1971) 54, 1206.
4. Bernstein, R.B. and Levine, R.D., J. Chem. Phys. (1972) 57, 434.
5. Levine, R.D. and Bernstein, R.B., "Molecular Reaction Dynamics", Clarendon, Oxford, 1974.

In State-to-State Chemistry; Brooks, P., et al.;
ACS Symposium Series; American Chemical Society: Washington, DC, 1977.

6. Parker, J.H. and Pimentel, G.C., J. Chem. Phys. (1969) 51, 91.
7. Polanyi, J.C., J. Chem. Phys. (1959) 31, 1338.
8. Polanyi, J.C. and Wong, W.H., J. Chem. Phys. (1969) 51, 1439.
9. Mok, M.H. and Polanyi, J.C., J. Chem. Phys. (1969) 51, 1451.
10. Raff, L.M., Sims, L.B., Thompson, D.L. and Porter, R.N., J. Chem. Phys. (1970) 53, 1606.
11. Anlauf, K.G., Maylotte, D.H., Polanyi, J.C. and Bernstein, R.B., J. Chem. Phys. (1969) 51, 5716.
12. Polanyi, J.C., Acc. Chem. Res. (1972) 5, 161.
13. Polanyi, J.C. and Schreiber, J.L., "Physical Chemistry-an Advanced Treatise, Kinetics of Gas Reactions", Vol. VI A, Chap. 6, ed. H. Eyring, W. Jost and D. Henderson, p. 383, Academic, New York 1974.
14. Levine, R.D. and Bernstein, R.B., Acc. Chem. Res. (1974) 7, 393.
15. Berry, M.J., Ann. Rev. Phys. Chem. (1975) 26, 259.
16. Bauer, S.H., Ann. Rev. Phys. Chem. (1977) 28, 000.
17. Levine, R.D. and Manz, J., J. Chem. Phys. (1975) 63, 4280.
18. Pollak, E. and Levine, R.D., Chem. Phys. Lett. (1976) 39, 199.
19. Kaplan, H., Levine, R.D. and Manz, J., Chem. Phys. (1976) 12, 447.
20. Kaplan, H., Levine, R.D. and Manz, J., Mol. Phys. (1976) 31, 1765.
21. Bernstein, R.B. and Levine, R.D., J. Chem. Phys. (1972) 57, 434.
22. Ben-Shaul, A., Levine, R.D. and Bernstein, R.B., J. Chem. Phys. (1972) 57, 5427.
23. Levine, R.D. and Bernstein, R.B., Chem. Soc. Far. Disc. (1973) 55, 100.
24. Bernstein, R.B. and Levine, R.D., Adv. Atom. Molec. Phys. (1975) 11, 215.
25. Levine, R.D. and Bernstein, R.B., "Dynamics of Molecular Collisions", ed. W.H. Miller, Vol. II B, p. 323, Plenum, New York, 1976.
26. Chupka, W.A., Berkowitz, J. and Russell, M.E., Proc. VI ICPEAC, p. 71, M.I.T., Cambridge, Mass. (1969).
27. Bernstein, R.B., Isr. J. Chem. (1971) 9, 615.
28. Whitton, W.N. and Kuntz, P.J., J. Chem. Phys. (1976) 64, 3624.
29. Stedman, D.H., Steffenson, D. and Niki, H., Chem. Phys. Lett. (1970) 7, 173.
30. Heidner, R.F. and Kasper, J.V., Chem. Phys. Lett. (1972) 15, 179.

In State-to-State Chemistry; Brooks, P., et al.;
ACS Symposium Series; American Chemical Society: Washington, DC, 1977.

31. Birely, J.H., Kasper, J.V., Hai, F. and Darnton, L.A., Chem. Phys. Lett. (1975) 31, 220.
32. Bauer, S.H., Lederman, D.M., Resler, E.L. and Fisher, E.R., Intl. J. Chem. Kin. (1973) 5, 93.
33. Sims, L.B., Dosser, L.R. and Wilson, P.S., Chem. Phys. Lett. (1975) 32, 150.
34. Gordon, R.J. and Lin, M.C., Chem. Phys. Lett. (1973) 22, 262.
35. Kurylo, M.J., Braun, W., Xuan, C.N. and Kaldor, A., J. Chem. Phys. (1975) 62, 2065.
36. Freund, S.M. and Stephenson, J.C., Chem. Phys. Lett. (1976) 41, 157.
37. Arnoldi, D. and Wolfrum, J., Chem. Phys. Lett. (1974) 24, 234.
38. Karny, Z., Katz, B. and Szöke, A., Chem. Phys. Lett. (1975) 35, 100.
39. Craig, N.C. and Moore, C.B., J. Phys. Chem. (1971) 75, 1622.
40. Quigley, G.P. and Wolga, G.J., Chem. Phys. Lett. (1974) 27, 276.
41. Macdonald, R.G., Moore, C.B., Smith, I.W. and Wodarczyk, F.J., J. Chem. Phys. (1975) 62, 2934.
42. Brown, R.D., Glass, G.P. and Smith, I.W., Chem. Phys. Lett. (1975) 32, 517.
43. Kirsch, L.J. and Polanyi, J.C., J. Chem. Phys. (1972) 57, 4498.
44. Ding, A.M., Kirsch, L.J., Perry, D.S., Polanyi, J.C. and Schreiber, J.L., Far. Disc. Chem. Soc. (1973) 55, 252.
45. Douglas, D.J., Polanyi, J.C. and Sloan, J.J., J. Chem. Phys. (1973) 59, 6679.
46. Leone, S.R., Macdonald, R.G. and Moore, C.B., J. Chem. Phys. (1975) 63, 4735.
47. Arnoldi, D. and Wolfrum, J., Ber. Bunsenges. Phys. Chem. (1976) 80, 892.
48. Arnoldi, D., Kaufmann, K. and Wolfrum, J., Phys. Rev. Lett. (1975) 34, 1597.
49. Douglas, D.J., Polanyi, J.C. and Sloan, J.J., Chem. Phys. (1976) 13, 15.
50. Birely, J.H. and Lyman, J.L., J. Photochem. (1975) 4, 269.
51. Wolfrum, J., Ber. Bunsenges. Phys. Chem. (1977) 81, 000.
52. Odiorne, T.J., Brooks, P.R. and Kasper, J.V., J. Chem. Phys. (1971) 55, 1980.
53. Pruett, J.G., Grabiner, F.R. and Brooks, P.R., J. Chem. Phys. (1975) 63, 1173.
54. Pruett, J.G. and Zare, R.N., J. Chem. Phys. (1976) 64, 1774.
55. Wolga, G.J. and Chang, R., unpublished (1976); referred to by Bauer, S.H., Ref. 16.

In State-to-State Chemistry; Brooks, P., et al.;
ACS Symposium Series; American Chemical Society: Washington, DC, 1977.

56. Blackwell, B.A., Polanyi, J.C. and Sloan, J.J., Chem. Phys. (to be published 1977).
57. Blackwell, B.A., Polanyi, J.C. and Sloan, J.J., Chem. Soc. Far. Disc. (1976) 62, 000.
58. Stephenson, J.C. and Freund, S., J. Chem. Phys. (1976) 65, 4303.
59. Schmatjko, K.J. and Wolfrum, J., 16th Intl. Symp. on Combustion (1977), The Combustion Institute.
60. Levine, R.D., Johnson, B.R. and Bernstein, R.B., Chem. Phys. Lett. (1973) 19, 1.
61. Bernstein, R.B., J. Chem. Phys. (1975) 62, 4570.
62. Levine, R.D., Bernstein, R.B., Kahana, P., Procaccia, I. and Upchurch, E.T., J. Chem. Phys. (1976) 64, 796.
63. Bernstein, R.B., Int. J. Quant. Chem. (1976) S10, 267.
64. Kaplan, H. and Levine, R.D., Chem. Phys. (1976) 13, 161.
65. Pattengill, M.D. and Bernstein, R.B., J. Chem. Phys. (1976) 65, 4007.
66. Coombe, R.D. and Pimentel, G.C., J. Chem. Phys. (1973) 59, 1535.
67. Klein, F.S. and Persky, A., J. Chem. Phys. (1974) 61, 2472.
68. Perry, D.S., Polanyi, J.C. and Wilson, C.W., Chem. Phys. Lett. (1974) 24, 484.
69. Douglas, D.J. and Polanyi, J.C., Chem. Phys. (1976) 16, 1.
70. Blackwell, B.A., Polanyi, J.C. and Sloan, J.J., Chem. Soc. Far. Disc. (1976) 62, 000.
71. Stolte, S., Proctor, A.E. and Bernstein, R.B., J. Chem. Phys. (1975) 62, 2506.
72. Stolte, S., Proctor, A.E., Pope, W.M. and Bernstein, R.B., J. Chem. Phys. (1977) 66, 3468.
73. Stolte, S., Proctor, A.E. and Bernstein, R.B., J. Chem. Phys. (1976) 65, 4990.
74. Stolte, S., J. Chem. Phys. (to be published 1977).
75. Flynn, G.W., Pechukas, P., Stern, R.C. and Zare, R.N., eds., N.S.F. Workshop Report, "Gas-Phase Molecular Interactions and the Nation's Energy Problem", Columbia University, Harriman House, Arden, New York (1974).
76. Wilson, L., ed., A.F.O.S.R. Workshop Report, "State-to-State Molecular Dynamics", July 1974, University of Maryland, College Park, Md. (1976).
77. Steinfeld, J.I. and Wrighton, M.S., eds., "The Laser Revolution in Energy-Related Chemistry", M.I.T., Cambridge, Mass. (1976).

Supported by N.S.F. Grant MPS73-04940A03.

2

State-to-State Ion-Molecule Reactions

T. F. MORAN

Chemistry Department, Georgia Institute of Technology, Atlanta, GA 30332

The purpose of this paper is to examine some of the state to state processes that occur when an ion interacts with a neutral molecule. High resolution ion beam-neutral beam techniques have been so developed that detailed quantum state distributions can be obtained from a translational energy analysis of products scattered in ion-molecule interactions. When an ion, A^+, collides with a neutral molecule, BC, a number of scattering events can occur. Some of these processes are illustrated schematically.

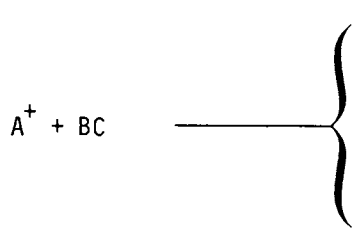

$A^+ + BC$	Elastic	(1)
$A^+ + BC^*$	Inelastic	(2)
$AB^+ + C$	Rearrangement	(3)
$(A + B + C)^+$	Dissociation	(4)
$A + BC^+$	Charge Exchange	(5)

In elastic scattering events (1) the velocities of the product species differ in direction and magnitude from the velocities of the reactants; however products and reactants occupy the same quantum states before and after collision. Elastic scattering processes are now routinely used in beam experiments to determine the interaction potential between the colliding reactant pair. Since state distributions are the same before and after collision, the elastic channels will not occupy our attention here. Inelastic scattering (2) results in a change of the reactant velocities and also a change in the occupation of various quantum states before and after collision. The rearrangement channels (3) involve chemical reactions in which the velocity, mass, and thus quantum state distribution of products are different from that of reactants. Dissociative collisions (4) give rise to an additional one or more heavy particle fragments emerging from the interaction

In State-to-State Chemistry; Brooks, P., et al.;
ACS Symposium Series; American Chemical Society: Washington, DC, 1977.

and can be classified as a particular type of inelastic process. Charge exchange collisions (5) involve a transfer of an electron from the target molecule to the incident ion with the products possibly leaving the interaction in excited quantum states.

Inelastic Processes

Inelastic scattering of ions by neutral molecules has been observed for several years (1-7) and, as the instrumental resolution and experimental techniques have improved, details concerning electronic, vibrational and rotational product state distributions have become available. A typical ion-impact spectrometer is shown in Figure 1. Reactant ions in this apparatus are generated in an electron impact source, accelerated through a slit system and then energy selected by a 127 degree electrostatic sector. Ions emerging from the sector pass through an ion optical system prior to entering the collision region where ion-molecule interactions take place with neutral molecules from a beam. Product ions scattered from the interaction region pass into the analyzing system consisting of a 127 degree electrostatic sector, a quadrupole mass filter and a multiplier detector. The analyzing system can be rotated with respect to the direction of the primary ion beam and both angular and energy distributions of the scattered ions can be determined. From this information

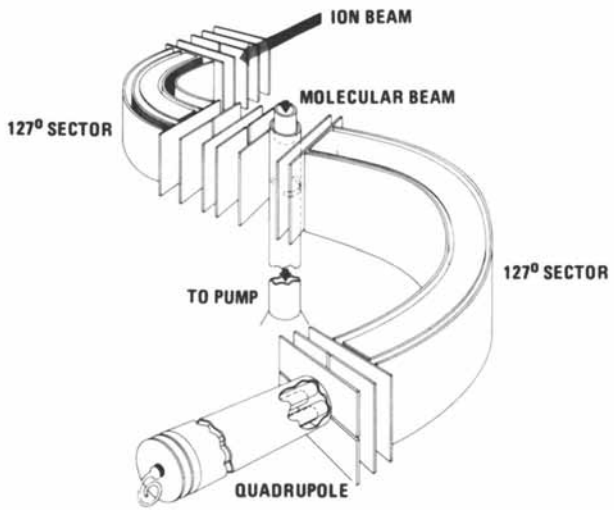

Figure 1. Schematic of typical ion beam–neutral beam apparatus employing electrostatic sectors for energy analysis of the reactant and scattered ion beams

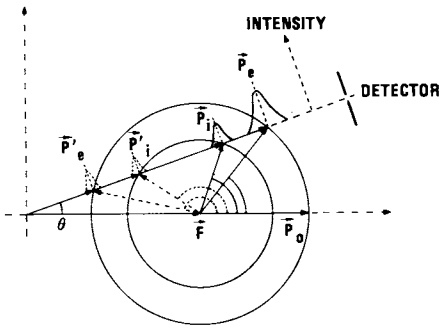

Figure 2. Schematic momentum vector for elastic and inelastic scattering of a system with one excited internal quantum state accessible to the products

the doubly differential cross sections are obtained. High resolution time-of-flight (T.O.F.) techniques have also been used successfully to measure inelastic energy loss in the scattering of ions from molecules. In this T.O.F. arrangement, the primary ion beam is chopped prior to reaction and the analyzing sector is replaced by a drift tube assembly with associated time-counting equipment.

Since classical mechanics provides a good description of the asymptotic translational states of a given ion and molecule, the energy loss in a particular process can be determined from the laboratory scattering angle and momentum of the product ion. This is schematically illustrated in Figure 2 for the in-plane scattering of an ion with initial momentum, $\vec{P}_0$, by a stationary target molecule. In this figure, $\vec{P}_e$ represents the momentum of the elastically scattered ion while $\vec{P}_i'$ and $\vec{P}_e'$ represent the momentum of the backward scattered inelastic and elastic ions respectively. The larger of the two circles in the figure is the locus of termini of all possible momentum vectors for elastically scattered ions, while the small circle is that for inelastically scattered ions in a collision system with only one accessible excited quantum state. In reality, collision systems will have a number of energetically accessible quantum states and the different momentum vectors $\vec{P}_i$ and $\vec{P}_i'$ reflect scattering to these product states at a particular laboratory angle. It is generally found that the signal intensities of the forward elastically scattered ions are significantly larger than those scattered in the backward

In State-to-State Chemistry; Brooks, P., et al.;
ACS Symposium Series; American Chemical Society: Washington, DC, 1977.

direction. Early data (8) of this type, obtained in a T.O.F. measurement of the scattering of 3.62 eV Li^+ ions from H_2, is displayed in Figure 3 for a 3^o scattering angle. The large peak on the left side of the figure is due to the elastic $\upsilon = 0 \rightarrow 0$ process while the smaller peaks on the right side are from backward elastic $\upsilon = 0 \rightarrow 0$ and inelastic $\upsilon = 0 \rightarrow 1$, $\upsilon = 0 \rightarrow 2$ processes. With instrumental improvements over the past few years, scattered ion spectra of the type given in Figure 3 have been used to obtain differential cross sections for individual vibrational scattering events as a function of scattering angle and reactant ion kinetic energy. Relative vibrational excitation cross sections from (8) for the Li^+-H_2 system are presented below for a 172^o center of mass angle.

TABLE I

Relative Differential Vibrational Cross Sections $\upsilon = 0 \rightarrow \upsilon'$

Li^+ Kinetic Energy (eV)	$\upsilon' = 0$	1	2	3	4	5	6
3.6	.73	.14	.07	.04	.02	-	-
5.5	.68	.16	.08	.05	.03	-	-
8.8	.60	.20	.06	.04	.03	.03	.03

As indicated in this table, the relative contributions of vibrationally inelastic processes increase with ion center of mass kinetic energy.

In addition to peaks in the inelastic energy loss spectrum corresponding to vibrational excitation, maxima are observed in high resolution experiments which result from rotational excitation. An example from ref. (9) of pure rotational excitation in the forward scattering of 0.60 eV Li^+ ions by H_2 at 3^o is given in Figure 4, where the $j = 0 \rightarrow 2$ and $j = 1 \rightarrow 3$ rotational transitions are found to dominate the forward inelastic scattering processes at low center of mass kinetic energies. The ratio of the differential cross sections $\sigma(j = 0 \rightarrow 2)/\sigma(\text{elastic})$ increases (9) from 0.07 to 0.13 as the center of mass scattering angle increases from 14 to 32 degrees while corresponding $\sigma(j = 1 \rightarrow 3)/\sigma(\text{elastic})$ ratio increases from 0.07 to 0.18. At very low Li^+-H_2 relative energies, rotational excitation is dominant but as the kinetic energy is increased, the differential cross sections for vibrational excitation become important. Although inelastic vibrational and rotational excitation processes have been observed in a number of systems (see references (10,11,12) for a survey), the Li^+-H_2 reaction has occupied a pivotal position in inelastic studies since accurate self consistent field, SCF, and configuration interaction, CI, potential hypersurfaces are available (13-15). Close

In State-to-State Chemistry; Brooks, P., et al.;
ACS Symposium Series; American Chemical Society: Washington, DC, 1977.

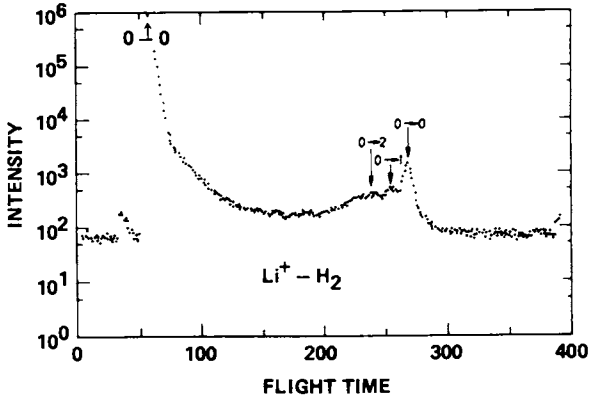

Figure 3. Experimental data taken from David, Faubel, and Toennies (8), giving the intensity of forward and backward Li^+ ions scattered in 3.62 eV Li^+-H_2 interactions as a function of time-of-flight for $\theta = 3°$. The arrow gives the position expected for pure vibrational excitation.

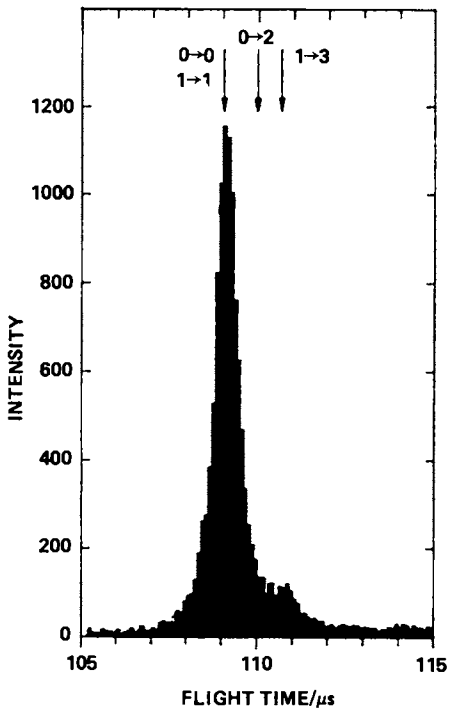

Figure 4. Experimental data taken from van den Bergh, Faubel and Toennies (9), giving the intensity of forward scattered Li^+ in 0.6 eV Li^+-H_2 interactions as a function of time-of-flight for $\theta = 3°$. The arrows give the position expected for pure rotational excitation.

In State-to-State Chemistry; Brooks, P., et al.;
ACS Symposium Series; American Chemical Society: Washington, DC, 1977.

coupling quantum mechanical calculations (16) have been carried out using this potential and have provided bench-mark scattering cross section that have stimulated further experimental and theoretical work (17-23). The accurate Li^+-H_2 interaction potential has been expanded in terms of the Legendre polynomials

$$V(R,r,\gamma) = \sum_{\lambda} V_{\lambda}(R,r)P_{\lambda}(\cos\gamma) \qquad (6)$$

where R is the ion-molecule center-of-mass distance, $\vec{r}$ is the H_2 internuclear distance and γ is the angle $\vec{R}$ makes with $\vec{r}$. The magnitude and variation of V_λ with R is displayed in Figure 5. The overall well depth is reasonably small with the V_2 term comparatively large and repulsive at all R. The coupled radial equations describing the scattering of Li^+ from H_2 are:

$$\left(\frac{d^2}{dR^2} + k^2_{\upsilon'j'} - \frac{\ell'(\ell'+1)}{R^2}\right) u^J_{\upsilon'j'\ell'\leftarrow\upsilon j\ell}(R)$$

$$= \frac{2\mu}{\hbar^2} \sum_{\upsilon''j''\ell''} \langle \upsilon'j'\ell' | V | \upsilon''j''\ell'' \rangle u^J_{\upsilon''j''\ell''\leftarrow\upsilon j\ell}(R) \ , \qquad (7)$$

where

$$k^2_{\upsilon'j'} = 2\mu(E_{\upsilon j} - \varepsilon_{\upsilon'j'})/\hbar^2 \ , \qquad (8)$$

and μ is the reduced mass of the ion-molecule system, $E_{\upsilon j}$ is the total energy of the reactants in the υ,j vibrational-rotational state, and $\varepsilon_{\upsilon',j'}$ is the corresponding energy of the H_2 final state. Differential cross sections, determined using the above coupled radial equations, are given in Figures 6 and 7 for the collisions of 0.6 eV (center of mass kinetic energy) Li^+ ions with ortho and para hydrogen respectively. The dashed line is the quantum result of ref. (16) and the squares encompass the experimental data and error limits estimated in ref. (11). The ratio of inelastic to elastic cross section is taken to be the most accurate experimentally measured quantity and thus ratios have been used when comparing theory and experiment. The solid line is the semi-classical multistate orbital approach of refs. (20,21). In this later approach the appropriate trajectories are evaluated from a certain optical potential which couples the response of the internal structure, as determined from a quantum multistate approach, to the orbit for relative motion and vice versa. A relatively large V_2 component ($V_0 > V_2 >> V_4$) in the Li^+-H_2 interaction potential leads to large $0 \rightarrow 2$ and $1 \rightarrow 3$ rotational transitions since it is this $\lambda = 2$ term that directly couples initial and final rotational states with $\Delta j = 2$, although we note that a

In State-to-State Chemistry; Brooks, P., et al.;
ACS Symposium Series; American Chemical Society: Washington, DC, 1977.

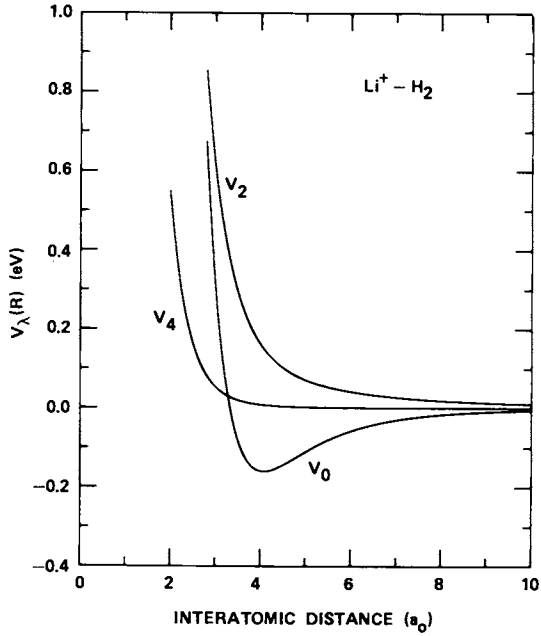

Figure 5. Interaction potential for the Li^+-H_2 system

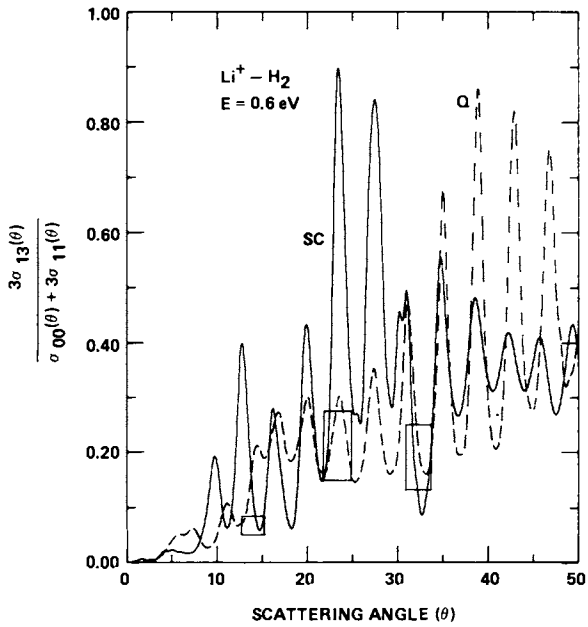

Figure 6. Ratio of the $j = 1 \rightarrow 3$ rotational cross sections to the elastic cross sections as a function of scattering angle in 0.6 eV Li^+-ortho H_2 interactions. The dashed line represents the full quantum calculations of Ref. 16, the solid line represents the semiclassical calculations of Ref. 21, and the squares give the experimental data of Ref. 11.

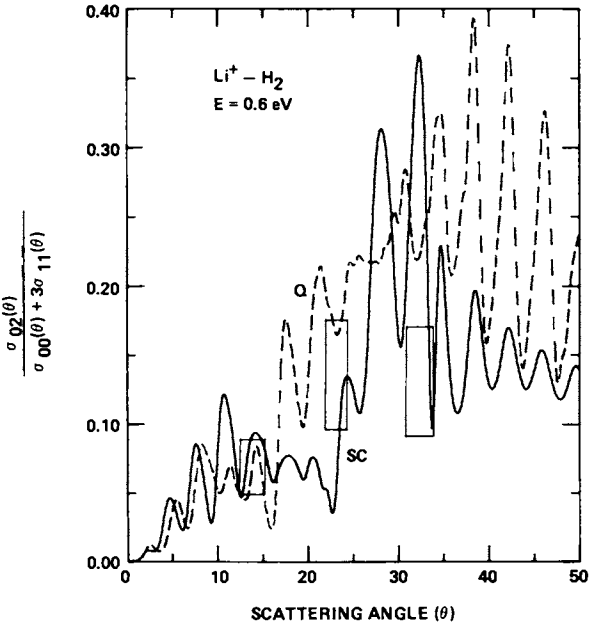

Figure 7. Ratio of the $j = 0 \rightarrow 2$ rotational cross sections to the elastic cross sections as a function of scattering angle in 0.6 eV Li^+-para H_2 interactions. The dashed line represents the full quantum calculations of Ref. 16, while the solid line represents the semi-classical calculations of Ref. 21, and the squares give the experimental data of Ref. 11.

large basis set is explicitly used in the coupled channel expansion (16) to obtain converged cross sections. Reasonably good agreement is observed in Figures 6 and 7 between theory and experiment. Classical calculations using the accurate hypersurfaces have also been performed (22) and the cross sections are found to be in reasonable accord with the quantum, Q, and semi-classical, SC, treatments. Semi-classical approaches are particularly attractive as the ion velocity is increased, since a large number of energetically accessible inelastic channels make the full close coupling calculations prohibitively time consuming.

Similar inelastic processes occurring in the H^+-H_2 system reported by ref. (23) are presented in Figure 8 for 20° lab scattering angle and 3.7 eV c.m. kinetic energy. The position of the lines indicates the flight times expected for H^+ scattered from H_2 in rotationally inelastic events. In contrast to the previously discussed Li^+-H_2 system, transitions corresponding to large

In State-to-State Chemistry; Brooks, P., et al.;
ACS Symposium Series; American Chemical Society: Washington, DC, 1977.

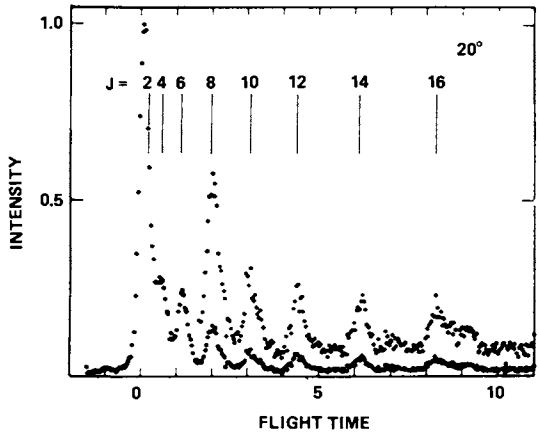

Figure 8. The intensity of H^+ scattered in 3.7 eV H^+-para H_2 interactions as a function of flight-time with respect to the elastic peak as measured in Ref. 23. The lines denote positions expected for pure rotational transitions $j = 0 \rightarrow 2. \ldots 16$ at $\theta = 20°$.

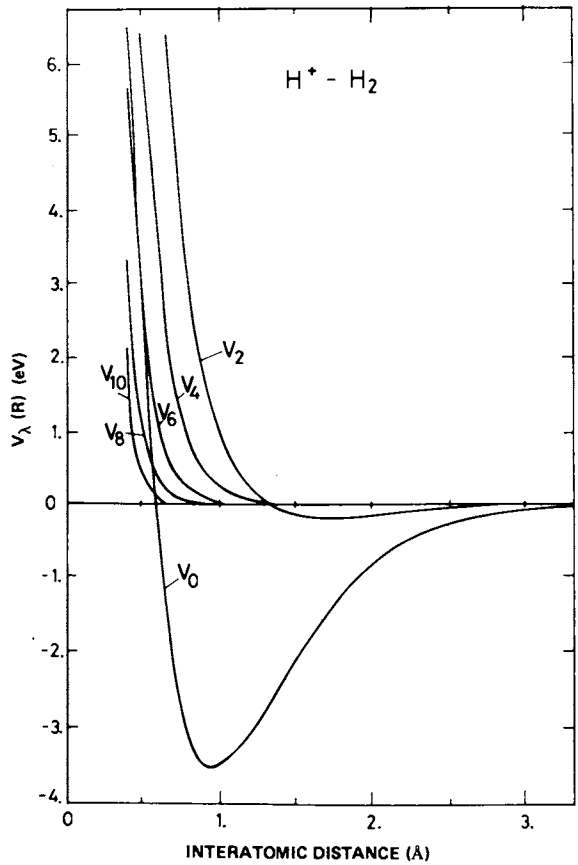

Figure 9. Interaction potential for the H^+–H_2 system

changes in rotational quantum number, Δj, are observed. The interaction potential for this system has been determined from an analytical fit (24) to the H_3^+ ab initio calculations of references (25,26,27) which have determined over a range of R, r and θ. As H^+ approaches H_2, the H_3^+ surface has an avoided crossing at $r \sim 2.5\ a_0$ with a surface asymptotically corresponding to $H_2^+ + H$ (28,29); however the ground state analytic potential is extrapolated smoothly through this seam (24). This ground state H_3^+ interaction potential, fitted to the Legendre expansion form, is shown in Figure 9. The H^+-H_2 surface is much deeper than that of Li^+-H_2. The V_4, V_6, V_8 and V_{10} terms in the H^+-H_2 potential are relatively large compared to V_2. The higher order anisotropic terms in the H^+-H potential give rise to transitions which occur with large values of Δj (processes of the type illustrated by the data in Figure 8). From measurements of the energy loss spectra, at specified angles and H^+ reactant energy, the ratio of the rotational inelastic cross section for a particular transition to the total differential cross section has been determined and compared with the quantum calculations by McGuire, Rudolph and Toennies (30). The measured ratios, or rotational transition probabilities, are given as the closed and open circles in Figure 10 along with the results of coupled states quantum mechanical calculation, which are denoted by the x's. Transition probabilities involving para-H_2 are given by the closed circles while the open circles refer to those for ortho-H_2. The agreement between the experimental inelastic transition probabilities and those obtained from converged theoretical cross sections provides qualitative verification of the theoretical H_3^+ hypersurface. A comparison of the coupled states quantum, Q, calculation and the semiclassical, SC, approach (21) is given in Figure 11 for the $0 \rightarrow 2$ rotational transition. Reasonable accord between the two approaches, at angles smaller than the rainbow, lends support for the semiclassical model which can be applied at high kinetic energies where it is more difficult to employ full quantum treatments. Classical calculations using accurate hypersurfaces also have been used to obtain information on the inelastic processes (24) and, in fact, have provided the original impetus for high resolution studies of the H^+-H_2 system.

Typical inelastic spectra measured (31) for reactions involving heavier molecules, that of 7 eV Li^+ ions scattered from N_2 and CO, are given in Figure 12 where the arrows denote positions expected for the elastic $\upsilon = 0 \rightarrow 0$ and vibrationally inelastic $\upsilon = 0 \rightarrow 1$ and $\upsilon = 0 \rightarrow 2$ transitions at a lab scattering angle of 40^o. Individual rotational transitions are not observed in this spectra due to the small spacing between rotational levels but there are clear indications of pure rotational transitions occurring below the threshold for the $\upsilon = 0 \rightarrow 1$ vibrational excitation. In these reactions Δj changes of ∿30 to 50 are common. A larger amount of vibrational excitation is measured in the Li^+-CO collisions as compared to that in Li^+-N_2 interactions.

In State-to-State Chemistry; Brooks, P., et al.;
ACS Symposium Series; American Chemical Society: Washington, DC, 1977.

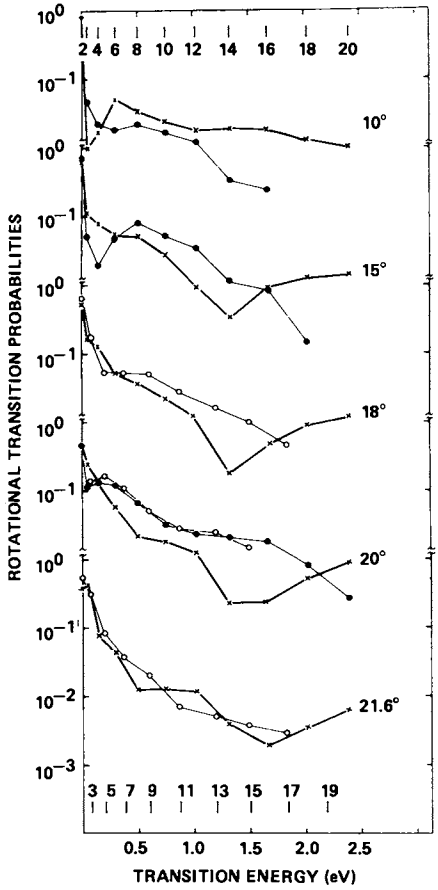

Figure 10. Comparison of experimental and theoretical rotational probabilities for 3.7 eV H^+–H_2 collisions at different scattering angles given in Ref. 30. The x's are computed using the quantum mechanical coupled states approach, and the circles give the experimental data (closed for para H_2 and open for ortho H_2).

The maxima are attributed to simultaneous vibrational-rotational excitation processes with the degree of inelasticity increasing as functions of both ion kinetic energy and scattering angle.

Rearrangement Processes

Ion beam techniques have been successfully applied (32-40) to the study of rearrangement channels in ion-molecule reactions. From measurements of the mass and energy of products emerging from reaction at a particular angle, it has been possible to obtain valuable information about the reaction mechanism as well as examine energy disposal pathways. In general, detailed product vibrational and rotational state distributions are difficult to determine due to the extremely high energy resolution requirements needed to obtain state to state cross sections. However, there are reactions where complementary experimental techniques have provided the necessary data to assess product state populations.

In State-to-State Chemistry; Brooks, P., et al.;
ACS Symposium Series; American Chemical Society: Washington, DC, 1977.

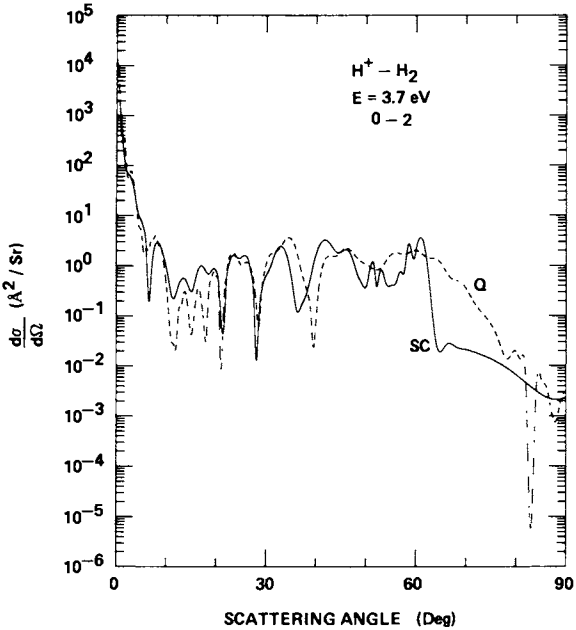

Figure 11. Differential cross sections for $j = 0 \rightarrow 2$ rotational transitions in 3.7 eV H^+–H_2 interactions as a function of scattering angle. The dashed line represents the quantum calculations, while the solid line represents the semi-classical computation of Ref. 21.

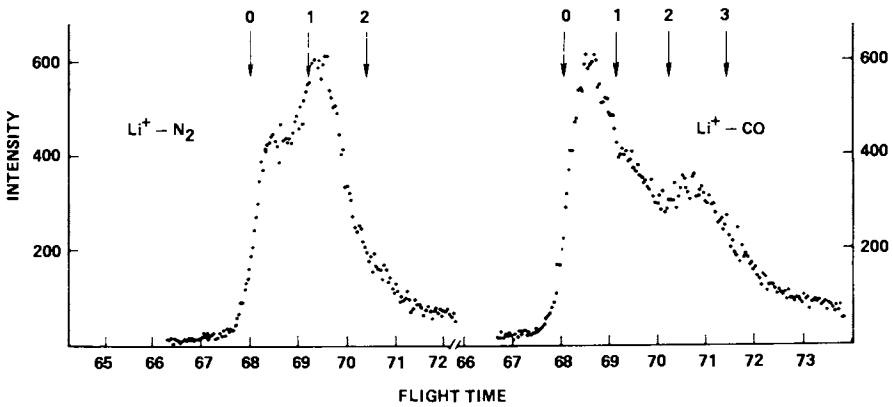

Figure 12. Inelastic energy loss spectra of Ref. 31 measured for 7.07 eV Li^+–N_2 and 7.07 eV Li^+–CO interactions at $\theta = 40°$. The arrows denote flight times of Li^+ ions scattered in collisions involving pure vibrational excitation of the target.

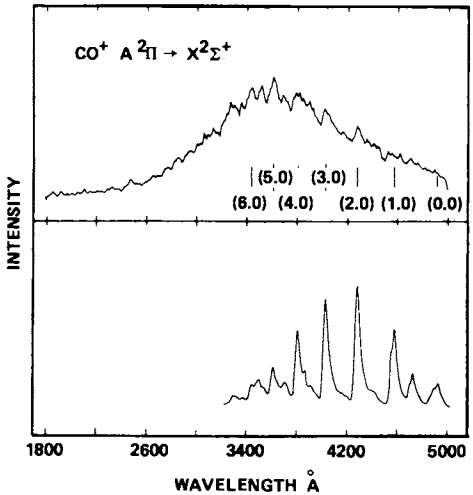

Figure 13. Variation of photon intensity as a function of wavelength for $CO^+(A^2\Pi,v'j') \rightarrow CO^+(X^2\Sigma^+,v''j'')$ transitions, adapted from Ref. 43. The upper curve gives the spectra obtained for $CO^+(A^2\Pi,v'j')$ ions produced in 5 eV $C^+ + O_2$ interactions while the lower curve gives the spectra of $CO^+(A^2\Pi,v'j')$ produced in 1 keV Ar^+–CO charge transfer reactions.

Such an example involves the $C^+ + O_2$ reactions where a tandem-mass spectrometer apparatus was first used to measure total cross sections for CO^+ product formation (41). Several years later, a kinetic energy analysis of the CO^+ product ions at a particular angle (42) showed that these $CO^+ + O$ product species accommodated a surprisingly large amount of energy, ~7 eV, in internal degrees of freedom. But the product kinetic energy distribution curve did not give indications of structure which could be used to ascertain the product quantum state distribution. A more recent examination (43) of the light emitted by products from the reactions of 5 eV C^+ ions with O_2 is displayed in the upper portion of Figure 13, where the photon intensity is plotted as a function of wavelength. The spectrum, although very broad, is characteristic of CO^+ $A^2\Pi$, $\upsilon'j' \rightarrow X^2\Sigma^+$, $\upsilon''j''$ transitions. Band head wavelengths are indicated as vertical lines. The spectrum in the lower portion of this figure is characteristic of $A \rightarrow X$ transitions in reactions where $CO^+(A^2\Pi,\upsilon'j')$ is produced in high kinetic energy Ar^+-CO charge transfer reactions, which serves as both a calibration reaction and a contrast to the high vibrational and rotational level population of $CO^+(A^2\Pi,\upsilon'j')$ when produced via $C^+ + O_2$ reactions. Many elegant experiments have been performed to determine the velocity and angular distributions of various ion-molecule

In State-to-State Chemistry; Brooks, P., et al.;
ACS Symposium Series; American Chemical Society: Washington, DC, 1977.

rearrangement collisions (10-12,32-40). Since these rearrangement channels have been the subject of recent reviews, they will not be discussed further.

Charge Transfer Processes

In many ion-molecule interactions, charge transfer processes (5) strongly compete with all other channels and it is not unusual for electron transfer channels to dominate the reaction. The Li^+-H_2 and H^+-H_2 reactions discussed previously are somewhat unique since the recombination energies (energy of the transition when an electron combines with an isolated ion to form a neutral molecule or atom/s) of the Li^+ and H^+ ions are smaller than the H_2 ionization potential and thus charge transfer channels are not energetically accessible at low reactant ion velocities. The ubiquitous charge transfer processes have found application in the charge transfer nitrogen ion laser which is pumped by the $He_2^+ + N_2\ (X^1\Sigma g^+,\upsilon j) \rightarrow N_2^+\ (B^2\Sigma_u^+,\upsilon' j') + 2He$ reaction. The reactant He_2^+ ion has a continuously variable recombination energy, due to the He-He repulsive final state, in the 18.3 to 20.3 eV range which is sufficient to produce N_2^+ in excited states. Nitrogen $(B^2\Sigma_u^+,\upsilon' j')$ product ions undergo spontaneous radiative decay with the emission of ∿3 eV photons. The spectrum observed (45) when an 11 eV He_2^+ beam interacts with $N_2(X^1\Sigma g^+,\upsilon,j)$ is displayed in Figure 14 where the intensity is plotted as a function of the wavelength of light emitted in the spontaneous $N_2^+\ (B^2\Sigma_u^+,\upsilon' j') \rightarrow N_2^+\ (X^2\Sigma g^+,\upsilon'' j'') + h\nu$ transitions. Charge transfer reactions producing excited ions are also observed in the reactions of He_2^+ ion beams with O_2. The He_2^+ recombination energy is close to the energy of the $O_2^+\ (b^4\Sigma g^-,\upsilon' j)$ state and charge transfer reactions readily take place. Product O_2^+ $(b^4\Sigma g^-,\upsilon' j')$ ions have a sufficiently short lifetime with respect to radiative $O_2^+\ (b^4\Sigma g^-,\upsilon' j') \rightarrow O_2^+\ (a^4\Pi_u,\upsilon'' j'')$ transitions, and the emitted light can be used to probe the product internal state distributions. The spectrum measured (45) for this reaction is given in Figure 15 where the labels refer to various vibrational changes associated with the spontaneous b → a electronic transition of the newly formed reaction product. Vibrational state distributions of the $N_2^+\ (B^2\Sigma_u^+,\upsilon' j')$ and $O_2^+\ (a^4\Pi_u,\upsilon' j')$ species produced in these two reactions are consistent with a vertical Franck-Condon type model in which an electron is transferred over long distances, with very little distortion of the target molecule. The paper of ref. (46) explicitly considers the more commonly encountered phenomena -- that of departures from vertical transitions in non-resonant charge transfer interactions.

Charge transfer processes between symmetric molecular systems can give rise to vibrationally excited products. An example is provided by the hydrogen ion-molecule system where the charge

In State-to-State Chemistry; Brooks, P., et al.;
ACS Symposium Series; American Chemical Society: Washington, DC, 1977.

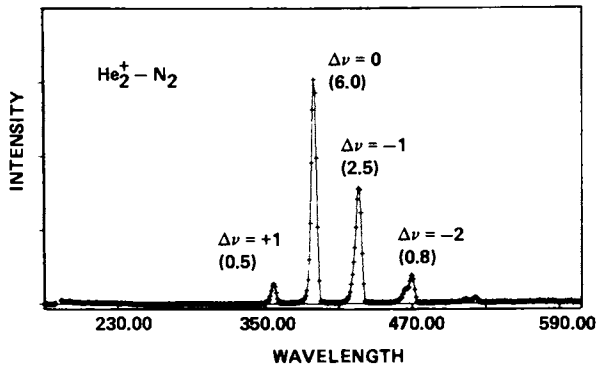

Figure 14. Variation of photon intensity as a function of wavelength for $N_2^+(B^2\Sigma_u^+,v'j')$ → $N_2^+(X^2\Sigma g^+,v''j'')$ transitions measured by Leventhal, Harris and co-workers in Ref. 45. The $N_2^+(B^2\Sigma_u^+,v'j')$ ions are produced in 11 eV He_2^+–N_2 collisions.

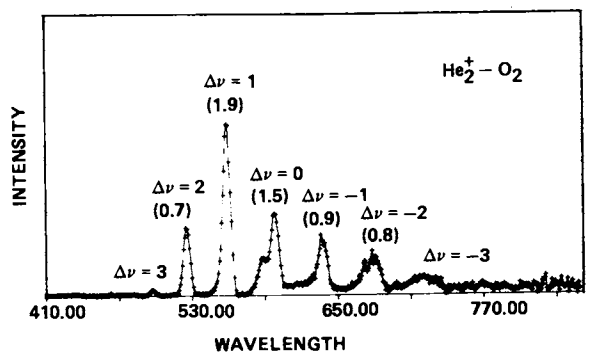

Figure 15. Variation of photon intensity as a function of wavelength for $O_2^+(b^4\Sigma g^-,v'j')$ → $O_2^+(a^4\Pi_u,v''j'')$ transitions measured by Leventhal, Harris, and co-workers in Ref. 45. The $O_2^+(b^4\Sigma g^-,v'j')$ ions are produced in 11 eV He_2^+–O_2 collisions.

In State-to-State Chemistry; Brooks, P., et al.;
ACS Symposium Series; American Chemical Society: Washington, DC, 1977.

transfer channels (9) are energy degenerate with the inelastic scattering channels (10) given below

$$\underline{\text{fast}} \qquad\qquad \underline{\text{slow}}$$

$$H_2^+(X^2\Sigma g^+,\upsilon_0',j) + H_2(X^1\Sigma g^+,\upsilon_0' = o,j) \longrightarrow$$

$$\underline{\text{fast}} \qquad\qquad \underline{\text{slow}}$$

$$H_2(X^1\Sigma g^+,\upsilon''j'') + H_2^+(X^2\Sigma g^+,\upsilon'j') \qquad (9)$$

$$H_2^+(X^2\Sigma g^+,\upsilon'j') + H_2(X^1\Sigma g^+,\upsilon''j'') . \qquad (10)$$

In these reactions a fast ion in vibrational level υ_0' captures an electron to form a fast neutral molecule in level υ'' and the target molecule initially in level υ_0'' is converted to a slow ion in level υ'. At high kinetic energies, the region where most charge transfer reactions have been studied, the ion-molecule collision times are small compared to a rotational period and significant rotational excitation of the products is not observed. However, merging beam studies (29) have indicated that fast neutral H_2 beams from reaction (9) are vibrationally excited when produced in high energy charge transfer processes. A realistic description of these symmetric ion-molecule interactions must take into account the coupling between the internal degrees of freedom during the collision. A multistate impact parameter treatment (47,48) appropriate to these processes has been used in which the wavefunction $\Psi(t)$ for the internal motions, denoted by $\vec{r}$, is expanded in the form

$$\Psi(t) = \sum_{\alpha=D,X} \sum_{n} a_n^\alpha(t)\phi_n^\alpha(\vec{r})\exp(-iE_n^\alpha t) , \qquad (11)$$

where ϕ_n^α are the molecular eigenfunction with electronic, vibrational and rotational parts describing the unperturbed Hamiltonian H_δ for the isolated molecular systems at infinite center-of-mass separation R with eigenenergies E_n^α. The index α denotes whether the labelled quantities refer to either direct channels D or to the X channels where electron transfer takes place. Use of this wavefunction in the time dependent Schrödinger equation results in the set of first order coupled differential equations for the transition amplitudes $C_m^\alpha(t)$,

$$i\partial C_f^\alpha(\rho,t)/\partial t = \sum_m V(\vec{R})P_{fm}C_m^{\bar{\alpha}}(\rho,t)\exp(i\varepsilon_{fm}t) ,$$

$$f = 1,2,\ldots,N \qquad (12)$$

In State-to-State Chemistry; Brooks, P., et al.;
ACS Symposium Series; American Chemical Society: Washington, DC, 1977.

which are solved numerically, subject to the boundary condition that only the direct channel, i, is initially populated, i.e., $C_m^D(\rho,-\infty) = \delta_{mi}$, $C_m^X(\rho,-\infty) = 0$. Matrix elements P_{fm} are equal to $F(\upsilon_f',\upsilon_m'')F(\upsilon_m',\upsilon_f'')$, where $F(\upsilon_i',\upsilon_n'')$ is the vibrational overlap for the $H_2^+(X^2\Sigma_g^+,\upsilon_i') \rightarrow H_2(X^1\Sigma_g^+,\upsilon_n'')$ transition). When α denotes X in (12) $\bar{\alpha}$ refers to D and vice versa. The difference ε_{if} in the internal energies between initial and final states of the system is $E_i^{\alpha} - E_f^{\bar{\alpha}}$. The scattering amplitude is computed in C.M. frame using the relation

$$f_{if}^{\alpha}(\theta,\phi) = \{-ik_i/2\pi\} \int \exp(i\{\vec{K}\cdot\vec{R} + m_{if}\Phi\}) \times \exp\{i\varepsilon_{if}Z/\hbar\upsilon_i\}(\partial C_f(\rho,Z)/\partial Z)d\vec{R} \quad , \qquad (13)$$

where the incident velocity is $\upsilon_i = \hbar k_i/\mu$, the momentum change K during the collision is $\vec{k}_i - \vec{k}_f$ with the final momentum vector $\vec{k}_f$ directed along (θ,ϕ), and m_{if} is the change in azimuthal quantum number, taken to be zero in the reactions investigated here. The ion-molecule separation vector R has spherical components (ρ,Φ,Z), where ρ is the impact parameter. From the amplitudes, (13), the differential cross section is given by

$$\sigma_{if}^{\alpha}(\theta) = 2\pi \frac{k_f}{k_i} |f_{if}^{\alpha}(\theta,\phi)|^2 \qquad (14)$$

when integrated over angle yields

$$Q_{if}^{\alpha}(\upsilon_i) = \int_{-1}^{1} \sigma_{if}^{\alpha}(\theta)d(\cos\theta) = 2\pi \int_0^{\infty} |C_f(\rho,\infty) - \delta_{if}|^2 \rho d\rho \quad , \qquad (15)$$

for the integral cross section. The relative probabilities for the various inelastic channels involving 49 eV ions in reaction (10) are displayed in Figure 16 as a function of distance. The numbers labeling the differently shaded areas in this figure refer to inelastic channels having product neutral and ion vibrational levels υ'' and υ' respectively. The coupling between these inelastic channels is indicated in Figure 16 but we note that these channels are also strongly coupled to the energy degenerate charge transfer channels which are not displayed here. Integral cross sections ($Å^2$) for some of the larger inelastic cross sections (49) are given in Figure 17 as a function of reactant ion kinetic energy. Each of the curves are labelled by the vibrational quantum numbers of the product neutral and ion in a particular channel. Product channels having small energy defects are dominant at low reactant ion kinetic energy but other pathways having good overlap become more important as the kinetic energy is increased. The solid curve at the top of Figure 17 represents the

In State-to-State Chemistry; Brooks, P., et al.;
ACS Symposium Series; American Chemical Society: Washington, DC, 1977.

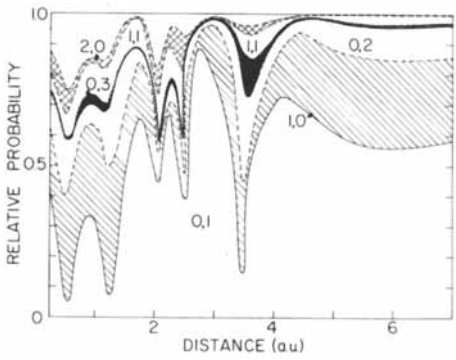

Figure 16. Relative probabilities for formation of different vibrational channels in 49 eV $H_2^+(X^2\Sigma g^+, v_0 = 0) + H_2(X^1\Sigma g^+, v_0'' = 0)$ interactions as a function of distance. The numbers labeling each of the areas refer to the vibrational quantum states of the neutral product and ion respectively.

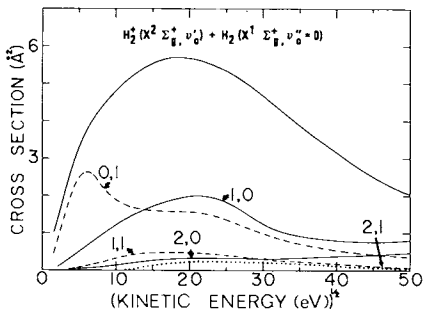

Figure 17. Integral multistate cross sections (Å²) for vibrational excitation in $H_2^+(X^2\Sigma g^+, v_0' = 0) + H_2(X^1\Sigma g^+, v_0'' = 0)$ collisions as functions of reactant ion kinetic energy. Numbers labeling each curve refer to vibrational states of product neutral and ions.

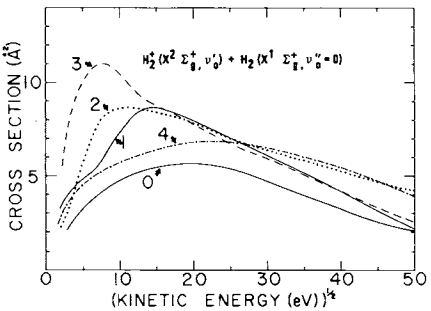

Figure 18. Total cross sections (Å²) for vibrational excitation in $H_2^+(X^2\Sigma g^+, v_0' = 0,1,2,3,4) + H_2(X^1\Sigma g^+, v_0'' = 0)$ collisions given as a function of reactant ion kinetic energy (Ref. 49). The numbers attached to each curve refer to the vibrational state of the reactant ion.

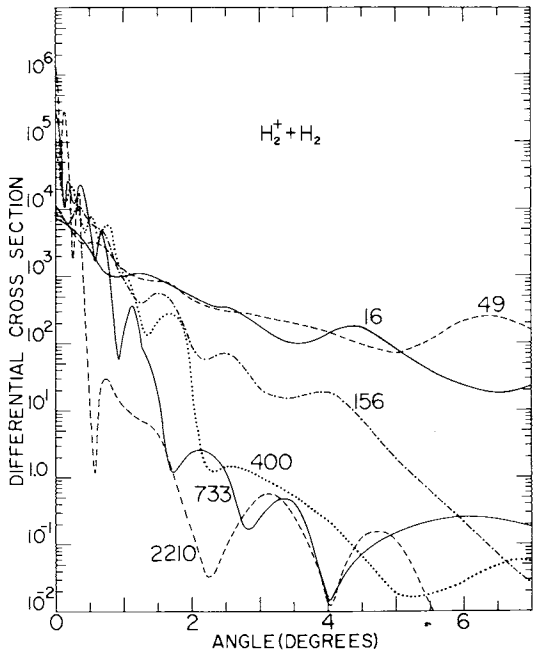

Figure 19. Differential charge transfer cross sections ($Å^2$/sr) for neutral product formation in $H_2^+(X^2\Sigma g^+, v_0' = 0) + H_2(X^1\Sigma g^+, v_0'' = 0)$ collisions given as a function of center of mass scattering angle. The differential cross sections are summed over the totality of product vibrational states. Reactant ion kinetic energies are given by the numbers near each curve.

total inelastic cross section for vibrational excitation in reactions involving ground state reactants. The influence of the reactant ion vibrational state on the inelastic processes is examined in Figure 18 where cross sections for total vibrational excitation are given for the reactions of $H_2^+(X^2\Sigma g^+, v_0' = 0,1,2,3,4)$ with $H_2(X^1\Sigma g^+, v_0'' = 0)$. Increasing v_0' tends to increase the number of product channels in near energy balance with the reactants leading to large cross sections at low reactant velocities. The angular distributions of the forward scattered fast $H_2(X^1\Sigma g^+, v'')$ product neutrals from reaction (9) are illustrated in Figure 19. Differential cross sections are presented (50) as a function of center of mass scattering angle for $H_2^+(X^2\Sigma g^+, v_1' = 0)$ ions having 16, 49, 156, 400, 733 and 2210 eV kinetic energies. At high energies the fast neutral products are forward collimated with the cross sections dropping by 10^5 as the angle is increased to several degrees. Integral charge transfer cross sections for

In State-to-State Chemistry; Brooks, P., et al.;
ACS Symposium Series; American Chemical Society: Washington, DC, 1977.

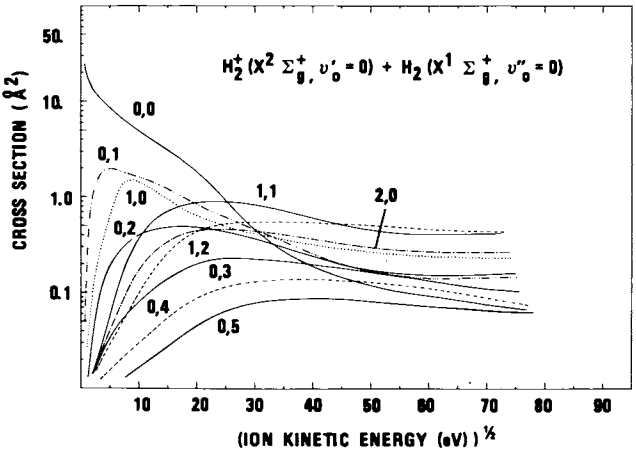

Figure 20. Integral multistate charge transfer cross sections ($Å^2$) for the formation of specific product channels as a function of ion kinetic energy. The vibrational states of the product neutral and ion are given by the numbers close to each curve.

the formation of the dominant channels are given in Figure 20. The numbers in this figure indicate the vibrational states of the product neutral and ion respectively. At low velocities the energy resonant 0,0 → 0,0 channel is the largest, but as the energy is increased this 0,0 channel is overwhelmed by those having close energy balance with the reactants and possessing favorable vibrational overlaps. A similar presentation of the integral charge transfer reactions of $D_2^+(X^2\Sigma g^+, \upsilon_0' = 0)$ ions with $D_2(X^2\Sigma g^+, \upsilon_0'' = 0)$ is given in Figure 21 for the 10 product channels with the smallest energy defects, ε_{fm}. At the low velocities, the channels with small ε_{fm} are the largest but as the reactant velocity is increased the relative magnitudes of the different channels becomes a complicated function of energy defects and vibrational overlaps.

Total charge transfer cross sections in the hydrogen system have been a puzzle for some time in that cross sections do not continually decrease with velocity as expected from an earlier resonant two-state model. As functions of velocity, the total charge transfer cross sections decrease with increasing kinetic energy but then slowly rise with kinetic energy above several hundred eV. This is shown in Figure 22 where the darkened area represents the data of ref. (51), the circles give data of ref. (52) and the solid line represents the measurements of ref. (53) for reactions involving incident H_2^+ ions produced via low energy

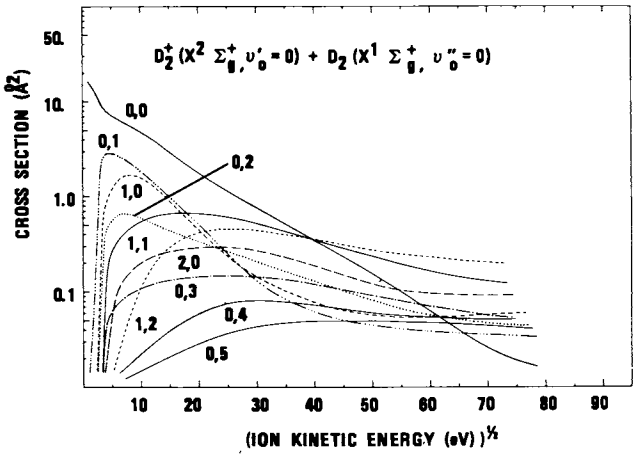

Figure 21. Integral multistate charge transfer cross sections (Å²) for the formation of specific product channels as a function of ion kinetic energy for $D_2^+(X^2\Sigma g^+, v_0' = 0) + D_2(X^1\Sigma g^+, v_0'' = 0)$ collisions. The vibrational states of the product neutral and ion are given by the numbers close to each curve.

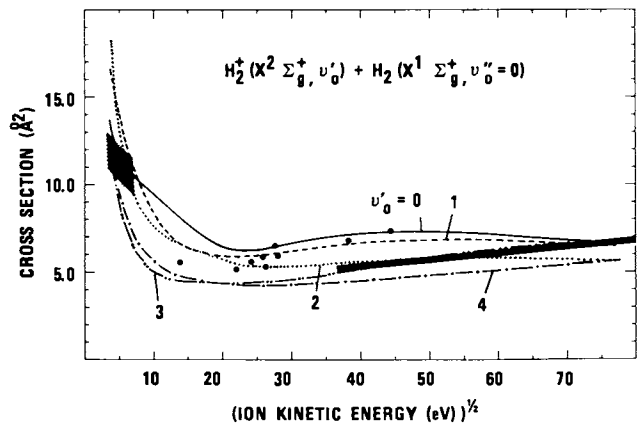

Figure 22. Total charge transfer cross sections (Å²) for $H_2^+(X^2\Sigma g^+, v_0' = 0,1,2,3,4) + H_2(X^1\Sigma g^+, v_0'' = 0)$ reactions over all product channels as a function of reactant ion kinetic energy. The shaded area represents the experimental data of Ref. 51, the circles the data of Ref. 52, and the wide solid line gives the results of Ref. 53.

In State-to-State Chemistry; Brooks, P., et al.;
ACS Symposium Series; American Chemical Society: Washington, DC, 1977.

electron impact ionization. The behavior of the total charge transfer cross sections can be understood by examination of the integral cross sections shown in Figure 20 where a number of channels with reasonably large cross sections are opened up, thereby resulting in large total cross sections as the kinetic energy is increased. Total charge transfer cross sections ($Å^2$) for neutralization of $H_2^+(X^2\Sigma g^+, \upsilon_0' = 0,1,2,3,4)$ ion beams by $H_2(X^1\Sigma g^+, \upsilon_0'' = 0)$ molecules, computed in the multistate model, are shown in Figure 22 where the numbers refer to cross sections computed for reactant ions in a particular vibrational level. Data in Figure 22 was obtained using beams of $H_2^+(X^2\Sigma g^+)$ state ions produced by electrons having energies close to the H_2 ionization potential. Reactant $H_2^+(X^2\Sigma g^+)$ beams formed in this way will occupy the lower 0-4 levels. Thus, a comparison between theory and experiment is one between the curves labelled $\upsilon = 0,1,2,3,4$ and the measurements spanning the range of kinetic energies given in Figure 22. The corresponding charge transfer reactions in the deuterium system are displayed in Figure 23 where the total cross sections drop rapidly as the ion kinetic energy is raised to several hundred eV but then show a slight increase with increasing translational energy. The experimental data (51-54) in Figures 22 and 23 are in harmony with the multistate approach which predicts a high degree of vibrational excitation for charge transfer reactions occurring in the hydrogen system at high energies.

Charge transfer reactions of heavier A_2^+-A_2 molecular systems have been examined (55) and certain similarities to the hydrogen are observed. The angular distributions of both the A_2 and H_2 systems are alike in that the fast neutral products of reaction are forward scattered with the forward scattering becoming more pronounced as the ion kinetic energy is increased, although the details of the differential cross sections with angle vary from system to system. The multistate angular distributions (50) of the fast neutral molecular products from $CO^+(X^2\Sigma^+, \upsilon_0' = 0)$ + $CO(X^1\Sigma^+, \upsilon_0'' = 0)$ charge transfer reactions (a typical systems) are presented in Figure 24. Numbers labeling each curve indicate the incident ion kinetic energy. At high energies the CO cross sections drop by 6 orders of magnitude as the scattering angle is increased by several degrees, a behavior that is paralleled in symmetric N_2, O_2 and NO reactions (50). Total charge transfer cross sections computed for $CO^+(X^2\Sigma^+, \upsilon_0 = 0)$ + $CO(X^1\Sigma^+, \upsilon_0'' = 0)$ interactions are given in Figure 25 as a function of reactant ion kinetic energy along with the experimental values determined by collecting all the slow ions (56) formed in the charge transfer process. A further comparison, between computed and experimental values, down to lower energies is shown in Figure 26. In this figure the computed values are given by the circles and the squares represent the experimental data obtained using ion cyclotron resonance techniques (57). The charge transfer cross sections in the CO system are observed to be larger than the corres-

In State-to-State Chemistry; Brooks, P., et al.;
ACS Symposium Series; American Chemical Society: Washington, DC, 1977.

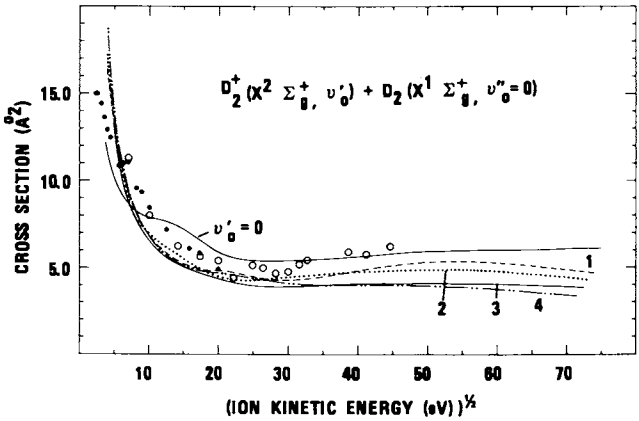

Figure 23. Total charge transfer cross sections (Å²) for $D_2^+(X^2\Sigma g^+, v_0' = 0,1,2,3,4) + D_2(X^1\Sigma g^+, v_0'' = 0)$ reactions over all product channels as a function of reactant ion kinetic energy. The numbers labeling the curves denote total cross sections for specific reactant ion vibrational states. The experimental data of Refs. 54 and 52 are given by the respective closed and open circles.

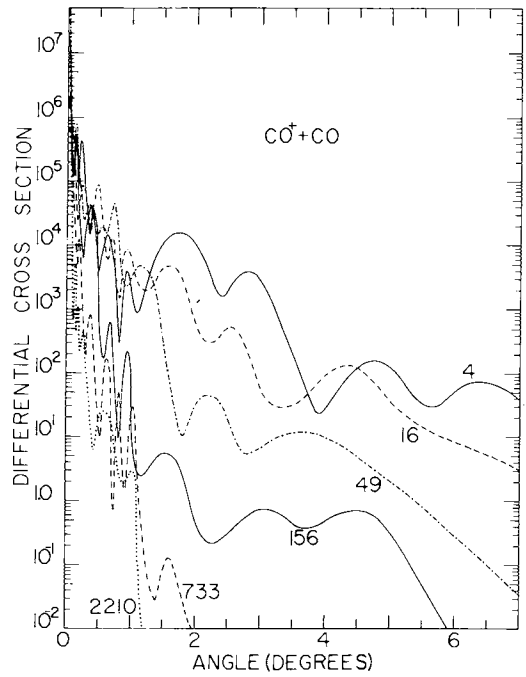

Figure 24. Differential charge transfer cross section (Å²/sr) for neutral product formation in $CO^+(X^2\Sigma^+, v_0' = 0) + CO(X^1\Sigma^+, v_0'' = 0)$ collisions given as a function of center of mass scattering angle. The differential cross sections have been summed over all product vibrational states. Reactant ion kinetic energies are given by the numbers labeling each curve.

In State-to-State Chemistry; Brooks, P., et al.;
ACS Symposium Series; American Chemical Society: Washington, DC, 1977.

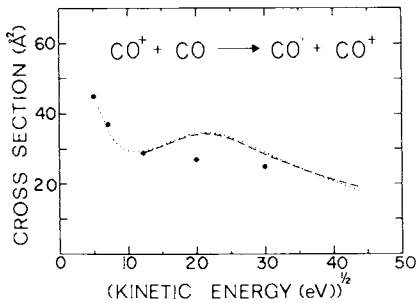

Figure 25. Total charge transfer cross sections (Å²) for CO⁺–CO interactions are given as a function of reactant ion kinetic energy. The circles are the data of Ref. 56.

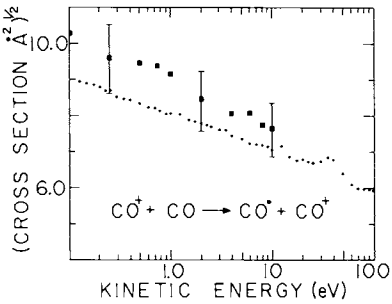

Figure 26. Total charge transfer cross sections (Å²) for CO⁺–CO interactions are given as a function of reactant ion kinetic energy. The squares are the data of Ref. 57.

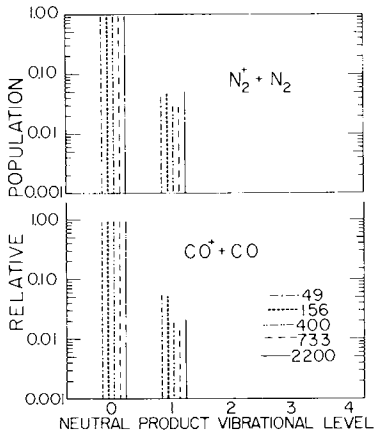

Figure 27. Neutral $N_2(X^1\Sigma g^+,v'')$ and $CO(X^1\Sigma^+,v'')$ product vibrational distributions from $N_2^+(X^2\Sigma g^+,v_0' = 0) + N_2(X^1\Sigma g^+,v_0'' = 0)$ and $CO^+(X^2\Sigma^+,v_0' = 0) + CO(X^1\Sigma^+,v_0' = 0)$ interactions are given for different reactant ion kinetic energies.

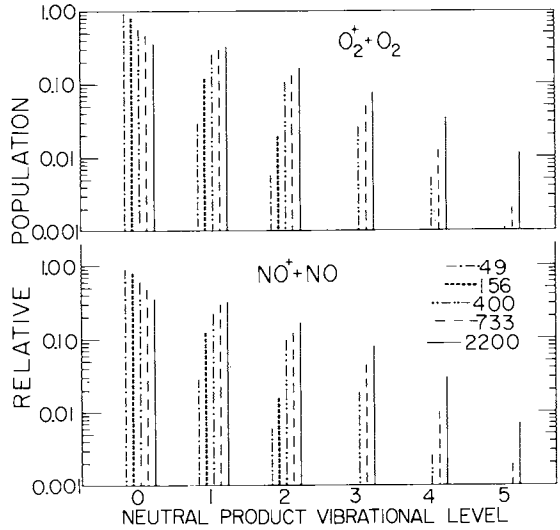

Figure 28. Neutral $O_2(X^3\Sigma g^-,v'')$ and $NO(X^2\Pi,v'')$ product vibrational distributions from $O_2^+(X^2\Pi g,v_0' = 0) + O_2(X^3\Sigma g^-,v_0'' = 0)$ and $NO^+(X^1\Sigma^+v_0' = 0) + NO(X^2\Pi,v_0'' = 0)$ interactions are given for different reactant ion kinetic energies.

ponding reactions in hydrogen due to a favorable combination of interaction matrix elements, vibrational overlaps and energy defects. The resonant channel, forming fast $CO(X^1\Sigma^+,\upsilon' = 0)$ and slow $CO^+(X^2\Sigma^+,\upsilon'' = 0)$ has the largest vibrational overlap and zero energy defect, while other near energy resonant channels leading to vibrationally excited species have poor overlap and are not strongly favored as products. The fast neutral product vibrational state distribution for the CO^+-CO and similar N_2^+-N_2 charge transfer reactions are given in Figure 27 where relative populations of particular neutral product states are presented as functions of product vibrational levels for different ion kinetic energies. Symmetric charge transfer processes in the N_2 and CO systems result in closely parallel neutral product state distributions. This is not surprising since the neutral product υ''=0 and 1 channels are dominant in the N_2 and CO reactions since these channels have the largest vibrational overlaps and the smallest energy defects.

An alternate situation occurs in the $O_2^+(X^2\Pi g,\upsilon_0' = 0)$ - $O_2(X^3\Sigma g^-,\upsilon_0'' = 0)$ and $NO^+(X^1\Sigma^+,\upsilon_0' = 0)$ - $NO(X^2\Pi,\upsilon_0'' = 0)$ systems where the energy resonant and near-resonant product channels with $\upsilon'' = 0$ and 1 have relatively small vibrational overlaps (58). The vibrational distribution of neutral products from these charge transfer reactions is presented in Figure 28 for different ion kinetic energies. At low velocities, the product channels forming ground vibrational state neutrals are favored by energy considerations. As the velocity of the incident ions is increased, the $O_2(X^3\Sigma g^-,\upsilon'')$ and $NO(X^2\Pi,\upsilon'')$ product distributions broaden since those product channels with $\upsilon'' > 0$ and large vibrational overlaps become energetically accessible.

In State-to-State Chemistry; Brooks, P., et al.;
ACS Symposium Series; American Chemical Society: Washington, DC, 1977.

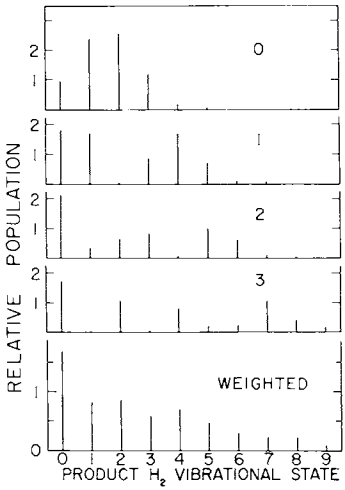

Figure 29. Neutral $H_2(X^1\Sigma g^+,v'')$ product vibrational distributions from $H_2^+(X^2\Sigma g^+,v_0' = 0,1,2,3) + H_2(X^1\Sigma g^+,v_0'' = 0)$ interactions.

The influence of reaction ion vibrational state on the neutral product vibrational distribution is shown in Figure 29 for 2.2 keV $H_2^+(X^2\Sigma g^+,\upsilon_0' = 0,1,2,3) + H_2(X^1\Sigma g^+,\upsilon_0'' = 0)$ charge transfer reactions. As the incident ion vibrational state goes from 0 to 3 there is significant broadening and structure in the product state distributions. The distribution in the lower portion of this figure has been constructed from cross sections involving incident ions in given vibrational states weighted according to the state population characteristic of reactant ion beams produced in high energy electron impact ionization. As indicated in Figures 28 and 29, a significant fraction of neutral products from symmetric charge transfer reactions are vibrationally excited.

Literature Cited

(1) Schöttler, J. and Toennies, J.P., Z. Phys. (1968) 214, 472.
(2) Dittner, P. and Datz, S., J. Chem. Phys. (1968) 49, 1969.
(3) Moran, T.F. and Cosby, P.C., J. Chem. Phys. (1969) 51, 5724.
(4) Moore, J.H., Jr. and Doering, J.P., Phys. Rev. Lett. (1969) 23, 564.
(5) Cosby, P.C. and Moran, T.F., J. Chem. Phys. (1970) 52, 6157.
(6) Cheng, M.H., Chiang, M.H., Gislason, E.A., Mahan, B.H., Tsao, C.W. and Werner, A.S., J. Chem. Phys. (1970) 52, 6150.
(7) Udseth, H., Giese, C.F. and Gentry, W.R., J. Chem. Phys. (1971) 54, 3642.
(8) David, R., Faubel, M. and Toennies, J.P., Chem. Phys. Lett. (1973) 18, 87.
(9) van den Bergh, H.E., Faubel, M. and Toennies, J.P., Faraday Disc. of the Chem. Soc. (1973) 55, 203.
(10) Toennies, J.P., Chem. Soc. Rev. (1973) 3, 407.
(11) Toennies, J.P., Ann. Rev. Phys. Chem. (1976) 27, 225.

(12) Koski, W., Adv. Chem. Phys. (1975) 30, 185.
(13) Lester, W.A., J. Chem. Phys. (1970) 53, 1551.
(14) Lester, W.A., J. Chem. Phys. (1971) 54, 3171.
(15) Kutzelnigg, W., Staemmler, V. and Hoheisel, K., Chem. Phys. (1973) 1, 27.
(16) Schaefer, J. and Lester, W.A., J. Chem. Phys. (1975) 62, 1913.
(17) McGuire, P., J. Chem. Phys. (1976) 65, 3275.
(18) Kouri, D.J., Shimoni, Y. and Heil, T.G., J. Chem. Phys. (1976) 65, 706.
(19) Dickinson, A.S., Kouri, D.J., Wells, C.A. and Lester, W.A., J. Chem. Phys. (1976) 65, 1501.
(20) McCann, K.J. and Flannery, M.R., J. Chem. Phys. (1975) 63, 4695.
(21) Flannery, M.R. and McCann, K.J., to be published.
(22) Barg, G.D., Kendall, G.M. and Toennies, J.P., Chem. Phys. (1976) 16, 243.
(23) Rudolph, K. and Toennies, J.P., J. Chem. Phys. (1976) 65, 4483.
(24) Giese, C.F. and Gentry, W.R., Phys. Rev. A (1974) 10, 2156.
(25) Csizmadia, I.G., Kari, R.E., Polanyi, J.C., Roach, A.C. and Robb, M.A., J. Chem. Phys. (1970) 52, 6205.
(26) Bauschlicher, C.W., O'Neil, S.V., Preston, R.K., Schaefer, H.F. and Bender, C.F., J. Chem. Phys. (1973) 59, 1286.
(27) Carney, G.D. and Porter, R.N., J. Chem. Phys. (1974) 60, 4251.
(28) Preston, R.K. and Tully, J.C., J. Chem. Phys. (1971) 54, 4297.
(29) Lees, A.B. and Rol, P.K., J. Chem. Phys. (1975) 63, 2461.
(30) McGuire, P., Rudolph, K. and Toennies, J.P., J. Chem. Phys. (1976) 65, 5522.
(31) Böttner, R., Ross, U. and Toennies, J.P., J. Chem. Phys. (1976) 65, 733.
(32) Franklin, J.L., ed., "Ion-Molecule Reactions", Plenum Press, New York, 1972.
(33) Mahan, B.H. and Schubart, P.J., J. Chem. Phys. (1977) 66, 3155.
(34) McClure, D.J., Douglass, C.H. and Gentry, W.R., J. Chem. Phys. (1977) 66, 2079.
(35) Schneider, F., Havemann, U., Zülicke, L., Pacák, V., Birkinshaw, K. and Herman, Z., Chem. Phys. Lett. (1976) 37, 323.
(36) Hopper, D.G., Wahl, A.C., Wu, R.L.C. and Tiernan, T.O., J. Chem. Phys. (1976) 65, 5474.
(37) Wyatt, J.R., Stattan, L.W., Snyder, S.C. and Hierl, P.M., J. Chem. Phys. (1976) 64, 3757.
(38) Blakley, C.R., Vestal, M.L. and Futrell, J.H., J. Chem. Phys. (1977) 66, 2392.
(39) Harris, H.H. and Leventhal, J.J., J. Chem. Phys. (1976) 64, 3185.

In State-to-State Chemistry; Brooks, P., et al.;
ACS Symposium Series; American Chemical Society: Washington, DC, 1977.

(40) Jones, C.A., Wendell, K.L., Kaufman, J.J. and Koski, W.S., J. Chem. Phys. (1976) 65, 2345.
(41) Lao, R.C.C., Rozett, R.W. and Koski, W.S., J. Chem. Phys. (1968) 49, 4204.
(42) Leventhal, J.J., J. Chem. Phys. (1971) 55, 4654.
(43) Ottinger, Ch. and Simonis, J., Phys. Rev. Lett. (1975) 35, 924.

(45) Bearman, G.H., Earl, J.D., Pieper, R.J., Harris, H.H. and Leventhal, J.J., Phys. Rev. A (1976) 13, 1734.
(46) Kelley, J.D., Bearman, G.H., Ranjbar, F., Harris, H.H., Leventhal, J.J., this volume.
(47) Moran, T.F., Flannery, M.R. and Albritton, D.L., J. Chem. Phys. (1975) 62, 2869.
(48) Moran, T.F., McCann, K.J., Flannery, M.R. and Albritton, D.L., J. Chem. Phys. (1976) 65, 3172.
(49) Flannery, M.R., McCann, K.J. and Moran, T.F., J. Chem. Phys. (1975) 63, 1462.
(50) McCann, K.J., Flannery, M.R., Hornstein, J.V. and Moran, T.F., J. Chem. Phys. (1975) 63, 4998.
(51) Moran, T.F. and Roberts, J.R., J. Chem. Phys. (1968) 49, 3411.
(52) Rothwell, H.R., Van Zyl, B. and Amme, R.C., J. Chem. Phys. (1974) 61, 3851.
(53) Latimer, C.J., Browning, R. and Gilbody, H.B., J. Phys. B (1969) 2, 1055.
(54) Cramer, W.H. and Marcus, A.B., J. Chem. Phys. (1960) 32, 186.
(55) Flannery, M.R., Cosby, P.C. and Moran, T.F., J. Chem. Phys. (1973) 59, 5494.
(56) Gustafsson, E. and Lindholm, E., Arkiv. Fys. (1960) 18, 219.
(57) Smith, D.L. and Futrell, J.H. (1973) 59, 463.
(58) Moran, T.F., McCann, K.J. and Flannery, M.R., J. Chem. Phys. (1975) 63, 3857.

In State-to-State Chemistry; Brooks, P., et al.;
ACS Symposium Series; American Chemical Society: Washington, DC, 1977.

3

Laser Techniques for Determining State-to-State Reaction Rates*

RICHARD N. ZARE†

Department of Chemistry, Columbia University, New York, NY 10027

This has been the most exciting symposium of the American Chemical Society that I have ever attended. I want to thank the Chairman very much for organizing this program and for giving me the opportunity to tell you how advances in molecular beam diagnostics using lasers are permitting us to learn about the internal state distributions of unrelaxed reaction products. I would like to start with a quote from Norman Ramsey's book, "Molecular Beams." He wrote that "the fundamental problem of molecular beams is the quantitative detection of the molecules in the beams." This little problem explains why molecular beams were for so long the exclusive playtoy of physicists; early on chemists would have gladly used beam techniques to investigate reaction dynamics, but with the inability to distinguish the scattered products from the elastically and inelastically scattered main beam and from the residual background gas there could be no chemistry studied.

This difficulty becomes all the more apparent as we examine the traditional detectors used in molecular beam research (Fig. 1). One of the first such detectors is based on the method of what I call "wait and weigh." Here one waits a sufficient period of time for deposition; then, one weighs the target to determine its mass gain. With patience and a good analytical balance this procedure certainly works - - but it does not distinguish one species from another. Other detectors rely upon pressure of the beam or chemical attack of the target by the beam. These detectors are often highly sensitive but seldom quantitative. Another class of detectors involves recombination. This works magnificently, particularly in the hands of Scoles and co-

*Edited talk presented at the New Orleans ACS Meeting, March 1977. Support by the National Science Foundation is gratefully acknowledged.

†Present address: Department of Chemistry, Stanford University, Stanford, CA 94305

In State-to-State Chemistry; Brooks, P., et al.;
ACS Symposium Series; American Chemical Society: Washington, DC, 1977.

Table 1. Traditional molecular beam detectors of neutral species.

Physical or chemical process	Detector
Condensation of beam on target	Analytical balance
Pressure of beam on target	Pirani gauge
Chemical attack of target by beam	Densitometer
Recombination of condensed beam on target	Bolometer
Radioactivity of condensed beam on target	Scintillation counter
Ejection of electrons from target by beam of metastables	Auger detector
Surface ionization of beam on target	Hot-wire detector
Electron bombardment ionization of beam	Mass spectrometer

Figure 1

workers, but has limited applicability. Counting radioactive disintegrations is also highly specific and very sensitive but again rather specialized. Now we come to ionization detectors. Because one can so skillfully handle ions, this type of detection has many advantages.

There are two ion detection methods on which I want to concentrate attention - - because these methods opened the use of molecular beam techniques to chemically interesting investigations. Figure 2 shows a schematic of a surface ionization detector. Here a beam impinges on a hot wire. If the work function of the wire surface exceeds the ionization potential of the atom or molecule bombarding it, ions are formed. In the hands of Datz, Taylor, and Trischka it is possible to treat the wire so that one type of wire ionizes only alkali atoms, another only alkali atoms and alkali-containing compounds, such as alkali halide salts. By subtracting the ion signal of the former from that of the latter one can detect alkali halide products from the reaction of alkali atoms with halogen-containing molecules. Using beams so that the products are detected without intervening collisions, the hot wire detector has allowed one to carry out all kinds of reactive alkali chemistry studies.

Note that surface ionization is a very special detector. Background molecules - - whatever remains in the evacuated beam chamber - - cannot be ionized because of their characteristic high ionization potentials. The detector is thus highly specific. Moreover, it is highly efficient; nearly 100% of the

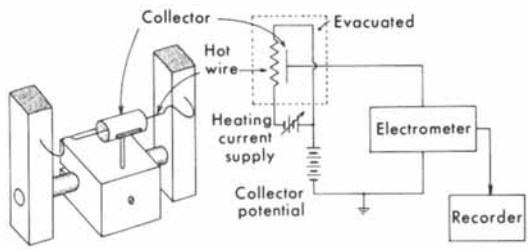

Figure 2

In State-to-State Chemistry; Brooks, P., et al.;
ACS Symposium Series; American Chemical Society: Washington, DC, 1977.

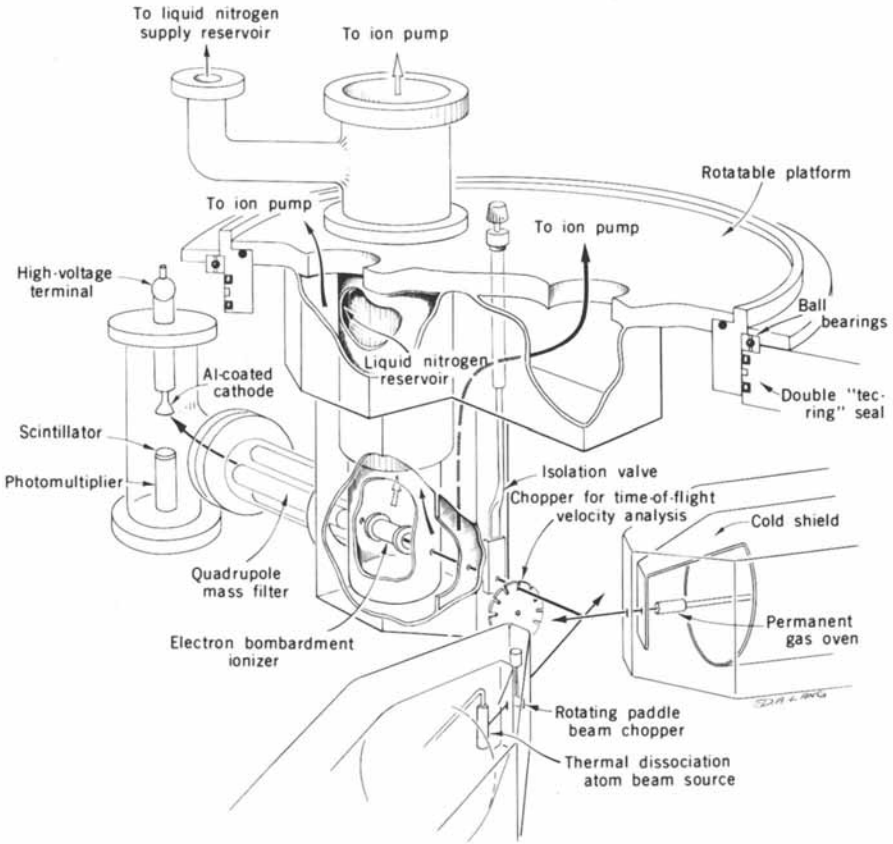

Figure 3

detectable particles striking the hot wire are ionized. It also provides a direct measure of the product flux rather than the particle number density. This latter fact is important when it is realized that kinetic rates are related directly to flux, not density.

A simple calculation suffices to show the sensitivity of surface ionization detection. Each charge carries about 10^{-19} coulombs; thus for a flux of only 10^{4} ionizable particles/sec, we get something like 10^{-15} coulombs/sec, i.e. 10^{-15} amperes, and this current, although small, can be readily measured or even counted.

The next major breakthrough in molecular beam detector technology is the replacement of the surface ionization detector by the universal ionizer. Figure 3 shows a cutaway view of the beautiful machine that Doug McDonald, Pierre LeBreton, and Yuan Lee assembled in Dudley Herschbach's laboratory. We have two

In State-to-State Chemistry; Brooks, P., et al.;
ACS Symposium Series; American Chemical Society: Washington, DC, 1977.

crossed beams; the product molecules fly from the reaction zone (beam intersection region) and some enter the detector; here a few tenths of a percent are ionized by electron bombardment; the ions are then sorted by mass in a quadrupole mass filter and counted. Because this detector will ionize anything that passes through it, this scheme has the virtue of being nearly universally applicable. However, this also requires that the background pressure in the main chamber must be reduced to about 10^{-11} torr to avoid interference from nearby mass peaks and to avoid disturbing the ion trajectories. Mass spectrometric detection does not have the high efficiency of the hot wire ionizer and it is not a flux detector but nominally a density detector. Nevertheless, its use opens up to investigation a vast variety of reaction systems that would remain otherwise unexplored.

Both the surface ionization detector and the quadrupole mass spectrometer are very well suited for measuring products, but if we inquire into the state of the products, we encounter an important limitation and/or complication. These ionization detectors are rather insensitive to the energy content (internal state) of the product, - - but there is some dependence - - and this dependence is generally unknown. If we place emphasis on the direct measurement of the internal energy distribution of the reaction products, then we are led to seek a way of combining molecular spectroscopy with molecular beams.

One such attempt, namely that of laser-induced fluorescence (LIF), is shown in Fig. 4. Here resonance fluorescence is

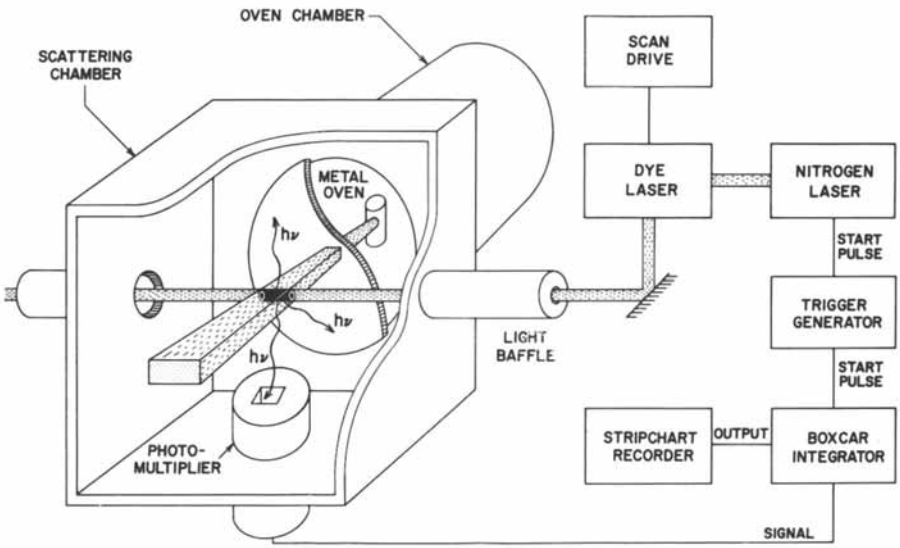

Figure 4

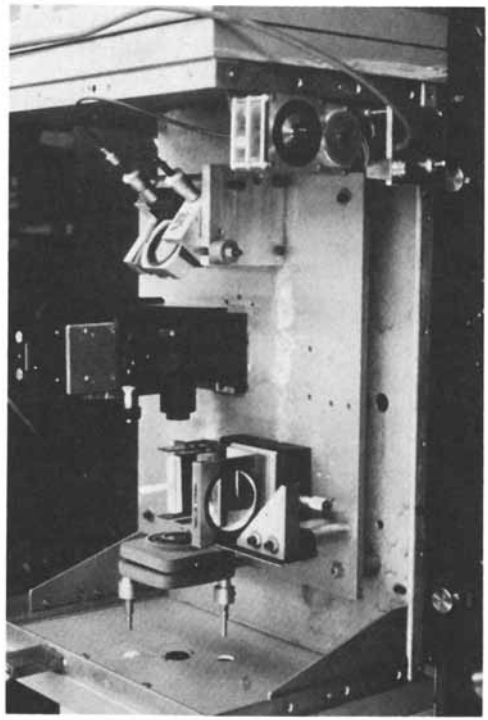

Figure 5

employed to detect the reaction products. A tunable dye laser is swept in wavelength. Whenever its output coincides with a molecular absorption line, some fraction of the molecules in the lower (v", J") level are pumped to the upper (v', J') level from which the molecules subsequently re-emit radiation. This fluorescence is detected by a photomultiplier which "views" the excitation zone. The fluorescence intensity is recorded as a function of laser wavelength to produce what we call "an excitation spectrum." The intensities are then converted to relative populations of the various product internal states, based on a knowledge of various vibrational and rotational intensity factors. Note that the fluorescence, itself, is not spectrally resolved, which would require some loss of signal. Instead, it is the narrow bandwidth of the scanning laser which provides the spectral resolution.

In Fig. 4 we show a "beam-gas arrangement" in which some beam of metal atoms is sent into a chamber filled with tenuous gas. The gas pressure is typically 10^{-4} to 10^{-5} torr so that the mean free path exceeds the dimensions of the vacuum chamber. Under these experimental conditions, we can be confident that the

In State-to-State Chemistry; Brooks, P., et al.;
ACS Symposium Series; American Chemical Society: Washington, DC, 1977.

observed products are not relaxed or disturbed by subsequent collisions. Here it is important to stress that the laser beam does not "drive" the reaction - - it is merely a probe of the state of the reaction products.

The dye laser is pumped by a nitrogen laser. This is a pulsed deivce; that is the nature of nitrogen lasers. Because of that, we use gated detection electronics. If you like, in Fig. 4 the photomultiplier is the "eye" and the boxcar integrator the "brain." The eye stares at the light; the brain tells the eye when to open, how long to look, and then when to close. We need the photomultiplier to blink shut because most of the time this experiment is off, i.e. has a very low duty cycle, and we would be looking at dark current from the photomultiplier if we did not turn it off.

Figure 5 shows the dye laser setup. The output from a pulsed AVCO nitrogen laser is directed by means of a mirror through a cylindrical lens which focusses the beam into a cuvette holding the organic dye solution. The laser cavity is formed by the output mirror on one side and the grating on the other. A beam expander is placed intra-cavity; this helps to fill the grating, giving us the necessary resolution. A simple analog motor rotates the grating causing the laser output to sweep in wavelength.

Figure 6 shows the dye laser in conjunction with the beam apparatus. Long black arms on the beam chamber provide the light baffling necessary to reduce scattered light. Under typically good conditions only 10 photoelectrons result from the pulse of 10^{14} photons directed through the apparatus. Angular distribution studies, which I will speak about later, are carried out by mounting two ovens on the rotating lid shown in this figure. To

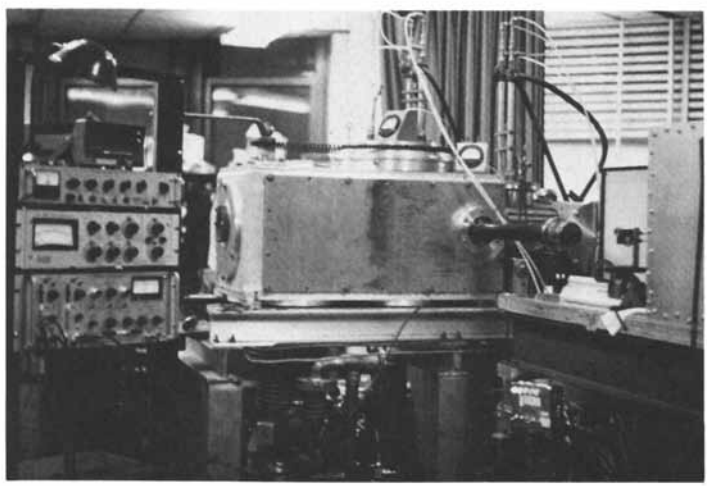

Figure 6

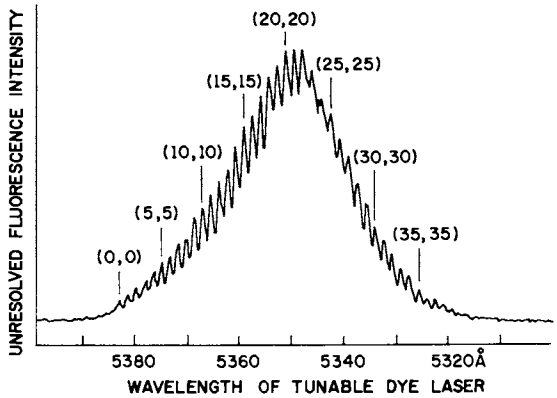

Figure 7. BaI excitation spectrum for the reaction $Ba + CH_3I \rightarrow BaI + CH_3$

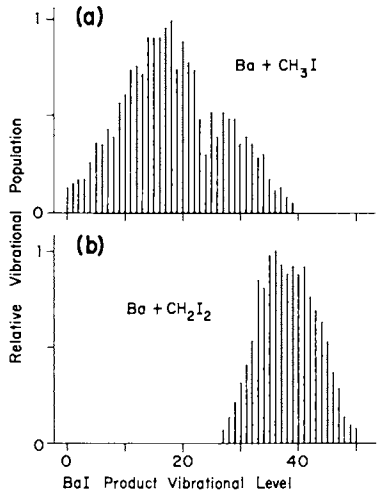

Figure 8. BaI product vibrational level vs. relative vibrational population for (a) $Ba + CH_3I$ *and (b)* $Ba + CH_2I_2$

In State-to-State Chemistry; Brooks, P., et al.;
ACS Symposium Series; American Chemical Society: Washington, DC, 1977.

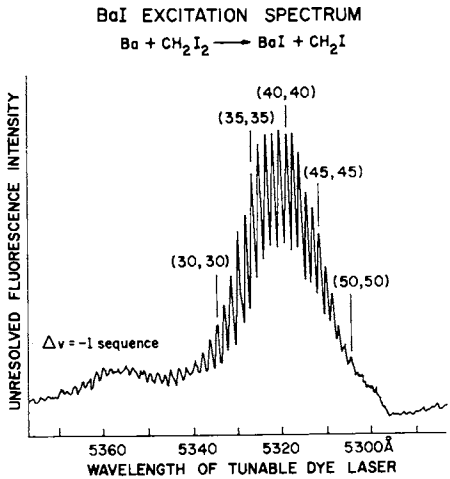

Figure 9. BaI excitation spectrum for Ba + CH_2I_2 → BaI + CH_2I

the side is the rack of electronics including the boxcar integrator. The photomultiplier is inside the beam apparatus. Now, let us look at some results.

Figure 7 is the excitation spectrum of the BaI product formed from the reaction of barium with methyl iodide (CH_3I). This work was carried out in my laboratory by Howard Cruse and Paul Dagdigian. It is possible to assign each peak to a (v', v") transition. Barium iodide, which may be regarded as Ba^+I^-, has an extra electron in an orbital primarily centered on the metal atom. This electron is easily excited, yielding a set of BaI Rydberg states. Because this electronic orbital is nonbonding in character, the potential curves of the excited state have the same shape, width, and location as the ground state. As a result nearly all the intensity is in the diagonal sequence of (0,0), (1,1), (2,2), etc. bands that have Franck-Condon factors which are nearly unity. Consequently, you can at a glance convert the excitation spectrum shown in Fig. 7 into the population distribution shown in Fig. 8. Clearly, we are observing unrelaxed reaction products since the vibrational population of BaI peaks around v" = 21, whereas a Boltzmann distribution will always have the v" = 0 level more populated than v" = 1, the v" = 1 level more populated than v" = 2, and so forth.

Figure 9 shows the same type of reaction with methylene iodide (CH_2I_2). Here the peak in the relative vibrational distribution is around v" = 39, even higher than in CH_3I. This reaction populates such high v" levels that the $\Delta v = -1$ sequence begins to overlap the $\Delta v = 0$ sequence and get in the way. The stick diagram of relative vibrational populations of the BaI product, Fig. 8, again shows a marked population inversion, but this distribution is smooth and bell-shaped.

Let us consider the energetics of these reactions. In my

In State-to-State Chemistry; Brooks, P., et al.;
ACS Symposium Series; American Chemical Society: Washington, DC, 1977.

lab, Ron Estler has recently redetermined the BaI dissociation energy by observing BaI chemiluminescence when metastable barium atoms collide with I_2. He finds the BaI bond energy to be about 73 kcal/mole. This corrects some early work of this lab. Now, if we take the known methyl iodide bond energy as 56 kcal/mole, we conclude that the reaction exothermicity is about 17 kcal/mole. From our relative vibrational population distribution (Fig. 8) we find that the average BaI vibrational energy is about 9 kcal/mole. Subtracting 9 from 17, we have 8 kcal/mole that must appear either in methyl excitation or in product translation. Ron Herm and coworkers have done some lovely work on this same reaction using mass spectrometric detection. They concluded that the average translational energy of the products is something like 10 kcal/mole. Consequently, we see that the methyl fragment is not very much excited as a result of the Ba + CH_3I reaction. With methylene iodide there is increasing vibrational excitation of the BaI product, but there is also more energy available from the reaction.

Figure 10 shows the remarkable data of Rommel and Schultz, University of Freiburg, on the reactions of barium with the various substituted bromides of methane. You can see clearly a trend that places more internal energy into the BaBr product with increasing substitution. The exothermicy limits, indicated by the arrows, are based on the recent BaBr bond energy determination (86 kcal/mole) by Estler.

At this point it is easy to become complacent and delude oneself into believing that the reactions of Ba with the nalogenated methanes have nothing new to teach us. Imagine then the surprise when Greg Smith, Chris Whitehead, and I ran the reaction Ba + CF_3I and saw the BaI excitation spectrum presented in Fig. 11. There is no escaping the conclusion that the BaI vibrational distribution is bimodal. This is quite unusual. There are just beginning to be a few examples of bimodal population distributions, most of them from the work of Polanyi and coworkers using infrared chemiluminescence to observe hydrogen halide products. If the distribution is bimodal, then it suggests that there is at least more than one reaction mechanism. I would like to share with you some speculation what mechanisms might be operative.

We see a high v and a low v peak; the former has about three times more population than the latter. The C-I bond energy of CF_3I is 53.5 kcal/more, quite similar to the value of 56 kcal/mole for the C-I bond energy of CH_3I. Taking the BaI bond energy as 73 kcal/mole, we have about 19.5 kcal/mole at the reaction's disposal. The average value of the internal energy in the BaI product is about 15.9 kcal/mole, and the maximum is about 22 kcal/mole. However, I have not included the relative translational energy of the reactants, so the total energy is going to balance closely.

Figure 12 shows the crossed beam study of Lin, Mims, and Herm

In State-to-State Chemistry; Brooks, P., et al.;
ACS Symposium Series; American Chemical Society: Washington, DC, 1977.

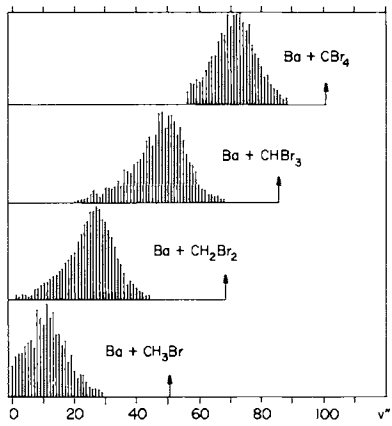

Figure 10. Reactions of barium with the various substituted bromides of methane. Data from M. Rommel and A. Schultz.

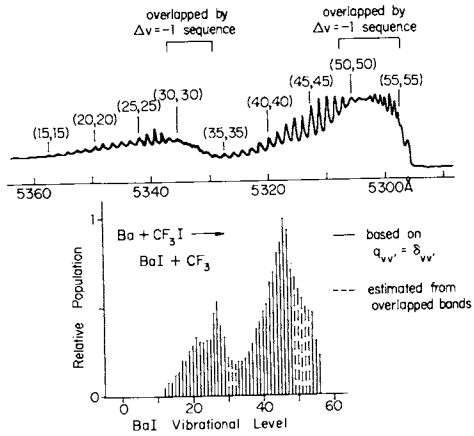

Figure 11

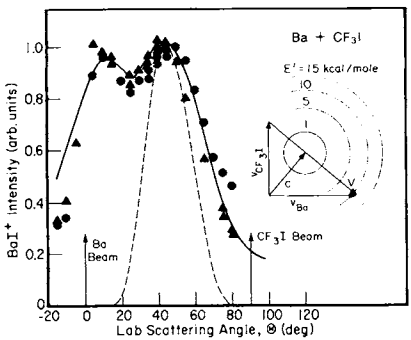

Journal of Physical Chemistry

Figure 12. Crossed beam study of Ba + CF_3I. (Lin, S.-M., Mims, C. A., Herm, R. R., J. Phys. Chem. (1973) 77, 569).

on Ba + CF_3I using mass spectrometric detection. Their angular distribution data has two peaks, from which they also suggested that more than one reaction mechanism occurs. They suggested that BaIF was one of the reaction products. The BaIF would be expected to give almost exclusively BaI^+ in the mass spectrometer. They observed a small BaF^+ signal as well.

Unfortunately, if BaIF is formed, we could not observe it, since this molecule does not absorb visible light. We can, however, distinguish BaI from BaF by their different excitation spectra. We find much BaI but no BaF product. This indirectly supports the idea that BaIF is formed. On examining the angular distribution data in Fig. 12 we can see that one distribution seems to peak closely along the centroid where the BaIF product would be expected to appear in the lab frame, while the other distribution is forward scattered. Yet, this reaction, Ba + CF_3I, might be thought to be typical of a rebound reaction, such as K + CH_3I, which produces primarily backward scattering. What is going on here?

We decided to perform our own angular distribution study. Figure 13 depicts the experimental setup. Two beam sources are mounted on a rotating lid; about 22 cm away from the reaction zone are slits which define the detection region. Figure 14 shows the results obtained. We are looking at the angular distribution of a particular vibrational state of BaI, namely v" = 47, which is characteristic of the high v peak. We found its distribution to be highly forward scattered, but we were unable to find the low v distribution when we searched for it. This suggests to us that the high v component may be related to the forward scattered peak seen by Lin, Mims, and Herm.

Let me move on to some further work. Figure 15 shows the investigation of Phil Brooks on the reaction of K with oriented CF_3I. I believe this gives us a clue to what is happening. Because CF_3I has a moderately large dipole moment and is a symmetric top, in this experiment it is possible to cause the K atom to strike either the CF_3 end or the I end of CF_3I. My friends in other disciplines of chemistry often ask why physical chemists spend so much time on an experiment whose outcome is obvious. The early studies of K with oriented CH_3I showed that reaction occurs only when the K approached the I end of methyl iodide. Everyone knew that. Figure 15 is an example where we see that reaction occurs when the K atom approaches either end of the CF_3I. What is happening here?

We must recall that we cannot restrict the collisions to zero impact parameter; afterall, we do not expect the potassium atom to pass through the carbon atom on its way to form KI. Instead, we are talking about initial directions of approach. We see in Fig. 15 that the KI product is back-scattered for initial attack of the I end, forward-scattered for initial attack of the CF_3 end.

All this leads to the model shown in Fig. 16. If Ba comes

In State-to-State Chemistry; Brooks, P., et al.;
ACS Symposium Series; American Chemical Society: Washington, DC, 1977.

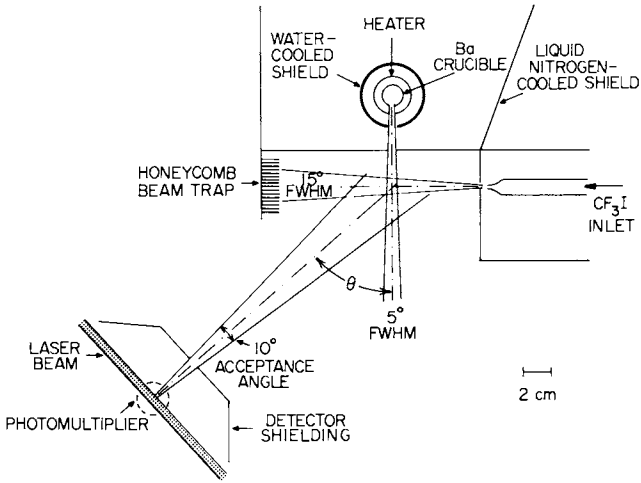

Figure 13

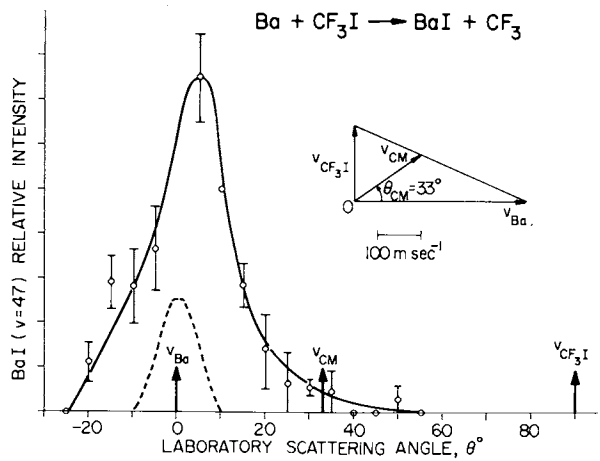

Figure 14. Laboratory scattering angle vs. BaI relative intensity for the reaction Ba + CF_3I → BaI + CF_3

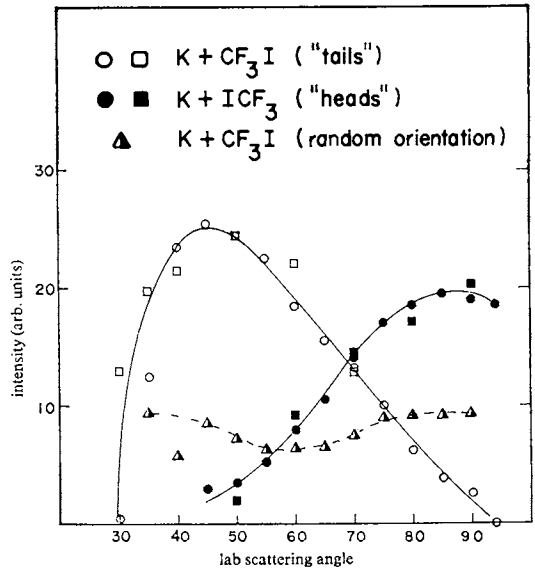

Faraday Discussions of the Chemical Society

Figure 15. Reaction of K with oriented CF_3I. (Brooks, P. R., Faraday Discuss. Chem. Soc. *(1973)* **55**, *299).*

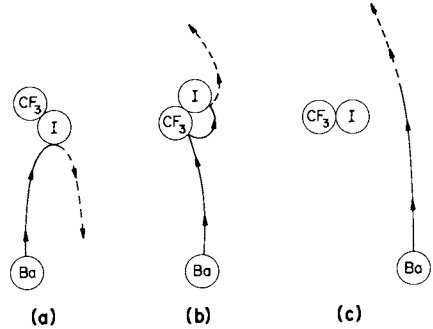

Figure 16

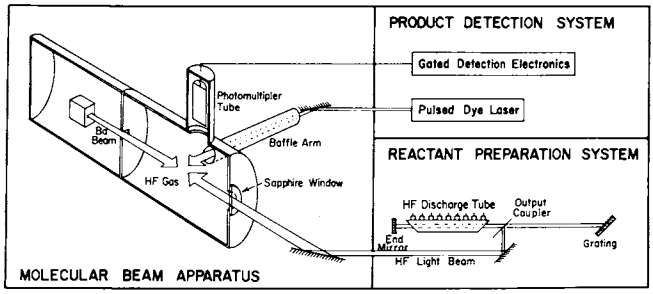

Figure 17

toward the I end (Fig. 16a), we expect backward scattering and a low v distribution; if Ba approaches the CF_3 end (Fig. 16b), an electron jump occurs - - remember that CF_3 is the electronegative end of CF_3I - - and the BaI product is scattered in the forward direction with high internal excitation. There are variants on the above, involving insertion of Ba into the C-I bond or glancing attack (Fig. 16c). The point of all this is that such studies are just beginning to permit us to learn about the stereochemistry of reactions and the presence of different reaction pathways leading to the same products but in different states of energization.

So far, I have emphasized the use of lasers in probing the products. However, lasers can also be used to prepare the reactants. An example of this is the work of Gary Pruett. The experimental setup is pictured in Fig. 17. A barium beam passes through a scattering chamber filled with HF gas at a very low pressure and reacts to form BaF. Like BaI, BaF can then be detected by laser-induced fluorescence. We vary the state of the HF gas. At room temperature nearly all the hydrogen fluoride molecules are in the gound vibrational level, v" = 0. There is about a 4000 cm^{-1} energy gap between v" = 1 and v" = 0. However, a chemically-driven HF laser can pump some fraction of the HF molecules from v" = 0 to v" = 1. We operate the laser on the $P_1(2)$ line so that we pump HF molecules at the peak of the rotational Boltzmann distribution. When we prepare a certain state of HF we want to know how that alters the states of the BaF product.

Figure 18 shows what happens to the BaF excitation spectrum with the HF laser on and the HF laser off. In the latter case, we see that v" = 0, 1, and 2 are populated but the vibrational distribution falls off to higher v" values. With the laser on, at first glance it seems that nothing happens. Further study indicates that there might be something going on in the region enclosed in the dashed box of Fig. 18. This region is enlarged in Fig. 19. Here we begin to see that HF(v" = 1) preferentially populates BaF molecules in high v" levels. With some electronics that substract the "laser-off" from the "laser-on" signal, we obtain the difference spectrum shown in Fig. 20.

By making some estimations of the fraction of HF pumped by the HF laser, we are able to deduce the relative state-to-state reaction rates, shown in Fig. 21. There are 12 kcal/mole initially available to the products; Ba + HF(v" = 0) is an exothermic reaction. We add an additional 11 kcal/mole when we pump HF to v" = 1. That is equivalent to 9 vibrational quanta of BaF. If there is full retention of vibrational energy from reactants to products, we could expect the rate distribution to shift by 9 quanta. If vibrational excitation of HF triggers more reaction exothermicity to appear in product vibration, then this rate distribution could be shifted even more. However, the rate distribution for Ba + HF(v" = 1) peaks at v" = 6. Therefore, only

In State-to-State Chemistry; Brooks, P., et al.;
ACS Symposium Series; American Chemical Society: Washington, DC, 1977.

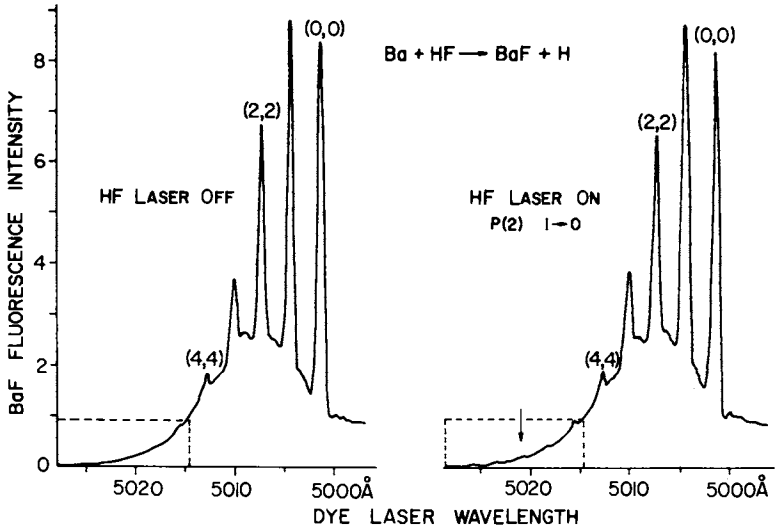

Figure 18

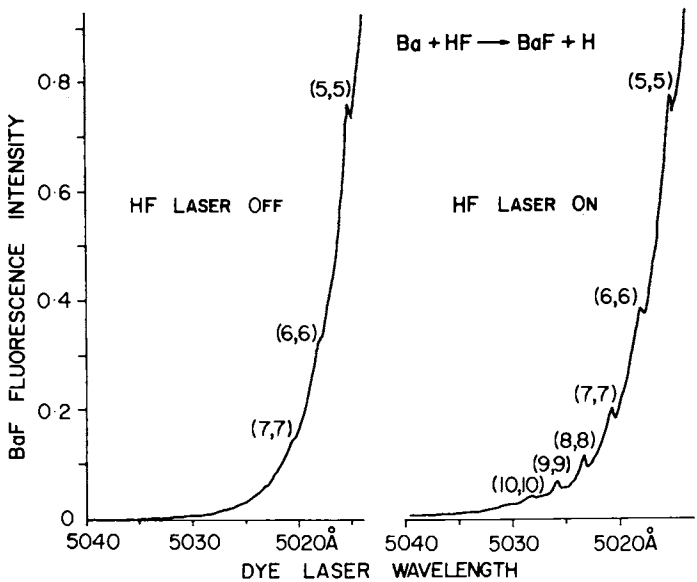

Figure 19

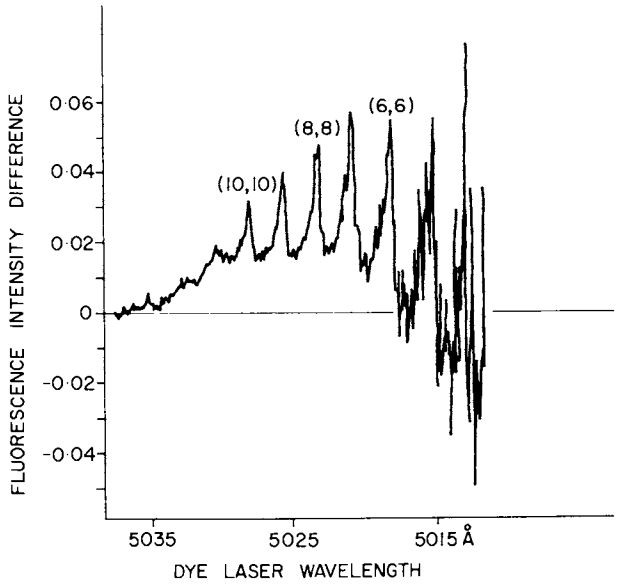

Figure 20

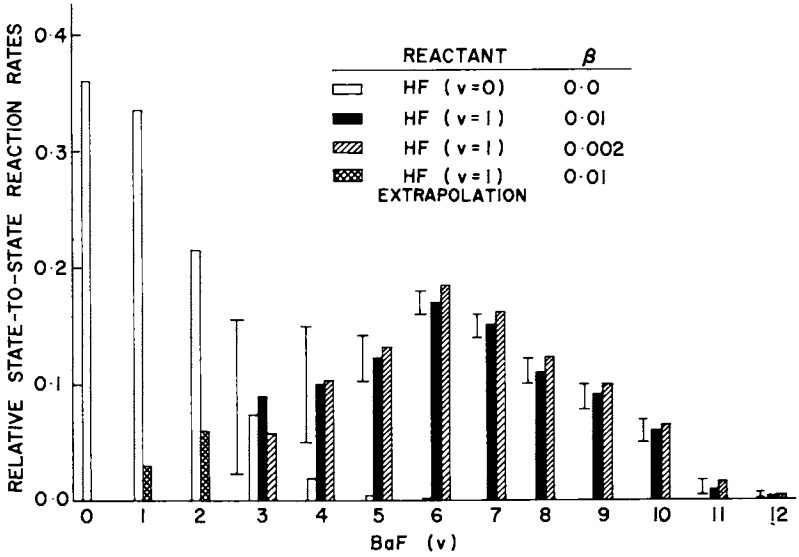

Figure 21

In State-to-State Chemistry; Brooks, P., et al.;
ACS Symposium Series; American Chemical Society: Washington, DC, 1977.

about 60% of the available vibrational energy is retained in the BaF product.

This leads to some thoughts about the reaction dynamics. Imagine the barium atom approaching the HF molecule on some reaction surface. One such surface is that calculated by Heloiza Schor for Be + HF (Fig. 22). For HF(v" = 0) we follow along the minimum energy path. After passing through some saddle point region the BaF product separates from the BaFH complex. Because the BaF has so much translational energy, we presume that the release of energy occurs after the BaF bond is formed, leading to a repulsive or late downhill surface. Suppose the HF is excited to v" = 1. This makes the HF vibrate as it climbs the valley to the saddle point region. We have the possibility that the bond might be extended or compressed on reaction. If this is true, then HF extension causes the BaF product to cut the corner and enter the product channel from the side rather than along the minimum energy path. This would lead to increased vibrational excitation of the BaF product. The other possibility is that reaction occurs when the HF bond is compressed. This places the BaF product deep into the far corner of the BaFH surface and might promote product translation. However, our rate distribution for Ba + HF(v" = 1) does not appear bimodal, suggesting that reaction is highly favored for one conformation over the other. From the data at hand we are not able to work backwards to a unique reaction surface. However, this state-to-state kinetics is just the type of data we need to judge the validity of proposed potential energy surfaces, and with such data a detailed understanding of reaction dynamics is within reach.

All the foregoing reactions were ground state reactions, that is, electronically ground state reactants evolved into electronically ground state products. However, laser excitation can be used to prepare electronically excited reactants, and if they react to form electronically excited products, then these products can be readily detected by their characteristic chemiluminescence. I would like to present to you some unpublished work of Ron C. Estler. He uses the 5145A argon ion laser line to pump I_2 to an excited state. Then the I_2* beam crosses a beam of metal atoms, such as indium or thallium. Figure 23 shows the laser-induced chemiluminescence spectrum of I_2* + In → InI* + I. With the laser off, there is no emission. This does not mean that reaction is absent. Indeed, In and I_2 probably react to form InI + I. However, this reaction does not give any visible light. With the laser on, peaks appear which are readily assigned to InI*. There is so much energy available that the InI* emission is to the blue of the pump line. This simplifies detection as we are then free of I_2* fluorescence. So we have yet another scheme where we can prepare one state of the reactants and observe the states of the products. There is, however, a special feature of this experiment which I wish to call to your attention. We can choose the polarization of the laser, and when we do that, we in

In State-to-State Chemistry; Brooks, P., et al.;
ACS Symposium Series; American Chemical Society: Washington, DC, 1977.

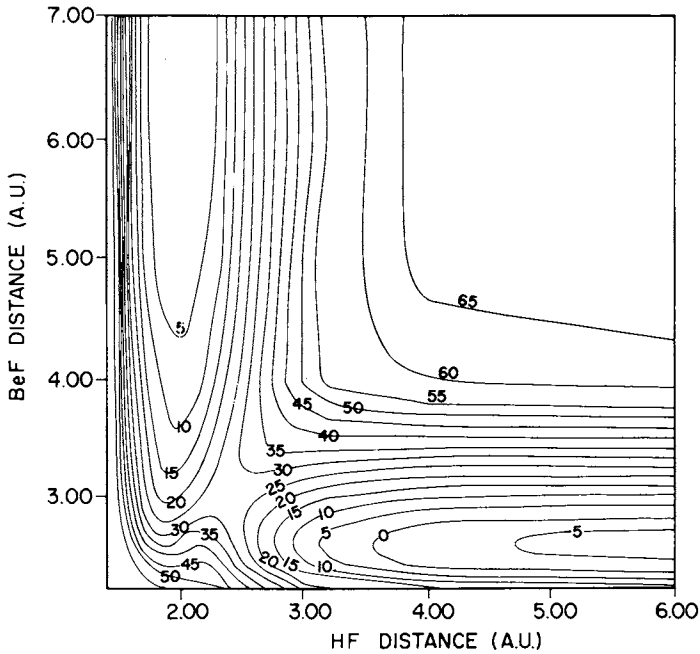

Figure 22. Contour plot for linear BeFH potential surface

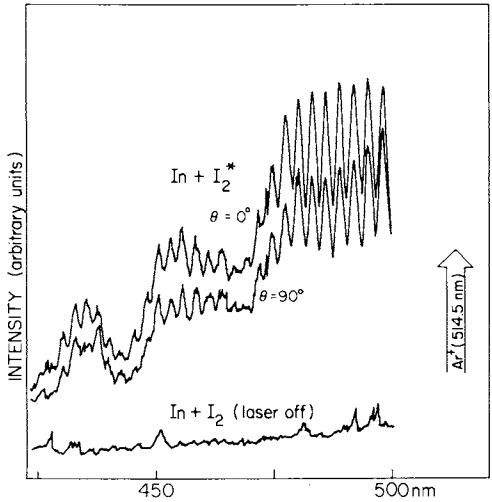

Figure 23

effect pick out the alignment of the I_2 molecule. The theory is relatively straightforward. With a beam of plane polarized light we initially photoselect the I_2 molecules in a $\cos^2\theta$ distribution, where θ is the angle between the electric vector of the light beam and the internuclear axis of the molecule. The molecules rotate before colliding with the In atoms. This rotation reduces the anisotropy of the original distribution, but does not completely remove it. Instead of a $\cos^2\theta$ distribution of the rotor axes, we have a $(1 + \cos^2\theta)$ distribution. A perfectly isotropic distribution corresponds to the angular momentum vectors of the I_2 molecules pointing equally in space every which way. However, the act of photoselection preferentially chooses I_2 molecules with their angular momenta in a plane at right angles to the electric vector. In the absence of collisions, this distribution cannot change as the I_2 molecules rotate. In the present crossed beam study of I_2^* + In, we find, as shown in Fig. 24, that reaction is more probable when the In atom strikes the I_2^* molecule head on - - collinear geometry - - than broadside - - C2v geometry.

Once again we all believe that there has to be some stereochemistry governing this reaction system...and indeed, one feels a little brainwashed from the numerous studies on the H + H_2 reaction to think that all A + BC reactions are collinear. This is not the case. However, this example does demonstrate a strong preference for a collinear approach to cause reaction. This may be the first instance where we have direct information on the role of orientation in atom-diatom reactive scattering. However, the point is that laser techniques should make such studies commonplace.

In closing, I want to mention one last laser technique for molecular beam studies. This is the thesis work of Diane Feldman. Figure 25 shows a spectrum of sodium dimers in a molecular beam. It is a fine spectrum, but what makes it unusual is that we are not recording the fluorescence or the absorption. Traditionally, spectroscopy is done by looking at light, but an alternative way is to look at the modified target. Our method is shown in Figure 26, which depicts the process of resonant multiphoton ionization. Here we pump from different levels of the Na_2 X state to the Na_2 B state and from thence to the ionization continuum. We then count the ion fragments with a channeltron (charged particle multiplier). Figure 27 shows this technique applied to a supersonic beam of Na_2. The extensive cooling is at once apparent. In this spectrum we plot ion count versus laser excitation wavelength.

Clearly, this scheme can provide us with much spectroscopic information, but what can it offer to the study of reaction dynamics? We have a chance here of combining mass spectrometry with laser spectroscopy in detecting reaction products. Already, in our laboratory Russ Lengel has been able to detect with this technique the BaCl product in the reaction Ba + HCl. There are

In State-to-State Chemistry; Brooks, P., et al.;
ACS Symposium Series; American Chemical Society: Washington, DC, 1977.

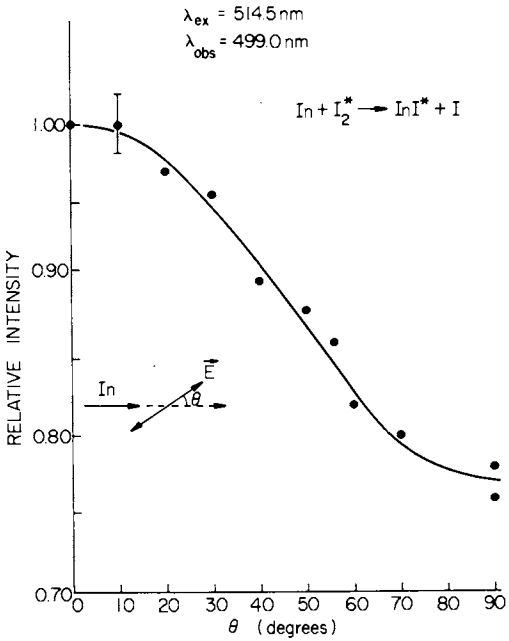

Figure 24

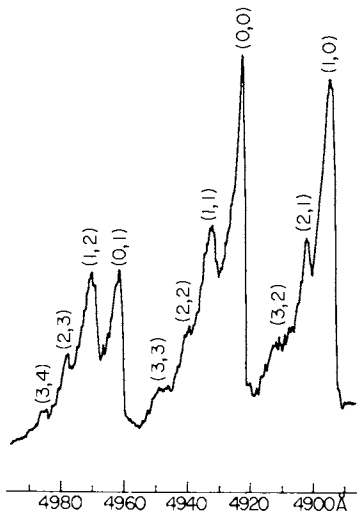

Figure 25. Na_2: molecular beam

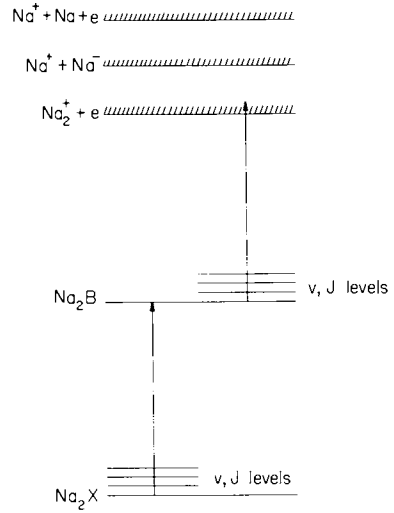

Figure 26. Detection of molecules by multi-photon resonant ionization

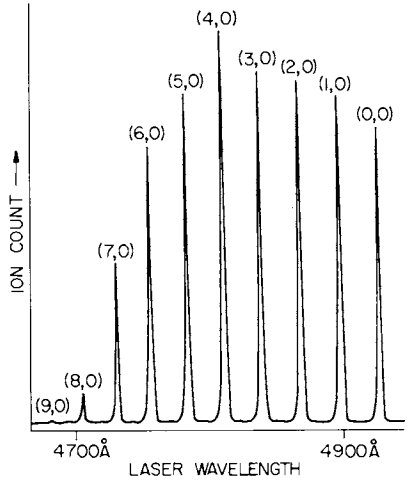

Figure 27. Na_2: supersonic beam (D. Feldman)

considerable advantages when this is applicable. Every ion we create can be collected; every ion we collect can be counted; and the natural ion background is exceedingly small. We have therefore a neutral detector with remarkable signal-to-noise characteristics. Indeed, Hurst and coworkers at Oak Ridge National Laboratory have recently demonstrated the use of this technique to detect one cesium atom in the presence of 10^{19} argon atoms. Presently, we are collecting charged particles, but it is not difficult to imagine using a mass filter in front of the channeltron. These new techniques may be quite useful in the future in studying state-to-state reaction processes, both on neutral and ionic systems. It remains to be seen, however, how easily we can relate the signal strength to initial internal state populations. If this problem can be overcome, then this laser technique will give us yet another powerful method of exploring chemistry, one collision at a time.

In State-to-State Chemistry; Brooks, P., et al.;
ACS Symposium Series; American Chemical Society: Washington, DC, 1977.

4

Studies of Multiphoton Dissociation of Polyatomic Molecules with Crossed Laser and Molecular Beams

E. R. GRANT, M. J. COGGIOLA,* and Y. T. LEE

Materials and Molecular Research Division, Lawrence Berkeley Laboratory and Department of Chemistry, University of California, Berkeley, CA 94720

P. A. SCHULZ, AA. S. SUDBO, and Y. R. SHEN

Materials and Molecular Research Division, Lawrence Berkeley Laboratory and Department of Physics, University of California, Berkeley, CA 94720

Recently, collisionless multiphoton dissociation (MPD) of polyatomic molecules by infrared lasers has become one of the most interesting and exciting problems in quantum electronics and laser chemistry (1). The process is isotopically selective and provides a potentially effective and inexpensive method for isotope separation (2). It has also been suggested that MPD could lead to mode-selective bond breaking (3). If this were indeed the case, the process would have a revolutionary effect on photochemical synthesis and other areas of chemistry.

From the scientific point of view, MPD is also an extremely intriguing problem. In order to reach the dissociation threshold, a single molecule has to absorb several tens of infrared photons. This is a nonlinear process. Usually, even a 3- or 4-photon absorption process would require a laser beam intensity of the order of MW/cm^2 or higher. For absorption of several tens of photons simultaneously, one would expect to take a laser intensity close to the gas breakdown threshold, namely, $\sim$ 10 GW/cm^2 or more. Therefore, it was quite surprising when it was found that only a laser intensity of $\sim$ 10 MW/cm^2 or a pulse energy of $\sim$ 1 J/cm^2 is needed for MPD (4,5). Then, the questions which must be answered are why can a single molecule absorb so many photons of same frequency with a large probability, how many photons are actually absorbed per molecule, how is the absorbed energy distributed in the excited molecule before dissociation, and what is the subsequent dynamics of dissociation. Here, we would like to discuss how we can answer most of these questions quantitatively from our recent molecular beam studies on MPD (6).

There already exists in the literature a large number of reports on the experimental and theoretical studies of MPD (1,7), and some of the questions related to the absorption have been answered. The techniques used in the experiments are, however, limited. In almost all cases, CO_2 TEA laser pulses were used to excite the low-pressure gas medium in a sample cell. One would

*Present address: Stanford Research Institute, Menlo Park, CA.

In State-to-State Chemistry; Brooks, P., et al.;
ACS Symposium Series; American Chemical Society: Washington, DC, 1977.

make 1000 or 2000 laser shots (8) and analyze the gas medium before and after the shots by optical absorption and mass spectroscopy. If possible, the induced luminescence in the medium was also monitored during the shots. The measurements were carried out as a function of laser power, energy, frequency, pulsewidth, gas pressure, gas mixtures, etc. An obvious difficulty of such experiments is that the observation of the dissociation process is always influenced by molecular collisions and chemical reactions following the laser excitation. Consequently, interpretation of the results is often uncertain, confusing, and sometimes even inconsistent. Direct, quantitative information about the dynamics of MPD is difficult to obtain. For example, such experiments sometimes cannot even tell for certain what the primary dissociation fragments are and how many infrared photons per molecule dissociated are absorbed. Then, the results on the dependence of MPD on laser power, energy, frequency, etc. can all be affected by molecular collisions and chemical reactions.

It is clear that in order to fully understand MPD one must try to avoid molecular collisions. With this in mind, the Harvard group has used subnanosecond CO_2 laser pulses much shorter than the mean free time between molecular collisions to study MPD in a gas cell (5). However, even though the laser excitation time is short, the dissociation lifetime of a molecule can still be longer than the collision time, and hence their results of MPD are still more or less affected by molecular collisions. It seems to us that the only way to eliminate molecular collisions in the studies of MPD is to use a molecular beam. A molecular beam experiment on CO_2 laser-induced dissociation of SF_6 was performed previously by Brunner et al., (14) in which the influence on the molecular beam of SF_6 itself by the CO_2 laser was studied using the mass spectrometer. In our experiments, using a rotatable mass spectrometer, direct identification of fragment species as well as the measurements of angular and velocity distributions of dissociated products were performed for the understanding of the dynamics of excitation and dissociation.

Experimental Arrangement

Our experimental setup is shown schematically in Fig. 1 (6). The molecular beam was a supersonic jet from a 0.1 mm nozzle. The beam diameter at the collision center was about 2 mm with a divergence angle of 0.8°. At 75-torr stagnation pressure, the molecular density in the beam was $\sim 3 \times 10^{11}$ cm^{-3}. The laser was a Tachisto CO_2 TEA laser putting out about 0.5 - 1 J/pulse. A 25-cm ZnSe lens was used to focus the laser beam. The two beams crossed at the collision center and the dissociation fragments from the collision region were then analyzed by a detector which consisted of an ionizer, a quadrupole mass spectrometer, and a gated counting system. The detector could be rotated with respect to the collision center so that the angular distribution of the fragments could be measured. The angular resolution was better

In State-to-State Chemistry; Brooks, P., et al.;
ACS Symposium Series; American Chemical Society: Washington, DC, 1977.

than ± 0.5°. At a given angle, the velocity distribution of the fragments could also be obtained from the time-of-flight measurement. The pressure in the collision chamber was about 5×10^{-7} torr and that of the ionization chamber of the detector was about 10^{-10} torr.

Experimental Results and Discussion

What have we learned from our experiment? We shall discuss mainly MPD of SF_6 since most of our experiments were done with this molecule. First of all, we found that the dissociation fragments could be readily detected and at high laser pulse intensities or energy densities, the signal appeared to be saturated indicating that almost all excited molecules in the beam were dissociated. This result constitutes a direct proof to the collisionless nature of MPD. That MPD can occur with large probability at not very high laser intensities has been the subject of many recent theoretical papers (1,9). It is now qualitatively understood as due to the following physical mechanism (10).

In order that a single molecule can absorb several tens of photons from a monochromatic laser beam with high probability, each one-photon transition step in the multiphoton excitation process must be resonant or nearly resonant. This would be possible if molecular vibration were strictly harmonic. In practice, however, the anharmonicity in a vibrational mode is always so large that no resonant stepwise excitation up the pure vibrational ladder can happen. Fortunately, the energy level diagram of a polyatomic molecule is more complicated. Superimposed on the vibrational levels, there are numerous rotational levels. In addition, the degeneracy of the excited vibrational levels can be lifted by Coriolis coupling and by anharmonic coupling with other modes. As a result, starting from a range of rotational levels in the ground vibrational state, it is possible to have the first 3-6 one-photon stepwise excitations nearly resonant up the rotation-vibrational ladder. Then, the density of states of a polyatomic molecule always increases rapidly with energy and soon the energy levels form a quasi-continuum. For example, the density of states of SF_6 at 5000 cm^{-1} is already as high as $10^3/cm^{-1}$ (10). Thus, after the first 3-6 stepwise one-photon excitations, the laser field essentially interacts with a continuum of states, and the subsequent individual steps in the stepwise multiphoton transition through the quasi-continuum to and beyond the dissociation limit are all "resonant." This then qualitatively explains why a relatively low infrared laser power or energy is sufficient for MPD of polyatomic molecules.

The second important aspect of our experiment was that we could identify the dissociation fragments before they undergo secondary collisions with other molecules on the wall. However,

In State-to-State Chemistry; Brooks, P., et al.;
ACS Symposium Series; American Chemical Society: Washington, DC, 1977.

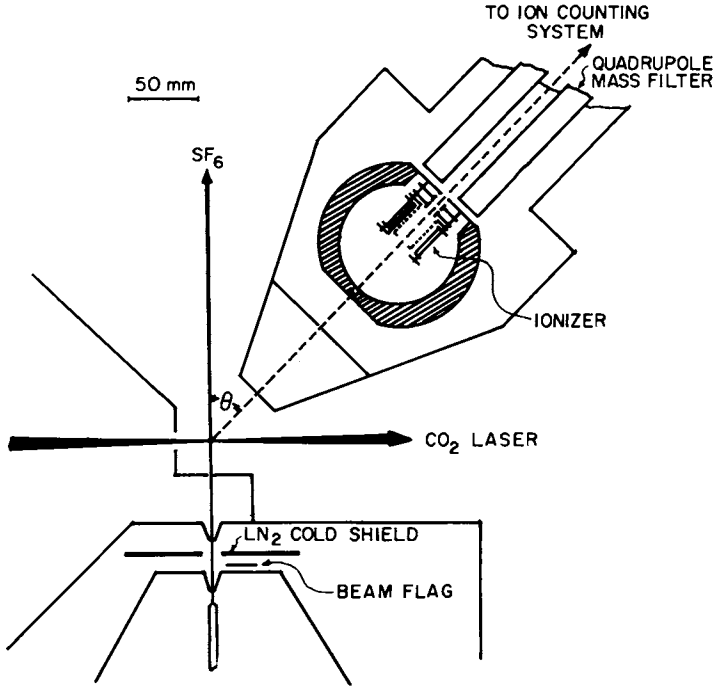

Figure 1. Schematic of the apparatus for studies of multiphoton dissociation of SF_6. The molecular beam is triply differentially pumped.

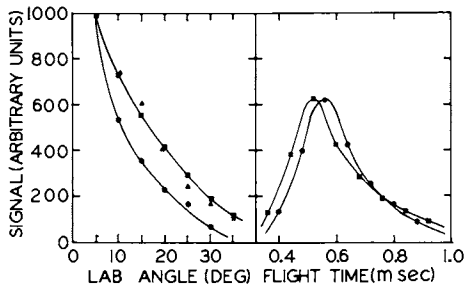

Figure 2. (a) Angular distribution of the SF_3^+ fragments from multiphoton dissociation of SF_6. (b) Flight time distribution of the SF_3^+ fragment. The narrow angular distribution and longer flight times ● are indicative of SF_5 at a laser energy density of ~ 6 J/cm². The wider angular distribution and shorter flight times ■ are indicative of SF_4 at a laser energy density of ~ 15 J/cm². The angular distribution ▲ was obtained at a laser energy density of ~ 50 J/cm².

In State-to-State Chemistry; Brooks, P., et al.;
ACS Symposium Series; American Chemical Society: Washington, DC, 1977.

the identification of the fragments of SF_6 is much more complicated than what we stated erroneously in our previous work (6). Sulfur polyfluorides are known to decompose almost completely in the ionization process into daughter ions. It was found that the ratio of SF_3^+/SF_2^+ is a much more reliable way of identifying products. We found that the primary dissociation products are SF_5 + F. This is in fact what one would expect from the energy consideration since SF_5 + F is the lowest dissociation channel. It has a dissociation threshold at 77 KCal/mole as compared to that of SF_4 + F_2 at 105 KCal/mole. Previous experiments by others had suggested that SF_4 and F_2 were the dissociation fragments (11). It turns out that SF_4 could actually appear as a secondary dissociation product when the laser energy is increased. No F_2 signal was ever detected. These results suggest a two-step mechanism for the production of SF_4:

$$SF_6 + nh\nu \xrightarrow{\tau} SF_5^* + F$$

$$+$$

$$n'h\nu$$

$$\longrightarrow SF_4^* + F$$

where τ indicates the average dissociation lifetime and * denotes internal excitation. Clearly, the laser pulse width, $T \gtrsim \tau$ in order for the second dissociation step to be significant. Our results therefore suggest that average τ must be close to or less than the laser pulse width of 50 nsec.

As we mentioned earlier, our apparatus also allowed us to measure the angular distribution and velocity distribution of the fragments. An example is shown in Fig. 2. Such results together with the velocity distribution of the primary beam could yield quantitative information about the dynamics of dissociation. Let $\vec{v}_0$ and $\vec{v}$ be the velocities of the primary beam and the fragment respectively, and θ be the angle between $\vec{v}_0$ and $\vec{v}$. Let $f(v,\theta)$ be the fragment velocity distribution at θ, $h(v_0)$ be the velocity distribution of the primary beam, and $g(u=|\vec{v} - \vec{v}_0|,\theta)$ be the fragment velocity and angular distribution in the center of mass coordinates. We first observed qualitatively that the angular distribution is isotropic in the center of mass coordinates so that $g(\vec{u}) = g(u)$. This was true for at least the case of SF_6 since our experimental results also showed no dependence on the laser polarization. We then have

$$f(v,\theta) = \int g(u = |\vec{v} - \vec{v}_0|)h(v_0)dv_0$$

from which we can deduce g(u) by deconvolution if $f(v,\theta)$ and $h(v_0)$ are known from measurements. The recoil kinetic energy $\mathcal{E}$ of the fragments is given by $\mathcal{E} = \frac{1}{2} m_f u^2$, so g(u) can be readily transformed into the fragment recoil-energy distribution $g(\mathcal{E})$. In Fig. 3, we show an example of $g(\mathcal{E})$ obtained with laser pulses of

In State-to-State Chemistry; Brooks, P., et al.;
ACS Symposium Series; American Chemical Society: Washington, DC, 1977.

~ 50 nsec in pulsewidth and ~ 6 J/cm^2 in energy. Theoretical curves are also shown for comparison.

Before we discuss the theoretical calculation of $g(\mathcal{E})$, we should point out that three qualitative but important conclusions can readily be drawn from the experimental data. (1) The fragment angular distribution in Fig. 2a suggests and the fragment recoil-energy distribution in Fig. 3 confirms that the average recoil energy of the fragments is low, approximately 2-3 KCal/mole which is about a CO_2 laser photon per molecule. This indicates that if SF_6 before dissociation absorbs many more than one photon above the dissociation level, a large fraction of this excess energy must be retained by the SF_5 fragment in its internal degrees of freedom. (2) If the dissociation has an appreciable exit barrier energy, then the fragment angular distribution would peak at $\theta \neq 0$ and the fragment recoil-energy distribution would correspondingly peak at $\mathcal{E} \neq 0$. This is apparently not the case for SF_6 as seen in Fig. 2a and Fig. 3, indicating that the barrier energy for $SF_6 \rightarrow SF_5 + F$ is essentially zero or less than 0.2 KCal/mole. (3) If MPD is mode-selective, a velocity distribution skewed to higher energy would be expected. Figure 3 shows that this is not the case for SF_6. The strong peaking of product molecules at zero kinetic energy is exactly what is expected if the energy in the excited molecule is completely randomized before decomposition.

We now discuss how we can deduce more quantitative information about MPD by comparing theory and experiment on $g(\mathcal{E})$. We believe that because of the very strong coupling among various vibrational modes at high excitations, the excitation energy deposited in the molecule should be randomly distributed in all vibrational degrees of freedom. We can therefore use the RRKM statistical model for unimolecular dissociation (12) to calculate $g(\mathcal{E})$. The model assumes that a molecule is initially excited to an energy level E (or statistically to many levels with a certain distribution) above the dissociation energy E_0, and that the excitation energy is randomly distributed in all composite vibrational states. If N_E is the density of vibrational states of the molecule at E, and $G_E(\mathcal{E})$ is the density of states in which the excited molecule will sooner or later dissociate with a fragment recoil energy $\mathcal{E}$, then the probability that the molecule will dissociate with a recoil energy $\mathcal{E}$ is

$$P_E(\mathcal{E}) = G_E(\mathcal{E})/N_E$$

and hence the fragment recoil-energy distribution is given by

$$g_E(\mathcal{E}) = P_E(\mathcal{E})/\int_0^{E-E_0} P_E(\mathcal{E})\,d\mathcal{E} \ .$$

In State-to-State Chemistry; Brooks, P., et al.;
ACS Symposium Series; American Chemical Society: Washington, DC, 1977.

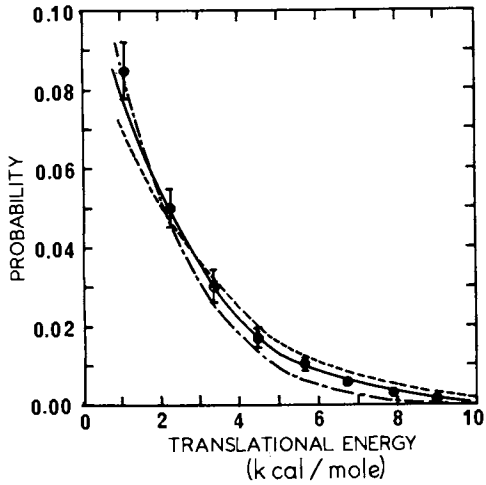

Figure 3. Fragment recoil energy distributions for $SF_6 \rightarrow SF_5 + F$. Experimental data points obtained with ~ 6 J/cm² laser pulses are denoted by ●. Curves are calculated from the RRKM theory assuming a molecular excitation of $E = E_0 + n\hbar\omega$ with $n = 7$ (— · —), $n = 9$(——), and $n = 11$ (– – –) where E_0 is the dissociation energy and $h\omega$ is the CO_2 laser photon energy.

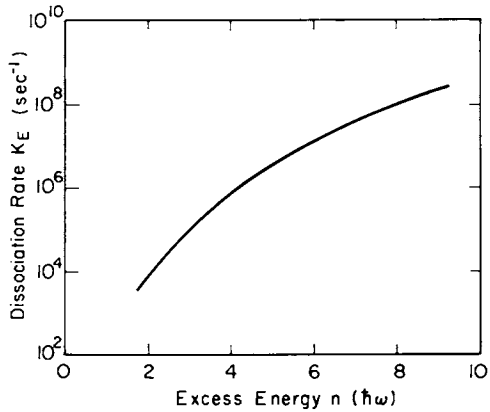

Figure 4. Dissociation rate of SF_6 calculated from the RRKM theory as a function of level of excitation $n\hbar\omega = E - E_0$.

In State-to-State Chemistry; Brooks, P., et al.;
ACS Symposium Series; American Chemical Society: Washington, DC, 1977.

For a given molecule, N_E and $g_E(\mathcal{E})$ can be obtained from model calculation. Therefore $g_E(\mathcal{E})$ [or $g(\mathcal{E})$ for excitation distributed over many levels] can be calculated and compared with the experimental data. In addition, the dissociation rate $k_E(\mathcal{E})$ which is proportional to $P_E(\mathcal{E})$ can also be obtained from the model calculation knowing $P_E(\mathcal{E})$. The total dissociation rate of the molecule is given by

$$K_E = \int_0^{E-E_0} k_E(\mathcal{E})\, d\,\mathcal{E}$$

and the corresponding dissociation lifetime is $\tau_E = 1/K_E$.

Figure 3 shows three $g_E(\mathcal{E})$ curves calculated by assuming $E = n\hbar\omega$ with $n = 7$, 9, and 11, where $\hbar\omega$ is the CO_2 laser photon energy. The $n = 9$ curve clearly fits well with the experimental date. Actually, there is a significant spread in the levels of excitation for a given laser energy, $n = 9$ merely means the average level of excitation. The agreement between theory and experiment leads to the following conclusions:

(1) The RRKM statistical model for unimolecular dissociation assuming random energy distribution in all vibrational degrees of freedom gives a correct description of the dynamics of MPD. The mode-selective dissociation is clearly not possible for at least MPD of SF_6 with nanosecond pulsed excitation.

(2) For MPD of SF_6, the molecule mostly likely dissociates from a level at 7 to 11 $\hbar\omega$ above E_0 depend on laser energies. In other words, since $E_0 \simeq 29\ \hbar\omega$, each SF_6 molecule actually absorbs on average 36 to 40 infrared photons before dissociation. This should be compared with the estimate of 200-250 photons reported earlier in the literature (13).

(3) The calculated dissociation rates versus $E - E_0 = n\hbar\omega$ for SF_6 are shown in Fig. 4. We find that for $n = 7$ to 11, the corresponding dissociation lifetime is ~ 50 to 0.5 nsec. This is in the same order of magnitude as laser pulsewidths.

(4) Figure 4 shows that the dissociation rate increases rapidly with n. This explains why the dissociated molecules appear to have originated from an energy level $E = E_0 + 7\ \hbar\omega$. For $E < E_0 + 6\ \hbar\omega$, the up-excitation rate is much larger than the dissociation rate and hence only a small fraction of molecules in these levels can dissociate. For $E > E_0 + 11\ \hbar\omega$, the dissociate rate is much larger than the up-excitation rate and only a small fraction of molecules can be excited to higher levels. The results also suggest that over a wide range of laser powers, the level of excitation would not vary significantly. This was found to be the case in SF_6.

We have also performed a number of other measurements of MPD. Limited by space here, we will only discuss briefly some of them:

(1) We have measured for MPD of SF_6 the dependence of the fragment intensity as a function of laser power and energy. The threshold energy (defined by the limit of our detection sensitivity) was around $2J/cm^2$ and appeared to be the same for laser

In State-to-State Chemistry; Brooks, P., et al.;
ACS Symposium Series; American Chemical Society: Washington, DC, 1977.

pulsewidths of 50 nsec and 500 nsec. For 500-nsec pulsewidth, this energy threshold corresponds to a power threshold of ~ 4 MW/cm^2 which is 6 times lower than the earlier reported value (4). For longer pulses, the power threshold could be even lower. This suggests that the energy threshold is probably more meaningful even though MPD must also depend on the laser peak power in some way. Above the threshold, the fragment intensity increased almost linearly and then quickly leveled off to saturation at ~ 10 J/cm^2. These results obtained under the strict collisionless condition should form the basis of any quantitative theory on MPD. With increasing laser energy, the fragment angular distribution first became somewhat broader. Then, above 15 J/cm^2, it remained essentially unchanged, indicating that it was difficult to excite the SF_6 molecules to $E - E_0 > 11\ \hbar\omega$.

(2) We have measured the excitation spectrum for MPD of SF_6. Compared to the one reported earlier by Ambartzumian et al (4), our spectrum had a full width of ~ 12 cm^{-1} instead of 19 cm^{-1} and a peak shifted from the Q branch by ~ 4 cm^{-1} instead of 8 cm^{-1}. In both cases, the vibrational temperatures and laser energies are supposed to be the same, but the vibrational temperature of the molecules in the gas cell experiments could become somewhat hotter during the experiment.

(3) We have found that MPD of SF_6 does not depend on the laser polarization. This indicates that the excitation energy is distributed isotropically in the rotational substate or/and the dissociation lifetime is much longer than the rotational periods.

(4) We have also made preliminary measurements on MPD of a number of other molecules, e.g., $CF\ Cl_3$ and CF_3Br. In all cases, the dissociation occurred through the lowest dissociation channel, indicating that the statistical model for MPD discussed earlier for SF_6 should also be applicable to other polyatomic molecules.

Concluding Remarks

In summary, we have shown that through molecular beam studies, we have learned a great deal about excitation and dissociation processes in MPD. Specifically, we have been able to identify the dissociation products, to learn about the excitation energy distribution in the excited molecule, to determine the level of excitation before dissociation, and to find the dissociation rate and lifetime. We have concluded that the RRKM statistical model for unimolecular dissociation gives a good description of the dynamics of MPD, and that the possibility of a mode-selective explosive type of MPD can be ruled out. There are, of course, many other experiments yet to be done in rigorously collisionless conditions of molecular beam in order to further our understanding on MPD. For example, we should measure MPD by varying the laser pulsewidth over a wide range, by using two exciting laser pulses with different energies and frequencies and a time delay between

In State-to-State Chemistry; Brooks, P., et al.;
ACS Symposium Series; American Chemical Society: Washington, DC, 1977.

them, and by heating and cooling the rotational and vibrational degrees of freedom of the molecular beam. These experiments are presently being carried out in our laboratory.

This work was done with support from the U.S. Energy Research and Development Administration.

ABSTRACT

It is shown that our crossed laser and molecular beam studies of collisionless multiphoton dissociation of polyatomic molecules have led to a much better understanding of the dynamics of excitation and dissociation of this important isotopically selective process.

Literature Cited

(1) See, for example, papers in "Tunable Lasers and Applications," Proceedings of the Nordfjord Conference, edited by A. Mooradian, T. Jaeger, and P. Stokseth, (Springer-Verlag, 1976), and references therein.
(2) Ambartzumian, R.V., Letokhov, V.S., Ryabov, E.A., and Chekalin, N.V., JETP Lett. (1974) 20, 273; Lyman, J.L., Jense, R.J., Rink, J., Robinson, C.P., and Rockwood, S.O., Appl. Phys. Lett. (1975) 27, 87.
(3) Denver, D.F. and Grunwald, E., J. Am. Chem. Soc. (1976) 98, 5055.
(4) Ambartzumian, R.V., Fuzikov, N.P., Gorokhov, Yu A., Letokhov, V.S., Marakhov, G.N., and Puretzky, A.A., Optics Comm. (1976) 18, 517.
(5) Kolodner, P., Winterfeld, C., and Yablonovitch, E., Optics Comm. (1977) 20, 119; Black, J.G., Yablonovitch, E., Bloembergen, N., and Mukamel, S. (to be published).
(6) Coggiola, M.J., Schulz, P.A., Lee, Y.T., and Shen, Y.R., Phys. Rev. Lett. (1977) 38, 17; Grant, E.R., Coggiola, M.J., Lee, Y.T., Schulz, P.A., and Shen, Y.R., Chem. Phys. Lett. (to be published).
(7) See, for example, review articles by Letokhov, V.S. and Moore, C.B., Sov. J. Quantum Electronics (1976) 3, 259 [English translation: Kvantovaia Elektronika (1976) 3, 485]; Lyman, J.L. and Rockwood, S.D., Proc. Conference on Lasers and Electro-Optics, Anaheim, Calif. (Nov., 1975) (to be published) and references therein.
(8) Recently, Gower, M.C. and Billman, K.W. [Optics Comm. (1977) 20, 123] have claimed that they could observe multiphoton dissociation of SF_6 with a single laser shot in a gass cell.
(9) See, for example, Stones, J., Goodman, M.F., and Dows, D.A., J. Chem. Phys. (1976) 65, 5062; Mukamel, S. and Jortner, J., J. Chem. Phys. (1976) 65, 5204; Cotter, T.P., J. Chem. Phys. (to be published).

(10) Larsen, D.M. and Bloembergen, N., Optics Comm. (1976) 17, 254; Letokhov, V.S. and Makarov, A.A., Optics Comm. (1976) 17, 250; Mukamel, S. and Jortner, J., Chem. Phys. Lett. (1976) 40, 150; Hodgkinson, D.P. and Briggs, J.S., Chem. Phys. Lett. (1976) 43, 45.
(11) Kompa, K.L. in Ref. 1, and also paper given at the Laser Chemistry Conference, Steamboat Springs, Colorado (1976).
(12) See, for example, Robinson, P.J. and Holbrook, K.A., "Unimolecular Reactions" (J. Wiley, New York, 1972).
(13) Ambartzumian, R.V., Gorokhov, Yu A., Letokhov, V.S., Makarov, G.N., Ryabov, E.A. and Chekalin, N.V., Sov. J. Quantum Electron. (1976) 6, 437.
(14) Brunner, F., Cotter, T.P., Kompa, K.L., and Pruch, D., J. Chem. Phys. (in press).

In State-to-State Chemistry; Brooks, P., et al.;
ACS Symposium Series; American Chemical Society: Washington, DC, 1977.

5

Molecular Beam Chemistry: Reaction Dynamics and Substituent Effects on the Electronic State of Carbonium Ions Produced in Ion-Molecule Reactions

S. A. SAFRON and R. C. HORVAT

Chemistry Department, Florida State University, Tallahassee, FL 32306

With polyatomic reactants the vibrational energy level density within an electronic manifold is too great and the energy randomization time [1,2] too rapid (measured against collision times $\gtrsim 10^{-12}$s) to allow the production of molecules in particular, well-defined states. However, "state-to-state" chemistry does have meaning when one is concerned with the possible product electronic states; for, the dynamics [3], symmetry [4] and spin [5] "selection rules" may inhibit the reactants from forming certain of these states. In the reactions of

$$Cs^+ + RC\ell \longrightarrow R^+ + CsC\ell \qquad (1)$$

$$\longrightarrow R'^+ + R'' + CsC\ell \qquad (2)$$

the data from crossed ion-molecule beam experiments [6,7,8] suggest (for R = benzyl, o-, m- and p-tolyl, and phenyl) that R^+ is probably a ground state singlet ion in the forward direction but an excited singlet state ion in the backward direction. Moreover, the type of fragment, R'^+ and R", produced at low collision energy is restricted to those which have singlet ground states, in keeping with the "propensity" for spin conservation. At higher energies other fragments are found (as in typical mass spectra of the parent $RC\ell$). We report here further scattering experiments of Cs^+ on RX (with X = F, Cℓ and Br) similar to (1), which implicate the halogen in determing the spin state of the product R^+ and which show the effect on the reaction cross-section of various substituent groups on the benzene ring.

These investigations have been carried out in the same apparatus described previously [6,7] with only minor improvements. Angular and energy distributions have been measured for the R^+ product and standard contour diagrams have been constructed from the data [9]. The energies (ΔH_r) of reaction [10] and measured product appearance potentials (A.P.) are shown in Table I.

In State-to-State Chemistry; Brooks, P., et al.;
ACS Symposium Series; American Chemical Society: Washington, DC, 1977.

Table I

Reactant RX	ΔH_r(eV)	A.P.(eV)
benzyl fluoride	2.2	~3.5
benzyl chloride	1.6	~3
benzyl bromide	1.5	<3
fluorobenzene	5.0	7.0
chlorobenzene	4.4	5.9
bromobenzene	4.3	4.6

The contour diagrams of the scattering experiments at about 9eV collision energy show remarkable similarity among the three benzyl halide systems and between the chlorobenzene and bromobenzene systems. Fluorobenzene has too small a reactive cross-section for us to obtain sufficient data to construct a contour diagram.

The pertinent results for this discussion are shown in Table II for the collision energy E, the maximum

Table II

Reactant RX	E(eV)	E'_{max}(eV)	W'_{min}(eV)
benzyl fluoride	9.2	4.4	2.6
benzyl chloride	9.5	5.5	2.4
benzyl bromide	9.3	6.2	1.6
chlorobenzene	8.9	3.4	1.1
bromobenzene	8.9	4.8	0

recoil energy for backward scattered product E'_{max} and the calculated minimum internal energy for this product W'_{min}. On the basis of the residual W'_{min} for benzyl chloride, it was suggested in [6] that the backward scattered benzyl ion was in the first excited singlet state. The data here for benzyl fluoride suggest a similar fate for its benzyl ion, but the benzyl bromide data point to a lower lying ion energy state, the triplet state. (A calculation for excited benzyl ions [11] gives 2.73 eV for the $^1B_1$ and 2.17 eV for the $^3B_1$ state above the ground $^1A_1$ state.) This behavior is consistent with the well-known enhancement of intersystem crossings by the heavier halogens compared to the lighter ones due to increased spin-orbit coupling [12].

Indeed, the same behavior can been seen for the halobenzenes. In [8] it was suggested that the phenyl ion product was formed in a singlet state, excited by ~1-1.5 eV above the ground state, based on the residual W'_{min} and the reaction A.P. This is in rough agreement with the A.P. for the fluorobenzene reaction. However, the bromobenzene data, both W'_{min} and A.P., suggest a lower energy product state, namely the ground state triplet (contrary to a calculation [13], but not intuition).

In State-to-State Chemistry; Brooks, P., et al.;
ACS Symposium Series; American Chemical Society: Washington, DC, 1977.

Scattering experiments were also tried on several ring substituted chlorobenzenes and one bromobenzene, the summary of the results of which are shown in Table III.

Table III

Reactant RX	Reactive Scattering Features
chlorobenzene	Strongly repulsive, backward scattered $C_6H_5^+$ [8].
o-, m- and p-chlorotoluenes	Direct reactions and complex formation, $C_7H_7^+$ probably rearranged to tropylium and benzyl ions [7].
o- and m-dichlorobenzenes	No R^+ formation; a few minor fragments produced.
o-, m- and p-chloroanisoles	No R^+ formation; a few minor fragments produced.
p-bromoanisole	No R^+ formation; a few minor fragments produced.

These substituents generally promote reactions which involve attack by positive ions on the ring π orbital electrons. In every case, except for the chlorotoluenes which react by rearranging [7], type (1) reactions are not observed. The charge in the R^+ ion is evidently produced, at least initially, in a σ-type orbital, which these substituents severely disfavor. Further theoretical work is obviously needed to explain the electronic coupling of the ring to the substituent, which stabilizes positive charge formation in π orbitals, but which suppresses such charge formation in σ molecular orbitals.

Literature Cited

1. D. L. Bunker and W. L. Hase, J. Chem. Phys. (1973) 59, 4621.
2. For example, J. F. Durana and J. D. McDonald, J. Chem. Phys. (1976) 64, 2518.
3. For example, B. H. Mahan, Accounts Chem. Res. (1975) 8, 55.
4. For example, D. L. King, D. A. Dixon, and D. R. Herschbach, J. Am. Chem. Soc. (1974) 96, 3328.
5. For example, J. C. Tully, J. Chem. Phys. (1974) 61, 61.
6. S. A. Safron, G. D. Miller, F. A. Rideout and R. C. Horvat, J. Chem. Phys. (1976) 64, 5051.
7. G. D. Miller and S. A. Safron, J. Chem. Phys. (1976) 64, 5065.
8. R. C. Horvat, G. D. Miller and S. A. Safron, J. Am. Chem. Soc. (1976) 98, 8274.
9. To be published.
10. J. L. Franklin, J. G. Dillard, H. M. Rosenstock, J. T. Herron, K. Drexl and F. H. Field, "Ionization Potentials, Appearance Potentials and Heats of Formation of Gaseous

Positive Ions", National Bureau of Standards, Washington, D. C., 1969.
11. C. Bertheuil, C. R. Acad. Sci. (Paris) (1963) 256, 5097.
12. N. J. Turro, "Molecular Photochemistry", Benjamin, New York, 1967.
13. C. G. Swain, J. E. Sheats, D. C. Gorenstein and K. G. Harbison, J. Am. Chem. Soc. (1975) 97, 791.

In State-to-State Chemistry; Brooks, P., et al.;
ACS Symposium Series; American Chemical Society: Washington, DC, 1977.

6

Reaction Product Identification from $O(^3P)$ + Benzene, Toluene, and 1,3,5-Trimethylbenzene Collisions

THOMPSON M. SLOANE

Physical Chemistry Department, General Motors Research Laboratories, Warren, MI 48090

Reactions of oxygen atoms with aromatic hydrocarbons have received a great deal of attention in recent years because of their potential importance in combustion processes and in atmospheric chemistry. (1) This paper presents the results of product analysis of single reactive collisions at room temperature between $O(^3P)$ atoms and benzene, toluene, and 1, 3, 5 - trimethylbenzene.

The apparatus used in these experiments consisted of a quadrupole mass spectrometer housed inside a two-chamber, diffusion-pumped, stainless steel vacuum system. The major features of the design were similar to the apparatus employed by Foner and Hudson. (2) The beam intersection angle was 60°.

Products were observed at m/e = 94 and 66 for the reaction of $O(^3P)$ with benzene. The product at m/e = 94 is a long-lived C_6H_6O complex which, if stable, is probably phenol. The product at m/e = 66 corresponds to the complex minus a molecule whose mass is 28. a.m.u., undoubtedly carbon monoxide. The ionization efficiency measurement for this C_5H_6 hydrocarbon product is shown in Figure 1. There appears to be a small amount of product with an ionization threshold near 9.0 eV, and a much larger amount with a threshold near 9.6 eV. Cyclopentadiene has an ionization potential of about 9 eV. Molecules similar to 3-penten-1-yne have ionization potentials in the range 9.8 to 10.2 eV. (4) Assuming that 3-penten-1-yne has an ionization potential close to those compounds, the major product at m/e = 66 is likely to be this open-chain C_5H_6 hydrocarbon. The less intense product is probably cyclopentadiene.

The hydrocarbon product must be in its ground electronic state for two reasons. First, the reaction would be too endothermic ($\Delta H \simeq 20$ kJ/mol) to take place at these low kinetic energies if the product were electronically excited. Second, the measured ionization potential would be about 3 eV smaller for the excited product.

Products were observed at m/e = 108, 106, and 80 for the reaction of oxygen atoms with toluene. These three product

In State-to-State Chemistry; Brooks, P., et al.;
ACS Symposium Series; American Chemical Society: Washington, DC, 1977.

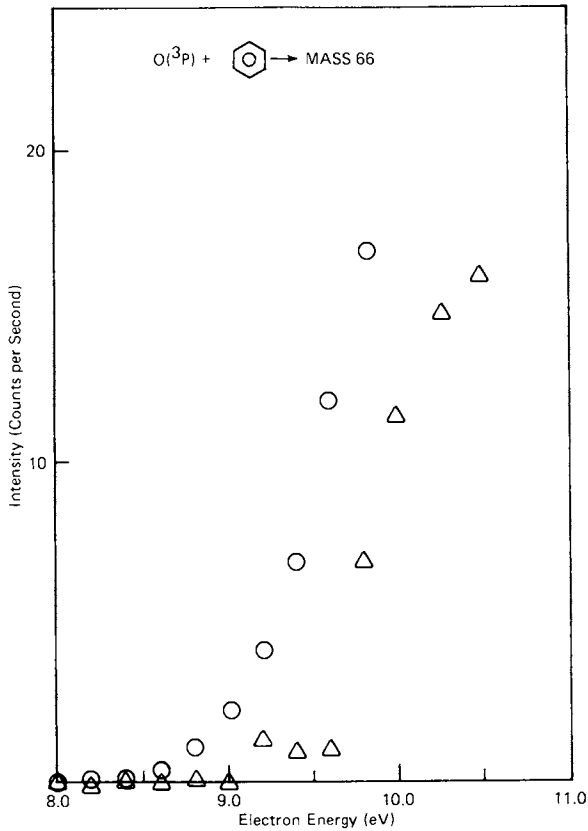

Figure 1. Ionization efficiency measurement for the O(³P) + benzene reaction product at m/e = 66. ○—measured intensity; △—intensity corrected for the finite energy width of the ionizing electrons using the procedure in Ref. 3.

masses correspond to the three products observed for $O(^3P)$ + 1, 3, 5 - trimethylbenzene. Since more extensive data were obtained for this latter reaction, the results for $O(^3P)$ + toluene will not be discussed further.

The reaction of $O(^3P)$ with 1, 3, 5 - trimethylbenzene yielded products at m/e = 136, 134, and 108. Figure 2 shows the ionization efficiency measurement for the product at m/e = 136. The ionization threshold is about 8.2 eV. This product could be 2, 4, 6 - trimethylphenol, 3, 5 - dimethylanisole, or 3, 5 - dimethylbenzyl alcohol. Since it is unclear how the internal energy of the $C_9H_{12}O$ adduct (~400 kJ/mol if it is the ground electronic state) might affect an ionization potential measurement, no conclusion can be drawn about this product's structure.

The ionization efficiency measurement for the product at m/e

= 134 is shown in Figure 3. A likely product at this mass is 3, 5 - dimethylbenzaldehyde because the ionization potential of methylbenzaldehyde is 9.33 eV. (4)

The ionization efficiency measurement for the product at m/e = 108 is shown in Figure 4. As in the case of $O(^3P)$ + benzene, when CO leaves the adduct the ring may close to form trimethylcyclopentadiene (I.P. = 7.96 eV (4)) or remain open to given an open-chain olefin similar to hydrocarbons having ionization potentials ranging from 8.6 to 9.1 eV. Although the measured data were too noisy for correction, they indicate that at least a major fraction of the products at m/e = 108 is an open-chain olefin rather than trimethylcyclopentadiene.

A reaction path which was not observed for these reactions is the hydrogen atom abstraction path to produce OH and an aromatic radical. Even if the aromatic radical is scattered "backward," it should still be observed due to poor beam collimation.

Tests for the participation of reactions of $O(^1D)$ or $O_2(^1\Delta)$ in the O atom beam and for reactions in the ionizer showed that these possible interfering processes were negligible.

The correlation diagram of Figure 5 shows for $O(^3P)$ + benzene that ground state reactants should correlate with excited products. The observed products must then be produced by a spin-

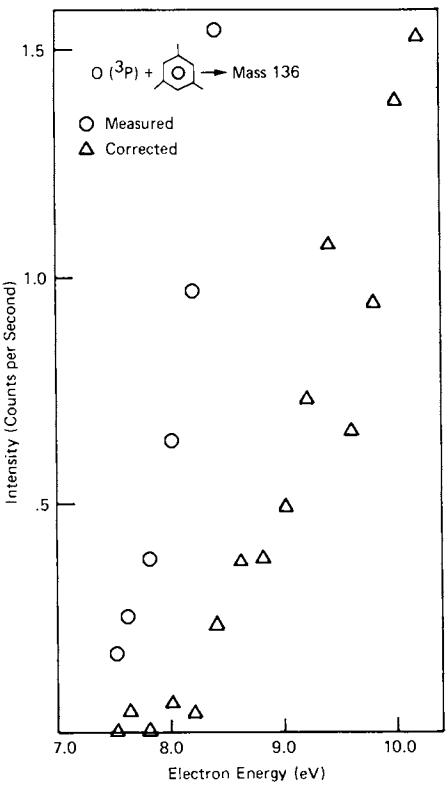

Figure 2. Ionization efficiency measurement for the $O(^3P)$ + 1,3,5-trimethylbenzene reaction product at m/e = 136

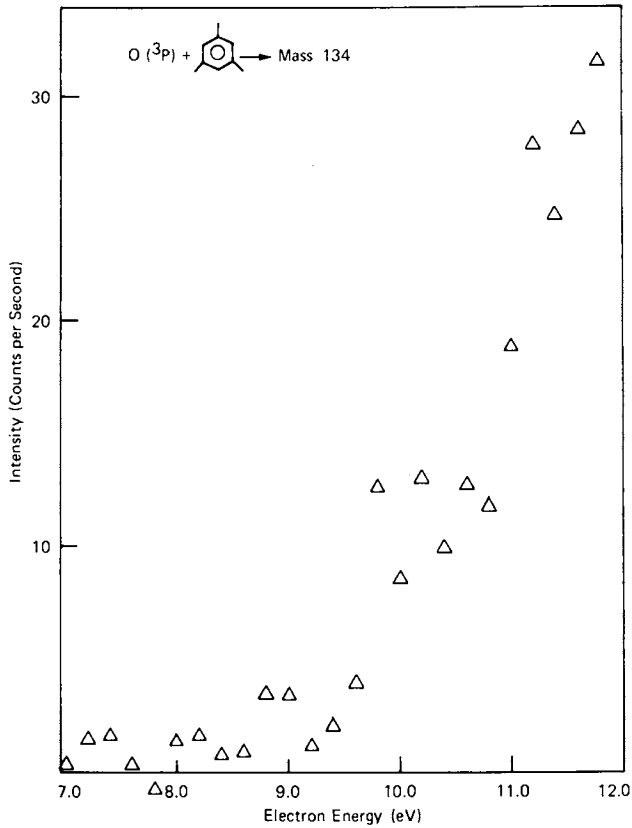

Figure 3. Ionization efficiency measurement for the O(^{3}P) + 1,3,5-trimethylbenzene reaction product at m/e = 134. Only the corrected measurement is shown.

forbidden process. Tully has successfully explained the rapid rates of a number of spin-forbidden reactions. (5) To determine whether his theory may explain the spin-forbidden nature of the O + benzene reaction, the following two questions must be answered: (1) is the lowest triplet state of phenol (T_1) long-lived enough? (2) Is the crossing region between T_1 and S_0 easily accessible during the lifetime of the complex?

To answer the first question, the RRKM lifetime of T_1 was estimated. For a relative kinetic energy of 2.7 kJ/mol, the estimated lifetime was 10^{-8} seconds. A crossing pointed located near the minimum of a 1300 cm^{-1} vibration could be traversed 3.5×10^5 times during this lifetime.

In order to answer the second question, that of the access-

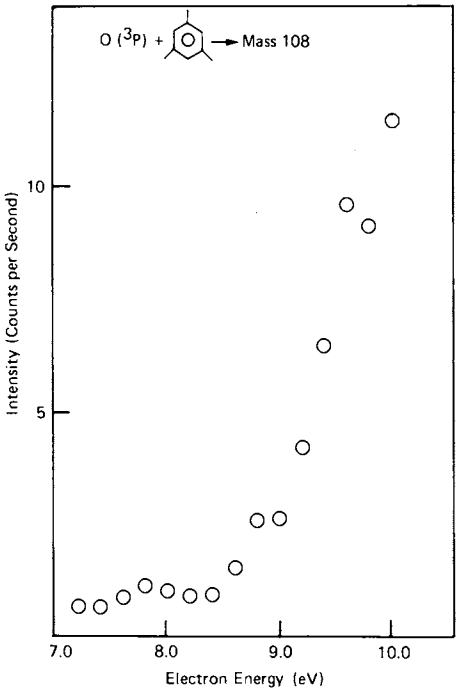

Figure 4. Ionization efficiency measurement for the O(³P) + 1,3,5-trimethylbenzene reaction product at m/e = 108. Only the uncorrected measurement is shown.

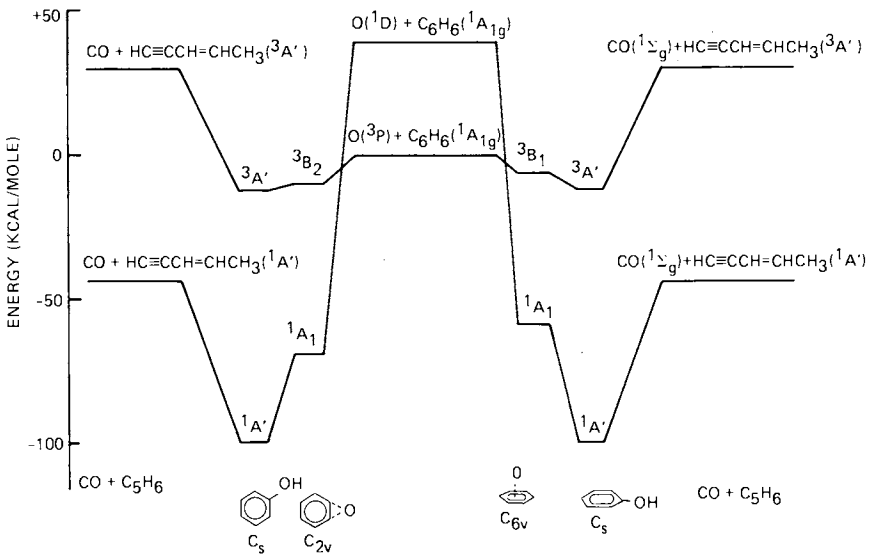

Figure 5. Electronic state correlation diagram for the O(³P) + benzene system

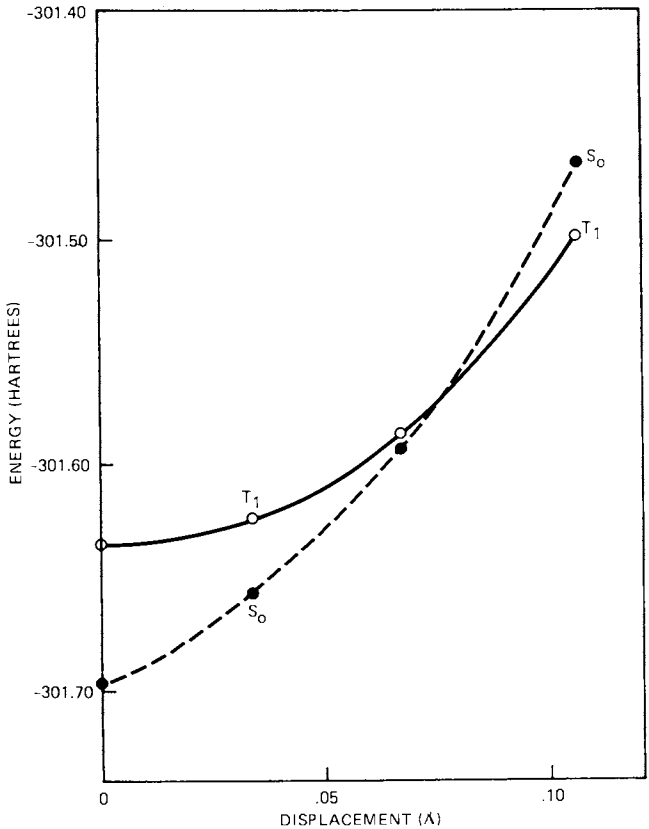

Figure 6. Energy of the T_1 and S_0 states of phenol as a function of displacement from the T_1 minimum along a ring stretching vibrational mode

ibility of the crossing region, calculations were carried out with the ab initio SCF-MO program Gaussian 70 (6) using the STO-3G basis set. (7) The T_1 and S_0 potential energy surfaces along eight vibrational modes of phenol were explored. For one mode, a crossing was located about 160 kJ/mol above the minimum energy configuration of T_1. The results for this mode are shown in Figure 6. Due to the primitive nature of these limited basis set single-configuration calculations, the relative positions of the two surfaces are uncertain. The two surfaces probably cross but where the crossing is located with respect to the minimum in the T_1 surface cannot be determined with chemical accuracy from these calculations.

These RRKM and molecular orbital calculations indicate that Tully's theory of spin-forbidden reactions is a plausible explanation for the spin-forbidden nature of the $O(^3P)$ + benzene and

methylbenzene reactions. More accurate calculations would be helpful in explaining more clearly the details of these reactions.

Literature Cited

1. See Colussi, A. J., Singleton, D. L., Irwin, R. S., and Cvetanovic, R. J., J. Phys. Chem., 79, 1900-3 (1975), and references cited therein.
2. Foner, S. N., and Hudson, R. L., J. Chem. Phys., 53, 4377-86 (1970).
3. Winters, R. E., Collins, J. H., and Courchene, W. L., J. Chem. Phys., 45, 1931-37 (1966).
4. Franklin, J. L., Dillard, J. C., Rosenstock, H. M., Herron, J. T., Draxl, K., and Field, F. H., "Ionization Potentials, Appearance Potentials, and Heats of Formation of Gaseous Positive Ions," NSRDS-NBS 26, U. S. Government Printing Office, Washington, D.C., 1969.
5. Tully, J. C., J. Chem. Phys., 62, 1893-8 (1975).
6. Hehre, W. J., Lathan, W. A., Ditchfield, R., Newton, M. D., and Pople, J. A., GAUSSIAN 70, Program #136, Quantum Chemistry Program Exchange, Indiana University, Bloomington, Indiana.
7. Hehre, W. J. and Pople, J. A., J. Amer. Chem. Soc., 92, 2191-7 (1970).

In State-to-State Chemistry; Brooks, P., et al.;
ACS Symposium Series; American Chemical Society: Washington, DC, 1977.

7

Threshold Behavior for Collision-Induced Dissociation*

E. K. PARKS, S. H. SHEEN, G. DIMOPLON, and S. WEXLER

Chemistry Division, Argonne National Laboratory, Argonne, IL 60439

A fundamental collisional process at elevated energies is the dissociation of a molecule into two or more fragments via a collision with a third body. This so called collision-induced dissociation (CID) has been observed extensively in ion-molecule reactions (1) and, in more recent years, between neutral species (2-4). CID of the alkali and thallium halides to ion pairs has been studied in this laboratory for the last few years, and the threshold behavior for the process has been determined (4,5).

Typical reactions observed are

$$M + CsCl \rightarrow M + Cs^+ + Cl^-$$
$$\rightarrow CsM^+ + Cl^-$$

for the monomer and

$$M + Cs_2Cl_2 \rightarrow M + Cs_2Cl^+ + Cl^-$$
$$\rightarrow M + Cs^+ + CsCl_2^-$$

for the dimer. The experiments involve accelerating the M species by the seeded jet method, with H_2 as the propellant, and crossing the beam of M with a beam of the cesium or thallium halide. The ions formed are then mass analyzed (by a TOF method) and counted. Absolute cross sections are obtained from the ion yields and the measured intensities of the two beams.

The behavior of the cross section as a function of energy for a few of the above reactions is shown in Figures 1, 2 and 3 with M = Xe, Kr, and SF_6 respectively. In Figure 1, both the $CsXe^+$ and CID channels are shown. The $CsXe^+$ product (from rearrangement ionization) shows a "step" behavior characteristic of reactions leading to oppositely charged ions (but no additional particles). The CID channel exhibits a power law rise in the threshold region and a less rapid rise at higher energies. The dashed lines in the

*Work performed under the auspices of USERDA.

In State-to-State Chemistry; Brooks, P., et al.;
ACS Symposium Series; American Chemical Society: Washington, DC, 1977.

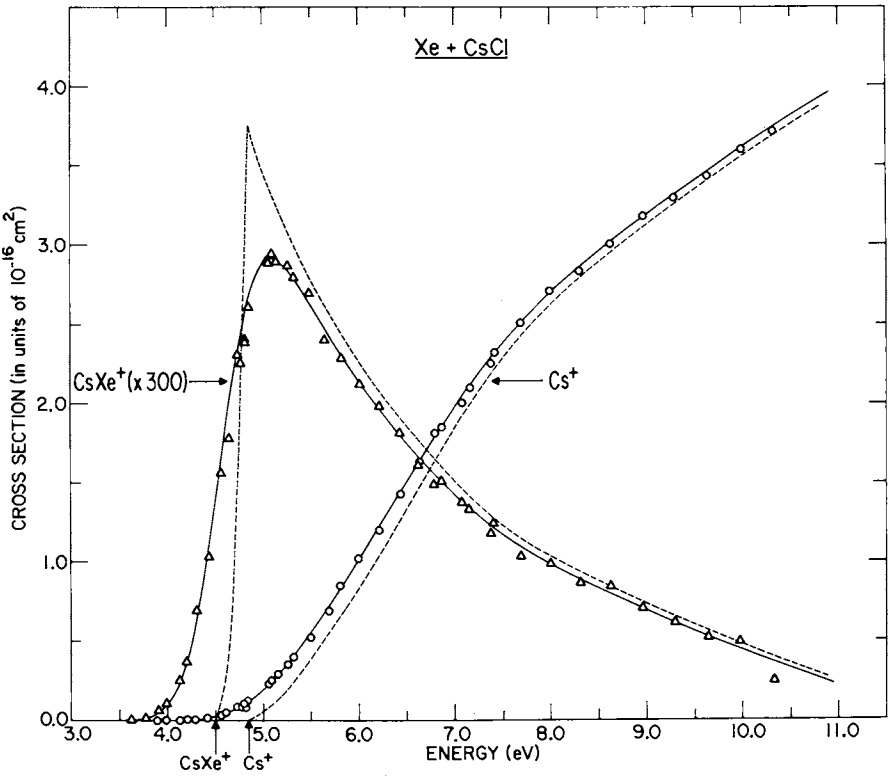

Figure 1. Cross sections for Cs^+ and $CsXe^+$ formation in Xe–CsCl collisions as functions of the center-of-mass kinetic energy

figures are the assumed cross sections, and the solid lines are the result of convoluting the latter with the various energy distributions in the experiments.

For CID, the power law

$$\sigma = A_o(E_{tot}-E_o)^n/E_{rel} \qquad (1)$$

was assumed to be operative in the threshold region, where E_o is the threshold energy, E_{tot} is the total energy (kinetic plus internal), and E_{rel} is the initial relative kinetic energy. This functionality has been obtained by a number of authors (6,7) from statistical theory for an atom-diatom reaction, with values of n of approximately 1.8-1.9. While A_o is in general a function of the internal energy of the diatom, it was assumed constant in our analysis. Values of A_o, E_o and n for the various systems studied are given in Table I.

In State-to-State Chemistry; Brooks, P., et al.;
ACS Symposium Series; American Chemical Society: Washington, DC, 1977.

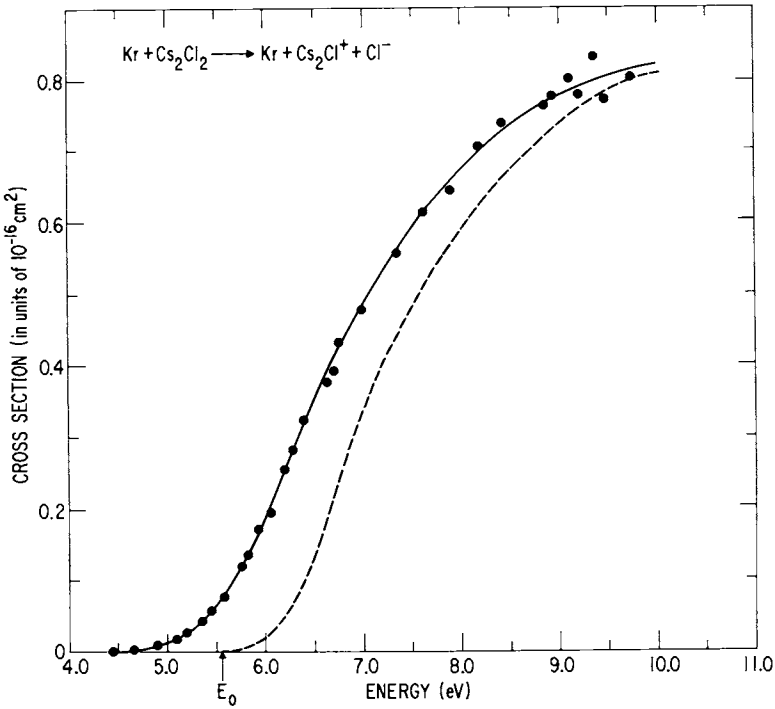

Figure 2. Cross sections for Cs_2Cl^+ formation in $Kr–Cs_2Cl_2$ collisions as a function of the center-of-mass kinetic energy

Experiments on the large number of systems in Table I demonstrate that Eq. (1) gives a good description of CID up to about 1 eV above threshold, and appears to be valid even for reactions which are decidedly not statistical (dissociation of TlF, for example, is probably a very dynamically constrained process (5)). This suggests the increase in the number of continuum states with increasing energy (which determines the functionality of Eq. (1)) dominates the threshold behavior irrespective of the reaction mechanism.

The specific (non-statistical) effect of internal energy of the diatom on the CID cross section has been studied only for TlCl (4). If the observed effect is taken into account in the coefficient A_0, the power n must be raised from ∿1.6 to ∿1.8 to fit the experimental data. If we assume a similar effect for the other atom-diatom reactions, then most of the n values in the upper section of Table I are in reasonable agreement with the 1.8-1.9 value obtained from statistical theory. The two high values for TlBr (2.0 and 2.3) result from a low transition probability to the ionic surface. If this is specifically taken into account in the co-

In State-to-State Chemistry; Brooks, P., et al.;
ACS Symposium Series; American Chemical Society: Washington, DC, 1977.

efficient A_0, both powers are lowered to ∿1.6 (excluding the internal energy correction). The high values of n for TlI are probably due to the same cause; however CID in TlI is also dynamically constrained (3), making similar corrections to the powers for this molecule intractable.

For the atom-dimer reactions, the same threshold analysis leads to higher powers of n ranging from 2.1 to 2.7. The high

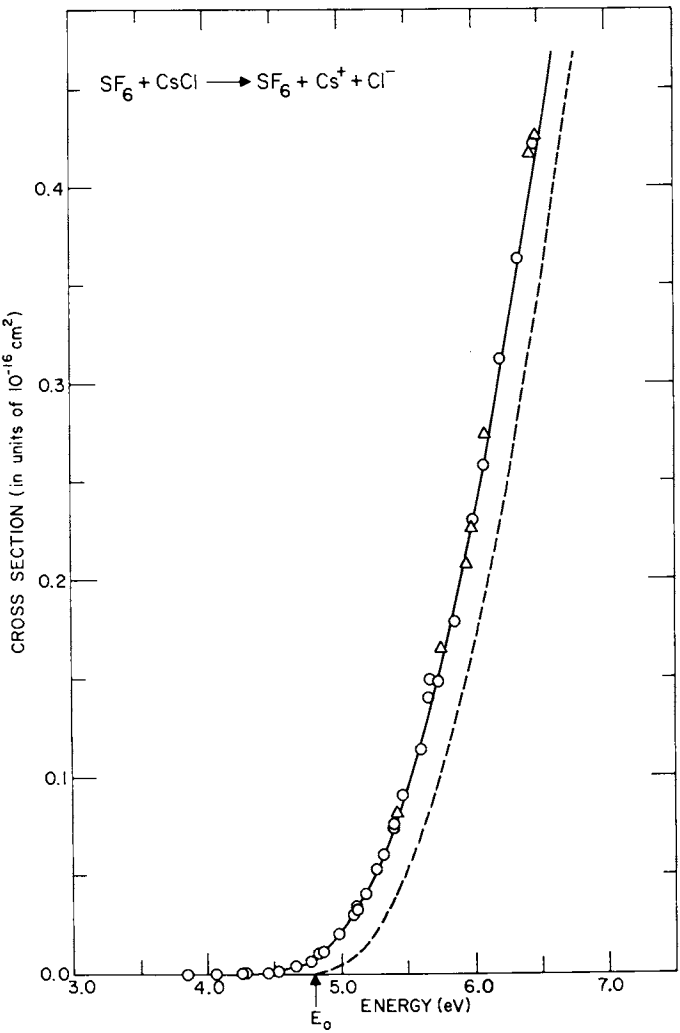

Figure 3. Cross sections for Cs^+ formation in SF_6–CsCl collisions as a function of the center-of-mass kinetic energy

powers are most likely due to the presence of energetically accessible internal states of the product molecular ions. As the collision energy increases, an increasing number of internal states becomes accessible, and thus the cross section, based on a statistical model, would rise more rapidly than in the atom-diatom case, where only the ground states of the products are accessible. This point of view is consistent with the results for SF_6 given in Table I. Since the SF_6 can absorb energy in the collision, the powers obtained for SF_6 would be expected to be higher than for analogous collisions involving the inert gases. Indeed, the increase in power from monomer to dimer, which reflects the additional internal states of the Cs_2Cl^+ product-ion, is approximately the same for SF_6 collisions (2.4 → 3.5) as for the inert gas collisions (1.5 → 2.5).

Table I: $\sigma = A_o(E_{tot}-E_o)^n/E_{rel}$

System	A_o ($cm^2 \cdot eV^{(1-n)} \cdot 10^{16}$)	E_o (eV)	n
$Xe+CsCl \rightarrow Xe+Cs^+ + Cl^-$	4.02	4.85±.08	1.5 ±.1
$Kr+CsCl$	6.64	4.85±.08	1.4 ±.1
$Ar+CsCl$	6.44	4.85±.08	1.4 ±.1
$Xe+TlF$	0.152	7.15±.08	1.85±.1
$Kr+TlF$	0.114	7.23±.08	1.95±.1
$Xe+TlCl$	1.41	6.31±.08	1.6 ±.1
$Kr+TlCl$	1.48	6.25±.08	1.45±.1
$Xe+TlBr$	0.063	6.17±.08	2.0 ±.1
$Kr+TlBr$	0.0077	6.20±.08	2.3 ±.1
$Xe+TlI$	0.00092	6.40±.08	2.1 ±.1
$Kr+TlI$	0.00118	6.40±.08	2.1 ±.1
$Xe+Cs_2Cl_2 \rightarrow Xe+Cs_2Cl^+ + Cl^-$	0.482	5.55±.1	2.65±.2
$Kr+Cs_2Cl_2$	1.00	5.60±.1	2.70±.2
$Ar+Cs_2Cl_2$	2.17	5.30±.1	2.70±.2
$Xe+Tl_2F_2$	0.139	8.1 ±.2	2.6 ±.2
$Kr+Tl_2F_2$	0.306	8.1 ±.2	2.7 ±.2
$Xe+Tl_2Cl_2$	2.30	6.6 ±.3	2.4 ±.3
$Xe+Tl_2Br_2$	6.17	6.1 ±.15	2.4 ±.2
$Kr+Tl_2Br_2$	6.03	6.2 ±.15	2.1 ±.2
$Xe+Tl_2I_2$	2.30	5.45±.2	2.45±.3
$SF_6+CsCl \rightarrow SF_6+Cs^+ + Cl^-$	0.600	4.75±.08	2.4 ±.1
$SF_6+Cs_2Cl_2 \rightarrow SF_6+Cs_2Cl^+ + Cl^-$	0.0501	5.65±.15	3.5 ±.1

Literature Cited

1. McClure, G.W. and Peek, J.M., "Dissociation in Heavy Particle Collisions" (Wiley-Interscience, New York, 1972).
2. Tully, F.P., Lee, Y.T. and Berry, R.S., Chem. Phys. Lett. (1971) 9, 80.

In State-to-State Chemistry; Brooks, P., et al.;
ACS Symposium Series; American Chemical Society: Washington, DC, 1977.

3. Parks, E.K., Hansen, N.J. and Wexler, S., J. Chem. Phys. (1973) 58, 5489.
4. Parks, E.K., Wagner, A. and Wexler, S., J. Chem. Phys. (1973) 58, 5502.
5. Parks, E.K., Kuhry, J.G. and Wexler, S., J. Chem. Phys. (in press).
6. Rebick, C. and Levine, R.D., J. Chem. Phys. (1973) 58, 3942.
7. Wagner, A. and Parks, E.K., (unpublished results).

In State-to-State Chemistry; Brooks, P., et al.;
ACS Symposium Series; American Chemical Society: Washington, DC, 1977.

8

Fourier Transform Doppler Spectroscopy: A New Tool for State-to-State Chemistry

JAMES L. KINSEY

Department of Chemistry, Massachusetts Institute of Technology, Cambridge, MA 02139

To achieve a complete description of the states of reactants or products in a chemical reaction, it is necessary to specify the translational states of the participants. A somewhat coarser level of detail still might include the dependence of the rate on the magnitude of the initial or final relative velocity. Molecular beam reactive scattering experiments are the principal sources of data on translational-energy dependence. For reactants this is achieved through velocity selection and for products by the combination of velocity analysis and angular distributions. In measurements involving resonant absorption or emission of light, the Doppler effect furnishes a different means of access to velocity information potentially as detailed as that attained by direct velocity analysis. This approach appears especially promising in measurements employing laser-induced fluorescence.

To first order, the Doppler shift ν_D in an absorption line produced by a velocity component of magnitude w in the direction of propagation of the incident light is given by $\nu_D = w/\lambda$ where λ is the wavelength of the resonant radiation. Under conditions that the main source of linewidth is Doppler broadening, the line shape directly reflects the sample's distribution in w. Such a one-dimensional determination at first seems inadequate for the general situation, since the Doppler effect is blind to the transverse velocity components. It has recently been demonstrated (1), however, that the set of Doppler profiles as a function of the direction of propagation of incident light can be directly inverted to recover the full three-dimensional velocity distribution $F(\underset{\sim}{v})$ of the sample, irrespective of the nature of $F(\underset{\sim}{v})$.

Let $D(w;\underset{\sim}{n})$ be the distribution in the parallel velocity component w as exhibited by the Doppler line profile for light incident along the direction of the unit vector $\underset{\sim}{n}$. The equivalence of $D(w;\underset{\sim}{n})$ and $F(\underset{\sim}{v})$ is established by the demonstration that the one-dimensional Fourier transform of $D(w;\underset{\sim}{n})$ is identical to the three-dimensional Fourier transform of $F(\underset{\sim}{v})$, evaluated along a line parallel to $\underset{\sim}{n}$ in Fourier space (1). I.e. if

In State-to-State Chemistry; Brooks, P., et al.;
ACS Symposium Series; American Chemical Society: Washington, DC, 1977.

$G(\underset{\sim}{k})\equiv\int d^3\underset{\sim}{v}F(\underset{\sim}{v})\exp(2\pi i\underset{\sim}{k}\cdot\underset{\sim}{v})$ then $\int dwD(w;\underset{\sim}{n})\exp(2\pi iKw)=G(\underset{\sim}{n}K)$. Hence, the term, Fourier-transform Doppler spectroscopy (FTDS).

In the conventional molecular beam experiments, angular distributions are accomplished with a detector that views only those molecules with velocities directed into a selected well-defined solid angle. Consequently, the magnitude of the signal is limited by the small solid angle subtended ($d^2\Omega$) no matter what means is used to probe the distribution in speed. FTDS affords an average gain over this method of $4\pi/d^2\Omega$ in the rate of signal acquisition, since every molecule formed has some value of the velocity component parallel to $\underset{\sim}{n}$ regardless of how $\underset{\sim}{n}$ is chosen. Estimation of the signal/noise improvement is more complex and depends on the nature of the noise as well as of the velocity distribution, but there are no circumstances in which FTDS has disfavorable signal/noise compared to conventional methods with equivalent detector characteristics.

Certain experimental arrangements permit simplified forms of FTDS, for example, processes of the type $A^*+B\rightarrow C+D$ where A^* is prepared by Doppler-selective absorption of light. In this case, the quantity whose velocity distribution is monitored will be the reaction rate $R(w;\underset{\sim}{n})=k(w;\underset{\sim}{n})[A^*(w;\underset{\sim}{n})]$ where $[A^*]$ is the concentration of A^* and k is the specific rate coefficient. If these measurements are carried out in a static gas, neither $[A^*]$ nor k depends on the direction $\underset{\sim}{n}$. The Fourier-transform relationship still holds, but takes on a simplified form: $-(2\pi w)^{-1}dR(w;\underset{\sim}{n})/dw=F(|\underset{\sim}{v}|)$ where F gives the dependence of the reaction rate on the magnitude of the vector $\underset{\sim}{v}$. For this technique to work, it is necessary that the observed process occur before the prepared A^* is translationally relaxed, but this is easily guaranteed if the radiative lifetime of A^* is short compared to the collision time.

Processes of the type $A^*+B\rightarrow C^*+D$ where A^* is selectively prepared using the Doppler effect and C^* is observed by a Doppler-selective method can be subjected to a similar analysis. Let $R(w_A, w_C; \underset{\sim}{n}_A, \underset{\sim}{n}_C)$ be the observed rate where A^* is selected at velocity component w_A parallel to $\underset{\sim}{n}_A$ and C^* is analyzed at component w_C parallel to n_C in a static gas. It is evident that this rate can depend only on the two magnitudes w_A, w_C and the angle between the two laser beams $\gamma_{AC}=\cos^{-1}(\underset{\sim}{n}_A\cdot\underset{\sim}{n}_C)$. The Fourier transform of this quantity (with respect to both w_A and w_C) can be inverted to obtain the six-dimensional distribution $F(\underset{\sim}{v}_A,\underset{\sim}{v}_C)$ giving the dependence rate on the vectors $\underset{\sim}{v}_A$ and $\underset{\sim}{v}_C$. However, this F can depend only on: $|\underset{\sim}{v}_A|, |\underset{\sim}{v}_C|, \theta_{AC}=$ angle between $\underset{\sim}{v}_A,\underset{\sim}{v}_C$. Hence, in principle the use of two lasers to measure the Doppler profiles of both reactant and product in a static gas can yield the reaction rate as a function of initial and final velocity and scattering angle. Again, it is necessary that the process being

In State-to-State Chemistry; Brooks, P., et al.;
ACS Symposium Series; American Chemical Society: Washington, DC, 1977.

studied occur with unrelaxed A^*, and that unrelaxed C^* be detected. The kernel for inversion of $D(w_A,w_C;\gamma_{AC})$ into $F(|\underline{v}_A|,|\underline{v}_C|,\theta_{AC})$, which results from integration over redundant angles in the six-dimensional Fourier transform, is not easily expressible in terms of simple functions, but it is susceptible to numerical computation.

Literature Cited

1. Kinsey, J. L., J. Chem. Phys. (1977), 66, 2560-2565.

9

Total Cross Section Measurements of the Reaction K + HCl → KCl + H as a Function of Translational Energy

M. W. GEIS, H. DISPERT, T. L. BUDZYNSKI, and P. R. BROOKS

Department of Chemistry, Rice University, Houston, TX 77001

The rates of most chemical reactions are accelerated when the temperature is raised, and this has long been interpreted as evidence for an energy requirement (the "activation energy") in excess of any thermodynamic requirement. This activation energy has traditionally been supplied by heating the reagents, but energy transfer among reagent modes is so rapid that no information is obtained to identify the critical mode for reaction. But, by isolating molecules in molecular beams, it becomes possible to prepare reagents in specific states, and for the prototype reaction K + HCl → KCl + H we have studied the results of vibrationally exciting HCl (1) and (separately) of increasing the kinetic energy of the reacting molecules (2). Both forms of energy increase the reaction cross section, but translational energy [T] is much less effective (10x) than vibrational energy [V] even at energies 50% higher than the HCl vibrational energy (8.3 kcal/mole). We have increased the range of translational energy [T] to see if further addition of [T] can ever be as effective as only one quantum of [V]. Our preliminary results suggest that this is not the case, and that the cross section maximizes near 10 kcal/mole for [T].

The difference between [T] and [V] is not clearly understood, although various theoretical studies on model potential energy surfaces have given some insight (3,4). Quite apart from considerations of the potential surface, we should recognize that a vibrationally excited molecule brings into a collision less angular momentum than does a translationally excited molecule (at the same impact parameter). Consequently, different product states will be populated in the two cases. The experimental rate constant will change with energy depending not only on how the number of available product states change, but also on how the state-to-state rate constant changes with energy. By dividing out the purely statistical variation of the available states, attention can then be drawn to the dynamically interesting variation in the state-to-state rate constant, $\bar{\omega}$. Analysis of our earlier data (2) suggested that $\bar{\omega}$ was an exponentially

In State-to-State Chemistry; Brooks, P., et al.;
ACS Symposium Series; American Chemical Society: Washington, DC, 1977.

decaying function of the energy in excess of the thermodynamic requirement, and simple extrapolation of $\bar{\omega}$ beyond our measurements predicted that the experimental cross section would decline at higher energies. The present measurements were undertaken to verify this prediction and are qualitatively consistent with this analysis.

The apparatus is largely described in reference 2. Briefly, it consists of five differentially pumped chambers in which a thermal K beam and supersonic, seeded, HCl beam cross at right angles. The angular distribution of scattered KCl is measured with a rotatable surface ionization detector; K beam intensity is monitored with an auxiliary surface ionization detector, and HCl intensity is monitored with a quadrupole mass spectrometer. Various HCl speeds are obtained by mixing ("seeding") small amounts of HCl in H_2; hydrodynamic expansion of the mixture "bumps" the HCl along to a faster speed determined by the composition of the mixture and the expansion conditions. By increasing the nozzle temperature, both the H_2 and, consequently, the HCl speeds are further increased. Changing either the temperature or composition of the gas mixture to vary the energy changes the intensity of the HCl beam, and it is necessary to carefully normalize cross sections measured under different conditions. For this reason the data collection apparatus has been modified to allow rapid comparision among data taken under different conditions. The HCl beam is chopped, the detector is rotated with a stepping motor, and a multichannel analyzer (MCA) records the beam-on and beam-off scattering as a function of angle. The MCA is interfaced to a computer which subtracts the two signals and calculates the area under the curve. A typical angular distribution obtained in this way is shown in Figure 1. Cross sections are calculated from beam intensities and integrated scattering intensities as described in reference 2.

The variation of the reactive cross section with [T] is shown in Figure 2. Velocity analyses of the HCl beam have not yet been performed, but, because of favorable kinematics, the HCl speed can be deduced from the maxima of the angular distributions, which are essentially the centroid angles. Because of slight uncertainties in collision energies, and because no allowance has yet been made for the effect of different rotational energies at different nozzle temperatures, the results must be regarded as preliminary. Nevertheless, the trend is clear: the cross section does not increase for energies higher than 10 kcal/mole. The results also qualitatively confirm the exponential decrease in the state-to-state rate constant extracted from the earlier results. While the factors responsible for this decay are not yet known, we note that contrary to the usual explanations no new channels are opening up to compete with reaction.

We are pleased to acknowledge financial support from the

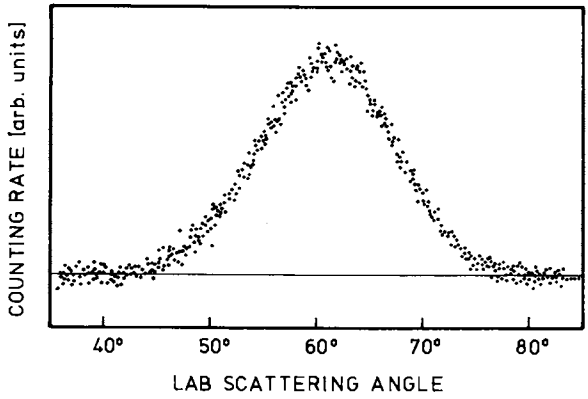

Figure 1. Laboratory angular distribution of scattered KCl for a collision energy of 7.9 kcal/mol

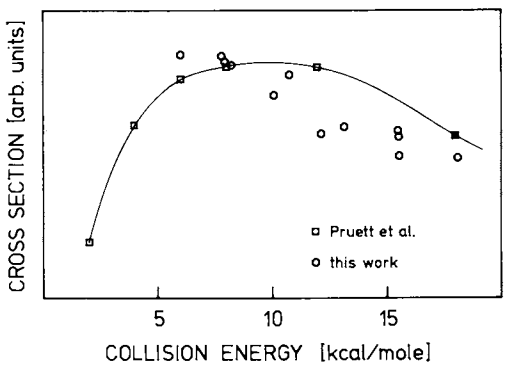

Figure 2. Reactive cross section for $K + HCl \rightarrow KCl + H$ as a function of center of mass translational energy. Circles display present results, open squares are experimental points of Ref. 2, and the closed square is the result of extrapolating the state-to-state rate constant of Ref. 2.

Robert A. Welch Foundation and from the Air Force Office of Scientific Research.

Literature Cited

1. Odiorne, T. J., Brooks, P. R., and Kasper, J. V. V., J. Chem. Phys., (1971), 55, 1980.
2. Pruett, J. G., Grabiner, F. R., and Brooks, P. R., J. Chem. Phys., (1975), 63, 1173.
3. Polanyi, J. C., and Wong, W. H., J. Chem. Phys., (1969), 51,1439.
4. Mok, M. H., and Polanyi, J. C., J. Chem. Phys., (1969), 51, 1451.

10

Inter- and Intramolecular Energy Transfer Deduced from Macroscopic Infrared Laser Chemistry

ERNEST GRUNWALD, CHARLES M. LONZETTA, and KENNETH J. OLSZYNA
Brandeis University, Waltham, MA 02154

As recently as three years ago, many experts in molecular dynamics thought that chemical activation by means of infrared lasers was not likely to be both practical and useful. There were essentially two reasons for this view. (1) The kinds of reactions which it would be most useful to induce have relatively high activation energies, in the range of 50-120 kcal/mole. Such energies are considerably greater than those of individual infrared photons: at 1000 cm^{-1}, $h\nu$ is equivalent to only 2.86 kcal/mole; and there were reasons to doubt that the required many-photon absorption could take place even at high infrared intensities. (2) It makes no economic sense to use expensive infrared radiation rather than conventional burner heat unless the radiatively activated molecules react more efficiently or in a distinctive, more desirable manner. Yet there were reasons to fear that the absorbed infrared energy at all but very low pressures might degrade into essentially random thermal energy prior to reaction.

That many-photon absorption takes place efficiently under suitable conditions is by now well established. For instance, the activation energy for decomposition of SF_6 is equivalent to that of ~ 29 photons at 940 cm^{-1}, yet decomposition is readily induced. Absorption and decomposition can be made preferential for a specific sulfur isotope of SF_6 by irradiating, at an appropriate frequency near 940 cm^{-1}, in short pulses at Gw/cm^2 peak intensities, under "collision-free" conditions at pressures well below 1 torr.

At Brandeis University we have studied infrared

In State-to-State Chemistry; Brooks, P., et al.;
ACS Symposium Series; American Chemical Society: Washington, DC, 1977.

laser chemistry at higher pressures, usually in the range of 10-100 torr, well above the "collision-free" range. The amounts of material used in our experiments are large enough to permit the monitoring of reaction yields and products by familiar methods of infrared analysis and gas-liquid chromatography. We use a tunable pulsed CO_2 laser with peak intensities around 1 Mw/cm^2 and effective pulse durations of 250-800 ns. In order to have approximately uniform excitation of the reactant gas, most experiments are done so that no more than 30% of the incident radiant dose is absorbed in the reaction cell.

Because our experiments are done well above the "collision-free" range, they provide information concerning the extent to which the absorbed energy becomes degraded into random thermal energy prior to reaction. For the sake of greater clarity, we shall limit this presentation to one specific example, the laser-induced decomposition of $CHClF_2$, which a group at Brandeis University consisting of the authors and D. F. Dever and B. Knishkowy has studied in some detail.

Relevant Properties of $CHClF_2$.

Homogeneous gas-phase pyrolysis of $CHClF_2$ yields C_2F_4 and HCl as primary products. Kinetics and thermochemistry are consistent with the following two-step mechanism. (1,2)

(1) $CHClF_2 \rightleftharpoons CF_2 + HCl$

$E_{act} = 234$ kj/mole; $\Delta H^\circ = 207$ kj/mole

(2) $CF_2 + CF_2 \rightarrow F_2C = CF_2$

Rate constant $\sim 10^7 - 10^8$ s^{-1} M^{-1} (2)

Because step (1) is reversible, the apparent rate constant decreases with progress of reaction. The initial rate constant is represented by the empirical equation

(3) $\log k = 12.60 - 11540/T$ (1)

The nine normal-mode frequencies of $CHClF_2$ have been reported to be 3023,1347,1311,1178,1114,809,595,

In State-to-State Chemistry; Brooks, P., et al.;
ACS Symposium Series; American Chemical Society: Washington, DC, 1977.

422, and 365 cm^{-1}. (3) Our laser was tuned to 1088 cm^{-1}; and its frequency is within the bandwidth of the antisymmetric CF_2 stretching band centered at 1114 cm^{-1}.

Vibration-to-translation/rotational relaxation (V-T/R relaxation) of $CHClF_2$ has been studied by ultrasonic measurements. (4) Relaxation from the first excited vibrational level (365 cm^{-1}) appears to be rate-determining; about 200 gas-kinetic collisions are required.

Photophysics of $CHClF_2$ at 1088 cm^{-1}.

Amount of energy absorbed per mole of irradiated gas (E_{abs}) was measured as a function of dose (or fluence D), effective pulse duration (τ), and pressure (P). For comparison with properties of the energy-absorbing oscillators, it is convenient to express E_{abs} as a multiple of the energy per mole of 1088 cm^{-1} photons.

$$(4) \quad E_{abs} = v_{abs} N_0 h\nu$$

v_{abs} is the mean excitation number of the oscillators, and $N_0 h\nu$ = 13.02 kj/einstein at 1088 cm^{-1}. Representative data, obtained at a fixed $CHClF_2$ pressure of 50 torr, are listed in Table I. The accuracy of v_{abs}/D is about 10%.

Table I. Irradiation of $CHClF_2$ (50 torr) at 1088 cm^{-1}

τ (ns)	v_{abs}	v_{abs}/D [a] (j^{-1} cm^2)	f [b] (%)
270	5.11	22.6	15.7
	4.01	22.5	3.0
	3.14	21.2	0.59
	2.00	18.0	0.030
	1.17	14.7	---
800	3.81	24.2	2.6

[a] Calculated from (5): 22.8 j^{-1} cm^2 at 50 torr

[b] Percent of $CHClF_2$ converted per flash to the products, C_2F_4 + HCl.

Numerous experiments in the pressure range 1.6 to 100 torr may be summarized as follows: When $v_{abs} > 2$ and $\tau = 270$ ns, at fixed pressure v_{abs} is practically proportional to D, up to values as high as $v_{abs} = 8.5$. The proportionality constant varies with pressure and is reproduced quite adequately by:

$$(5)\quad v_{abs}/D = 1.50 + 30.64\ \frac{P}{(P+22.06)}$$

The high-pressure limit according to (5) is 32.1 j^{-1} cm^2. Within experimental error, this limit has been reached in experiments at higher total pressure, involving an added nonabsorbing gas, but has not been exceeded. For low-intensity non-laser irradiation, v_{abs}/D is ~ 20 j^{-1} cm^2. The small increase in v_{abs}/D with increasing τ, shown in Table I, is not clearly significant.

Photochemistry.

The products and reaction mechanism of laser-induced decomposition of $CHClF_2$ are essentially identical with those of thermal pyrolysis and thus are described by (1) and (2). C_2F_4 and HCl are the stable products; the amount of product per flash decreases as HCl accumulates; and the intervention of CF_2 as a metastable intermediate is demonstrated by kinetic spectroscopy. Representative values of conversion per flash (f) during the initial 10-20% reaction of $CHClF_2$ are listed in Table I. It can be seen that f is highly sensitive to v_{abs}. Closer analysis shows that a 10% change in v_{abs} causes about a 40% change in f.

Effect of Cell Geometry. In an attempt to determine whether the laser-induced reaction proceeds by a thermal mechanism, experiments were performed in which the surface/volume ratio of the irradiated gas was varied. Other variables, such as E_{abs}, pulse duration, gas pressure and composition were kept constant. If reaction were proceeding by a thermal mechanism, one would expect a smaller conversion per flash in the experiments with the greater surface/volume ratio in which the laser-heated gas cools more quickly

Results, which cover a representative range of pressure and E_{abs}, are listed in Table II. Because

In State-to-State Chemistry; Brooks, P., et al.;
ACS Symposium Series; American Chemical Society: Washington, DC, 1977.

in comparable experiments, deviations of E_{abs} from exact equality owing to experimental error may be as high as 10%, differences in f of < 40% are not statistically significant. Actual differences in f, on increasing the surface/volume ratio, range from +29% to -9%. Thus, within the experimental error, the amount of reaction per flash is unaffected by the cooling dynamics.

Table II. Effect of Cell Geometry

P (torr)	E_{abs} (kj/mole)	Surface/Volume [a]	f(%) (obs)	f(%) (calc.) C+R	f(%) (calc.) C+R+M
14.2	32.0	2.8	0.17	(0.17)	(0.17)
		7.0	0.22	0.044	0.018
13.0	75.5	2.8	15.2	(15.2)	(15.2)
		7.0	15.5	4.5	1.7
29.5	110.7	2.8	49.8	(49.8)	(49.8)
		4.5	45.2	37	21

[a] cm^{-1}. Cell radius = 1 cm; cell length = 2.6, 0.8, or 0.4 cm.

The last two columns in Table II show model predictions for the hypothetical case that reaction proceeds by a thermal mechanism. In each case, the energy absorbed from the infrared beam by hypothesis is converted rapidly into random thermal energy and thus produces a T-jump. Reaction then takes place according to the known thermal rate constant while the gas is cooling back to room temperature. In model C+R, cooling takes place by thermal conduction and radiation only. In model C+R+M, cooling by conduction and radiation is accompanied by mass flow so as to produce perfect mixing and a gas phase of uniform temperature throughout. Although neither model is quite realistic, the calculated results suggest that the experimental changes in cell geometry should have produced marked differences in f if the reaction were proceeding by a thermal mechanism.

Kinetic Spectroscopy. The formation and decay of CF_2 following an infrared laser flash can be

monitored by ultraviolet kinetic absorption spectroscopy in the region of the $\bar{X}^1A_1 \rightarrow \bar{A}^1B_1$ absorption band near 250 nm. (2,5-7) Typical results of percent transmission (% T) vs. time along an axis parallel to that of the infrared laser beam are shown in Figs. 1 and 2. The upper horizontal trace indicates 100% T; The lower one indicates 52% T in Fig. 1 and 0% T in Fig. 2. Fig. 1 is recorded at 500 μs/division and shows the rapid rise and much slower decay of the CF_2 concentration. Fig. 2 is recorded at 5 μs/division and details the initial rise of the CF_2 concentration. (The two experiments are not duplicates.) The oscillations of the CF_2 concentration in both Figures are due to acoustical standing waves, a perturbation discussed by Bates et al. (8), and will be neglected for the present.

Of interest in the present context is the kinetics of the initial rise in the CF_2 concentration. In Fig. 2, the vertical signal on the left is the output of a photon drag detector and indicates the laser pulse. This is followed by a reproducible lag of ~ 1 μs, and then by a rise in the CF_2 concentration with a rise half-time which varies between 5 and 15 μs in different experiments. The rise half-time is much shorter than one would expect for a mechanism of temperature jump-followed-by-thermal-reaction. For instance, one experiment in which E_{abs} was measured, the maximum temperature after the hypothetical temperature jump was 1200° K at which temperature the half-time for thermal decomposition of $CHClF_2$ is 720 μs, (12), while the observed rise half-time of the CF_2 absorption was only 15 μs. It seems clear, both from kinetic spectroscopy and from the effect of cell geometry on product yield, that laser-induced decomposition of $CHClF_2$ does not proceed by a thermal mechanism.

Effect of Molecular Collisions During Laser Pulse.

If it be granted that decomposition takes place from a nonequilibrium molecular energy distribution, then the nature of that distribution, and in particular the fraction of molecules with energy in excess of the activation energy for decomposition, should have a marked effect on the product yield. This fraction will be greatest if the energy remains in the original levels of excitation, and becomes reduced as additional levels become populated owing to inelastic collisions.

In State-to-State Chemistry; Brooks, P., et al.;
ACS Symposium Series; American Chemical Society: Washington, DC, 1977.

Thus a study of reaction yield as a function of laser pulse duration and gas pressure should give information about inelastic collisions.

Effect of Pulse Duration. Data for f vs. τ at otherwise constant conditions are listed in Table III for a threefold change in τ and representative values of P and v_{abs}. As in previous comparisons, differences of f of < 40% are not statistically significant. Bearing this in mind, f is independent of τ, with a high statistical probability, under all conditions.

Table III Effect of Pulse Duration on Yield per Flash for $CHClF_2$ at 1088 cm^{-1}.

P (torr)	v_{abs}	τ (ns)	f (%)	$\delta f/f$ x 10^2	Z_τ [a]
50/$CHClF_2$	3.81	270	2.1		177
		800	2.6	+ 24	524
9.4/$CHClF_2$	3.78 [b]	270	1.6		33
		800	1.7	+ 6	99
9.4/$CHClF_2$	5.16 [b]	270	11.6		33
		800	8.8	- 24	99
50/$CHClF_2$	7.26	270	0.11		850
+ 250/N_2		800	0.11	0	2500

[a] $Z_\tau = 1.31 \times 10^7 P\tau$, where P is in torr and τ in seconds (4).

[b] Measured with a pyroelectric energy meter. Absolute value of v_{abs} is less accurate, but comparison of f at two values of τ is as precise as in experiments with a disc calorimeter.

Table III also lists values of Z_τ, the mean number of gas-kinetic collisions experienced by a molecule of $CHClF_2$ during the time τ. For neat $CHClF_2$, these values range from 33 to 524 and bracket the value of Z_{10}, 268 collisions, required for V-T/R relaxation of $CHClF_2$. (4)

In State-to-State Chemistry; Brooks, P., et al.;
ACS Symposium Series; American Chemical Society: Washington, DC, 1977.

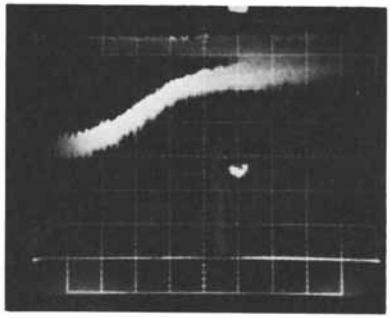

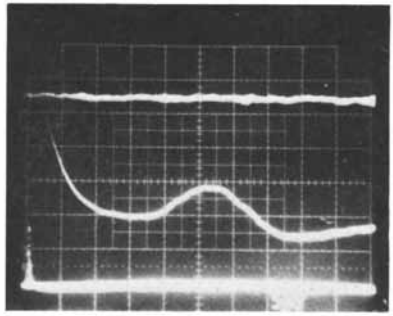

Figures 1 and 2. Kinetic spectroscopy of $CHClF_2$ (14 Torr) after megawatt infrared flash irradiation at 1088 cm^{-1}

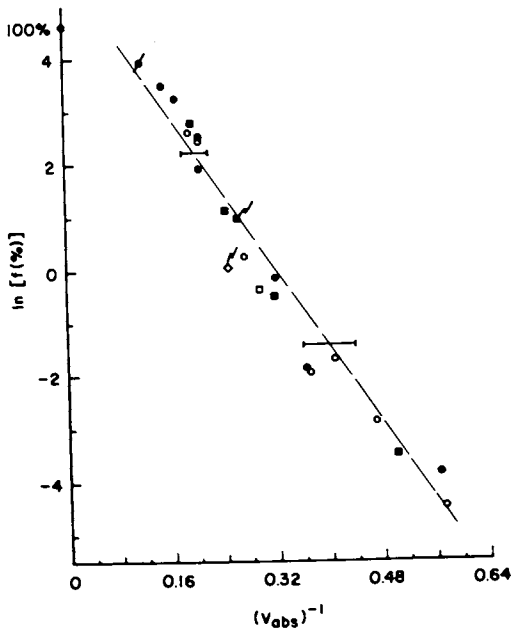

Figure 3. Photochemical results for neat $CHClF_2$ as a function of pressure. ● 100 Torr, ■ 50 Torr, ● 29.5 Torr, ○ 14.2, 13.7, 13.0 Torr, □ 5.8 Torr, ◇ 1.6 Torr. Points marked by a flagellum, $\tau = 800$ ns; others, $\tau = 270$ ns. The dashed line is drawn with a slope equivalent to $E_{act} = 234$ kj/mol.

In State-to-State Chemistry; Brooks, P., et al.;
ACS Symposium Series; American Chemical Society: Washington, DC, 1977.

Effect of Pressure. Results for f vs. v_{abs} for neat $CHClF_2$ are plotted in Fig. 3. As indicated in the caption, the data span the pressure range from 100 torr to 1.6 torr. Between 100 and 5.8 torr, all experimental points clearly define a single, pressure-independent relationship. The deviation from this relationship at 1.6 torr is only marginally significant. Thus, both variations of τ and of pressure show consistently that the relationship between f and E_{abs} is independent of the number of collisions which the absorbing molecules experience during the time of the laser pulse. In the 100 to 5.8 torr experiments plotted in Fig. 3, Z_τ ranges from 500 to 20 collisions.

Exponential Dependence on E_{abs}^{-1}. It has been found in previous studies (9-11) that the variation of f with E_{abs} at pressures and excitation energies similar to those studied in the present work conforms rather well to the equation, where A is a parameter of

$$(6) \quad f = A \exp(-E_{act}/E_{abs})$$

order unity and E_{act} is the activation energy of the laser-induced primary decomposition step. In the present case E_{act} = 234 kj/mole (v_{act} = 18.0). Accordingly, the dashed line in Fig. 4 represents the relationship, f(%) = constant x exp $(-18.0/v_{abs})$, which clearly gives a respectable fit.

Discussion.

Three conclusions seem to emerge from our results. (1) The laser-induced decomposition of $CHClF_2$ under the present conditions does not proceed by a thermal mechanism. (2) The amount of energy absorbed from a given dose increases with the pressure and approaches asymptotically to a high-pressure limit. (3) For a given amount of absorbed energy, the amount of reaction per flash is independent of the number of collisions during the flash.

Because of (3), we infer that collisions during the laser flash do not alter the molecular energy distribution. Moreover, because the energy is being absorbed in quanta of $h\nu$, the radiation field, by the same inference, constrains the excitation energies of

In State-to-State Chemistry; Brooks, P., et al.;
ACS Symposium Series; American Chemical Society: Washington, DC, 1977.

the molecules to integral multiples of $h\nu$. That is, the levels of excitation are equidistant, just like those of a harmonic oscillator.

In previous publications from this laboratory (9, 10) the working hypothesis was made that the molecular energy distribution among the equidistant levels of excitation is a Boltzmann distribution for a single harmonic oscillator. On that basis, the relationship between f and E_{abs} could reasonably be expressed by Eq. (6), in agreement with available data.

Acknowledgment.

It is a pleasure to acknowledge financial support by the National Science Foundation.

Literature Cited

(1) Barnes, R.G., Cox, R.A., Simmons, R.F., J. Chem. Soc. B (1971) 1176.
(2) Dalby, F.W., J. Chem. Phys. (1964) 41 2297.
(3) Plyler, E.K. and Benedict, W.S., J. Research Natl. Bureau Stand., (1951) 47 202.
(4) Rossing, T.D. and Legvold, S., J. Chem. Phys. (1955) 23, 1118.
(5) Mathews, C.W., Canad. J. Physics (1967) 45 2355.
(6) Mann, D.E. and Thrush, B.A., J. Chem. Phys. (1960) 33 1732.
(7) Modica, A.P. and LaGraff, J.E., J. Chem. Phys. (1965) 43 3383.
(8) Bates, R.D., Flynn, G.W., Knudtson, J.T., J. Chem. Phys. (1970) 53 3621.
(9) Dever, D.F. and Grunwald, E., J. Amer. Chem. Soc. (1976) 98 5055.
(10) Grunwald, E. and Olszyna, K., Laser Focus (1976) 12 (6), 41.
(11) Preses, J.M., Weston, R.E., Flynn, G.W., Chem. Phys. Letters (1977) 46 69.
(12) Because of the 207 kj/mole endothermicity of reaction (1) and the relative slowness of reaction (2), the temperature drops as CF_2 is formed so that decomposition by the T-jump mechanism appears to be self-quenching. We estimate a minimum rise half-time of 300 μs.

11

Temperature Dependence of the Reaction of Nitric Oxide and Vibrationally Excited Ozone

ROBERT J. GORDON, JERRY MOY, and EZRA BAR-ZIV

Department of Chemistry, University of Illinois at Chicago Circle, Chicago, IL 60680

There currently is considerable interest in the chemistry of vibrationally excited molecules. By selecting the vibrational states of reagents it is possible to control the rates and pathways of chemical reactions. Such experiments can provide detailed information regarding microscopic reaction mechanisms.

Particular attention has been paid to the gas phase reaction of nitric oxide and ozone. Clough and Thrush (1) showed that there are two reactive channels, one producing electronically excited NO_2^*, and the other yielding ground state NO_2. It has been found that the rates of both processes are increased by an order of magnitude when either O_3 (2-5) or NO (6) is vibrationally excited.

In the present study we have used a pulsed CO_2 laser to populate $O_3(001)$ in a rapidly flowing mixture of NO, O_3 and Ar, while monitoring the visible chemiluminescence from NO_2^*. With the laser off, a steady signal, I_{dc}, was detected. When the laser was fired a certain fraction, f, (4-8%) of the ozone molecules was vibrationally excited. The enhanced reaction rate of the excited molecules resulted in a rapid increase in the chemiluminescence, followed by a slow ($\sim 10^{-4}$ sec) decay. A simple kinetic model (2, 7) consisting of the reactions

$$\begin{aligned}
NO + O_3(000) &\xrightarrow{k_{1a}} NO_2^* + O_2, \\
&\xrightarrow{k_{1b}} NO_2 + O_2, \\
NO + O_3(001) &\xrightarrow{k_{2a}} NO_2^* + O_2, \\
&\xrightarrow{k_{2b}} NO_2 + O_2, \\
&\xrightarrow{k_3} NO + O_3(000),
\end{aligned}$$

In State-to-State Chemistry; Brooks, P., et al.;
ACS Symposium Series; American Chemical Society: Washington, DC, 1977.

$$NO_2^* + NO \xrightarrow{k_4} NO_2 + NO,$$

predicts that the decaying part of the laser-induced signal is described by the function

$$I(t) = A \exp(-k_{23}[NO]t) - B \exp(-k_1[NO]t) \quad (1)$$

where $k_{23} = k_{2a} + k_{2b} + k_3$, $k_1 = k_{1a} + k_{1b}$, and A and B are constants. The second term in Eq. (1) arises from the fact that at large t, when the $O_3(001)$ is consumed, there is a net depletion of $O_3(000)$, resulting in a faster than exponential decay of I(t). (A more complete model (8) including coupling to $O_3(010)$ does not alter the conclusions presented here.) The peak value of I(t), denoted by I_{ac}, is related to the dc signal by the expression (7)

$$I_{ac}/I_{dc} = (R_a-1)X_o/f, \quad (2)$$

where R_a is the enhancement ratio for the chemiluminescent reaction,

$$R_a = k_{2a}/k_{ta}, \quad (3)$$

X_o is the mole fraction of $O_3(000)$, and k_{ta} is the thermal rate coefficient (1) of the luminescent reaction.

Our objective in this study was to determine the temperature dependence of k_{2a}, k_{2b}, and k_3. The ratio R_a was determined from measurements (7) of I_{ac}/I_{dc} and f over the temperature range 155-303 K. We found that R_a has an Arrhenius form,

$$R_a(T) = C \exp(\Delta E_a/\underset{\sim}{k}T) \quad (4)$$

where $C = 0.87^{+0.44}_{-0.55}$ and $\Delta E_a = 1.29^{+0.25}_{-0.22}$ kcal/mole (with 95% confidence). ΔE_a is the reduction in activation energy due to vibrational excitation. This value corresponds to 42% of the vibrational quantum supplied by the laser.

The total rate coefficient, k_{23}, was determined from the decay rate of I(t), which was measured over the temperature range 143-457 K (8). As shown in Fig. 1, an Arrhenius plot of k_{23} displays strong curvature. Similar behavior has been observed in other laboratories (3, 5). This non-Arrhenius curvature is due to the different temperature dependences of k_{2a}, k_{2b} and k_3. Approximate values of k_{2b} and k_3 were obtained

In State-to-State Chemistry; Brooks, P., et al.;
ACS Symposium Series; American Chemical Society: Washington, DC, 1977.

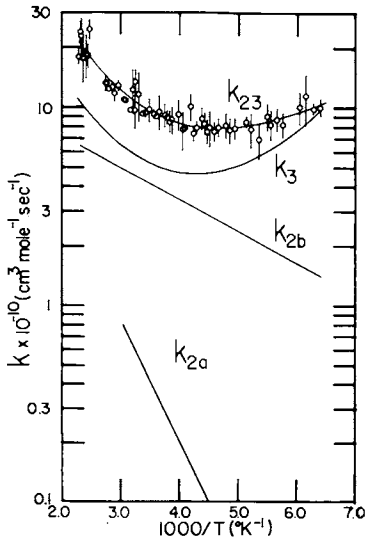

Figure 1. Arrhenius plot of k_{2a} *(the rate coefficient for the laser-enhanced luminescent reaction),* k_{2b} *(the rate coefficient for the non-luminescent reaction),* k_3 *(the relaxation rate coefficient), and the sum* $k_{23} = k_{2a} + k_{2b} + k_3$.

from an analysis of the shape of the laser-induced signal. From a least squares fit of the ratio A/B in Eq. (1), it was possible to estimate k_{2b} and k_3 (8). Results of this analysis are shown in Fig. 1. k_{2b} has an Arrhenius form, while k_3 has a minimum near 235 K. The activation energy associated with k_{2b} is lower than the thermal value by 1.6±0.4 kcal/mole, or by 53% of the vibrational energy.

From these experiments we conclude that vibrational energy is approximately 50% effective in overcoming the barrier in both reactive channels. This effect can be compared with the nearly 100% efficiency found for translational energy (9) and the very low efficiency predicted by information theory for exothermic reactions (10). The non-statistical behavior of these reactions, and the comparative inefficiency of vibrational vs. translational energy, are suggestive of a direct reaction mechanism with a barrier in the approach coordinate (11). The negative temperature dependence of k_3 at low temperatures is indicative of a strong chemical interaction in the non-reactive channel.

Literature Cited

1. Clough, P. N. and Thrush, B. A., Trans. Faraday Soc. (1967) 63, 915.
2. Gordon, R. J. and Lin, M. C., J. Chem. Phys. (1976) 64, 1058.

In State-to-State Chemistry; Brooks, P., et al.;
ACS Symposium Series; American Chemical Society: Washington, DC, 1977.

3. Kurylo, M. J., Braun, W., Xuan, C. N., and Kaldor, A., J. Chem. Phys. (1975) 62, 2065.
4. Freund, S. M. and Stephenson, J. C., Chem. Phys. Lett. (1976) 41, 157.
5. Hui, K. K. and Cool, T. A., to be published.
6. Stephenson, J. C. and Freund, S. M., J. Chem. Phys. (1976) 65, 4303.
7. Moy, J., Bar-Ziv, E., and Gordon, R. J., J. Chem. Phys. (1977) 66, 5439.
8. Bar-Ziv, E., Moy, J., and Gordon, R. J., to be published.
9. Redpath, A. E., Ph.D. dissertation (1976), University of Toronto.
10. Levine, R. D. and Manz, J., J. Chem. Phys. (1975) 63, 4280.
11. Polanyi, J. C. and Wong, W. H., J. Chem. Phys. (1969) 51, 1439.

In State-to-State Chemistry; Brooks, P., et al.;
ACS Symposium Series; American Chemical Society: Washington, DC, 1977.

12

CO Product Vibrational Energy Distribution in the $O(^3P) + C_3O_2$ Reaction

D. S. Y. HSU and M. C. LIN

Chemistry Division, Naval Research Laboratory, Washington, D. C. 20375

The reaction of the $O(^3P)$ atom with C_3O_2 (carbon suboxide) was proposed to be one of several possible laser pumping reactions in an electrically initiated C_3O_2/O_2/He pulsed chemical CO laser system (1). The $O + C_3O_2$ reaction has now been shown to occur mainly via the spin-forbidden path producing three ground electronic state CO molecules (2-4)

$$O(^3P) + C_3O_2(^1\Sigma_g^+) \rightarrow 3CO(X\ ^1\Sigma^+) \qquad (1)$$

$$\Delta H_1^o = -115 \text{ kcal/mole.}$$

The spin-conserved route associated with the formation of CO_2 and C_2O, however, was found to be less than 0.2% of the overall rate (2). In order to understand the dynamics of this unique process, we employed a cw CO laser to measure the vibrational population of the CO formed in the initial stage of the reaction.

A detailed description of the laser-probing apparatus can be found elsewhere (5,6). A Pyrex flash tube was used in the present study to avoid the photodissociation of C_3O_2 below 300 nm. The $O(^3P)$ atom was generated by the photodissociation of NO_2. In all runs, 10 torr mixtures of C_3O_2 and NO_2, diluted with He or SF_6, were flash-photolyzed at 290°K. C_3O_2 was prepared by pyrolyzing the vapor of diacetyltartaric anhydride (7) at about 900°K, using a 10 mm ID x 500 mm length quartz tube. The products of decomposition were purified by trap-to-trap distillation employing appropriate slush baths. He, SF_6 and NO_2 were obtained in lecture bottles of the highest purity available from the Matheson Gas Products Company.

The CO vibrational population distribution was determined by analyzing the initial portion of the time-resolved absorption curves according to the method described previously (5,6). The initial distribution was evaluated by least-square extrapolating (5) the relative population ratios N_v/N_2 to the appearance time of absorption, 6.8 μsec after flash initiation. A typical mixture used in the experiments was $NO_2:C_3O_2:SF_6$ = 3:1:46, flashed at

In State-to-State Chemistry; Brooks, P., et al.;
ACS Symposium Series; American Chemical Society: Washington, DC, 1977.

0.64 kJ. The CO vibrational energy distributions presented in Table 1 were normalized to v=2 because of the presence of slight C_3O_2 dissociation near 300 nm producing a small amount of CO at v=0 and 1. However, corrections were made by photolyzing the mixtures of C_3O_2 and SF_6 under the same experimental conditions employed in the reaction.

Table 1. CO Vibrational Energy Distribution in the $O(^3P) + C_3O_2$ Reaction

V	0	1	2	3	4	5	6	7	8	9	10
Expt	4.0	1.7	1.0	.56	.35	.23	.15	.09	.06	.03	.01
Calc	2.5	1.6	1.0	.61	.36	.21	.12	.06	.03	.02	.01

To elucidate the dynamics of this rather unique reaction, we compared the observed distribution with that predicted by a simple statistical model based on the method employed previously (6,8). Assuming that the C_3O_2 complex consists of three indistinguishable CO-stretching modes, each having an average vibrational energy E_v, then the population of the CO molecules formed at the vth level in the $O + C_3O_2$ reaction can be estimated by the following expression,

$$N_v \propto \sum_{n \geq v \geq 0} g(n,v) \, (E_{tot} - nE_v + aE_z)^s \qquad (3)$$

where $g(n,v) = 3(n-v+1)$ represents the number of ways one can populate the vth level of the three CO modes with n vibrational quanta. $(E_{tot}-nE_v+aE_z)^s$ is a quantity which is proportional to the total number of ways (9) the remaining energy $(E_{tot}-nE_v)$ can be randomly distributed among the rest of vibrational modes, excluding the one which becomes the reaction coordinate. Practically, the choice of the reaction coordinate and the assignments of the vibrational frequencies of the activated complex are not critical in these calculations because the zero-point energy correction term, $aE_z = a\Sigma h\nu/2$ is unimportant at lower n's (or v's), which are more densely populated.

The predicted statistical distribution based on $E_{tot} = -\Delta H_1^o + E_a + 5RT/2 = 118.3$ kcal/mole (taking $E_a = 2.2$ kcal/mole (2) and $T = 290°K$), $E_v = 5.8$ kcal/mole and $s = 3N-6-4 = 8$, agrees closely with the observed distribution as shown in the Table. This seems to indicate that the $O + C_3O_2$ reaction probably occurs via a C_3O_3 complex which may survive several vibrations before breaking into three CO's. In a preliminary experiment carried out with $N^{18}O_2$, however, it was found that the $C^{16}O$ formed in the reaction is noticeably cooler. This finding could be explained by the following mechanism, using the labeled reaction as an example:

In State-to-State Chemistry; Brooks, P., et al.;
ACS Symposium Series; American Chemical Society: Washington, DC, 1977.

$$*O(^3P) + O{=}C{=}C{=}C{=}O \rightarrow O{=}C(*O){-}C{=}C{=}O \leftrightarrow O{=}C{-}C(*O){=}C{=}O \rightarrow$$

$$*OC^{\dagger} + (C_2O_2)^{\dagger} \rightarrow *OC^{\dagger} + 2CO^{\dagger}.$$

Since the attack of O atoms occurs sideways, the most likely reaction coordinate is the skeletal O=C=C=C=O bending motion. This bending vibration, aided by the overlapping of the unpaired electrons, may lead to the concerted decomposition of $*OC_3O_2$ into a hotter C*O and transient $(CO)_2$ that immediately dissociates into two CO's each carrying equal amount of energy. Further study on this reaction is underway; more detailed results will be reported in a future publication.

Literature Cited

1. Lin, M. C. and Bauer, S. H., Chem. Phys. Lett., (1970), 7, 223.
2. Pilz, C. and Wagner, H. Gr., Z. Physik. Chem., N. F., (1974), 92, 323.
3. Liuti, G., Kunz, C. and Dondes, S., J. Amer. Chem. Soc., (1967), 89, 5542.
4. Williamson, D. G. and Bayes, K. D., J. Amer. Chem. Soc., (1967), 89, 3390.
5. Lin, M. C. and Shortridge, R. G., Chem. Phys. Lett., (1974), 29, 42.
6. Shortridge, R. G. and Lin, M. C., J. Chem. Phys., (1976), 64, 4076.
7. Melville, H. and Gowenlock, B. G., "Experimental Methods in Gas Reactions", MacMillan and Co. Ltd., London, 1964, p. 197.
8. Lin, M. C., Shortridge, R. G., and Umstead, M. E., Chem. Phys. Lett., (1976), 37, 279.
9. Whitten, G. Z. and Rabinovitch, B. S., J. Chem. Phys., (1964), 41, 1883.

In State-to-State Chemistry; Brooks, P., et al.;
ACS Symposium Series; American Chemical Society: Washington, DC, 1977.

13

Infrared Chemiluminescence from F + RH and H + ClF Reactions

KEIETSU TAMAGAKE and D. W. SETSER

Department of Chemistry, Kansas State University, Manhattan, KS 66506

Infrared emission spectra from newly formed HF and HCl product molecules were observed under nearly arrested relaxation conditions with a cold wall reaction vessel at 77°K and a Digilab Fourier Transform Spectrometer. The reactions examined were F + HCl, HBr, HI, H_2S, GeH_4, CH_4, CH_3CH_3, CH_3Cl, CH_3Br, $C(CH_3)_4$, CH_3OCH_3 (plus some others not reported here) and H + ClF. The flow rates and pressure in the vessel were 0.5-30 μmol/sec and 0.5-5 x 10^{-5} torr, respectively. These experiments are an improvement over previous work from this laboratory and permit assignment of both the initial vibrational and rotational distributions of the HF and HCl product molecules.

F + RH

The data from the F + HCl reaction gave virtually the same vibrational and rotational distributions as previously reported (1). However, our results for the F + HBr and F + HI reactions have greater populations in the highest vibrational levels than the previous report (2), which was based on extrapolated distributions in a 1 torr fast flow reactor. With a few exceptions, the highest observed vibrational-rotational level is that permitted by the thermochemistry. In some cases the thermochemical limit is so close to v_{max} that only a few rotational levels are permitted and the relative population of v_{max} is low; an example is HCl for which only J=8 is permitted in the v=3 level. A similar limit holds for F + GeH_4. There also can be dynamical limitations such as for F + toluene (3). The most highly populated rotational levels are at high J for the diatomic cases, but for the polyatomic cases low J levels are favored. Initial vibrational distributions, P_v, and the fractions of the total available energy released to vibration, $\langle f_v \rangle$, and rotation, $\langle f_R \rangle$, of HF are listed in Table I. The reduced rotational energy for individual vibrational states $\langle g_R(v) \rangle = \langle f_R(v) \rangle / \langle 1-f_v \rangle$, and reduced total rotational energy $\langle g_R \rangle = \langle f_R \rangle / \langle 1-f_v \rangle$ also are listed. From the tables the following conclusions can be reached. (A) The vibrational distributions P_v and $\langle f_v \rangle$ are similar for both diatomic and

In State-to-State Chemistry; Brooks, P., et al.;
ACS Symposium Series; American Chemical Society: Washington, DC, 1977.

Table I. Summary of Vibrational and Rotational Energy Disposal

		HCl	HBr	HI	H_2S	CH_4	CH_3CH_3	CH_3Cl	CH_3Br	$C(CH_3)_4$	$(CH_3)_2O$	GeH_4
$\langle E \rangle$ kcal mole^{-1}		36.5	51	67	47	35	41	39	38	40	45	55
P_v	v = 1	.25	.12	.10	.23	.18	.12	.09	.11	.19	.27	.14
	v = 2	.63	.17	.12	.25	.69	.46	.36	.45	.64	.38	.20
	v = 3	.11	.30	.13	.34	.14	.42	.55	.44	.16	.35	.28
	v = 4		.41	.16	.18							.37
	v = 5			.22								.02
	v = 6			.28								
$\langle f_V \rangle$		.57	.63	.65	.57	.62	.61	.69	.67	.54	.51	.57
$\langle f_R \rangle$		.15	.13	.14	.12	.058	.055	.070	.069	.022	.084	.18
$\langle g_R^{(v)} \rangle$	v = 1	.43	.30	.29	.25	.24	.24	.32	.25	.039	.17	.43
	v = 2	.40	.35	.33	.30	.11	.13	.26	.22	.058	.17	.50
	v = 3	.52	.38	.37	.26	.10	.08	.13	.13	.015	.17	.42
	v = 4		.42	.40	.24							.26
	v = 5			.45								.26
	v = 6			.47								
$\langle g_R \rangle$		.35	.35	.40	.28	.15	.14	.23	.21	.049	.17	.42

In State-to-State Chemistry; Brooks, P., et al.;
ACS Symposium Series; American Chemical Society: Washington, DC, 1977.

polyatomic reagents. (B) The $\langle f_R \rangle$ is high (0.13-0.17) for diatomic and low (0.05-0.08) for polyatomic cases. (C) The triatomic molecule H_2S gives intermediate $\langle f_R \rangle$ (0.12). (D) the GeH_4 reaction is unusual and gives exceptionally high $\langle f_R \rangle$ like a diatomic case. (E) The $\langle g_R(v) \rangle$ values increase with v for diatomic reactants and decreases for polyatomic reactants. (F) The overall $\langle g_R \rangle$ for diatomic, triatomic and some polyatomic reagents (CH_3Cl, CH_3Br) are close to 0.4, 0.29, and 0.25, respectively. Such $\langle g_R \rangle$ values are expected if the remaining energy, after subtraction of the fraction released to vibration of HF, is distributed statistically between the 2 rotations of HF, the 3 relative translations plus 2 or 3 rotations of the parent radical (for tri- or polyatomic reagent, respectively). (G) The hydrocarbons CH_4, C_2H_6 and $C(CH_3)_4$ give smaller $\langle g_R \rangle$ than the expected value based upon the above model for a polyatomic reagent. (H) The $\langle g_R \rangle$ for GeH_4 is as high as a diatomic reagent.

Rotational relaxation may be more significant for CH_4 and C_2H_6 because of the relatively high vapor pressure at 77°K. The low $\langle g_R \rangle$ for $C(CH_3)_4$, as well as the non linear surprisal plot (3), may be attributed to collision dynamics which transfers energy to vibrations of the parent radical. Interpretation of the $(CH_3)_2O$ results must be done with caution because of the radical stabilization energy, which reduces the overall available energy (4). The diatomic-like behavior of GeH_4 may be explained by the very large reactive cross section, which is more than 7 times larger than F + CH_4 (5). Such a large cross section allows the hydrogen atom to move from GeH_4 to the F atom with an impact parameter that is large enough to keep the parent radical GeH_3 unexcited by the interaction with the newly formed HF molecule.

H + ClF

This reaction gave emission from HF and HCl. Using the latest Einstein coefficient, the ratio of k_{HF} and k_{HCl} was obtained as 1 to 3.9. The $\langle f_V \rangle$ values for HF and HCl are 0.53 and 0.44, respectively. The HF rotational distribution is very broad and much more extended than from H + F_2.

Literature Cited

1) Ding, A.M.G., Kirsch, L.J., Perry, D.S., Polanyi, J.C. and Schreiber, L., Faraday Disc. Chem. Soc. (1973) 55, 252.
2) Jonathan, N., Melliar-Smith, C.M., Okuda, S., Slater, D.H., and Timilin, D., Mol. Phys. (1971) 22, 561.
3) Bogan, D.J. and Setser, D.W., J. Chem. Phys. (1976) 64, 586.
4) Bogan, D.J., Setser, D.W., and Sung, J.P., J. Phys. Chem., May (1977).
5) Smith, D.J., Setser, D.W., Kim, K.C. and Bogan, D.J., J. Phys. Chem., May (1977).

In State-to-State Chemistry; Brooks, P., et al.;
ACS Symposium Series; American Chemical Society: Washington, DC, 1977.

14

Dynamics of the Electronically Chemiluminescent Reactions of $O_2(^1\Delta)$ with Olefins

DENIS J. BOGAN, RONALD S. SHEINSON, and FREDERICK W. WILLIAMS
Chemistry Division, Code 6180, Naval Research Laboratory, Washington, D. C. 20375

The reactions of ethylene and vinyl ethers (H_2CCHOR, R = Me, Et, n-Bu) with $O_2(^1\Delta_g)$ in the gas phase have been shown (1,2,3) to produce excited H_2CO (A^1A_2) via a vibrationally excited dioxetane adduct. Thus these reactions are chemically activated unimolecular fragmentations with the interesting and important feature that the product UV-Visible chemiluminescence can be used for characterization. We are engaged in a detailed study of the dynamics of these reactions. Chemiluminescence spectra are analyzed for $O_2(^1\Delta)$ plus various olefin reactions, chosen such that the overall thermochemistry and the possible excited products are different (4,5). A schematic of the reaction coordinate is shown as Figure 1. The dioxetane complex has not been collisionally stabilized in any of our experiments and has a lifetime, $\tau < 10^{-8}$ sec (3). In all cases the product chemiluminescence (and hence rate of product formation) is first order in both $O_2(^1\Delta)$ and olefin concentrations. A summary of experimental activation energies and thermochemistry, estimated in some cases, appears as Table 1. These E_a values are for passage from reactants to complex (Fig. 1), and not for passage from complex to products. Experiments of the latter type have been reported by many others (6), but ours is the only published work which probes the entire reaction coordinate diagram of Figure 1.

Vibronic hot bands appear in product formaldehyde spectra with different intensities for different reactant olefins. In general, the hot band intensity is directly related to the available energy and inversely related to the number of vibrational modes of the dioxetane complex. With the exception of the reaction of C_2F_3H (5), the lowest lying electronically excited product is observed exclusively. For the vinyl ether series, the quantum yield for formaldehyde chemiluminescence is constant, hence the electronic energy partitioning is not sensitive to the number of vibrational modes of the alkoxy side chain. These results suggest that electronic energy is partitioned non-statistically and controlled by the interactions of at least two potential energy surfaces; and that the excess vibrational energy is partitioned statistically (4,5).

In State-to-State Chemistry; Brooks, P., et al.;
ACS Symposium Series; American Chemical Society: Washington, DC, 1977.

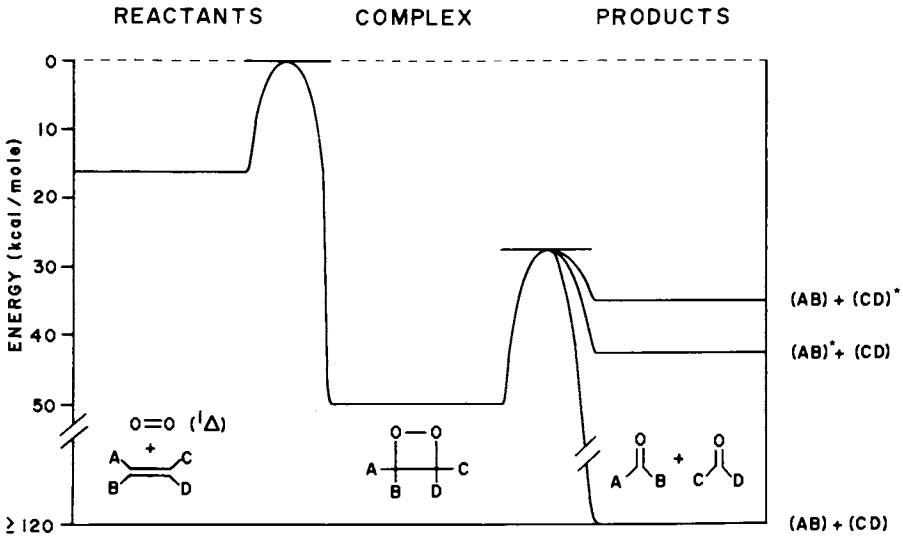

Figure 1. General reaction coordinate diagram for $O_2(^1\Delta)$ plus olefin reaction (approximate scale only)

TABLE 1. Data Summary

Olefin	$E_a \pm 3\sigma$ (Kcal/mole)		Emission	$-\Delta H_{Rxn}$ (Kcal/mole)
$H_2C{=}CH_2$	21.4	1.8	H_2CO	90.5
$H_2C{=}CHOMe$	13.4	0.4	H_2CO	107*
$H_2C{=}CHOEt$	12.5	0.3	H_2CO	107*
$H_2C{=}CHOnBu$	13.0	0.3	H_2CO	107*
$H_2C{=}C{=}O$	15.3	0.8	H_2CO	129
$H_2C{=}CHF$	18.3	1.1	H_2CO	109
$H_2C{=}CF_2$			H_2CO	122
$HFC{=}CF_2$	15.6	0.4	F_2CO,HFCO	148
$F_2C{=}CF_2$	17.9	0.4	F_2CO	171
$H_2C{=}CHCl$	15.5	1.6	H_2CO	129*
$H_2C{=}CCl_2$	16.9	0.7	H_2CO	103

*estimated

In State-to-State Chemistry; Brooks, P., et al.;
ACS Symposium Series; American Chemical Society: Washington, DC, 1977.

LITERATURE CITED

1. Bogan, D. J., Sheinson, R. S., Gann, R. G. and Williams, F. W.; J. Am. Chem. Soc., (1975), 97, 2560.
2. Bogan, D. J., Sheinson, R. S. and Williams, F. W.; J. Am. Chem. Soc., (1976), 98, 1034.
3. Bogan, D. J., Sheinson, R. S. and Williams, F. W.; J. Photochem., (1976), 7, 156.
4. Bogan, D. J., Sheinson, R. S., Williams, F. W. and Durant, Jr., J. L.; Chem. Phys. Lett., to be submitted, 1977.
5. Bogan, D. J., Sheinson, R. S., Durant, Jr., J. L. and Chiu, Y-N.; Chem. Phys. Lett., to be submitted, 1977.
6. Adam, W.; "The Chemistry of 1,2-Dioxetanes," in "Advances in Heterocyclic Chemistry," Vol. 22, edited by A. R. Katritzky, Academic Press, in press, 1977.

In State-to-State Chemistry; Brooks, P., et al.;
ACS Symposium Series; American Chemical Society: Washington, DC, 1977.

15

Laser Induced Reaction Rate and Optical Absorption at Various Frequencies in the Absorption Bands of CF_2ClCF_2Cl and of CH_3CF_2Cl

R. N. ZITTER
Department of Physics and Astronomy, Southern Illinois University, Carbondale, IL 62901

D. F. KOSTER
Department of Chemistry and Biochemistry, Southern Illinois University, Carbondale, IL 62901

Infrared laser induced reactions more often than not lead to products that are consistent with the purely thermal reaction and hence it is difficult to discern whether the laser is acting as more than a heat source. This is particularly true when using C.W. irradiation of gases at relatively high pressures, where rapid V-T/R process should be operating. It is under these latter conditions, however, that we feel we have strong evidence for a non-thermal component in the reaction pathway, although we do not discount a simultaneous thermal component as well.

In an earlier paper [1] on CF_2ClCF_2Cl we noted a large difference in the reaction rate on irradiation of two separate bands of the compound (921 cm^{-1} and 1051 cm^{-1}) at the band centers. Since the slightly stronger 1051 cm^{-1} band gave the slower rate, it appeared that compartmentalization of energy in the vibrational mode was operating to a significant degree, despite V-V transfer.

Further studies of this reaction now allow us to modify our original interpretation. As Figure 1 shows, the reaction rate [2] maximizes at frequencies $\sim$ 30 cm^{-1} below the 921 and 1051 cm^{-1} band centers. This "red shift" effect has been observed in at least one other compound [3] and has been ascribed to vibrational anharmonicity. The 1051 cm^{-1} band now gives the faster rate, but only at red-shifted frequencies.

Figure 1 also shows the absorption band profiles as measured normally in a spectrophotometer (curve α_o) and as measured under laser irradiation (curve α). The latter were obtained from measurements of beam transmission through a short cell for the same gas pressure and laser power conditions as the rate measurements. Under laser irradiation, absorption is lowered at frequencies near the α_o band centers and is enhanced at red-shifted frequencies, to the extent that absorption is virtually frequency-independent over broad ranges.

Standard equations for steady-state heat flow predict that temperatures in the beam region will be determined by the power absorbed per unit volume (all other factors being equal), which

In State-to-State Chemistry; Brooks, P., et al.;
ACS Symposium Series; American Chemical Society: Washington, DC, 1977.

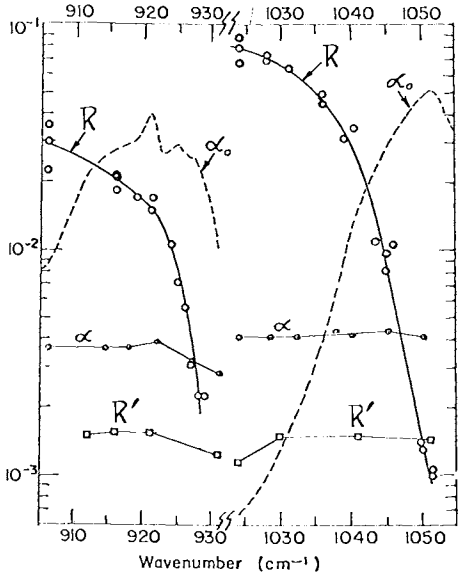

Figure 1. Data for various frequencies through two bands of CF_2ClCF_2Cl. Curves α_0 are the "ground-state" optical absorption coefficients (in units of cm^{-1} $Torr^{-1}$). Curves α are absorption coefficients (cm^{-1} $Torr^{-1}$) induced by a 4-watt, 1-mm diameter laser beam in 200 Torr CF_2ClCF_2Cl. Curves R *are the reaction rates (arbitrary units) of 200 Torr CF_2ClCF_2Cl for a 4-watt, 1-mm diameter laser beam. Curves* R′ *are the reaction rates (arbitrary units) of the "temperature probe" gas PFB. The logarithmic scale refers to both* R *and* α.

in turn is given by αI (absorption coefficient times intensity). Since α is essentially independent of frequency over the range of interest, to a first approximation temperature also should be constant. On the other hand, reaction rates increase sharply with decreasing frequency. We consider this strong evidence for a non-thermal, vibrationally enhanced component in the reaction process.

To corroborate the results, we introduced a small amount (2.44%) of a "temperature probe" gas perfluorobutadiene (PFB), which cyclizes thermally to perfluorocyclobutene (PFCB) according to well known kinetics [4]. PFB has no appreciable absorption in the 920 cm^{-1} and 1050 cm^{-1} regions, and alone at pressures equivalent to its partial pressure in the mixture, undergoes negligible reactions when irradiated at these frequencies. Therefore, PFB should serve as a temperature probe in the mixture since most of input energy is expected to lie in modes of CF_2ClCF_2Cl that are already equilibrated at the translational temperature.

In State-to-State Chemistry; Brooks, P., et al.;
ACS Symposium Series; American Chemical Society: Washington, DC, 1977.

The curve R' in Figure 1 shows that the rate constant for cyclization of PFB, obtained by monitoring the production of PFCB at 1416 cm^{-1}, is nearly independent of frequency. If indeed the probe is monitoring translational temperature, then the results are entirely consistent with those for absorption of CF_2ClCF_2Cl, namely, constant translational temperature over the frequency range.

A second reaction of interest is the elimination of HCl from CH_3CF_2Cl to give CH_2CF_2. This reaction is known to proceed thermally with a rate constant given by the expression [5]

$$k = 10^{14.35} \exp [-252kJ/RT]$$

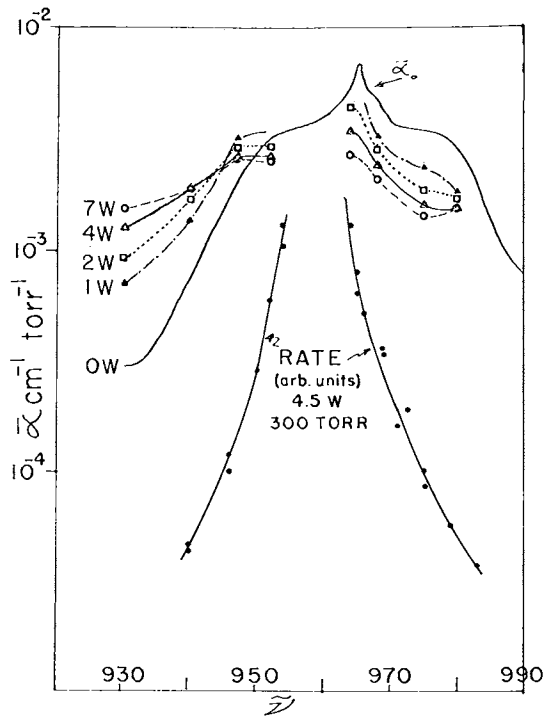

Figure 2. Absorption coefficient of the 966 cm^{-1} band of CH_3CF_2Cl and initial reaction rate vs. frequency. Absorption coefficient data are taken at 40 Torr, rate data at 300 Torr. Upper absorption curve is the standard spectrophotometer trace; other curves are for various laser power (watts). The laser has no appreciable output in the 955–965 cm^{-1} region. The logarithmic scale (now in arbitrary units) is also used to plot the reaction rate.

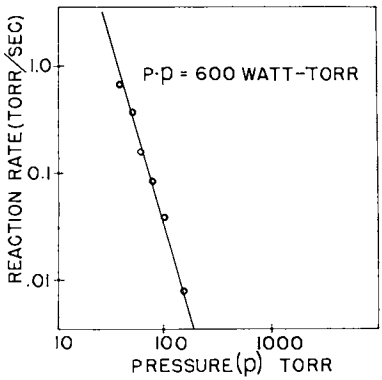

Figure 3. Reaction rate at 952 cm^{-1} vs. pressure for CH_3CF_2Cl, with laser power P varying inversely with pressure p to give constant product pP. The latter condition is intended to keep translational temperature in the beam region at a constant value.

Figure 2 gives the absorption curves and rate data. As observed in the previous compound there is a distinct "red shift" in both absorption and rate, the latter maximizing 6-10 cm^{-1} below the low intensity curve band center. Unfortunately there is a gap in our laser frequencies in the region where the rate is maximizing. The relationship between the rate and absorption coefficient curves is not clear here but it is evident that they do not scale in the same manner. That is, widely differing rates are obtained at frequencies where the absorption is essentially the same, indicating a non-thermal component to the reaction rate [6].

In addition, we have measured rates with laser power P varying inversely to reactant gas pressure p. Under these conditions, translational temperature in the beam region should remain fixed, since it is determined by the product αI, which in turn is proportional to pP. For a purely thermal process, the rate should remain unchanged for pP=constant. That this is not so can be seen in Figure 3. In all instances, high powers and low pressures give faster rates, a picture consistent with excitation of higher vibrational states at higher power levels.

It is interesting to consider the quantum requirement Q, defined as the number of photons absorbed per product molecule produced for this reaction. Figure 4 shows Q values obtained for various laser powers and gas pressures of CH_3CF_2Cl. Q decreases monotonically with increasing power and pressure. At a beam power of 23 W and starting gas pressure of 400 torr, Q has reached the value of 17 photons absorbed per product molecule (CH_2CF_2) produced, and the trend of the curves indicate that even lower Q values may be attained. (See footnote [7].)

These values are significantly less than the 22 photons required per molecule to reach the thermal activation barrier of 252 kJ [5]. As a tentative explanation, we propose that part of the activation energy released in the reaction is being fed back to reactant molecules, rather than being lost to the cell walls. Under this mechanism, the limiting value of Q for this endother-

In State-to-State Chemistry; Brooks, P., et al.;
ACS Symposium Series; American Chemical Society: Washington, DC, 1977.

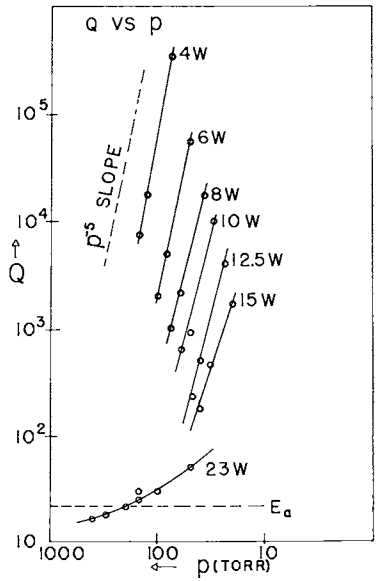

Figure 4. Quantum requirement for the CH_3CF_2Cl reaction at 952 cm^{-1} vs. pressure at various laser powers. The thermal activation energy E_a corresponds to 22 photons/molecule at this frequency.

mic reaction would be set by ΔH (∿7 photons per molecule [8]) and not by the activation energy. In any event, it appears that essentially all of the input laser energy can be channeled into the reaction, with negligible loss to the cell walls before reaction occurs.

The lowest Q values we have obtained for CF_2ClCF_2Cl have been in the range of 80. Under conditions needed to achieve these values a strong visible emission is evident, which may be effectively removing energy from the system.

In all the experiments reported here, the laser beam had an approximate diameter of 1 mm and was essentially parallel over the 10 cm path through the reaction cell.

Acknowledgement: This work was supported in part by the National Science Foundation through grant no. CHE 76-01162.

Literature Cited

1. Zitter, R.N. and Koster, D.F., J. Amer. Chem. Soc.(1976),98, 1614.
2. Major initial products are C_2F_4 and CF_2Cl_2. Initial rates of formation of the former are monitored at 1331 cm^{-1}.
3. Rinck, R., Bachmann, R., Noth, H., and Kompa, K.L., Ninth International Conference on Quantum Electronics, (Digest), Amsterdam, Netherlands June (1976).
4. Prober, M. and Miller, W.T., J. Amer. Chem. Soc. (1949), 71, 598.
5. Martens, G.J., Godfroid, M., Decelle, R. and Verbeyst, Jr., Int. J. of Chem Kinetics, IV (1972), 645-55.
6. More recent improved absorption coefficient measurements are

more definitive. For example, the absorbances at 952 cm^{-1} and 979 cm^{-1} are virtually identical for all laser input powers, yet the rates at these frequencies differ by more than an order of magnitude.
7. More recent results at higher powers and pressures give Q as low as 13 photons/molecule.
8. Sianesi, D., Nelli, G. and Fontanelli, R., Chim. Ind. (1968), 50 (6), 619.

In State-to-State Chemistry; Brooks, P., et al.;
ACS Symposium Series; American Chemical Society: Washington, DC, 1977.

16

Chemiluminescence from the Gas Phase Reaction of Atomic Boron with the Alkali Metal Fluorides

U. C. SRIDHARAN, D. L. MC FADDEN, and P. DAVIDOVITS
Department of Chemistry, Boston College, Chestnut Hill, MA 02167

During the past few years there has been considerable interest in chemical reactions that produce excited alkali metal atoms. Chemiluminescence from alkali atoms has been studied recently in both beam experiments (1-3) where single collision processes can be observed as well as in flames (4-8) where complex collisional energy transfer plays an important role in the excitation process. These studies were motivated in part by the possibility that these reactions may produce inversion in the excited states of the alkali atoms, suitable for chemical lasers.

We are studying the chemiluminescence produced by the reaction of boron with the alkali fluorides (MF), that is

$$B + MF \rightarrow BF + M$$

With the reactants in the ground state the exoergicity of these reactions is about 3 ev. This amount of energy can excite only the first p states in sodium and potassium but in rubidium and cesium higher lying excited states can be reached. Our aim is to determine the distribution of excited states produced in these reactions and ultimately to understand the reaction mechanism. It is expected that the results from experiments with these relatively simple reactions will lead also to a better general understanding of energy partitioning in exoergic reactions.

Both crossed flow and molecular beam techniques are being used to study these chemiluminescent reactions. A simplified schematic drawing of the flow apparatus is shown in Fig. 1. The flow containing the boron atoms is produced inside the vacuum chamber by a microwave discharge in a mixture of 1% B_2H_6, 99% helium. The alkali fluoride molecules are produced in an oven heated between 925-1275 K (depending on the

In State-to-State Chemistry; Brooks, P., et al.;
ACS Symposium Series; American Chemical Society: Washington, DC, 1977.

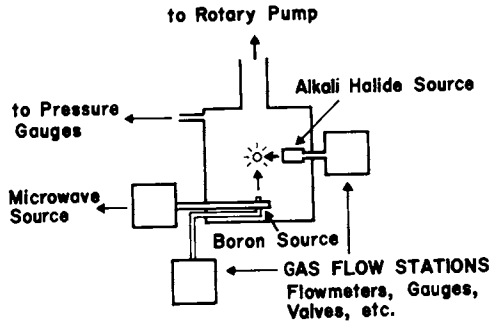

Figure 1. Schematic of the crossed flow apparatus

salt) and are carried into the reaction region through a 1 mm hole in the oven by helium carrier gas. The total pressure in the reaction chamber is about 0.5 torr. In the molecular beam apparatus, an effusive atomic boron beam is produced by vaporization of elemental boron at 2400 K in a knudsen cell. The alkali fluoride beam source consists of an oven heated to about 1000 K. Photon counting techniques are used in the low pressure (10^{-5} torr) beam experiments.

We have performed experiments in the flow apparatus with the salts CsF, RbF, KF and NaF (9). The spectrum from each reaction was recorded and the relative number of photons from the various transition was computed. From these data we obtained the relative steady state population distribution. We observe excitation of states with energies up to and in some cases above the exoergicity for the reaction of boron with the metal fluorides. The results show that while the population of the excited states tends to decrease with energy there are population inversions between some of the states. Experiments indicate that the first excited P states are produced mainly in the primary chemical reaction of boron with thermal MF molecules. The photon yield from the first excited state is estimated to be as high as 0.5 photons per boron atom reacted. The mechanism for the excitation of the states lying above the first P levels cannot be determined from the flow experiments. We can only conclude that several secondary energy transfer processes contribute to the production of the higher excited states. Preliminary results from the single collision beam studies confirm the above results and are in the process of yielding quantitative values for the chemiluminescence cross sections.

In State-to-State Chemistry; Brooks, P., et al.;
ACS Symposium Series; American Chemical Society: Washington, DC, 1977.

Literature Cited

1. Struve, W.S., Kitagawa, T., and Herschbach, D.R., J. Chem. Phys. (1971) 54, 2759.
2. Oldenborg, R.C., Gole, J.L., and Zare, R.N., J. Chem. Phys. (1974) 60, 4032.
3. Struve, W.S., Krenos, J.R., McFadden, D.L., and Herschbach, D.R., J. Chem. Phys.(1975) 62, 404.
4. Luria, M., Eckstrom, D.J. and Benson, S.W., J. Chem. Phys. (1976) 64, 3103.
5. Luria, M., Eckstrom, D.J., Edelstein, S.A., Berry, B.E. and Benson, S.W., (1976) 64, 2247.
6. Hall, L.H., Appl. Phys. Lett. (1975) 27, 335.
7. Hall, L.H., IEEE J. Quantum Electron. (1975) 11, 693.
8. Hall, L.H., J. Chem. Phys. (1977) 66, 2435.
9. Sridharan, U.C., McFadden, D.L., and Davidovits, P., J. Chem. Phys. (1976) 65, 5373.

In State-to-State Chemistry; Brooks, P., et al.;
ACS Symposium Series; American Chemical Society: Washington, DC, 1977.

17

Dark Products in Chemiluminescent Flames of Ba + N_2O

J. GARY PRUETT and AFRANIO TORRES-FILHO

Department of Chemistry, University of Pennsylvania, Philadelphia, PA 19174

Chemiluminescent flames resulting from the reactions between metal atoms and various oxidant gases have been studied extensively in emission under molecular beam and low pressure flow conditions(1). In all cases it is found that the initial reaction products which spontaneously emit light represent a small fraction of the total products.

We are examining the dark states of BaO present in a flow reaction of 200μ pressure using laser induced fluorescence and would like to report our preliminary results.

Experimental

The technique of laser-induced fluorescence as applied to gas phase reaction products has been well documented by Zare and co-workers(2). Briefly it involves gated optical detection of a pulsed fluorescence signal resulting from pulsed electronic excitation of product molecules by a tunable visible dye laser. However, in the present studies the presence of very bright visible chemiluminescence emanating from the same reaction volume as the laser induced fluorescence, precludes simple collection of the total light with an unprotected photocathode surface.

The chemiluminescence and the expected pulsed laser-induced fluorescence differ, of course, in two key ways which may be utilized for selective detection. First, if the light flux from the flame region is integrated only during the lifetime of the pulsed fluorescence much chemiluminescence can be avoided. This technique is adequate as long as the background light is sufficiently low that it does not saturate the photomultiplier tube, thus eliminating gain on the pulsed signal.

The second distinction between the pulsed fluorescence and the chemiluminescence is their spectral difference. In general the chemiluminescence covers a very wide range of wavelengths, whereas the pulsed fluorescence occurs only to the dipole allowed Franck-Condon regulated transitions from the state produced by the excitation laser. This fact can be utilized in two ways.

In State-to-State Chemistry; Brooks, P., et al.;
ACS Symposium Series; American Chemical Society: Washington, DC, 1977.

First, if any of the pulsed fluorescence lines occur completely outside the chemiluminescence wavelength range, cut-off filters may be used to observe only those wavelengths. Second, the excitation wavelength will always be one of the fluorescence pathways, so dispersion of the total light from the reaction zone by an optically fast, low resolution monochromator, followed by detection at the laser wavelength throws away a much higher fraction of the broad-band chemiluminescence than of the pulsed fluorescence. Both of these techniques have been utilized in this study.

The reaction

$$Ba + N_2O \rightarrow BaO + N_2$$

was chosen for initial study because of the large amount of work which has been done on this reaction in flames(3). It is known that the emission under beam and low pressure conditions is primarily due to the low probability (<1%) production of molecules in the $A\,^1\Sigma^+$ and $A'\,^1\pi$ states, which have radiative lifetimes of .3 and 10 μsec respectively. Some information has also been obtained on the populations of the low vibrational levels of the BaO product(4).

Results

Now in order to observe pulsed fluorescence following excitation from one of the dark states ($X\,^1\Sigma^+$ or a $^3\pi$), we must excite molecules to yet another excited electronic state to observe the fluorescence. Thus we must have spectroscopic information on even higher lying excited electronic states. By exciting with visible light and observing fluorescence outside of the chemiluminescence range, we have observed ultraviolet fluorescence (400 $>\lambda>$ 250 nm) with a radiative lifetime of 20 nsec. This radiation represents emission from a new electronic state of BaO to the ground electronic state, following excitation from high vibrational levels of the ground electronic state (laser λ between 390 nm and 590 nm). The red degraded band heads form regular series corresponding to lower state vibration spacings from 614 cm^{-1} to 584 cm^{-1} and upper state spacings from 443 cm^{-1} to 420 cm^{-1}. Vibrational assignments of the lower state have been made by matching the spacings with known ground electronic state vibrational spacings. The assignments of the upper state numbering was accomplished by spectrally resolving the total fluorescence and counting nodes in the Franck-Condon factor envelopes. This technique is unambiguous in the present case because the upper state internuclear separation is sufficiently shifted that the low vibrational levels of the upper state sample the wave function maxima of the ground state wave functions at their outer turning points. Thus, for low vibrational levels (0-4), the Franck-Condon factor nodes are well developed and easily recognized.

In State-to-State Chemistry; Brooks, P., et al.;
ACS Symposium Series; American Chemical Society: Washington, DC, 1977.

TABLE 1

Band Heads ($cm^{-1} \pm 15\ cm^{-1}$) of Observed BaO Bands
ν_{oo}(calc) = $32750 \pm 15\ cm^{-1}$

v',v''	Head Position	v',v''	Head Position
0,12	25045	2,16	23488
1,13	24886	3,17	23329
2,14	24699	0,15	23214
3,15	24525	4,18	23150
0,13	24431	1,16	23032
1,14	24275	2,17	22890
2,15	24088	3,18	22732
3,16	23925	4,19	22563
0,14	23829	1,17	22448
4,17	23753	2,18	22296
1,15	23641	3,19	22146
		4,20	21979

Table 1 gives our tentative transition energies and vibrational assignments. The upper state seems to be the same as one already observed by Field et. al. using double resonance techniques (5). Thus far we have been able to: (A) Confirm the existence of highly vibrationally excited states of the $X\ ^1\Sigma$ state in the flame at 200 torr. (B) Obtain the lifetime, rough vibrational spacing, ν_{oo}, and approximate shape of a highly electronically excited state of BaO. (C) Confirm our ability to probe very highly vibrationally excited states of BaO $X\ ^1\Sigma$ by excitation using red light and observation in the deep U.V. (D) Prove the feasibility and usefulness of laser induced fluorescence techniques on systems with high background light fluxes.

We are now extending our present studies to the higher vibrational states of BaO $X\ ^1\Sigma$ and with the aid of Franck-Condon factor calculations to assign relative populations to the high vibrational levels of the $X\ ^1\Sigma$ state at reaction zone pressures of 200 μ. As yet we have not observed any features characteristic of exciting fluorescence in molecules from the $^3\pi$ levels of BaO, although we have not yet ruled out their existence.

Literature Cited

1. Ekstrom, D.J.; Edlestein, S.A.; Huestis, D.L.; Perry, B.E.; Benson, S.W.; J. Chem. Phys. (1975), 63(9), 3828.
2. Zare, R.N.; Dagdigian, P.J.; Science, (1974), 185, 739.
3. Jones, C.R.; Broida, H.P.; J. Chem. Phys. (1974),60(11), 4369.
4. Revelli, M.A.; Wicke, B.G.; Harris, D.O.; J. Chem. Phys. (1977), 66(2), 732.
5. Field, R.W.; Capelle, G.A.; Revelli, M.A.; J. Chem. Phys. (1975), 63(8), 3228.

18

Laser Fluorescence and Thermal Lensing Studies of Intermode Energy Transfer and Chemical Reactivity in Small Polyatomic Molecules

GEORGE W. FLYNN

Department of Chemistry and Columbia Radiation Laboratory, Columbia University, New York, NY 10027

Energy transfer processes in molecules have been of interest to chemists for well over 50 years simply because the majority of chemical reactions proceed through molecular bond breaking. The rupture of chemical bonds requires energy, but not necessarily just any form of energy. The relative importance of vibrational, rotational, and translational energy in controlling the magnitude of cross sections for chemical reaction can only be determined by careful consideration of the potential energy surfaces leading from reactants to products. There are reactions in which translational and rotational energy are expected to be as important or more important than vibrational energy in determining the overall chemical reaction rate. Nevertheless, the flow of energy between the various degrees of freedom of a molecule remains a topic of crucial importance in the development of a complete theory of chemical reactivity.

More recently chemists and physicists working on the development of powerful, versatile, and efficient laser systems have become interested in the details of molecular energy transfer. It is in fact the relative rates of energy flow between vibrational modes and among the translational, rotational, and vibrational degrees of freedom which controls the gain, energy, and power characteristics of most infrared gas lasers. A knowledge of the factors affecting energy transfer can often be used to increase the efficiency and power of a given laser system. At the present time a relatively small number of molecules exhibit laser action, but it is reasonable to expect that many new molecular lasers can be developed as the factors which determine energy transfer pathways and mechanisms become understood.

Experimental studies of molecular energy flow also offer good tests for energy transfer theories. Agreement between theory and experiment has improved steadily over the past few years, but for most molecules only qualitative theoretical correlations seem to be valid. Theoretical efforts are hampered by a lack of knowledge of the complete interaction potential

In State-to-State Chemistry; Brooks, P., et al.;
ACS Symposium Series; American Chemical Society: Washington, DC, 1977.

between two colliding molecules. Furthermore, for polyatomic molecules, so many energy transfer paths are available during a particular collision, that an enormous effort would be required to compute the total energy transfer cross section even if the full interaction potential were accurately known. Thus experimental data serve as excellent tests for the necessarily approximate treatments of most energy transfer theories.

Lasers have had a significant impact on studies of energy flow and chemical reactivity in gases over the past 12 years because they have provided the first monochromatic, high power, short pulse radiation sources in the infrared spectral region. Lasers are being used now, not only to study energy transfer processes, but also to initiate chemical reactions by infrared pumping. A brief description of some laser energy transfer and laser "catalysis" experiments is given below.

Experimental Methods

For the experimental results reviewed here, two basic techniques have been used to obtain energy transfer data. The first is infrared laser induced fluorescence (1 - 4), which employs a Q-switched CO_2 laser to vibrationally excite gaseous molecules. Typical laser characteristics are a pulse width $\lesssim 10^{-6}$ sec, an energy per pulse of 0.5 - 4 mJ, a pulse repetition rate of 10^2 sec^{-1}, and a wavelength between 9.2 and 10.6 microns. Following laser excitation, time resolved infrared fluorescence is observed with a fast, sensitive detector at right angles to the direction of propagation of the laser radiation. In general, all states which emit spontaneously can be studied by the proper choice of infrared interference filters, but in practice many weakly fluorescing modes cannot be monitored because of the low efficiency of infrared detectors and the relatively long radiative lifetimes which characterize the infrared region. The growth and decay rates of these fluorescence signals give a direct measure of the dynamical changes in the populations of various vibrational states which occur due to relaxation processes following laser excitation. The pressure dependence of these rates can be used to determine average collision cross sections for energy transfer.

The second technique which is used to study energy transfer processes is the time resolved thermal lensing method (5, 6). This experimental device employs a Q-switched CO_2 laser, essentially identical to the one used in fluorescence studies, to vibrationally excite gaseous molecules. A He-Ne laser operating continuously at 6328Å and propagating colinearly with the CO_2 laser, is used to monitor time dependent translational energy changes in the gas following laser pumping. This opto-acoustic detection method can distinguish vibrational energy transfer events that are translationally endothermic from those which are translationally exothermic.

In State-to-State Chemistry; Brooks, P., et al.;
ACS Symposium Series; American Chemical Society: Washington, DC, 1977.

In the study of infrared laser driven chemical reactions a high power CO_2 laser is generally used to excite molecules. Typical characteristics for these laser are a pulse duration $\lesssim 5 \times 10^{-7}$ sec., an energy per pulse of 0.5 - 1 J, a pulse repetition rate of 2 sec^{-1}, and a wavelength between 9.2 and 10.6 microns. Product analysis is performed by standard I.R. absorption, gas chromatography, or mass spectroscopy. The laser driven production of HF from $SF_6 + H_2$ mixtures, which is discussed below, was monitored by observing time resolved HF infrared fluorescence as noted above (7, 8).

Intermode Energy Transfer in SO_2

Energy transfer processes in SO_2 have been studied using both infrared fluorescence (9) and thermal lensing techniques(6). Laser excitation and energy transfer processes for SO_2 can be described by the following equations:

Laser pump: $SO_2(0) + h\nu \rightarrow SO_2(\nu_1)$ (1)

V-V relaxation: $SO_2(\nu_1) + M \rightleftarrows SO_2(\nu_3) + M - 210\ cm^{-1}$ (2)

V-V relaxation: $SO_2(\nu_1) + M \rightarrow SO_2(2\nu_2) + M + 120\ cm^{-1}$ (3)

The laser excites the ν_1 (symmetric stretch) vibration while vibration-vibration (V-V) energy transfer processes carry population to other vibrational modes via collision events (2) and (3) which are, respectively, translationally endothermic by 210 cm^{-1} and exothermic by 120 cm^{-1}. An abbreviated vibrational energy level diagram for SO_2 is shown in Fig. 1. At pressures of a few Torr, the excitation step (1) is much faster than the collision processes so that the growth and decay of antisymmetric stretch fluorescence ($\nu_3 \rightarrow 0$ $\lambda \sim 7.4\mu$) can be easily measured as a function of pressure. Translational cooling is observed with the thermal lens technique giving strong evidence for step (2). When $M = SO_2$, the V-V collisional equilibration of ν_1 and ν_2 (Eqn. (2)) requires approximately 135 gas kinetic collisions on the average. On the other hand, the V-V collisional relaxation attributed to step (3) requires about 2600 gas kinetic collisions. Thus even though process (2) is 210 cm^{-1} endothermic while (3) is 120 cm^{-1} exothermic, process (2) is almost 20 times more efficient than (3)! This remarkable fact suggests quite strongly that there are qualitative collisional propensity rules for V-V energy transfer processes (10). A formulation of these "rules" will be given later.

Because of the tight collisional coupling between ν_1 and ν_3 compared to the weak collisional coupling of these states to the bending mode overtone ($2\nu_2$), laser pumping causes the stretches to become vibrationally hot while the bends remain cold. In pure SO_2 this condition lasts for approximately 2600

In Water in Polymers; Rowland, S. P., et al.;
ACS Symposium Series; American Chemical Society: Washington, DC, 1977.

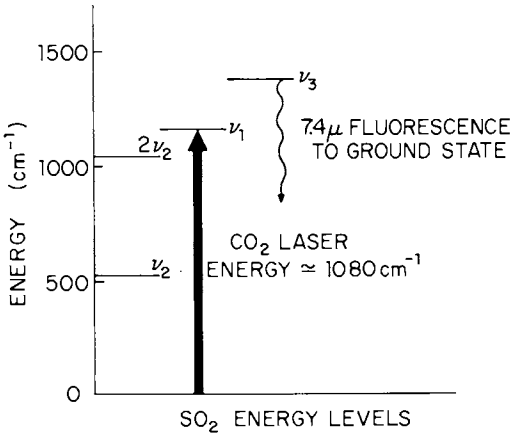

Figure 1. Partial vibrational energy level diagram for SO_2. ν_1 is the symmetric stretch, ν_2 the bend, and ν_3 the antisymmetric stretch frequency.

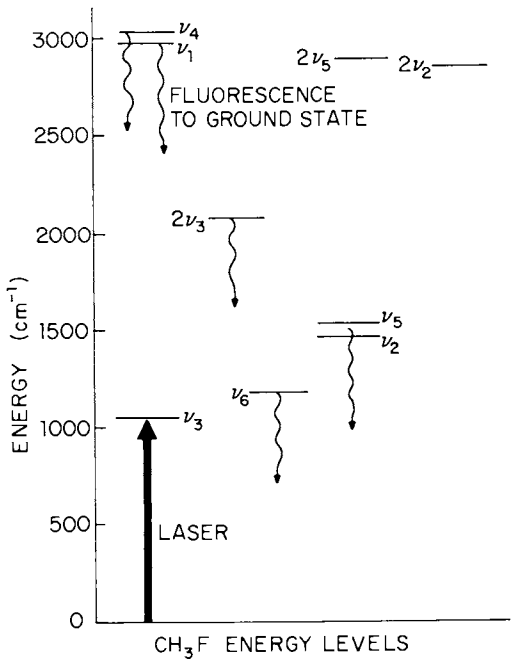

Figure 2. Partial vibrational energy level diagram for CH_3F. Wavy lines indicate fluorescence to the ground state has been observed. ν_1 and ν_4 are C–H stretches, ν_2 and ν_5 are CH_2 bends, ν_3 is a C–F stretch, and ν_6 is a methyl deformation.

In State-to-State Chemistry; Brooks, P., et al.;
ACS Symposium Series; American Chemical Society: Washington, DC, 1977.

collisions. Such a metastable system offers several interesting possibilities for mode specific chemical reaction studies and optically pumped molecular laser action.

Intermode Energy Transfer in CH_3F

Though SO_2 represents a particularly simple and pleasing milestone in the study of vibrational energy transfer processes, CH_3F has proven to be a substantially more complex challenge. Experimental efforts to define "completely" the vibrational energy transfer mechanism of this 9 mode molecule have only recently been successful. Sophisticated, careful work with both the infrared fluorescence and thermal lensing techniques has allowed us to unravel the detailed vibrational energy flow-map for this molecule. Fig. 2 shows an abbreviated vibrational energy level diagram for CH_3F. The modes are: ν_1 (C-H stretch), ν_2 (CH_2 bend), ν_3 (C-F stretch), ν_4 (C-H stretch, doubly degenerate), ν_5 (CH_2 bend, doubly degenerate), and ν_6 (CH_3 deformation, doubly degenerate). Because ν_1 and ν_4 are only slightly split in energy, the collisional energy transfer event

$$CH_3F(\nu_1) + M \rightleftarrows CH_3F(\nu_4) + M \qquad (4)$$

is too fast to measure with present state-of-the art equipment. A similar argument holds for ν_2 and ν_5. Thus for the purposes of vibrational energy transfer, CH_3F may be thought of as a pseudo 4 mode molecule with the modes or mode sets being ν_3, ν_6, (ν_2, ν_5), and (ν_1, ν_4). Experimental evidence to date (4, 5, 11-16) indicates that the following set of equations describes with good accuracy the CH_3F laser excitation and energy redistribution scheme:

Laser excitation: $CH_3F(0) + h\nu \rightarrow CH_3F(\nu_3)$ (5)

V-V Relaxation: $CH_3F(\nu_3) + M \rightleftarrows CH_3F(\nu_6) + M - 133\ cm^{-1}$ (6)

V-V Relaxation: $CH_3F(\nu_6) + M \rightleftarrows CH_3F(\nu_2,\nu_5) + M - 284\ cm^{-1}$ (7)

V-V Relaxation: $2CH_3F\ (\nu_2,\nu_5) \rightleftarrows CH_3F(2\nu_2,\ 2\nu_5) + CH_3F(0)$ (8)

V-V Relaxation: $CH_3F(2\nu_2,\ 2\nu_5) + M \rightleftarrows CH_3F(\nu_1,\nu_4) + M - 60\ cm^{-1}$ (9)

V-T/R Relaxation: $CH_3F(\nu_3) + M \rightarrow CH_3F(0) + M + 1049\ cm^{-1}$ (10)

The final step (Eqn. 10) represents overall loss of energy from the vibrational manifold via vibration-translation/rotation (V-T/R) relaxation. When M = CH_3F this last process requires approximately 15,000 gas kinetic collisions while for M = Xe it requires roughly 400,000 gas kinetic collisions. On the other hand, all of the V-V energy redistribution steps (6-9) reach

In State-to-State Chemistry; Brooks, P., et al.;
ACS Symposium Series; American Chemical Society: Washington, DC, 1977.

equilibrium in less than 100 gas kinetic collisions for pure CH_3F. Thus the vibrational modes come into metastable equilibrium with each other shortly after laser excitation. This metastable state in turn lasts nearly 15,000 collisions due to the relative inefficiency of overall V-T/R relaxation (Eqn. 10).

Not all of the V-V processes (6-9) are equally important in determining the rate of vibrational energy redistribution in CH_3F. The rate limiting steps seem to be (7) which requires approximately 70 collisions in pure CH_3F and (6) which requires roughly 20 gas kinetic collisions. The dynamic changes in (ν_1, ν_4) population appear to mimic nearly identically the changes in (ν_2, ν_5) population suggesting that the events (8) and (9) are much faster than (6) and (7) (17).

Unlike SO_2 (6, 9) and CO_2 (1, 2) all of the vibrational modes of CH_3F are rapidly equilibrated by collisions so that free flow of vibrational energy between modes occurs with remarkable ease. Nevertheless, the entire vibrational manifold does remain hot for long periods of time after laser pumping due to the inefficiency of V-T/R relaxation (Eqn. 10). Perhaps even more interesting is the fact that the energy distribution which characterizes this vibrationally hot metastable state cannot be described by a single vibrational temperature and differs significantly from any one temperature Boltzmann distribution (18, 19). This point is considered in more detail below.

Energy Transfer in CH_3F/SO_2 Mixtures

A particularly interesting system, which illustrates again the importance of collisional propensity rules, is the vibrational energy transfer scheme in CH_3F/SO_2 mixtures. CH_3F can be easily excited by a CO_2 laser pulse (Eqn. 5) and fluorescence from $SO_2(\nu_3)$ and $SO_2(\nu_2)$ can be observed after laser excitation of the CH_3F in CH_3F/SO_2 mixtures (10). Fig. 3 is an abbreviated vibrational energy level diagram which is sufficient to describe energy transfer between CH_3F and SO_2. Vibrational energy exchange between these two molecules is tremendously efficient, requiring only about 30 gas kinetic collisions. Nevertheless, all available evidence indicates that the highly resonant energy transfer process

$$CH_3F(\nu_3) + SO_2(0) \rightleftarrows CH_3F(0) + SO_2(2\nu_2) + 18\ cm^{-1} \qquad (11)$$

is approximately 100 times less efficient than other channels which lead to the exchange of energy between CH_3F and SO_2 (10)! All of these channels are less resonant than (11). An interesting characteristic of the SO_2 molecule is that the $0 \rightarrow 2\nu_2$ absorption has never been observed spectroscopically indicating that the $2\nu_2$ state is negligibly mixed with ν_1 or ν_3 and exhibits little electrical or mechanical anharmonicity. Thus the scattering process (11) appears to require a nearly pure 2

In State-to-State Chemistry; Brooks, P., et al.;
ACS Symposium Series; American Chemical Society: Washington, DC, 1977.

quantum exchange for the SO_2 bending states. Such a process must necessarily be second order in the SO_2 bending mode normal coordinate, and this may well explain the relative inefficiency of the energy transfer processes (3) and (11).

Collisional Propensity Rules for Vibrational Energy Transfer

Based on the data reviewed here plus a large quantity of experimental evidence which now exists in the literature (20), a set of qualitative propensity rules can be formulated. These rules appear to be useful for making rough guesses about the relative efficiency of some energy transfer processes. Molecules which undergo "sticky" collisions (hydrogen bonding, pseudo-molecule complex formation), molecules with low frequency torsional modes, or "large" molecules almost certainly will not be well represented by these rules. Nevertheless, for molecules with relatively dilute vibrational levels (e.g. less than $\sim$ 50 vibrational states below 3000 cm^{-1}) under conditions of low to moderate vibrational excitation (less than $\sim$ 7 Kcal/mole), propensity rules do appear to be operative in vibrational energy transfer processes.

Rule 1. Within a mode, "up-the-ladder" energy transfer is "fast". This simply means that nearly resonant V-V energy transfer events of the type

$$X(v) + X(1) \rightleftarrows X(v+1) + X(0) + \Delta E \qquad (12)$$

are very efficient. For high v states where anharmonicity becomes sizeable (ΔE of the order of kT) the efficiency is expected and observed to drop-off (20). A compensating factor which slows this drop-off is the increase in the square of the matrix element for $v \rightarrow v + 1$ processes which scales like v for a harmonic oscillator. Fig. 4 gives a pictorial representation of Rule 1.

Rule 2. Energy transfer between 2 modes is "fast" if the v = 1 levels of the different modes are close to each other in energy (within $\sim$ kT). This rule can be illustrated by the equation

$$X(\nu_i) + M \rightleftarrows X(\nu_j) + M + h(\nu_i - \nu_j) \qquad (13)$$

If $h(\nu_j - \nu_i) \lesssim kT$, such V-V energy transfer steps generally occur rapidly ($\lesssim$ 100 gas kinetic collisions where M is the parent gas). There is some slight evidence that indicates such intermode exchanges are somewhat slower (100-200 gas kinetic collisions) for molecules which contain all heavy atoms (no hydrogen or deuterium). Figure 5 gives a pictorial representation of Rule 2.

In State-to-State Chemistry; Brooks, P., et al.;
ACS Symposium Series; American Chemical Society: Washington, DC, 1977.

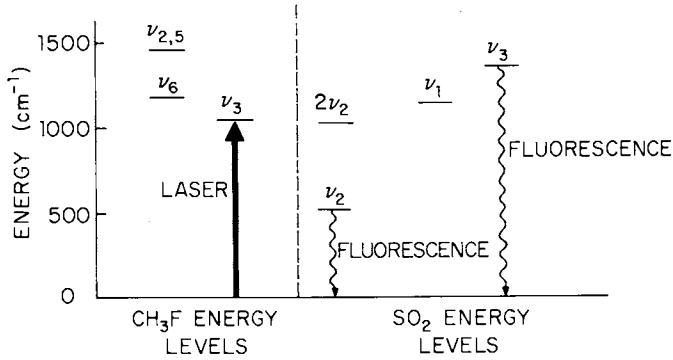

Figure 3. Partial vibrational energy level diagrams for CH_3F and SO_2. Mode descriptions are given in captions for Figures 1 and 2.

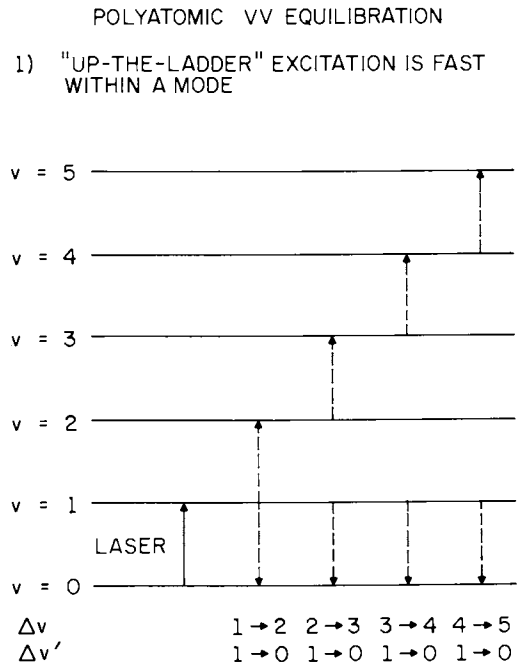

Figure 4. Qualitative rule #1 for V–V energy transfer processes in polyatomic molecules

In State-to-State Chemistry; Brooks, P., et al.;
ACS Symposium Series; American Chemical Society: Washington, DC, 1977.

Rule 3. If the v = 1 levels of two modes are not close in energy, V-V exchange between the modes is enhanced by mechanical Fermi mixing of the modes, or by a large mechanical or electrical anharmonicity for the mode of lowest frequency. To illustrate this rule consider the equation

$$X(n\nu_i) + M \rightleftarrows X(\nu_j) + M + h\,(n\nu_i - \nu_j) \qquad (14)$$

where $n\nu_i$ is the nth level of mode i (the level of mode i which is closest to v = 1 level of mode j) and $h(n\nu_i - \nu_j)$ is $\lesssim kT$. Rule 3 simply indicates that a process of the type (14) will be enhanced if there is someway of coupling $n\nu_i$ to the ground state by a process which is first order in some normal coordinate. Alternatively, such energy transfer events will be enhanced if the potential field of the molecule is not a rapidly converging function of the normal coordinates for mode i (large mechanical or electrical anharmonicity). Energy exchange involving the $SO_2(2\nu_2)$ state appears to "anti"-demonstrate this rule quite well since (3) and (11) are both inefficient. On the other hand, efficient energy exchange between the bending and stretching modes of OCS has been observed and attributed to the large electrical anharmonicity of the bending mode (21). Figure 6 gives a pictorial illustration of Rule 3.

These rules are quite obviously what one would expect on the basis of a first order time dependent perturbation theory approach to collisional energy transfer in which the interaction potential is expanded only to first order in the molecular normal coordinates. There will certainly be many situations where such a simple picture is expected to fail. One may ask why these simple rules are even qualitatively successful in many cases. The answer may be that V-V energy transfer processes which have been observed to date using laser techniques have almost always been faster than V-T/R relaxation or they could not have been detected. (Among the obvious exceptions to this statement are CO_2 (1, 2) and SO_2 (6, 9)). Since V-T/R relaxation probabilities per collision are typically 10^{-2} - 10^{-4}, only rather efficient V-V processes can be observed. Rules 1 - 3, based as they are on a first order perturbation picture, clearly emphasize collision events with large cross sections. A more insidious possibility exists, however. At this early stage in the study of intermode V-V energy transfer, the data base may be so restricted that these rules are valid for the cases studied but have no general long range validity. The answers to this question will become clear as more data is collected.

Metastable Vibrational Energy Distributions

For many small polyatomic molecules overall relaxation of the vibrational states by V-T/R energy transfer is slow compared to mode-to-mode equilibration of vibrational energy. Thus the

In State-to-State Chemistry; Brooks, P., et al.;
ACS Symposium Series; American Chemical Society: Washington, DC, 1977.

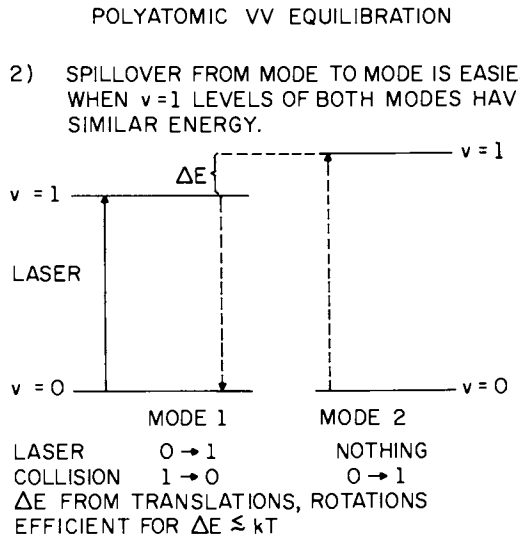

Figure 5. Qualitative rule #2 for V–V energy transfer processes in polyatomic molecules

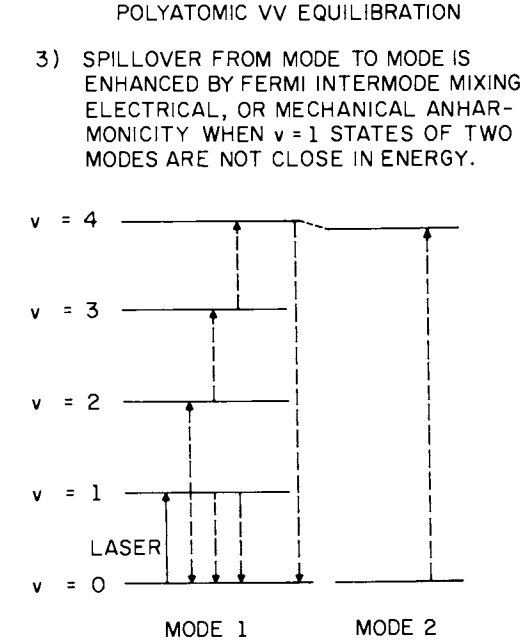

Figure 6. Qualitative rule #3 for V–V energy transfer processes in polyatomic molecules

vibrational states are metastable for relatively long periods of time. During this interval, the vibrational levels may be thought of as "hot" while the translational/rotational degrees of freedom remain "cold". For example, in CH_3F processes (6-9) reach steady state in approximately 75 gas kinetic collisions for the pure gas, while process (10) requires 15,000 collisions. The six modes of CH_3F are in a quasi-equilibrium state during the time between 75 and 15,000 collisions after laser excitation. This metastable state, however, cannot be described by a single vibrational temperature for the vibrational modes, even though the translational/rotational degrees of freedom have a well defined temperature T'. To illustrate these features consider just the CH_3F energy transfer process (6) which brings ν_3 and ν_6 into "equilibrium" or steady-state. The steady state or equilibrium condition for (6) is simply

$$k_6[CH_3F(\nu_3)][M] = k_{-6}[CH_3F(\nu_6)][M] \qquad (15)$$

where k_6 and k_{-6} are the kinetic rate constants in the forward and backward directions for the collision event (6). This leads immediately to

$$(k_6/k_{-6}) = k_{eq} = [CH_3F(\nu_6)]/[CH_3F(\nu_3)]. \qquad (16)$$

Boltzmann statistics give a value for K_{eq} as follows

$$K_{eq} = 2 \exp\{-h(\nu_6 - \nu_3)/kT'\} \qquad (17)$$

where h is Planck's constant, k is Boltzmann's constant, and T' is the temperature of the translational degrees of freedom. The factor of 2 arises from the degeneracy of ν_6. K_{eq} is a function only of T' because k_6, k_{-6} are the products of a cross section and a velocity, both of which depend only on the translational temperature. On the other hand, because of laser pumping, the concentrations $[CH_3F(\nu_3)]$and $[CH_3F(\nu_6)]$ are considerably larger than would be predicted for an equilibrium system at the temperature T'. To take this fact into account, we may define a set of temperatures T_i for the vibrational states i by the equation

$$[CH_3F(i)]/[CH_3F(0)] = g_i \exp[-E_i/kT_i] \qquad (18)$$

where g_i is the degeneracy and E_i the energy of state i. $[CH_3F(0)]$ is the concentration of ground state molecules. Inserting (18) into (16) and (17) gives a parametric equation relating T_3, T_6, and T'

$$\frac{-(\nu_6 - \nu_3)}{T'} = \frac{-\nu_6}{T_6} + \frac{\nu_3}{T_3} \qquad (19)$$

Essentially, T' clamps the ratio between the ν_3 and ν_6 populations while T_i defines the population ratio between state i and the ground state. Since the system is not completely at equilibrium, but only at steady state $T' \neq T_3 \neq T_6$.

The significance of (19) may be understood by setting $T' = 300^{\circ}K$ and noting $\nu_3 = 1049\ cm^{-1}$, $\nu_6 = 1182\ cm^{-1}$. Inserting these values into (19) gives

$$-(133/300) = -(1182/T_6) + (1049/T_3) \qquad (20)$$

Assuming the modes ν_3 and ν_6 are harmonic requres that T_6, $T_3 \geq 0$ (non-inverted populations with respect to the ground state). Thus we may ask what happens when $(1182/T_6) = (133/300)$ or $T_6 \approx 2667$ K. Under such conditions $T_3 = \infty$! Of course, such a result is not possible in practice since an infinite temperature would require infinite pump energy. The model used to describe the system simply breaks down at very high excitation levels. Nevertheless, the general result $T_3 > T_6$ holds. In a similar manner, temperature relationships for all the modes can be derived using equations (6-9). The temperature relationships, when combined with energy and population conservation equations, can in turn be used to determine the vibrational and translational energy distribution at steady-state. The procedure required is non-trivial and has been given in detail elsewhere (18, 19). Fig. 7 compares the laser pumped, V-V steady-state energy distribution in CH_3F with that obtained from Bunsen burner (one temperature) heating. Note that the metastable distribution has a decreasing translational energy (because eqns. 6-9 are overall translationally endothermic) while the Bunsen burner heated gas shows a rapidly increasing translational energy. In the metastable case the energy of the ν_3 mode is maximized while Bunsen burner heating maximizes the ν_2, ν_5 mode energy. Finally, the absolute magnitude of the vibrational energy change is clearly larger in the metastable case. The laser pumped V-V equilibrated steady-state lasts for $\sim$ 15,000 collisions in pure CH_3F.

The distribution of energy in laser pumped CH_3F shown in Fig. 7 can clearly have a significant effect on chemical reactions of this species. For example, the metastable state is expected to favor reactions from the ν_3(C-F) mode rather than the ν_2, ν_5(CH_2 bend) modes as in the Bunsen burner case. In addition, several possibilities exist for the development of laser action from the metastable distribution. Although CH_3F has been used as an example in this discussion, the above results are quite general for any molecule whose V-V rates are fast compared to V-T/R relaxation. A metastable state is achieved in which the energy distribution, controlled by the relaxation or energy transfer mechanisms, cannot be described by one temperature Boltzmann statistics.

In State-to-State Chemistry; Brooks, P., et al.;
ACS Symposium Series; American Chemical Society: Washington, DC, 1977.

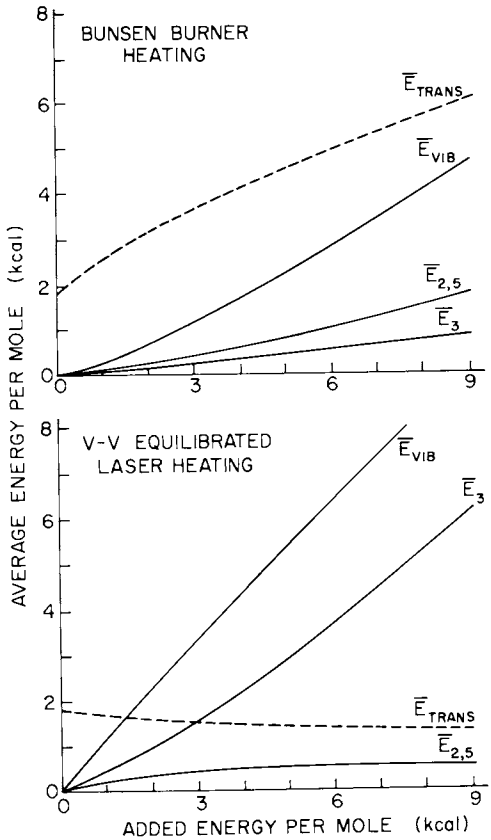

Figure 7. Comparison between Bunsen burner and laser heating of CH_3F. E_{Trans} and E_{vib} are the average total translational plus rotational energy and the average total vibrational energy respectively. E_3 is the average energy of the ν_3 C–F stretching mode while $E_{2,5}$ is the average energy of the ν_2, ν_5 CH_2 bending modes.

In State-to-State Chemistry; Brooks, P., et al.;
ACS Symposium Series; American Chemical Society: Washington, DC, 1977.

Laser Driven Chemical Reactions

Though there have been many reports of laser driven chemical reactions, just two will be mentioned here: (1) the multiphoton dissociation of SF_6 and (2) the laser driven explosion of perfluoro-Dewar benzene.

Laser Driven Reaction of $SF_6 + H_2$ SF_6 absorbs many photons from a high power CO_2 pulsed laser (22- 24). Strong evidence now exists that under certain conditions F atoms are produced by laser excitation (7, 8, 22-24).

$$SF_6 + nh\nu \rightarrow SF_{6-m} + mF \ . \qquad (21)$$

A study of the subsequent reaction of F atoms with hydrogen donors has been made (7, 8, 24)

$$F + H_2 \rightarrow HF + H \qquad (22)$$

$$F + D_2 \rightarrow DF + D \qquad (23)$$

Even at pressures of a few Torr, the HF and DF produced can be observed before significant relaxation sets in by monitoring infrared fluorescence from the v = 3, 2, 1 HF or DF levels. The growth rate of this infrared chemiluminescence is a measure of the reaction rate for (22) and (23) while the vibrational state population distributions clearly identify F atoms as the precursor for HF formation. A particularly interesting feature of this study is that the ratio of the rates for (22) and (23) is consistent with an F atom temperature which is fairly close to ambient (300°K). This strongly suggests that the multiphoton dissociation process for SF_6 produces F atoms with little excess energy (7, 8, 23).

Laser Driven Explosion of Perfluoro-Dewar Benzene Perfluoro-Dewar benzene (FDB) is a metastable form of perfluoro-benzene (FB) which absorbs CO_2 laser radiation quite strongly. Some preliminary experiments on this system have been performed using a focused Q-switched CO_2 laser (25). Such a laser is very low energy (0.5-4 mJ/pulse) by comparision with high energy lasers (0.5-10 J/pulse) ordinarily used to initiate laser driven reactions. Complete isomerization of (FDB) to (FB) can be achieved in one laser shot or gradually over many shots depending on pressure and laser conditions. Once triggered by the laser the large exothermicity of this reaction appears to drive the system into the explosive regime at higher (FDB) pressures. Many questions, such as the relative importance of translational versus vibrational energy on the rate, the degree of vibrational excitation of products, and the importance of

In State-to-State Chemistry; Brooks, P., et al.;
ACS Symposium Series; American Chemical Society: Washington, DC, 1977.

triplet states in the reaction coordinate, remain to be answered for this system.

Acknowledgements. I wish to thank my present and past collaborators, whose work has been discussed here, for many stimulating and exciting hours of fruitful interaction. They are Donald Siebert and Fred Grabiner (SO_2); Eric Weitz, Fred Grabiner, Jack Preses, Richard Slater, Irwin Shamah, and Rekha Sheorey (CH_3F); Irwin Shamah (vibrational temperature and energy distributions); Ralph Weston and Jack Preses ($SF_6 + H_2$ chemistry); and Nick Turro and Bill Farneth (perfluoro-Dewar benzene chemistry). This work was supported by the Joint Services Electronics Program (U. S. Army, U. S. Navy, and U. S. Air Force) under Contract DAAB07-74-C-0341 (currently being continued under Contract DAAG29-77-C-0019), the National Science Foundation under Grant MPS75-04118, and the Advanced Research Projects Agency of the Department of Defense administered by the Office of Naval Research (Boston) under Contract N00014-75-C-1106.

Literature Cited

1) Hocker, L. O., Kovacs, M. A., Rhodes, C. K., Flynn, G. W., and Javan, A., Phys. Rev. Lett. (1966) 17, 233.
2) Yardley, J. T. and Moore, C. B., J. Chem. Phys. (1967) 46, 4491.
3) Bates, R. D., Jr., Knudtson, J. T., Flynn, G. W., and Ronn, A. M., Chem. Phys. Lett. (1971) 8, 103.
4) Weitz, E. and Flynn, G. W., J. Chem. Phys. (1973) 58, 2679.
5) Grabiner, F. R., Siebert, D. R., and Flynn, G. W., Chem. Phys. Lett. (1972) 17, 189.
6) Siebert, D. R., Grabiner, F. R., and Flynn, G. W., J. Chem. Phys. (1974) 60, 1564.
7) Preses, J., Weston, R., and Flynn, G., Chem. Phys. Lett. (1977) to be published.
8) Quick, C. R., Jr., and Wittig, C., Chem. Phys. Lett. (1977) to be published.
9) Siebert, D. R. and Flynn, G. W., J. Chem. Phys. (1975) 62, 1212.
10) Slater, R. C. and Flynn, G. W., J. Chem. Phys. (1976) 65, 425.
11) Grabiner, F. R., Flynn, G. W., and Ronn, A. M., J. Chem. Phys. (1973) 59, 2330.
12) Karny, Z., Ronn, A. M., Weitz, E., and Flynn, G. W., Chem. Phys. Lett. (1972) 17, 347.
13) Weitz, E., Flynn, G. W., and Ronn, A. M., J. Chem. Phys. (1972) 56, 6060.
14) Preses, J., Weitz, E., and Flynn, G. W., "Vibrational Energy Transfer in CH_3F-O_2 Mixtures: Impurity Molecules as Probes of Vibrational Relaxation Mechanisms" manuscript in

preparation.
15) Shamah, I. and Flynn, G. W., "Laser Catalyzed Translation to Vibration Energy Conversion in CH_3F-O_2 Mixtures," to be published.
16) Sheorey, R., Slater, R. C., and Flynn, G. W., "Laser Fluorescence Study of $2\nu_3$ Overtone Relaxation in CH_3F," manuscript in preparation.
17) Sheorey, R., and Flynn, G. W., work in progress.
18) Shamah, I., and Flynn, G. W., J. Am. Chem. Soc. (1977) 99, 3191.
19) Shamah, I., and Flynn, G. W., "Translational and Vibrational Energy Distributions in Metastable Laser Pumped Polyatomic Molecules: A Quasithermodynamic Description," manuscript in preparation.
20) For a recent review see Weitz, E., and Flynn, G. W., Ann. Rev. Phys. Chem. (1974) 25, 275.
21) Siebert, D. R., and Flynn, G. W., J. Chem. Phys. (1976) 64, 4973.
22) Ambartsumyan, R. V., Gorokhov, Yu. A., Letokohov, V. S., and Makarov, G. N., JETP (1976) 42, 993 (and references sited therein).
23) Coggiola, M. J., Schulz, P. A., Lee, Y. T., and Shen, Y. R., Phys. Rev. Lett. (1977) 38, 17.
24) Lyman, J. L., Jensen, R. J., Rink, J., Robinson, C. P., and Rockwood, S. D., Appl. Phys. Lett. (1975) 27, 87.
25) Farneth, W., Flynn, G. W., and Turro, N. J., work in progress.

In State-to-State Chemistry; Brooks, P., et al.;
ACS Symposium Series; American Chemical Society: Washington, DC, 1977.

19

Molecular Dynamics of Electronic Energy Transfer: Quenching of $Na(3^2P_{3/2})$ Atoms by NO Molecules

JOEL A. SILVER, N. C. BLAIS, and G. H. KWEI

University of California, Los Alamos Scientific Laboratory, Los Alamos, NM 87545

The collisional quenching of electronically excited alkali atoms has long served as a prototype for nonadiabatic processes. Many of these studies have been total quenching cross section measurements for collisions of excited $Na(3^2P)$ atoms with rare gas atoms and diatomic molecules (1). Recently, relative rates of transfer of energy from excited Na atoms into individual vibrational levels of CO molecules have been measured by infrared absorption (2) and the recoil velocities of quenched Na atoms inelastically scattered from several small molecules have been determined in a molecular beam scattering experiment (3). Neither of these studies has provided any information on the detailed mechanism for energy transfer or on the partitioning of internal energy between vibration and rotation. At this Meeting, we report initial results from a crossed molecular beam study of the process

$$Na(3^2P_{3/2}) + NO(O,J) \rightarrow Na(3^2S_{1/2}) + NO(v',J')$$

in which both scattering angle and product velocity distributions are measured. The results provide the first direct evidence that energy transfer takes place via the formation and subsequent decomposition of a collision complex and that rotational excitation is low. Thus the electronic energy is partitioned primarily between relative translation (~25%) and vibration of the NO molecule (~75%).

A block diagram of the apparatus is shown in Figure 1. A nearly effusive Na atom beam (at 720 K) is crossed with an H_2-seeded nozzle beam of NO molecules. Under these conditions, the NO molecules are internally relaxed and we estimate that the most probable initial rotational angular momentum is $\lesssim 4\hbar$. Approximately 1 to 5% of the Na atoms in the collision region are excited to the $3^2P_{3/2}$ state by an argon ion pumped cw dye laser. The dye laser is frequency stabilized by a feedback system which monitors the fluorescence at the scattering center. Processes involving electronically excited atoms are distinguished from ground state processes by modulation of the laser beam. A simple chopping

In State-to-State Chemistry; Brooks, P., et al.;
ACS Symposium Series; American Chemical Society: Washington, DC, 1977.

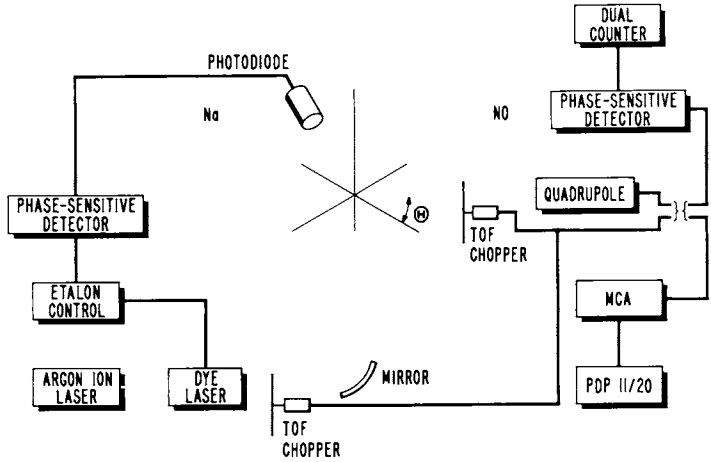

Figure 1. Block diagram of the experimental apparatus

wheel is used for total intensity measurements while a pseudo-random binary wheel is used for cross correlation time-of-flight measurements. A second pseudorandom wheel inside the vacuum chamber is used for obtaining ground state particle velocity distributions. The remainder of the apparatus has been described elsewhere in greater detail (4).

The angular distribution of NO molecules scattered from excited Na atoms is shown in Figure 2(a). The velocity distribution for NO at $\Theta = -14°$ shown in Figure 2(b), together with time-of-flight data taken at other laboratory angles, confirm that inelastically scattered NO molecules are responsible for the signals that contribute to this angular distribution. The shape of the angular distribution, with the peak near -10° and the rise at large angles, suggests that energy transfer takes place via a complex mechanism. Unfortunately, the backward peak (with respect to the initial NO direction) in the angular distribution is expected to be at $\sim 105°$ and is not accessible in these experiments. However, evidence for complex formation is provided by the velocity distribution of Na atoms scattered at $\Theta = -18°$ as shown in Figure 2(b). Scattering of Na at this angle corresponds to scattering of NO in the backward direction and the measured Na velocity is commensurate with the velocity of the inelastically forward scattered NO. This is illustrated by the recoil energy distributions [Figure 3(b)] for Na(-18°) and NO(-14°). An approximate transformation of the laboratory angular distribution to the center-of-mass (c.m.) system using only the most probable NO recoil velocity produces a distribution that is shown in Figure 3(a). This distribution is sharply peaked in the forward direction and displays approximate forward-backward symmetry over the limited range of

In State-to-State Chemistry; Brooks, P., et al.;
ACS Symposium Series; American Chemical Society: Washington, DC, 1977.

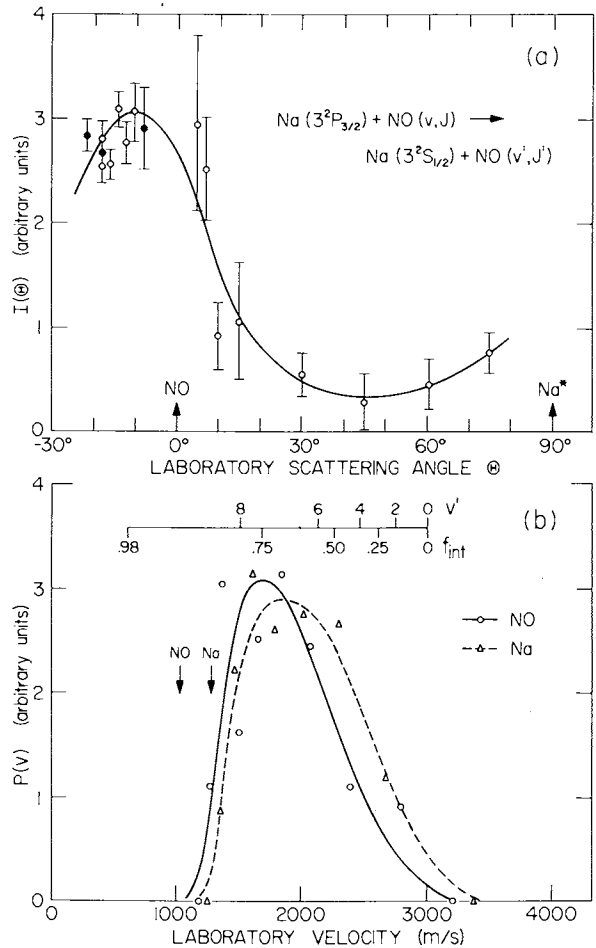

Figure 2. Laboratory distributions. (a) Laboratory angular distribution of NO molecules scattered from excited Na($3^2P_{3/2}$) atoms. Different symbols refer to data taken in separate runs; arrows denote the location of the primary beams, and error bars represent ± one standard deviation. At laboratory angles within ~8° of the NO beam, the data includes partially offsetting contributions from NO molecules elastically scattered from excited Na atoms and from modulation of elastic scattering of ground state species resulting from laser depletion of the ground state Na concentration in the collision region. (b) Laboratory flux density velocity distributions for NO and Na at laboratory angles of −14° and −18°, respectively. The upper scales show the fraction of the total available energy converted to internal energy, f_{int}, and the final vibrational state of NO (if there were no rotational excitation) for given values of the NO laboratory velocity. Arrows indicate the most probable recoil velocities for elastically scattered NO and Na (both $3^2S_{1/2}$ and $3^2P_{3/2}$).

In State-to-State Chemistry; Brooks, P., et al.;
ACS Symposium Series; American Chemical Society: Washington, DC, 1977.

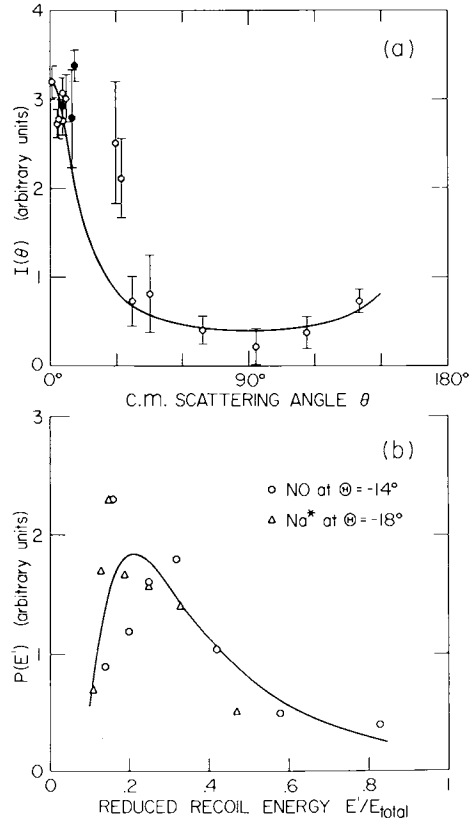

Figure 3. Approximate center-of-mass distributions. (a) Center-of-mass angular distribution of NO obtained from the data in Figure 2(a) using an approximate transformation with a fixed value of 1420 ms^{-1} for the c.m. recoil velocity. The error bars again represent ± one standard deviation. The solid curve is the calculated distribution for the decomposition of a prolate complex having a thermal distribution of rotational states with $L_m/J_{mp} = 10$. (b) Approximate recoil energy distributions taken from the velocity distributions shown in Figure 2(b).

In State-to-State Chemistry; Brooks, P., et al.;
ACS Symposium Series; American Chemical Society: Washington, DC, 1977.

c.m. scattering angles from 0° to 140°. This implies that the shape of the complex is roughly prolate (5). However, the lack of precise knowledge of the c.m. distribution near 180° precludes an estimate of the mean lifetime of the complex (6).

The anisotropy in the c.m. angular distribution (ratio of cross sections at 0° and 90°) is unusually large with a value of ∿8 and, since the initial rotational angular momentum is small, provides an estimate of ∿10 for the ratio of the maximum initial orbital angular momentum, L_m, to the most probable final rotational angular momentum, J'_{mp} (5). Since the quenching cross section is large (7), L_m is also expected to be large. Estimating L_m from the crossing between covalent and ionic surfaces in the "harpoon" mechanism (8) gives a value of ∿165ħ; therefore $J'_{mp} \simeq 17\hbar$. The solid curve in Figure 3(a) is the calculated distribution for $L_m/J'_{mp} = 10$ (5). Except for the two points which were taken near the NO primary beam (and may therefore include contributions from elastically scattered NO molecules), the agreement is reasonably good.

The recoil velocity and energy distributions [Figures 2(b) and 3(b)] show that energy transfer is nonresonant, with ∿75% of the available energy of 220 kJ/mol appearing as internal excitation. Since rotational excitation (∿6 kJ/mol) is negligible, these distributions provide a direct measure of the relative vibrational state populations of the scattered NO. As shown in Figure 2(b), the v' = 7 and 8 levels are preferentially populated with some shading to lower values of v'.

The quenching of excited alkali atoms by diatomic molecules has traditionally been treated as a process involving multiple potential surface crossings where a stongly attractive ionic state couples the upper and lower covalent states. Excited atoms and diatomic molecules which approach each other in states that cross adiabatically to the ionic state form complexes which later decompose to ground state products via a nonadiabatic transition. This picture has been used in theoretical treatments of the quenching of $O(^1D)$ by N_2 where the long complex lifetimes imposed by the spin-forbidden transition result in statistical energy partitioning (9). In the $Na(3^2P_{3/2}) + NO$ system, the nonadiabatic transitions have greater probability and we would not expect statistical behavior. The final vibrational distribution we observe is in fact strongly reminiscent of the distributions predicted for the quenching of $Na(3^2P)$ by N_2 using a simple multiple-crossing electron-jump model (10).

This work was done under the auspices of the United States Energy Research and Development Administration.

Literature Cited

1. Barker, J. R., and Weston, R. E., J. Chem. Phys. (1976) 65, 1427, and references cited therein.
2. Hsu, D. S. Y., and Lin, M. C., Chem. Phys. Letters (1976) 42, 78.
3. Hertel, I. V., Hofmann, H., and Rost, K. J., Chem. Phys. Letters (1977) 47, 163.

4. Blais, N. C., Cross, J. B., and Kwei, G. H., J. Chem. Phys. (1977) 66, 2488.
5. Miller, W. B., Safron, S. A., and Herschbach, D. R., Discussions Faraday Soc. (1967) 44, 112.
6. Bullitt, M. K., Fisher, C. H., and Kinsey, J. L., J. Chem. Phys. (1974) 60, 478.
7. Kondratiev, V., and Siskind, M., Physik. Z. Sowjetunion (1935) 8, 644. However, these results display a velocity dependence contrary to those found more recently for other systems (see Reference 1).
8. For a "harpoon" model, a value of r_c = 4.7 Å can be calculated from the electron affinity of NO (0.024 eV) and the ionization potential of Na(3^2P) (3.03 eV); this value, used with the most probable initial relative velocity of 1670 ms^{-1}, gives $L_m \cong 165\hbar$. The quenching cross section is then $Q = f\pi r_c^2 = 28$ Å^2, where f = 3/8 is the fraction of excited potential surfaces that correlate with the ionic surface in C_s symmetry.
9. Tully, J. C., J. Chem. Phys. (1974) 61, 61.
10. Bauer, E., Fisher, E. R., and Gilmore, F. R., J. Chem. Phys. (1969) 51, 4173.

In State-to-State Chemistry; Brooks, P., et al.;
ACS Symposium Series; American Chemical Society: Washington, DC, 1977.

20

Energy Transfer and Reaction in LiH $A^1\Sigma$

L. A. MELTON and P. H. WINE

The University of Texas at Dallas, Box 688, Richardson, TX 75080

We report here a series of measurements on the simple triatomic system LiH $A^1\Sigma$, v', J' + Li(^{2}S) → products. This system was chosen because the existence of tunable dye lasers in the near ultraviolet region makes possible selective excitation of the LiH, and because systematic data on the energy transfer and reactions of this system, which contains only three nuclei and seven electrons, might lead to fruitful comparison with ab initio calculations now available. (1,2,3,4)

The experimental procedure has been described previously, and only a brief summary need be given here. (5) The nitrogen laser pumped dye laser used a PBD solution in dimethyl formamide and was continuously tunable from 3600 Å to 3800 Å with a typical bandwidth of 0.5 Å. Because the lines of LiH are in general well separated, this bandwidth was sufficient to insure excitation of a single vibrational-rotational level of the $A^1\Sigma$ state. The LiH was prepared by allowing H_2 to react with the lithium vapor present in a lithium heat pipe. The predominant species in the center of the T-shaped heat pipe, where the fluorescence was excited, was Li(^{2}S), with trace amounts of Li_2, (∿2%) H_2, LiH, and He present. The only significant collision partner for the LiH $A^1\Sigma$ molecule was Li(^{2}S) atoms. The lithium density in the center of the heat pipe was determined by measuring the buffer gas pressure in the cool zones with a capacitance manometer. The pulsed fluorescence was detected through a 1-m monochromator with a 1P28 phototube, whose output was fed to a PAR model 162/164 boxcar integrator. Calibration of the time base was confirmed by regular scans of the output of a crystal controlled 50 Mhz oscillator. The entire fluorescence, including the rise, was least square fit to the convolution of a single exponential decay with the separately detected dye laser scattered light.

The fluorescence decay times τ obtained from the least squares fitting procedure were used to determine the collision free radiative lifetimes and total quenching rates by plotting τ^{-1} versus P_{Li}. The total rates of collisional transfer, out of the initially excited LiH $A\Sigma v'$, J' level, in collisions with Li

In State-to-State Chemistry; Brooks, P., et al.;
ACS Symposium Series; American Chemical Society: Washington, DC, 1977.

atoms, were found to depend very strongly on the initial rotational quantum number. In addition, in a separate series of experiments, the total rates of collisional transfer by collisions with He atoms were determined by plotting the ratio of the LiH fluorescence with only Li atoms present to that obtained when a variable, known amount of He was also present, all other conditions being held constant, versus the helium pressure. Table I summarizes the results obtained thus far.

TABLE I.

LiH $A^1\Sigma^+$ Total Quenching Data

v'	J'	τ_o(nsec)	$\sigma_{Li}\pm2\sigma(\AA^2)$	$\sigma_{He}\pm2\sigma(\AA^2)$
5	0	33.0±3.5	543±60	56.2±6.9
5	5	32.6±3.0	363±51	43.2±6.9
5	10	32.6±3.0	229±28	43.0±5.5
5	15	29.0±3.2	127±28	-
8	15	32.2±5.9	307±69	46.5±10.2

τ_o, the collision free radiative lifetime, is remarkably constant with J', and in very close agreement with independent measurements by Dagdigian, (6) and with calculations using RKR Franck-Condon factors and the ab initio transition moment calculated by Docken and Hinze. (7)

The last two columns in Table I give the effective cross sections, σ, for the total quenching processes ($\sigma=k/v$ where v is the mean collision velocity). For collisions with Li atoms, the cross sections are several times the gas kinetic cross section ($\sim$50 A^2) and decrease rapidly with increasing rotational quantum number J', of the initially prepared state. The cross sections for quenching collisions with He are constant at roughly the gas kinetic cross section. In addition, in LiH/Li collision work, a spectral scan with Li pressures of 1-2 torr shows very little evidence of new features in the LiH fluorescence spectrum, as might arise from collision induced rotational transfer; we estimate the total rotational transfer cross sections to be $<30A^2$ in these cases. In contrast, with He, many new rotational line emissions are observed even at pressures of 0.5 torr.

We interpret these data as follows. The LiH/He collisions represent hard impulsive collisions in which changes in the rotational angular momentum of the initially prepared state -- and very little else -- occur. Every collision results in a change in the initial angular momentum. In the case of collisions with Li atoms, because of the magnitude of the observed cross sections, long range forces are clearly involved, and the strong dependence on J' suggests that dynamical effects may be important. Whatever the mechanism(s) responsible, it results in destruction of the LiH $A^1\Sigma$ state, because very little emission from other levels,

In State-to-State Chemistry; Brooks, P., et al.;
ACS Symposium Series; American Chemical Society: Washington, DC, 1977.

populated by collisional transfer, is observed.

We have made calculations of the long range energy transfer cross sections for the process

$$LiH\ A^1\Sigma,\ v'=5,\ J' + Li(^2S) \rightarrow$$

$$LiH\ X^1\Sigma,\ v''=11,\ J'\pm 1 + Li(^2P) + \Delta E$$

in which the energy defect ΔE is minimized. The interaction in this case is a transition dipole-transition dipole potential; the method of calculation follows that of Cross and Gordon (8) and Melton and Klemperer (9). We define a critical impact paramater b by $P(b^*) = 1/2$, and for $b \leq b^*$, we take $P(b) = 1/2$. The collision velocity was taken to be the mean collision velocity at 1000°K. The electronic transition moment for the LiH A-X(5,11) band (1.33D) was provided by Zempke and Stwalley, and is based on RKR Franck-Condon factors and the ab initio transition moment function of Docken and Hinze. (10,4) The energy defects were computed from recent spectroscopic data on LiH provided by Stwalley. (11) The calculated cross sections are, of course, very sensitive to the values of ΔE used, and the present data is believed to be accurate to better than $\pm 1 cm^{-1}$. Table II summarizes these calculations.

Table II.

J'	J"	$\Delta E(cm^{-1})$	σ_{Li}(Calc)(Å^2)		σ_{Li}(Expt)(Å^2)$\pm 2\sigma$
0	1	+69	144		543±60
5	4	+62	58	184	363±51
5	6	-52	126		
10	9	-71	109	111	229±28
10	11	-284	2		
15	14	-316	2	2	127±28
15	16	-619	0		

These calculations emphasize that much of the decrease in total quenching cross section with increasing J' is due to the increasing energy defect, rather than to important dynamical constraints. The discrepancy between the calculated and measured cross sections would be much diminished if for $b \leq b^*$, one takes $P(b) = 1$. To do this, however, would require the assumption of an additional efficient destruction channel for $Li(^2P)$ during a collision with LiH $X^1\Sigma$. Even with such an assumption, there would remain a significant discrepancy for the J'=0 results.

Further experiments, on additional LiH $A^1\Sigma$ levels, are underway in order to clarify these points.

Acknowledgement is made to the Robert A. Welch Foundation for their generous support of this work.

Literature Cited

(1) England, W. B., Sabelli, N. H., and Wahl, A. C., J. Chem. Phys., (1975), 63, 4596.
(2) England, W. B., Sabelli, N. H., Wahl, A. C., and Karo, A., J. Chem. Phys. (1977), 81, 772.
(3) Docken, K. K., and Hinze, J., J. Chem. Phys., (1972), 57, 4928.
(4) Docken, K. K., and Hinze, J., J. Chem. Phys., (1972), 57, 4936.
(5) Wine, P. H., and Melton, L. A., J. Chem. Phys., (1976), 64, 2692.
(6) Dagdigian, P. J., J. Chem. Phys., (1976), 64, 2609.
(7) Stwalley, W. C., Paper FB4, 31st Symposium on Molecular Spectroscopy, Ohio State University, (June 14-18, 1976).
(8) Cross, R. J., and Gordon, R. G., J. Chem. Phys., (1966), 45, 3571.
(9) Melton, L. A., and Klemperer, W., J. Chem. Phys., (1973), 59, 1099.
(10) Zempke, W., and Stwalley, W. C., private communication.
(11) Stwalley, W. C., private communication.

In State-to-State Chemistry; Brooks, P., et al.;
ACS Symposium Series; American Chemical Society: Washington, DC, 1977.

21

Vibronic Excitation in Atom–Diatom Systems: N_2^+–He Collisions

J. D. KELLEY
McDonnell Douglas Research Laboratories, St. Louis, MO 63166

G. H. BEARMAN, H. H. HARRIS, and J. J. LEVENTHAL
University of Missouri–St. Louis, St. Louis, MO 63121

Spectroscopic analysis of collision-produced emissions is a powerful method for study of state-to-state chemistry. By employing mass-selected ion beams (or neutral beams), the reactant species and collision energy are well defined; luminescence resulting from the collisions then provides definitive information on state distributions of excited products. Examples of processes which may lead to excited products are charge transfer-excitation (CTE), collision-induced excitation (CIE), excitation transfer and atomic rearrangement.

Processes of particular interest are those which lend themselves to interpretation using simple theoretical models. As a starting point, the Franck-Condon (FC) model in which excitation is assumed to proceed vertically can be applied when electronically excited molecules are produced. However, it has been observed that the vibrational state distributions resulting from CTE processes deviate substantially from those predicted from the FC model (1); usually these distributions tend toward the FC picture as the collision energy is increased. A popular model used to rationalize these deviations in CTE processes is based on the assumption that target molecule distortion by the electric field of the incoming ion causes vertical transitions from a deformed neutral molecule so that FC factors calculated from the undistorted ground-state potential energy curve are not applicable. In an effort to further test these models, we have undertaken an extensive study of $N_2^+[X^1\Sigma_g^+(v=0)]$ - rare gas CIE processes. Since the most abundant observable product (using spectroscopic techniques) is $N_2^+(B^2\Sigma_u^+)$, ion-induced polarization is unimportant.

Figure 1 is representative of the data and illustrates two of the features common to these systems: 1) over the entire energy range the vibrational state distributions are decidedly non-FC, and 2) as the collision energy is increased, the average vibrational energy in the B state decreases and the distribution

In State-to-State Chemistry; Brooks, P., et al.;
ACS Symposium Series; American Chemical Society: Washington, DC, 1977.

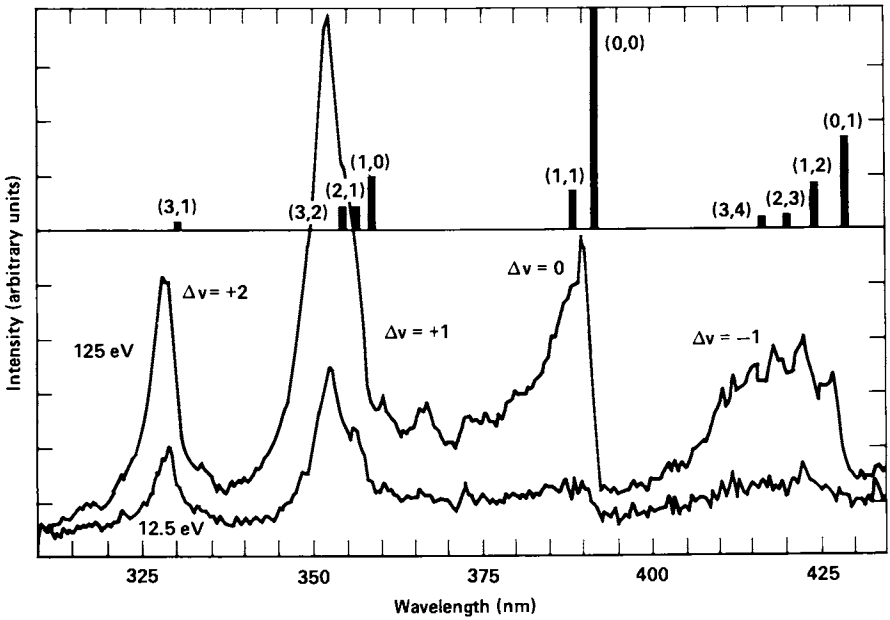

Figure 1. Spectra resulting from $N_2^+(X)$–He CIE at 12.5 eV and 125 eV (c.m.). Emissions are from the N_2^+ first negative ($B \rightarrow X$) band system. The bars represent a vertical model spectrum.

approaches the FC picture. Both of these features also occur in the CTE case indicating that a more general model than polarization-distortion is required.

The model which we have developed (2) and applied to N_2^+-He CIE is based on the assumption that deviations from FC behavior are caused by direct translational-vibrational (T-V) excitation in both the initial (X) and final (B) electronic states of N_2^+. This T-V transfer proceeds via the short-range N_2^+-He interaction. The potential hypersurfaces describing $N_2^+(X)$-He and $N_2^+(B)$-He are taken to have an avoided crossing for some value of R, the N_2^+-He separation. For simplicity, we have assumed that these two hypersurfaces $V_X(r,\theta,R)$ and $V_B(r,\theta,R)$ are independent of the N_2^+-He orientation angle θ, and that the dependence on N-N separation, r, can be approximated as

$$V_{X,B}(r,R) \approx V_{X,B}(r_e,R) + (r-r_e)\frac{\partial V_{X,B}(r_e,R)}{\partial r} + \frac{1}{2}(r-r_e)^2 \frac{\partial^2 V_{X,B}(r_e,R)}{\partial r^2} . \quad (1)$$

In State-to-State Chemistry; Brooks, P., et al.;
ACS Symposium Series; American Chemical Society: Washington, DC, 1977.

The term $\frac{\partial^2 V_{X,B}(r_e,R)}{\partial r^2}$ can be written as $k_0 + k_1(R) \approx k_0$, the unperturbed N_2^+ force constant. In this study, we have replaced the adiabatic surfaces with diabatic surfaces which cross at R_C; these diabatic states are coupled by a potential operator. For mathematical convenience, these surfaces are taken to vary as exp-R/L. A number of calculations were performed in which the important parameters were varied; these parameters are: the range parameter, L; the X-B coupling matrix element; and the potential energy at the crossing point, V*. R-motion was treated classically, but all other calculations were quantum mechanical.

Two conclusions can be drawn from the calculations. First, for a given collision energy $E_{COLL} > V^*$, the opacity function $P_{X\to B}(b)$, which represents the total electronic transition probability as a function of impact parameter b, rises as b increases from b=0 to b=R_C and then falls rapidly for b > R_C. For $E_{COLL} > V^*$, the surface crossing region is accessible for b < R_C but not for b > R_C; in the latter case, the transition proceeds by tunnelling through an energy gap which increases rapidly with b.

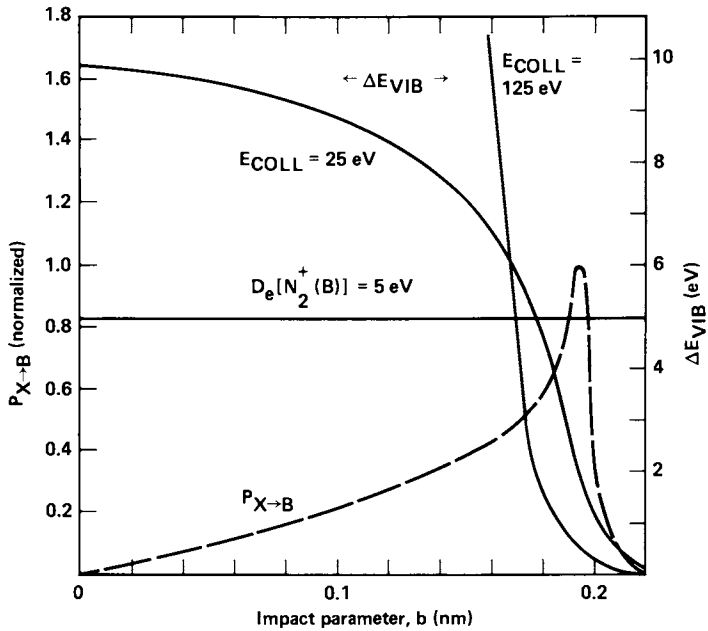

Figure 2. Total relative $N_2^+(X \to B)$ transition probability, $P_{X\to B}(b)$, and vibrational energy transfer to $N_2^+(X, v = 0)$, $\Delta E_{VIB}(b)$. The potential parameters are (see text): *L = 0.02 nm, V* = 4.0 eV, R_c = 0.2 nm. The $P_{X\to B}(b)$ curve shown accurately represents results for E_{COLL} between 25 and 125 eV.*

In State-to-State Chemistry; Brooks, P., et al.;
ACS Symposium Series; American Chemical Society: Washington, DC, 1977.

The second conclusion is that the average vibrational energy, $\overline{\Delta E}_{VIB}$, transferred to $N_2^+(X)$ by T-V coupling, is a decreasing function of E_{COLL} for $b \gtrsim R_c$ ($\Delta E_{VIB}(b \gtrsim R_c) \propto 1/E_{COLL}$). This occurs because E_{COLL} is much greater than the N_2^+ vibrational spacing ($\hbar\omega_{VIB} \gtrsim 0.25$ eV) and also because the trajectories are approximately rectilinear for large b. For small b, however, $\Delta E_{VIB}(b)$ increases with E_{COLL}, and can become so large that the $N_2^+(B)$ formed from such highly excited $N_2^+(X)$ immediately dissociates [D_e ($N_2^+(B)$) $\gtrsim$ 5 eV]. The experimental technique does not allow observation of such collision-induced dissociation, so that a calculation for comparison with data need only consider b greater than some value b* for which $\Delta E_{VIB}(b^*) = 5$ eV. Note that we are inferring the extent of B-state vibrational excitation from the X-state excitation in a given collision; a full calculation requires a more complex treatment than afforded by our present model. Figure 2 shows the form of $P_{X\to B}(b)$ when $E_{COLL} > V^*$; superimposed are $\Delta E_{VIB}(b)$ curves for two values of E_{COLL}. Since

$$\overline{\Delta E}_{VIB} = \int_{b^*}^{\infty} P(b)\ \Delta E_{VIB}(b)\ b\,db \Big/ \int_{b^*}^{\infty} P(b)\ b\,db,$$

the observed decrease in $\overline{\Delta E}_{VIB}$ with increasing E_{COLL} can be qualitatively understood.

Although these calculations have been applied specifically to N_2^+-He CIE, the model is applicable to any atom-diatom process having electronically excited molecular products. The decrease in $\overline{\Delta E}_{VIB}$ with increasing E_{COLL} is not peculiar to the present system but rather is to be expected for systems with an accessible avoided surface crossing, provided E_{COLL} is high enough. Since this T-V excitation is superposed on the usual vertical (FC) distribution, such systems will tend toward the FC picture at high collision energy.

Research supported in part by US ERDA under Contract no. EY 76-S-02-2718.*000, and in part by the McDonnell Douglas Independent Research and Development Program.

Literature Cited

(1) Bearman, G. H., Earl, J. D., Pieper, R. J., Harris, H. H., and Leventhal, J. J., Phys. Rev., (1976), A13, 1734 and references cited therein.
(2) Kelley, J. D., Bearman, G. H., Harris, H. H., and Leventhal, J. J. (submitted).

22

Mode-to-Mode Collisional Flow of Vibrational Energy within the S_1 State of Benzene Vapor

C. S. PARMENTER and KENNETH Y. TANG

Department of Chemistry, Indiana University, Bloomington, IN 47401

If low pressure benzene is excited to a single vibronic level low in the S_1 manifold, one obtains a simple fluorescence spectrum which is uniquely characteristic of molecules emitting from the prepared level. Changes in this spectrum occur upon addition of foreign gas, and in most cases these changes are due solely to the collisional flow of vibrational energy in the S_1 state before fluorescence.

We have monitored these changes at the very initial stages of foreign gas addition to get absolute cross sections for transfer from the S_1 vibrational level $\nu_6'=522cm^{-1}$ (6^1) to each of a number of neighboring levels. A schematic in Fig. 1 shows the levels to which transfer can be seen. Ten added gases have been used, and the resulting ensemble of 40 cross sections comprises our experimental picture of the vibrational energy flow.

The data are given in Fig. 2. Numerous IR studies describe energy flow in ground electronic states, and their results form a base for comparison. What is new about vibrational energy flow in excited electronic states?

The answers dwell on two points. First we find that the absolute cross sections are much larger in the excited state than the ground state. Second, we find that the partitioning of flow among the many final levels is governed by strong propensity rules, and the same rules seem to operate in both electronic states.

The magnitude of the cross sections for level-to-level transfer can be gauged from the total transfer efficiencies. Large cross sections are the rule. For example, the addition of a quantum of ν_{16}' (channel D) requires a TR → V exchange of $237cm^{-1}$, yet He accomplishes this in only 18 collisions. Channel D cross sections for N_2, CO and CO_2 are equally large, with collision numbers of 11, 9 and 5 respectively. Data from numerous diatomics (1) and from glyoxal (2) suggest generality in these large upper state cross sections.

The Σ column for each gas in Fig. 2 shows that over seventy percent of the flow goes into four (or fewer) channels, in spite

In State-to-State Chemistry; Brooks, P., et al.;
ACS Symposium Series; American Chemical Society: Washington, DC, 1977.

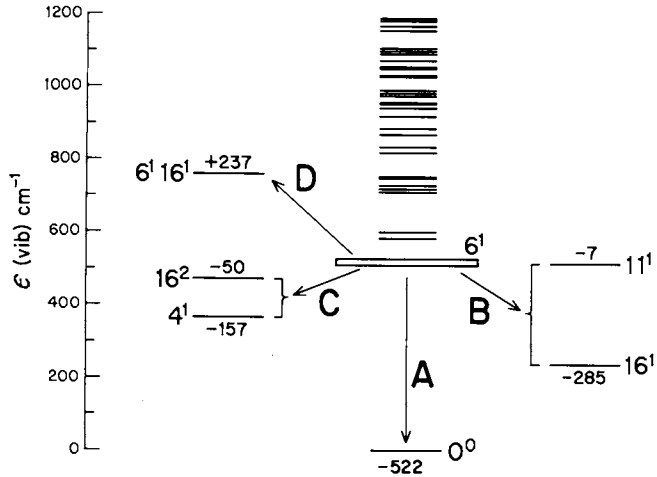

Figure 1. Schematic showing every vibrational level in the first 1200 cm⁻¹ of S_1 benzene. Heavy lines show level pairs too close to separate in the schematic. The level 6′ is pumped by the exciting light. Collisional slow of vibrational energy can be followed from this level to the zero point level (Channel A), to the level $6^1 16^1$, to the pair of levels 11^1 and 16^1 (Channel B), and to the pair of levels 4^1 and 16^2.

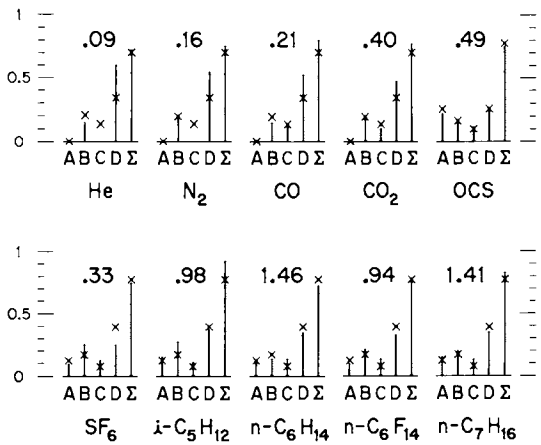

Figure 2. The numbers give the total collision efficiencies of various collision partners for vibrational energy transfer from the level 6^1 into the nearby field of S_1 levels. The vertical bars indicate the function of total vibrational energy transfer which goes into specific channels, with the Σ columns indicating the fraction into the channels A, B, C, and D combined. The crosses indicate the fractions calculated from the propensity rules.

In State-to-State Chemistry; Brooks, P., et al.;
ACS Symposium Series; American Chemical Society: Washington, DC, 1977.

of the large number of nearby final levels. Thus, strong propensity rules govern the transfer.

The rules also establish fairly common flow patterns for partners transferring energy by V-TR transfer alone (He, N_2, CO, CO_2), and another set of common patterns for V-VTR partners. Note that loss of the ν_6 fundamental (Channel A) is inefficient with V-TR partners, but important with V-VTR partners. Adding a fundamental of ν_{16}^1=237cm^{-1} (Channel D) is the dominant transfer for every gas in spite of opportunity for transfer to a level only 7 cm^{-1} away from the initial level (Channel B). By comparison of CO_2 and OCS channel A efficiencies, one observes clearly the effect of resonance transfer from ν_6^1=522 of benzene to $\nu_2^{1\prime}$=520cm^{-1} of OCS.

From SSH calculations made by others on ground state systems (3-7), we have formulated rules which describe these transfers. The relative probability P for a given level-to-level transition in which, say, mode A changes i→j and mode B (in either benzene or the collision partner) changes k→ℓ is given by

$$P(A_{ij}, B_{k\ell}) \propto g_j . g_\ell . U_A^2 . U_B^2 . I$$

The final level degeneracies g_j and g_ℓ enter in a straight forward way. U_A and U_B are matrix elements dependent principally upon vibrational quantum number changes, and we use U^2=10^{-1} for each $\Delta\upsilon$=1 change. I is a prohibition dependent principally on the amount of energy ΔE switched between V and TR degrees of freedom. We gauge its magnitude from prohibitions calculated for transfers in CH_4, CH_3F, and CH_3Cl (5-7).

We have used these rules to calculate transfer probabilities from 6^1 to every level in the first 1000cm^{-1} of S_1 benzene, assuming vibrational resonances whenever the rules allow them to help. The fractions of transfer into various channels were derived from these results, and are given for each gas in Fig. 2.

The rules, with a few exceptions, describe the flow patterns remarkably well. Not only is the channel-to-channel competition replicated, but also the fraction of total transfer appearing in the four channels combined. Exploration of the calculations show that the competition among channels is governed principally by a trade-off between the prohibitions of large ΔE switching and multiple quantum changes.

In summary, a number of generalities about collisional flow of vibrational energy are suggested. (i) Cross sections for energy flow are much larger in excited states than in ground electronic states. (ii) Strong propensity rules control the energy flow, and these rules are simply expressed in terms of $\Delta\upsilon$ changes and V-TR energy gaps ΔE. (iii) A common set of rules describes both V-TR and V-V processes. (iv) A common set of rules describes energy flow in both excited and ground electronic states. (v) A V-V resonance between a vibrationally complex molecule (benzene) and a simple collision partner (OCS) is explicitly recognized.

In State-to-State Chemistry; Brooks, P., et al.;
ACS Symposium Series; American Chemical Society: Washington, DC, 1977.

(vi) Resonances between S_1 benzene levels and levels in vibrationally complex collision partners are recognized.

Acknowledgement: Contribution 2986 from the Chemical Laboratories of Indiana University. We are grateful for the financial support provided by the National Science Foundation. Help by Drs. G.H. Atkinson and A.E.W. Knight on aspects of the work is appreciated.

Literature Cited

1. Ennen, G., and Ottinger, C., Chem. Phys. (1974) 3, 404.
2. Beyer, R.A., Zittel, P.F., and Lineberger, C.W., J. Chem. Phys. (1975) 62, 4016, 4024.
3. Yardley, J.T., and Moore, C.B., J. Chem. Phys. (1966) 45, 1066; (1967) 46, 4491.
4. Flynn, G.W., and Yuan, R.C.L., J. Chem. Phys. (1973) 58, 649.
5. Yardley, J.T., and Moore, C.B. J. Chem. Phys (1968) 49, 1111.
6. Weitz, E., and Flynn, G.W., J. Chem. Phys. (1973) 58, 2781.
7. Grabiner, F.R., and Flynn, G.W., J. Chem. Phys. (1974) 60, 398.

23

State-to-State Relaxation in $A^2\Sigma^+$ OH and OD

RUSSELL K. LENGEL
Columbia University, New York, NY 10027
DAVID R. CROSLEY
Ballistic Research Laboratory, Aberdeen Proving Ground, MD 21005

The measurement of collisional energy transfer rates, under conditions in which both initial and final states can be identified, plays a key role in our understanding of the dynamics of the collision process. In addition, there are a number of chemical kinetic and diagnostic applications in which such data may be used directly. We here present a brief summary of our findings concerning state-to-state rotational (1) and vibrational (2) transfer within the electronically excited $A^2\Sigma^+$ state of the OH and OD molecules. Rather than list the numerical results, which may be found in other publications (1,2), we will here concentrate on qualitative highlights of the study, and consider their implications for the occurrence of the energy transfer through a long-lived collision involving anisotropic attractive forces.

The experimental method is that of laser-excited fluorescence in the presence of a known pressure of collision partner. The OH (OD) is produced in a fast flow system by the H(D) + NO_2 reaction; the pressure of the collision gas (He, Ar, H_2, D_2 or N_2) ranges from tens of mTorr to about one Torr. Initial state selection is provided by a frequency doubled dye laser, which pumps individual rotational levels N,J in the v=0, 1 or 2 vibrational level of the $A^2\Sigma^+$ state. A 0.35m monochromator furnishes rotationally resolved fluorescent spectra of the A-X system. In the case of vibrational transfer, total populations in a given v level are obtained from the integrated intensities of the appropriate bands; populations of individual rotational levels, for both vibrational and rotational relaxation, are deduced from fits to the observed spectra (although there is some overlapping of spectral features, each level emits several rotational branches, rendering such a fit feasible). Rate constants (and cross sections) for transfer between given initial and final states are obtained by fitting the population data to appropriate steady state equations (which contain some correction terms due to the influence of background gases, and the pulsed nature of the laser). These equations are quite simple in the case of vibrational transfer, but must be solved by an iterative technique

In State-to-State Chemistry; Brooks, P., et al.;
ACS Symposium Series; American Chemical Society: Washington, DC, 1977.

for rotational transfer. The resulting fitted parameters describe the observed data (in which there exists significant redundancy) quite well, and independent methods of analysis provide further checks on the precision of the results.

Our early findings concerning vibrational relaxation from v=1 to v=0 proved most intriguing. The collision partners He and Ar behaved in an expected manner, that is, the v=1 level became significantly rotationally relaxed before appreciable vibrational relaxation began to occur. However, this was not the case for the diatomic collision partners H_2, D_2, or N_2. Here, the vibrational transfer occurs at a faster rate than the rotational relaxation within v=1. Consequently, the vibrationally transferred molecules have originated predominantly from that rotational level N,J within v=1 which is initially pumped by the laser. Tuning the laser to different absorption lines then permits a measurement of the vibrational transfer cross section $\sigma_v(1\rightarrow0)$ as a function of the initial level N,J in v=1. It is found that the cross section decreases markedly as N increases, e.g., for collisions with N_2 it falls from 24Å^2 at N=0 to 5Å^2 at N=9. The size of $\sigma_v(1\rightarrow0)$ suggests the importance of attractive forces and a long-lived collision. We have hypothesized (2) that the dependence of σ_v on N is due to rotational averaging of an anisotropy in this attraction, which reduces the ability of the OH and its collision partner to maintain a favorable orientation in the entrance channel.

A variety of further experiments has been undertaken to provide further evidence on these points, and the findings (for the diatomics) are briefly listed. 1) The nascent rotational distribution of the vibrationally relaxed OH in v=0 is thermal, though significantly hotter (670K for H_2 collisions) than the translational temperature of the system (300K). This temperature depends on collision partner but not significantly on initial N,J in v=1. 2) Isoenergetic transfer [E(v=1, N=5) - E(v=0, N=14) = 3 cm^{-1}] occurs at a rate < 1% of the rate of transfer to low-N levels in v=0. 3) Resonant effects [$\Delta G_{1/2}$ (D_2) - $\Delta G_{1/2}$(OH) = 2 cm^{-1}] are not important, although the light diatomics behave differently from the monatomics. 4) "Reactive transfer," i.e., OH(v=1) + D_2 → OD (v=0) + HD, does not occur. 5) Initially pumped F_1(i.e., J = N + ½) and F_2(J = N - ½) levels have the same $\sigma_v(1\rightarrow0)$ for the same value of N. 6) In OD, $\sigma_v(1\rightarrow0)$ shows a similar but somewhat smaller variation with N, as expected for its more closely spaced rotational levels. Here again, isoenergetic, resonant, and reactive transfer are not observed. 7) $\sigma_v(2\rightarrow0)$ and $\sigma_v(2\rightarrow1)$ have been measured for initial N values of 1 and 4 in OH. They are of comparable magnitude to $\sigma_v(1\rightarrow0)$, and smaller for the higher value of N. Again, a thermal (though here much hotter) nascent rotational population distribution is found for those molecules which have undergone 2→0 transfer.

These details are all in accord with the long-lived collision picture. While rotational energy transfer within v=0

In State-to-State Chemistry; Brooks, P., et al.;
ACS Symposium Series; American Chemical Society: Washington, DC, 1977.

presents fewer details bearing directly on the mechanism, the results here are also compatible with this view. In the case of collisions with N_2, a total of 5 different initially pumped F_1 levels (N=0,1,3,4 and 6) were used and the populations monitored for 15 levels in each case; one series of runs was made initially populating $F_2(4)$. The cross sections result from fits to all the F_1 data. Only two initially pumped levels are used in the case of H_2 or Ar collisions, although the qualitative results are essentially the same.

The cross sections are again large: total rotational transfer by N_2 out of any one level has a cross section of 60Å^2. State-to-state cross sections $\sigma_R(N,J \rightarrow N'J')$ fall off slowly and smoothly with increasing value of ΔN, although multiquantum transfers are quite noticeable. Cross sections involving simultaneous changes in spin projection as well as rotational quantum number ($\Delta J \neq \Delta N$, i.e., $F_1 \rightarrow F_2$ or vice versa) are smaller by a factor of two than those where $\Delta N = \Delta J$ ($F_1 \rightarrow F_1$ or $F_2 \rightarrow F_2$). The principle of detailed balancing may be examined through ten pairs of rate constants, involving initially pumped levels for which independent determinations have been made for both the forward and backward rates. The ratios are well described by a "detailed balancing temperature" of 420K. Less complete studies have also been made of rotational relaxation in OD colliding with N_2; while these data have not yet been fully analyzed, preliminary results indicate that similar trends will be seen.

The vibrational and rotational relaxation processes may be more directly compared through the use of surprisal analysis. Surprisal plots for vibrational transfer as functions of both initial and final rotational energy are well described by straight lines having slopes with absolute magnitudes of ~ 0.3. However, the points corresponding to initial values of $N \geq 10$ in v=1 fall off the line, suggesting to us that the rotational averaging of the anisotropy is here essentially complete. Rotational surprisal plots show a great deal of apparent scatter even though the cross sections yield reasonably smooth trends with ΔN. Assuming that a linear fit is nonetheless suitable, slopes of 0.6 and 0.1 are obtained for the $F_1 \rightarrow F_1$ and $F_1 \rightarrow F_2$ processes respectively; it is unambiguously clear that a much higher value is inappropriate. These values of surprisal parameters, for both types of transfer, are close to the limit of zero corresponding to a full equipartition of energy, providing further suggestion of the energy transfer occurring through a long-lived collision.

Literature Cited:

1. Lengel, R. K., and Crosley, D. R., J. Chem. Phys. (submitted for publication).
2. Lengel, R. K., and Crosley, D. R., Chem. Phys. Lett. (1975) 32, 261, and J. Chem. Phys. (in preparation).

In State-to-State Chemistry; Brooks, P., et al.;
ACS Symposium Series; American Chemical Society: Washington, DC, 1977.

24

Quantum Mechanics of Neutral Atom-Diatomic Molecule Reactions

ROBERT E. WYATT

Department of Chemistry, University of Texas, Austin, TX 78712

Very significant progress in the quantum mechanical study of chemical reactions has occurred during the past several years (1-4). Early distorted wave calculations on the three-dimensional $H + H_2$ reaction (5,6) were rapidly followed by the development of new theoretical and computational techniques which were applied to collinear and coplanar atom-diatom reactions (2-4). Recent calculations on collinear (7-10) and coplanar reactions (11,12) have led to the near perfection of several numerical techniques, and have provided remarkable dynamical details aimed at answering the question "What happens during a chemical reaction?" Calculations on full three-dimensional reactions employing accurate close-coupling techniques are just beginning to yield a wealth of new dynamical information on the $H + H_2$ reaction (13-18) and to a lesser extent the $F + H_2$ chemical laser reaction (19,20). Distorted-wave techniques have recently been applied to the hydrogen-isotope reactions (21,22).

This chapter is not intended as a comprehensive review of quantum reactive scattering theory or results. However, one approach is briefly reviewed in Section I. Selected recent results on the three-dimensional $H + H_2$ reaction are discussed in Section II. Then, new dynamical results on the collinear and three-dimensional $F + H_2$ reaction are presented in Sections III and IV, respectively. It is hoped that the array of results presented here will illustrate the depth of detail that quantum scattering theory is now able to provide for simple chemical reactions. As a disclaimer, it should be mentioned that these results concern neutral electronically adiabatic reactions on a single potential surface at energies below three-body dissociation. Electronic transitions in reactive collisions and dissociation processes will receive much more attention in the near future. The status of theories for electronic nonadiabatic reactions are reviewed by Tully in this volume.

In State-to-State Chemistry; Brooks, P., et al.;
ACS Symposium Series; American Chemical Society: Washington, DC, 1977.

I. Reactive Scattering Theory

A. Coordinates and Tubes. The calculation of reactive scattering probabilities involves several steps, beginning with the choice of a coordinate system in which to represent the motions of the reacting species. We have been using natural collision coordinates (NCC) (23), with an approximate representation of the kinetic energy operator (24). These coordinates are attractive because the bending motion of the system is represented by a "natural" angle γ that smoothly varies from a rotational coordinate in reactants or products to a bending angle in the transition state. In NCC, we orient the instantaneous three-particle triangle with Euler angles $\theta\phi$ and χ, and specify the size and shape of the triangle with two distances s and ρ, and a bend-rotation angle γ. The angles θ,ϕ orient a rotating z-axis relative to a nonrotating frame such that z changes orientation during the reaction from the AB to C relative vector in reactants to the A to BC relative vector in products. The internal coordinates s, ρ, and γ have a simple geometric interpretation in terms of the three arrangement tubes shown in Fig. 1. The reactant tube leading from AB + C toward the two transition states ABC or BAC bifurcates into A + BC and B + AC product tubes. The electronic potential hypersurface at subdissociative energies restricts the nuclear vibration-bend motion near the surface of the bifurcating tube shown in the figure. It is convenient to split the tube into three arrangement tubes (one leading toward each of three bound diatom regions) along two matching surfaces. Internal coordinates s, ρ, and γ are then introduced separately on each arrangement tube. The translational coordinate s defines evolution along the surface of each tube, from $s = -\infty$ in separated reactants to $s = 0$ on the matching surface to $s = +\infty$ for separated products. The vibrational coordinate ρ defines motion perpendicular to the tube, while γ defines bending motion around the tube at fixed values of s and ρ. Scattering wavefunctions are calculated on each tube and are required to be continuous across the matching surfaces. In these coordinates, the scattering problem involves directing flux (in a specified reactant state) in along the reactant tube and finding how much comes out on each product tube (in specified product states).

A difficulty with NCC is that the kinetic energy is rather complicated. Alternative sets of coordinates using geometrical angles defined separately for reactant or product configurations have been used for $H + H_2$ (25,15) and have recently been generalized for the treatment of an A + BC reaction which can have two distinguishable product arrangement channels (26). The use of geometrical angles describing atom-molecule orientations does lead to much simpler expressions for the kinetic energy operator, but introduces complicated coordinate transformations on the matching surfaces. A novel method for generating reaction

In State-to-State Chemistry; Brooks, P., et al.;
ACS Symposium Series; American Chemical Society: Washington, DC, 1977.

coordinates for collinear reactions (based on a point transformation procedure) has recently been presented (27).

B. Hamiltonian Partitioning. On each of the three arrangement tubes, we decompose the Hamiltonian operator into a translational term for s motion, a vibrational term for ρ motion, and a rotational term for θφχ and γ motion (24)

$$\hat{H} = \hat{H}_{tr} + \hat{H}_{vib} + \hat{H}_{rot}. \tag{1}$$

The translational Hamiltonian includes a kinetic energy operator and the reaction path potential $V_{tr}(s)$, $\hat{H}_{tr} = \hat{T}_s + \hat{V}_{tr}(s)$. The vibrational Hamiltonian includes the local vibrational potential (e.g. a Morse potential curve), $\hat{H}_{vib} = \hat{T}_\rho + V_{vib}(\rho;s)$. The rotational Hamiltonian is more complicated; it is the Hamiltonian for a hindered asymmetric top (28-30) wherein θ, φ, and χ describe free tumbling, with γ motion (hindered internal rotation) governed by a local bending potential $V_{bend}(\gamma;s)$. The rotational Hamiltonian is thus

$$\hat{H}_{rot} = \hat{H}_{st} + \hat{H}_{asym} + \hat{H}_{bend} + \hat{H}_{cor}, \tag{2}$$

where

$$\hat{H}_{bend} = \hat{T}_\gamma + V_{bend}(\gamma;s). \tag{3}$$

The sum of the symmetric top Hamiltonian $\hat{H}_{st}$ and the asymmetry term $\hat{H}_{asym}$ describes a tumbling asymmetric top; $\hat{H}_{cor}$ is the Coriolis interaction which couples triangle tumbling to internal bending. Vibration-rotation coupling is neglected in decomposing the potential $V(s, \rho, \gamma)$ into the three terms mentioned above.

At each s, local adiabatic vibrational and hindered asymmetric top basis sets are defined by the equations

$$\begin{aligned} \hat{H}_{vib}\, H_v(\rho;s) &= E_v(s)\, H_v(\rho;s), \\ \hat{H}_{rot}\Omega^{JM}_{jl}(\theta\phi\chi\gamma;s) &= W^J_{jl}(s)\Omega^{JM}_{jl}(\theta\phi\chi\gamma;s) \end{aligned} \tag{4}$$

where v is the (local) vibrational quantum number, and where j (molecular rotation quantum number) and l (atom-molecule relative angular momentum quantum number) define the sources of angular momentum (at total angular momentum JM) in reactants, where $V_{bend} = 0$. We generally choose the H_v to be Morse oscillator states. The hindered asymmetric top states are conveniently expanded in normalized symmetric top states $\{N^J_{MK}(\theta\phi\chi)\}$:

$$\Omega^{JM}_{jl}(\theta\phi\chi\gamma;s) = \sum_{K=-J}^{+J} N^J_{MK}(\theta\phi\chi) R^{JK}_{jl}(\gamma;s), \tag{5}$$

where R^{JK}_{jl} is a hindered rotor function for angular momentum

In State-to-State Chemistry; Brooks, P., et al.;
ACS Symposium Series; American Chemical Society: Washington, DC, 1977.

component K along the rotating z-axis. The hindered rotor functions are found numerically by diagonalizing $\hat{H}_{rot}$ in the basis of free-rotor functions. Both the hindered asymmetric top energy correlation diagram ($W^J_{j\tau}$ vs. s) and the J and K dependence of the hindered rotor functions have been extensively studied for the H + H_2 reaction (28,30).

C. Wavefunction Expansion and Close-Coupling Equations. In the theory of scattering, channels (alternatives for flux) are labeled by the eigenvalues of operators which commute with the Hamiltonian. In atom-diatom scattering, this set may be chosen as JMjlv, where jv define the rotation-vibration state of the diatom. During the collision, JM remain good quantum numbers with mixing among jlv basis states induced by the interaction potential and by dynamic coupling terms. If the reactants start in the channel JMjlv, then the total wavefunction at position s along each arrangement tube may be expanded in N members of the set of local hindered asymmetric top-oscillator states which were previously calculated at that s:

$$\Psi^{JM}_{jlv}(\theta\phi\chi s\rho\gamma) = \frac{\eta^{\frac{1}{2}}}{\omega r^2} \sum_{j'l'v'}^{N} T^J_{jlvj'l'v'}(s) \times \Omega^{JM}_{j'l'}(\theta\phi\chi\gamma;s) H_{v'}(\rho;s), \quad (6)$$

where $\eta^{\frac{1}{2}}/\omega r^2$ is a local scale factor (31) chosen to simplify and symmetrize the resultant equations for the expansion coefficients $\{T^J_{jlvj'l'v'}\}$, which are called translational wavefunctions. The function $T^J_{jlvj'l'v'}(s)$ is proportional to the amplitude that the system makes a transition from state jlv at s=-∞ to local "state" j'l'v' at position s. In order to derive equations for the translational wavefunctions, we operate on Eq. (6) with $(\hat{H}-E)$ and then project on each basis state, one at a time: $0 = \langle \Omega^{JM}_{j'l'} H_{v'} | (H-E) | \Psi^{JM}_{jlv} \rangle$ where the integration is over all variables except s. The close-coupled equations for the translational wavefunctions are then (with α = jlv)

$$\frac{d^2T^J_{\alpha\alpha'}}{ds^2} - \sum_{\alpha''} V^J_{\alpha'\alpha''} T^J_{\alpha\alpha''} - \sum_{\alpha''} \hat{V}^J_{\alpha'\alpha''} \frac{dT^J_{\alpha\alpha''}}{ds} = 0 \quad (7)$$

where the coupling matrix $\underline{\underline{V}}$ contains the total energy, the local channel vibration-rotation energies, and matrix elements involving derivatives of local basis functions with respect to s. The other coupling matrix $\underline{\underline{\hat{V}}}$ contains matrix elements over first-derivatives of basis functions with respect to s.

Equations of this type (with as many as 50 basis functions) were solved for the H + H_2 reaction (17,18) at many values of E and J. More recently, we have considered an alternate method

In State-to-State Chemistry; Brooks, P., et al.;
ACS Symposium Series; American Chemical Society: Washington, DC, 1977.

(20) in which the local adiabatic basis functions are constant within each of many "boxes," thus eliminating $\bar{\bar{V}}$ and those parts of $\bar{\bar{V}}$ which depend upon derivatives of basis functions with respect to s. The translational wavefunctions in adjacent boxes are then joined by orthogonal connection matrices which insure that the total wavefunction and its first derivative are continuous across each box junction. This technique has recently been applied to the three-dimensional F + H_2 reaction (20)(Section IV).

Solution of the close-coupled equations yields elements of the scattering matrix, the amplitudes to make transitions from initial channels jlv as $s \to -\infty$ into product channels j'l'v' as $s \to +\infty$. Once the S-matrix elements are known at a given energy, reaction probabilities and differential and total reaction cross sections may be calculated. Explicit formulas for these quantities will not be given here (15,16), but they may be easily computed once the time consuming process of integrating the close-coupled equations is complete.

II. The Three-Dimensional H + H_2 Reaction

A. Threshold Energies. In this section, classical and quantal threshold energies for the reaction H + H_2(v=0) → H_2(v'=0) + H on the Porter-Karplus H_3 surface (32) will be reviewed and compared (17,18,1). The term "threshold energy" will be used to denote the total energy at which the reaction probability (collinear nuclear motion), cross length (coplanar nuclear motion), or cross section (full three-dimensional reaction) reaches 0.01 of maximum. A quantum reaction is "unsafe at any speed" in the sense that virtually any positive reagent kinetic energy produces some amount of reaction, hence a cutoff value of the reactivity must be used to define the threshold, particularly for comparison with quasiclassical trajectory results. Table I shows threshold energies defined via this criterion. This table shows several quite interesting trends. Note that the classical threshold energy always exceeds the quantum value, but that the difference $\delta = E_{th}(cl) - E_{th}(qu)$ decreases as the dimensionality increases from 1D to 2D to 3D (δ decreases from 0.06 to 0.04 to 0.02 eV). The collinear world thus accentuates the classical-quantum threshold defect for this reaction.

In State-to-State Chemistry; Brooks, P., et al.;
ACS Symposium Series; American Chemical Society: Washington, DC, 1977.

Table I

Classical and quantum threshold energies on the Porter-Karplus H_3 surface for the reaction $H + H_2(v=0) \rightarrow H_2(v'=0) + H$.

Physical Dimensions	Classical Threshold(eV)	Quantum Threshold(eV)
1	0.47	0.41
2	0.51	0.47
3	0.55	0.53

In addition, note that the quantum threshold increases by about 0.06eV with each increase of dimension (1):

$$E_{th}(qu) = E_{th}(qu,1D) + (p-1)(0.06), \qquad (8)$$

where p = 1, 2, or 3. The threshold increase with dimension correlates nicely with the bending zero-point energy of the H_3 transition state (0.0eV in 1D, 0.06eV in 2D for one bending degree of freedom, 0.12eV in 3D for two degenerate bending degrees of freedom). Requiring that increasing amounts of available energy be siphoned off into bending energy in the transition state in going from 1D to 2D to 3D thus requires corresponding increases in total energy to reach the same degree of reactivity. There is recent evidence that these correlations between bending energy in the transition state and the quantum threshold energy also apply for vibrationally excited reagents (33,34) (Section IIID).

B. J_z-Conserving Approximation. Because of the large computer time requirements for close-coupling calculations, it is essential to develop efficient approximate methods for obtaining quantum results on three-dimensional reactions. The J_z-conserving approximation, developed originally by Pack (35) and by McGuire and Kouri (36) for nonreactive collisions, has been extended successfully to the hydrogen exchange reaction (37,38). In the formulation of Elkowitz and Wyatt (37), instead of scattering on all symmetry allowed l-branches of each asymmetric-top energy correlation diagram $W_{jj}^{J}(s)$ (J,j fixed; $|J-j| \leq l \leq J+j$), only a single l was used for each value of J and j. The required value of l for each Jj was found by examining (at small s, where the bending potential is significant) the distribution over K produced by the hindered rotor functions. Examination of Eq. (5) shows that in each hindered asymmetric top state Ω_{jj}^{JM} the relative probability of obtaining each value of K is determined

In State-to-State Chemistry; Brooks, P., et al.;
ACS Symposium Series; American Chemical Society: Washington, DC, 1977.

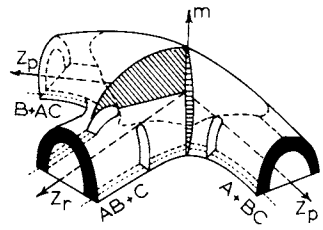

Figure 1. Schematic of arrangement tubes for atom–diatom chemical reactions. The reactant tube (lower left) for AB + C bifurcates into two product tubes. Collinear reactions occur in the horizontal plane and m *measures deviations from collinearity. The potential favors vibration-bending motion within the rings shown emerging from the tube ends. Scattering wavefunctions on the separate tubes are joined on the matching surfaces (cross-hatched). Collinear reaction paths are shown as dotted lines.*

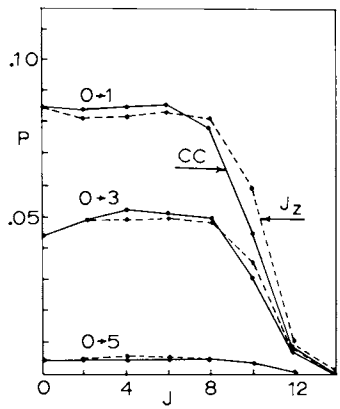

Figure 2. Comparison of J_z*-conserving and close-coupling reaction probabilities vs. total angular momentum (J) for para (j = 0) to ortho (j′ = 1,3,5) transitions in H + H_2 collisions at* E_{TOTAL} *= 0.80 eV on the Yates–Lester–Liu potential surface.*

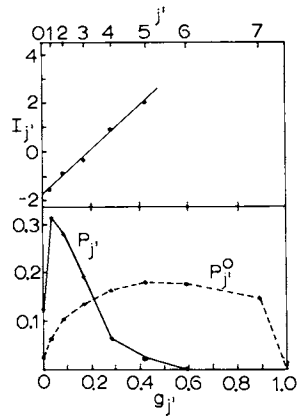

Figure 3. Rotational surprisal plot (top panel) and reaction probabilities $P_{j'}$ *(lower panel) vs. fraction of available energy in each rotational level at* E_{TOTAL} *= 0.80 for the Yates–Lester–Liu* H_3 *surface.*

In State-to-State Chemistry; Brooks, P., et al.;
ACS Symposium Series; American Chemical Society: Washington, DC, 1977.

by the integral (over γ) $|\langle R_{jj'}^{JK}|R_{jj'}^{JK}\rangle|^2$. Examination of these K-distributions showed that at small s, an asymmetric top state with Jj and l fixed tends to concentrate into a specific value of $|K|$. The bending potential for H_3 favors collinear geometries, which in the hindered rotor distributions implies that K = 0 is favored for reaction. The value of l to use for each Jj was found by maximizing the concentration of hindered rotor density into K = 0. This method thus led to a simple algorithm for selecting l for arbitrary J and j. The result was that in the reaction zone, the hindered asymmetric top was approximated by a near-prolate symmetric top (i.e., a tumbling "cigar"). Because many fewer rotational channels (jl) were used, the saving in computer time was substantial (about a factor of 30 in typical calculations).

In Fig. 2, both close-coupling and J_z-conserving para → ortho reaction probabilities vs. J are shown at E_{TOTAL} = 0.80eV for the Yates-Lester-Liu H_3 surface (39) (with a simple fit to the bending potential). When reaction cross sections are calculated over a range of post-threshold energies, the J_z results are within 5% of the full close-coupling results. This approximation has made it possible to obtain low energy reaction cross sections for F + H_2 (Section IV).

C. Product Rotational Distribution. As a final example of results obtained in the three-dimensional H + H_2(v=0) reaction, we use information theory (40) to analyze the product rotational distribution at one energy. In this approach, we compare the actual rotational probability distribution $P_{j'}$ to the "prior" distribution $P_{j'}^{o}$ obtained by democratic partitioning of probability into the available cells in the microcanonical (E = fixed) phase space. The comparison for rotational energy transfer is made via the rotational surprisal function

$$I_{j'} = -\ln\frac{P_{j'}}{P_{j'}^{o}} . \qquad (9)$$

In Fig. 3, $I_{j'}$ is plotted vs. $g_{j'}$, the fraction of available energy in the j-th product rotational level ($g_{j'} = E_{j'}/(E_{TOTAL} - E_{v'})$). Amazingly, the surprisal is linear in $g_{j'}$, and is clearly of a simpler structure than $P_{j'}$, which is plotted in the lower panel in Fig. 3. (Also, note how "cold" the actual rotational distribution is compared to the microcanonical distribution.) Surprisal plots for rotationally excited reagents are also linear (16), and have approximately the same slope as the curve resulting from excitation from j=0. The fact that these surprisal plots are linear implies that the actual rotational distribution can be written in the form

$$P_{j'} = P_{j'}^{o} e^{-\theta_o} e^{-\theta_R g_{j'}} ,$$

In State-to-State Chemistry; Brooks, P., et al.;
ACS Symposium Series; American Chemical Society: Washington, DC, 1977.

where $e^{+\theta_0}$ plays the role of a "partition function." The dynamical information is thus entirely contained within the slope parameter θ_R, which determines (or, is determined by) the average product rotational energy.

D. Cooling of $H_2(v=1)$. We now consider the cooling of vibrationally excited $H_2(v=1)$ in collisions with H atoms (34). At each energy, there is competition between the nonreactive and reactive pathways:

$$H + H_2(v=1,j=0) \begin{cases} \xrightarrow{N} H + H_2(v'=0;j'=0,2,4\cdots) \\ \xrightarrow{R} H_2(v'=0;j'=0,1,2,3\cdots) + H \end{cases}$$

Previous quantum collinear (41) and classical three-dimensional calculations (42,43) have indicated dominance of the reactive pathway. Heidner and Kasper (44) have experimentally measured the net (reactive plus nonreactive) cooling rate constant $k_{1\to0}(T=298°K)$ for $H + H_2(v=1)$.

We have recently obtained quantum collinear and three-dimensional vibrational cooling probabilities (34) on a fit to the Yates-Lester-Liu H_3 potential surface(39). The upper panel in Fig. 4 shows the collinear 1 → 0 reactive and nonreactive transition probabilities; the results are very similar to previous quantum results on a different potential surface (41) and confirm the dominance of nonreactive cooling in the collinear world. However, the three-dimensional quantum results for collisions with total angular momentum J=0 in the lower panel show that nonreactive cooling dominates at low translational energies, $E_{TR} \lesssim 0.25$ eV. The reactive 1 → 0 probability is similar in shape to the collinear result, except that the resonance peak is shifted to higher energy by 0.16eV, close to the bending zero point energy (0.13eV) of the H_3 transition state. In contrast, the low energy nonreactive 1 → 0 probability increases with translational energy until the threshold (at 0.06eV) is reached for j=0 → j'=2 nonreactive rotational excitation within the v=1 vibrational manifold. The nonreactive cooling probability then drops, but eventually (near E_{TR} = 0.14eV) increases again. Qualitatively similar results have been obtained for J > 0 in the J_z-conserving approximation. Thermal rate constants for the alternate cooling processes will be computed and compared with available experimental and classical trajectory results.

III. The Collinear F + H_2 Reaction

A. Reaction Probabilities. Over the past several years, vibrational transition probabilities from quantum close-coupling calculations have been reported on several different FH_2 potential surfaces (7,8,45,46). These papers have emphasized the

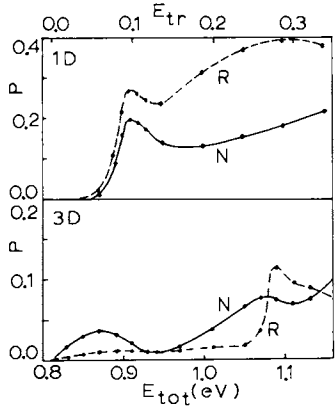

Figure 4. Reaction probabilities for nonreactive (N) and reactive cooling (R) of H_2(v = 1) for collinear (upper panel) and three-dimensional collisions (lower panel) at total angular momentum J = 0. A fit to the Yates–Lester–Liu H_3 surface was used in the calculations.

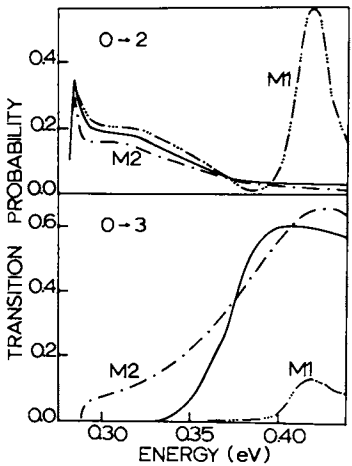

Figure 5. Reaction probabilities from 10 channel collinear F + H_2 calculations for the v = 0 → v′ = 2,3 processes. M1 and M2 are results from the modified v = 3 vibrational energy curve in Figure 13.

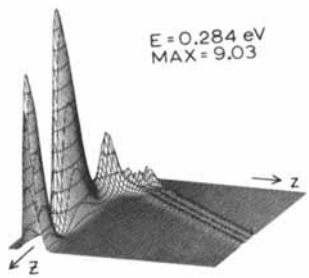

Figure 6. Scattering probability density for the F + H_2 reaction at E_{TOTAL} = 0.284 eV, viewed from the F + H + H region in skewed coordinates. The F + H_2 reactant region is at the left and the FH + H product region emerges on the right. The maximum density (atomic units) is indicated on the figure.

In State-to-State Chemistry; Brooks, P., et al.;
ACS Symposium Series; American Chemical Society: Washington, DC, 1977.

highly specific energy disposal in products, but Manz has also analyzed the quantal vibrational state distributions at several intermediate stages along the reaction path (47). During the past several years, we have analyzed the probability density and flux distributions associated with scattering wavefunctions for this reaction and attempts have been made to develop models for the resonance structure in the reaction probability curves with particular emphasis on the v=0 → v'=2,3 low energy processes (48,49). In these studies, the Muckerman V potential surface has been employed (7).

Collinear reaction probabilities $P_{v\to v'}(E)$ for v=0 to v'=2,3 are shown in Fig. 5. These results were obtained with a 10-term vibrational basis set. (Probabilities calculated with a 12 term basis were very similar, except that the $P_{0\to 2}$ resonance peak near E_{TOTAL} = 0.28eV is about 10% higher for the larger basis.) The probabilities in this figure are similar to those of Schatz, Bowman, and Kuppermann (7), who studied both the F + H_2 and F + D_2 reactions. Striking features of these curves are: (1) the rapid rise of $P_{0\to 2}$ to a resonance peak at 0.284eV, followed by a gradually declining region above 0.30eV; (2) the very slow growth of $P_{0\to 3}$ from its energetic threshold at 0.288eV. Clearly, an important feature to understand about this reaction is the origin of the difference in post-threshold behavior between the processes which produce HF(v'=2) and HF(v'=3). We will return to this point in Section IIIC, but first we will examine the probability density and flux associated with the scattering wavefunction.

B. Density and Flux. Once the S-matrix, with elements $S_{vv'}(E)$, is calculated for the collinear F + H_2 reaction, it is possible to calculate the scattering wavefunction $\Psi_v(\rho,s)$ at each coordinate point (ρ,s), for reactants with incoming flux in the F + $H_2(v)$ channel. From this wavefunction, both the probability density and flux may be calculated at a series of grid points:

$$P(\rho,s) = |\Psi_v(\rho,s)|^2,$$

$$\vec{J}(\rho,s) = \frac{\hbar}{2\mu i}[\Psi_v^* \vec{\nabla} \Psi_v - \Psi_v \vec{\nabla} \Psi_v^*]. \qquad (11)$$

Of course, P measures the tendency of probability to accumulate near a given point, while $\vec{J}$ measures both the flow rate and direction of probability past the point. Surprisingly, although reaction probabilities have been calculated for many collinear processes, density and flux analyses have been reported only for the H + H_2 reaction (50,51). These quantities are nevertheless important, since they show how the quantum reaction occurs.

The probability density at the energy (0.284eV) of the 0 → 2 resonance is shown in Fig. 6. From the observation point in the F + H + H region, the density in the F + H_2 reactant region is on

In State-to-State Chemistry; Brooks, P., et al.;
ACS Symposium Series; American Chemical Society: Washington, DC, 1977.

the left of the figure, while the FH + H product region is at the lower right, skewed 46.4° relative to the reactant valley. Clearly seen in this figure are extrema in the entrance valley due to interference between incoming flux and elastically scattered flux (only the H_2(v=0) channel is open in reagents although HF(v'=0,1,2) are open in products). Also, the product density, with three maxima along the vibrational axis corresponding to v'=2, is seen to emerge from the "lumpy" density in the FHH interaction region. A better view of the density in the interaction region is shown in the contour map in Fig. 7, where the three-peaked product density is seen to be preceded by the three sharp peaks at the lower left of the figure.

In order to find out how the probability in Figs. 6-7 flows from point-to-point, consider the flux map in Fig. 8, which covers the same region as the contour map in Fig. 7. The v=0 flow in the F + H_2 region and the three-peaked v'=2 flow in the FH + H region are clearly shown. But the remarkable feature is the set of flux vectors swirling around the three whirlpools in the interaction region! In addition, notice the flow from the whirlpool region into the product valley in the upper right of the figure.

Hirschfelder and co-workers (52,53) have recently presented detailed analyses of the density and flux in a series of model scattering problems. They have emphasized that whirlpools formed in these problems must have quantized circulation integrals:

$$\oint \vec{p} \cdot d\vec{r} = mh; m = \pm 1, \pm 2 \cdots, \tag{12}$$

where the circulation number m determines the "state of excitation" of the whirlpool and where the integral is taken around any closed loop enclosing the wavefunction node at the center of the whirlpool. In a collinear scattering process, whirlpools may form around points where P = 0. On comparing Figs. 7 and 8, we note that the three whirlpools in Fig. 8 are formed around the nodes separating the four density peaks in the lower part of Fig. 7.

In order to find the circulation number of these whirlpools, it is useful to write the wavefunction (a complex number) as $\Psi(\rho,s) = P^{\pm}e^{iS}$, where the phase S is unique (within a multiple of $\alpha\pi$), except at nodal points. The flux is then easily shown to be $\vec{J} = \hbar\vec{\nabla}S/\mu$ where the velocity is $\vec{v} = \hbar\vec{\nabla}S/\mu$, so that the circulation integral becomes

$$\oint \vec{p} \cdot d\vec{r} = \hbar \oint \vec{\nabla} S \cdot d\vec{r} = \hbar \Delta S = mh, \tag{13}$$

in which ΔS is the phase change of the wavefunction as the closed loop is traversed about the nodal point. This equation thus requires that $\Delta S = 2\pi m$. The circulation number for these whirlpools (read directly from a contour map of wavefunction phase) is $|m| = 1$; they are "ground state" vortices. We have not

In State-to-State Chemistry; Brooks, P., et al.;
ACS Symposium Series; American Chemical Society: Washington, DC, 1977.

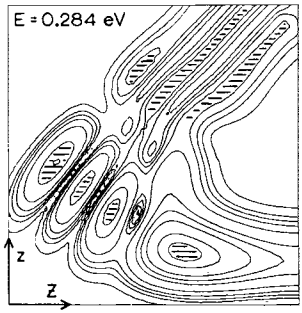

Figure 7. Contour map of scattering probability density at E_{TOTAL} *= 0.284 eV. Maxima are cross-hatched. The top center of Figure 6 is being viewed from above, with the reactant region to the lower right.*

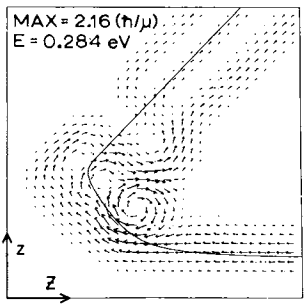

Figure 8. Scattering probability current vectors at E_{TOTAL} *= 0.284 eV, showing flow direction of probability. The magnitude of the longest vector is indicated on the figure. The viewing region is the same as Figure 7.*

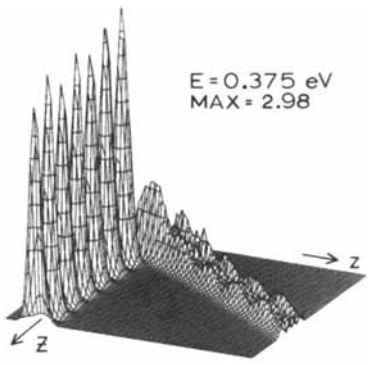

Figure 9. Scattering probability density for the F + H_2 reaction at E_{TOTAL} *= 0.375 eV. See the caption to Figure 6 for details.*

In State-to-State Chemistry; Brooks, P., et al.;
ACS Symposium Series; American Chemical Society: Washington, DC, 1977.

observed excited whirlpools with $|m| \geq 2$ at any energy below 0.40eV in this reaction.

We will now briefly examine density and flux maps at one higher energy, 0.375eV. Referring back to the probability curves in Fig. 5, we see that $P_{0\to2} = 0.05$ and $P_{0\to3} = 0.36$ at this energy, which is on the high energy side of the 0→2 resonance peak. The density in the reactant channel, Fig. 9, again shows strong interference extrema, although the separation is shorter due to the higher translational wavenumber in the v=0 channel. The density in the product channel is qualitatively different from that in Fig. 6, where most of the product flux was in the v'=2 channel. At this higher energy, the product total density is given approximately by

$$P = \left| S_{02} \frac{e^{+ik_2 s}}{\sqrt{k_2}} H_2(\rho) + S_{03} \frac{e^{+ik_3 s}}{\sqrt{k_3}} H_3(\rho) \right|^2, \qquad (14)$$

where $S_{0v'}$ is an S-matrix element for production in channel v'. The interference cross-term in this expression is what leads to the oscillations along the product translational coordinate in Fig. 9. The flux map at this energy is shown in Fig. 10. Again, note the whirlpool patterns in the interaction region. Also, the product flux oscillates out into the product valley (the "bobsled effect" (54)). One other feature of this map is quite interesting: there is extensive "corner-cutting" by the flux on the inside of the reaction path. Polanyi and Schreiber (55), through examination of classical trajectories, have pointed out that the potential "ledge" in this region of the potential surface is very important in the vibrational inversion mechanism. We hope that density and flux analyses of other reactions will be performed, so that further understanding of quantum reaction mechanisms will be obtained.

C. Resonance Models. In this section, the origin of the resonances in the reaction probability curves will be discussed in more detail (48). First, consider in Fig. 11 a vibrational energy correlation diagram for the F + H_2 reaction. The curve $V_{tr}(s)$ is the potential along the reaction path; note the steep exoergic plunge (-1.38eV) following the small (0.05 eV) barrier. Measured up from V_{tr} at each s are the local vibrational eigenvalues, obtained by fitting a Morse curve to the potential in constant s cuts through the collinear potential surface. An important feature of these curves is the presence of wells for v>1 in the region $-0.5a_0 \lesssim s \lesssim +1.0a_0$. These wells do not arise from an actual depression in the potential surface, but are caused by the broadening and subsequent contraction of the vibrational valley on turning through the interaction region.

Also shown in this figure is a horizontal line at 0.284eV, the 0→2 resonance energy, and the average vibrational energy $\langle E_v \rangle$

In State-to-State Chemistry; Brooks, P., et al.;
ACS Symposium Series; American Chemical Society: Washington, DC, 1977.

computed from the scattering wavefunction at this energy. In reactants, the system is in v=0, in products in v'=2, with extensive vibrational excitation occurring near $s=0.0a_0$. Note the oscillatory dependence of $\langle E_v \rangle$ upon s in the well region.

If $P_v(v=0,1\cdots)$, the normalized probabilities of finding the system in various vibrational levels at position s, are computed from the scattering wavefunction, then extensive excitation out of v=0 is observed near s=0, and excitation into a number of competing wells (about 10) occurs in the region $0.0 \lesssim s \lesssim 1.0a_0$. One measure of the spread of probability over the vibrational channels is through the entropy plot in Fig. 12. The (unitless) entropy is defined here as $S = -\sum_v P_v \ln P_v$, where the sum ranges over all channels included in the calculation at each s. Toward the end of the reaction ($s \gtrsim +1.5a_0$), the entropy drops to a small value due to the highly specific energy disposal into v'=2.

We will now consider in more detail the relationship between the well structure in Fig. 11 and the resonance structure of the reaction probability curves. In order to demonstrate that the lower vibrational wells strongly influence the reaction probabilities, we considered a modified FH_2 potential surface (obtained at each s by adjusting the curvature parameter in the Morse vibrational potentials) which eliminated all wells below v=5, although wells were present for $v \geq 5$. This modified surface (the L5 model) does not expand and then contract (in the vibrational direction) like the actual FH_2 surface. Reaction probabilities computed on the modified surface did not show inversion into the v'=2 HF vibrational level. There was hardly any reaction for $E_{TOTAL} \lesssim 0.40$eV. Other models were then considered in which a single well, or a pair of wells from the "exact" correlation diagram were re-introduced into the L5 model. Calculations employing single wells were not successful in producing sharp 0→2 resonance structure, but a pair of wells reintroduced into v=2 and 3 did lead to 0→2 inversion at low energy, although the resonance width was a factor of five too large. The energy of the resonance maximum was about 0.03eV too high, but this is a sensitive function of the selection of the Morse parameters in the L5 model in the region around s=0, where the correlation curves are steeply plunging (this is where extensive 0→v' excitation first occurs). However, the shape of the model resonance improves as more wells are allowed to interact. The main result from these studies is that the low energy 0→2 inversion resonance in the $F + H_2$ reaction arises from temporary interaction among probability excited mainly into wells in the v=2 and 3 vibrational energy correlation curves.

The model results mentioned so far provide no clues as to why the 0→3 reaction probability curve shows such a gradual growth, in obvious contrast to the sudden growth of the 0→2 curve. A quite different collision system, $K+SO_2$ (56) shows cross section curves for photon ($K^*(4^2P) + SO_2; K^*(4^2P) \rightarrow K(4^2S) + h\nu$) and ionic ($K^+ + SO_2^-$) channels which have a remarkably similar

In State-to-State Chemistry; Brooks, P., et al.;
ACS Symposium Series; American Chemical Society: Washington, DC, 1977.

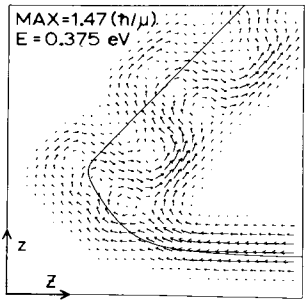

Figure 10. Scattering probability current for the F + H_2 reaction at E_{TOTAL} = 0.375 eV. See the caption to Figure 8 for details.

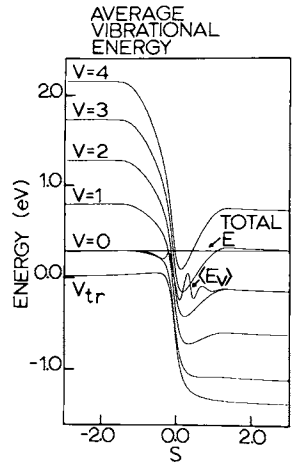

Figure 11. Vibrational energy correlation diagram for the F + H_2 reaction, showing alteration of vibrational energies between reactants (s = $-\infty$) and products (s = $+\infty$). $V_{tr}(s)$ is the local reaction path potential. The local average vibrational energy at E_{TOTAL} = 0.284 eV is also shown.

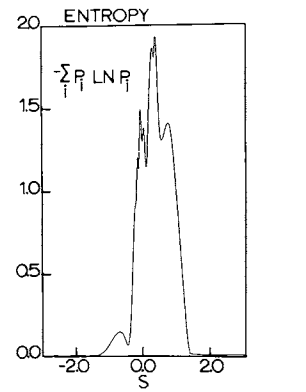

Figure 12. Vibrational entropy vs. reaction coordinate for the collinear F + H_2 reaction at E_{TOTAL} = 0.284 eV.

energy dependence to the F + H_2 0→2 and 0→3 probabilities. In K + SO_2 collisions, σ_{photon} increases rapidly with E_{TOTAL}, then drops suddenly as the threshold is reached for the relatively slow initial growth of σ_{ionic}. Below the ionic threshold probability traps in a well in the $K^+ + SO_2^-$ potential curve, which crosses the rising $K^* + SO_2$ curve. The shape of the ionic potential curve in the uphill region would appear to be an important factor in controlling the shapes of σ_{ionic} and σ_{photon}. Encouraged by this analogy to the K + SO_2 threshold behavior, we recall in Fig. 5 that the 0→2 resonance peak occurs only 0.004eV below the v'=3 energetic threshold (Schatz, Bowman, and Kuppermann (7) have noticed that a 0→v' reactive resonance occurs very close to the 0→v'+1 energetic threshold). Below 0.288eV, probability temporarily trapped in the v=3 well decays down onto the v'=2 exit channel. But as 0.288eV is approached from below the translational wavefunction in v=3 penetrates further up the side of the v=3 well between s=0.10 a_0 and s=1.00 a_0. Finally, just above 0.288eV, penetration into the asymptotic v=3 channel is possible, i.e. with increasing energy, more of the "hill" emerging out of the v=3 valley is sampled. This suggests that the shape of this hill in the v=3 vibrational energy curve may be the controlling factor in determining the ultimate shape of the 0→3 probability curve just above threshold.

This notion is correct! In Fig. 13 we see a blownup view of part of the vibrational correlation diagram. The uphill portion of the v=3 curve was either hardened in "Model 1" (M1 in the figure) or softened in "Model 2" (M2). Looking back to the lower panel of Fig. 5, we see that these apparently minor alterations in the shape of one part of the v=3 correlation curve produces drastic variations in the shape of the 0→3 reaction probability. In fact, the "soft model" (M2) leads to a sharp increase of reactivity just as soon as the threshold energy is exceeded. The eventual experimental detection of resonance structure in reactive processes should serve as a very sensitive probe of restricted portions of the potential surface (the near exit valley for the reaction discussed here.) Resonance structure in quantum collinear He + H_2^+ and I + H_2 collisions has recently been investigated (57,58).

IV. The Three-Dimensional F + H_2 Reaction

Quantum mechanical studies of the 3D F + H_2 reaction are very difficult because of the large number of vibration-rotation basis functions required in the wavefunction expansion. Of necessity, we have employed the J_Z-conserving approximation (Section II), using the same algorithm that was successfully employed in the 3D H + H_2 calculations. In the first quantum close-coupling calculations on this reaction, Redmon and Wyatt (19) employed a 10 channel vibrational basis, with only two hindered rotor functions in each vibrational manifold. This is

In State-to-State Chemistry; Brooks, P., et al.;
ACS Symposium Series; American Chemical Society: Washington, DC, 1977.

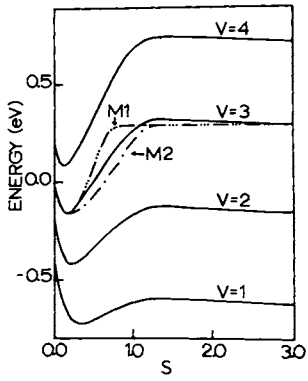

Figure 13. Blow-up of part of the F + H_2 vibrational energy correlation diagram in Figure 11. M1 and M2 are "hard" or "soft" modifications of the uphill portion of the v = 3 curve.

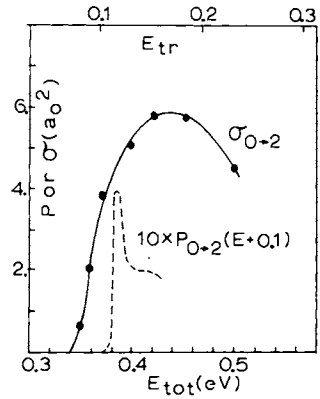

Figure 14. Total cross section for the three-dimensional F + H_2(v = 0) → FH(v′ = 2) + H reaction compared with the collinear reaction probability. The 3D cross section is summed over all final rotational levels. The collinear probability curve has been shifted to higher energies by 0.10 eV.

In State-to-State Chemistry; Brooks, P., et al.;
ACS Symposium Series; American Chemical Society: Washington, DC, 1977.

the minimum number of rotor functions that allows wavefunction bifurcation (into either FH_aH_b or FH_bH_a intermediates) so that the incoming F atom can react with either end of the H_2 molecule. These early calculations showed resonance structure in the 0→2 and 0→3 reaction probabilities at each value of J. Much more extensive calculations have recently been completed (20). The Muckerman potential surface was again employed, but the bending potential was fit to the simple form $\frac{1}{2}V_0(s)(1-\cos 2\gamma)$. In these calculations, a 60 channel vibration-rotation basis was typically employed at each J.

The energy dependence of the total reaction cross section for the process $F + H_2(v=0,j=0) \rightarrow FH(v'=2,\Sigma j') + H$ is shown in Fig. 14. Also shown is the collinear reaction probability curve $P_{0\rightarrow 2}(1D)$ shifted to higher energy by 0.10eV, the bending zero-point energy of the FHH intermediate in the 3D calculation. There are several dramatic differences between the two curves displayed in this figure. First, the threshold for the 3D reaction is shifted to higher energy-relative to the collinear threshold--by approximately the bending zero-point energy. This trend is analogous to that in the 1D and 3D $H + H_2$ reactions that was mentioned in Sec. II.A. This threshold shift is apparently not predicted in quasiclassical trajectory calculations (59). The second major difference between the two curves in Fig. 14 is the width of the 0→2 resonance peak. The 3D cross section curve is about a factor of twenty wider than the sharp collinear peak. There is significant rotational broadening in 3D, but not enough to completely wash out the resonance structure. The origin of the broadening is not hard to understand. In each partial wave (labeled by J), there is a sharp 0→2 resonance peak, but the energy at which the peak occurs increases as J increases. Thus, at each energy, as J is scanned, a series of "resonance blips" in several different partial waves are added together to finally produce the total cross section in Fig. 14. The story behind the broadened resonance is thus understood in terms of well-defined quantum effects in each partial wave.

Product rotational distributions within each vibrational manifold have been computed. The rotational distributions become compressed toward low j' values as v' increases. The sensitivity of these j' distributions to the form of the bending potential is being investigated. Once this is known, detailed comparisons with experimental v'j' distributions (60,61) should be possible.

Many discussions with Michael Redmon, Joe McNutt, and Sue Latham on their $F + H_2$ studies are gratefully appreciated. John Hutchinson is thanked for assistance with the graphs. Financial support was provided by the National Science Foundation and the Robert A. Welch Foundation.

Literature Cited

1. Truhlar, D.G. and Wyatt, R.E., Ann. Rev. Phys. Chem.,(1976)

36, 1.
2. Micha, D.A., Adv. Chem. Phys. (1975) 30, 7.
3. George, T.F. and Ross, J., Ann. Rev. Phys. Chem. (1973) 24, 263.
4. Levine, R.D., "Theoretical Chemistry," W. Beyers Brown (ed.), MTP Int. Review of Science, Vol. 1 (University Park Press, Baltimore, 1972).
5. Micha, D.A., Ark. Fys. (1965) 30, 411, 425, 437.
6. Tang, K.T. and Karplus, M., Phys. Rev. (1971) A4, 1844.
7. Schatz, G.C., Bowman, J.M., and Kuppermann, A., J. Chem. Phys. (1975) 63, 674.
8. Connor, J.N.L., Jakubetz, W., and Manz, J., Mol. Phys. (1975) 29, 347.
9. Wu, S.F., Johnson, B.R., and Levine, R.D., Mol. Phys. (1973) 25, 839.
10. Adams, J.T., Smith, R.L., and Hayes, E.F., J. Chem. Phys. (1974) 61, 2193.
11. Schatz, G.C., and Kuppermann, A., J. Chem. Phys. (1976) 65, 4624.
12. Baer, M., J. Chem. Phys. (1976) 65, 493.
13. Wolken, G., and Karplus, M., J. Chem. Phys. (1974) 60, 351.
14. Schatz, G.C.and Kuppermann, A., J. Chem. Phys. (1975) 62, 2502.
15. Schatz, G.C. and Kuppermann, A., J. Chem. Phys. (1976) 65, 4642.
16. Schatz, G.C. and Kuppermann, A., J. Chem. Phys. (1976) 65, 4668.
17. Elkowitz, A.B. and Wyatt, R.E., J. Chem. Phys. (1975) 63, 702.
18. Elkowitz, A.B. and Wyatt, R.E., J. Chem. Phys. (1975) 62, 2504.
19. Redmon, M.J. and Wyatt, R.E., Int. J. Quantum Chem. Symp. (1975) 9, 403.
20. Redmon, M.J. and Wyatt, R.E., Int. J. Quantum Chem. Symp. (1977) 11, 0000.
21. Choi, B.H. and Tang, K.T., J. Chem Phys. (1976) 65, 5617.
22. Tang, K.T. and Choi, B.H., J. Chem. Phys. (1975) 62, 3642.
23. Marcus, R.A., J. Chem. Phys. (1968) 49, 2610.
24. Wyatt, R.E., J. Chem. Phys. (1972) 56, 390.
25. Kuppermann, A., Chem. Phys. Lett. (1975) 32, 374.
26. Walker, R.B., Light, J.C., and Altenberger-Siczek, A., J. Chem. Phys. (1976) 64, 1166.
27. Wittriol, N.M., Stettler, J.D., Ratner, M.A., Sabin, J.R. and Trickey, S.B., J. Chem. Phys. (1977) 66, 1141.
28. Harms, S.H. and Wyatt, R.E., J. Chem. Phys. (1975) 62, 3173.
29. Elkowitz, A.B. and Wyatt, R.E., J. Chem. Phys. (1975) 62, 3683.
30. Harms, S.H., Elkowitz, A.B. and Wyatt, R.E. Mol. Phys. (1976) 31, 177.
31. Light, J.C. and Walker, R.B., J. Chem. Phys. (1976) 65, 1598.
32. Porter, R.N. and Karplus, M., J. Chem. Phys. (1964) 40, 1105.

In State-to-State Chemistry; Brooks, P., et al.;
ACS Symposium Series; American Chemical Society: Washington, DC, 1977.

33. Schatz, G.C. and Kuppermann, A., Phys. Rev. Lett. (1975) 35, 1267.
34. Wyatt, R.E., Redmon, M.J. and Wolfrum, J., to be published.
35. Pack, R.T., J. Chem. Phys. (1974) 60, 633.
36. McGuire, P. and Kouri, D.J., J. Chem. Phys. (1974) 60, 2438.
37. Elkowitz, A.B. and Wyatt, R.E., Mol. Phys. (1976) 31, 189.
38. Kuppermann, A., Schatz, G.C. and Dwyer, J.P., Chem. Phys. Lett. (1977) 45, 71.
39. Yates, A.C. and Lester, W.A., Chem. Phys. Lett. (1974) 24, 305.
40. Bernstein, R.B. and Levine, R.D., "Advances in Atomic and Molecular Physics, Vol. 11", D.R. Bates and B. Bederson (eds (eds.) p. 215 (Academic Press, New York, 1975).
41. Truhlar, D.G. and Kuppermann, A., J. Chem. Phys. (1972) 56, 2232.
42. Smith, I.W.M. and Wood, P.M., Mol. Phys. (1973) 25, 441.
43. Karplus, M. and Wang, I., quoted in Ref. 44.
44. Heidner, R.E. and Kasper, J.V.V. III, Chem. Phys. Lett. (1972) 15, 179.
45. Zuhrt, C., Kamal, T., and Zülicke, L., Chem. Phys. Lett. (1975) 36, 396.
46. Jakubetz, W. and Connor, J.N.L., Disc. Farad. Soc. (1976) 62, 324.
47. Manz, J., Mol. Phys. (1975) 30, 899.
48. Latham, S., McNutt, J., Redmon, M. and Wyatt, R.E., to be published.
49. Wyatt, R.E., McNutt, J., Latham, S., and Redmon, M.J., Disc. Farad. Soc. (1976) 62, 322.
50. McCullough, E.A.,Jr.and Wyatt, R.E., J. Chem. Phys. (1972) 54, 3578.
51. Kuppermann, A., Adams, J.T., and Truhlar, D.G., ICPEAC Abstracts VIII, (1973) 149.
52. Hirschfelder, J.O., Goebel, C.J. and Bruch, L.W., J. Chem. Phys. (1974) 61, 5456.
53. Hirschfelder, J.O. and Tang, K.T., J. Chem. Phys. (1976) 65, 470 and references therein.
54. Marcus, R.A., J. Chem. Phys. (1966) 45, 4493.
55. Polanyi, J.C. and Schreiber, J.L., Chem Phys. Lett. (1974) 29, 319.
56. Lacmann, K. and Herschbach, D.R., Chem Phys. Lett. (1970) 6, 106.
57. Chapman, F.M. and Hayes, E.F., J. Chem. Phys. (1975) 62, 4400.
58. Chapman, F.M. and Hayes, E.F., J. Chem. Phys. (1976) 65, 1032.
59. Leasure, S.C. and Bowman, J.M., Chem. Phys. Lett. (1976) 39, 462.
60. Polanyi, J.C. and Woodall, K.B., J. Chem. Phys. (1972) 57, 1574.
61. Perry, D.S. and Polanyi, J.C., Chem. Phys. (1976) 12, 419.

In State-to-State Chemistry; Brooks, P., et al.;
ACS Symposium Series; American Chemical Society: Washington, DC, 1977.

25

Collisions Involving Electronic Transitions

JOHN C. TULLY

Bell Laboratories, Murray Hill, NJ 07974

Electronic transitions - transitions between one potential energy surface and another - occur in a variety of low-energy molecular collision processes. Among them are electronic energy transfer, spin-forbidden processes, quenching of excited electronic states (E → V,R,T transfer), and charge transfer. With the maturing of the laser as a laboratory tool, detailed experimental information about each of these types of processes is becoming increasingly available. For example, experimental studies of the destruction of electronically excited halogen atoms by hydrogen halides,

$$X_a^*(^2P_{1/2}) + HX_b \rightarrow \begin{cases} X_b^*(^2P_{1/2}) + HX_a \\ X_b(^2P_{3/2}) + HX_a \\ X_a(^2P_{3/2}) + HX_b \end{cases}$$

have been reported for most of the 16 combinations of the halogens F, Cl, Br, and I. A schematic illustration of the potential energy surfaces operative in these systems is shown in Figure 1. The dynamics of these processes are not simple. Near-resonances between the electronic energy of the excited halogen and particular vibrational-rotational transitions of the diatomic appear to play an important role in some cases (1). Chemical reaction has been shown to occur in other cases (2). Curve-crossing mechanisms have been suggested for still others (3). Although many theoretical approaches have been applied successfully to particular classes of electronically nonadiabatic collisions, there are at present no practical techniques that are capable of providing reliable descriptions of processes that involve all of the complications of the above reaction. Development of a practical theory that can provide quantitative state-to-

In State-to-State Chemistry; Brooks, P., et al.;
ACS Symposium Series; American Chemical Society: Washington, DC, 1977.

state information about the type of collision process exemplified by this reaction is our goal. In this talk we will summarize advances toward this goal and suggest some possible directions for future work.

Impact Parameter Treatments

Most work in this area has been based on the large impact parameter assumption: interacting molecules pass by each other along a simple two-body trajectory and electronic transitions occur as a response to the time-dependent interaction along this trajectory. The multiple curve-crossing model of Bauer, Fisher and Gilmore (4) and the near-resonant transfer approach of Sharma, Brau and Ewing (5,6) are examples of methods based on this assumption that have been used successfully in certain situations. But the impact parameter assumption cannot be useful in most low-energy molecular collisions. It is obvious that for chemically reactive encounters simple two-body trajectories are totally inadequate. However, at low (thermal) velocities, even simple nonreactive ($E \rightarrow V,R,T$) collisions cannot be described by these methods in most cases.

An example that illustrates this point is provided by the simple quenching process,

$$O(^1D) + N_2 \rightarrow O(^3P) + N_2$$

Two theoretical treatments based on straight-line trajectories (7,8) do not provide satisfactory descriptions of this process. The reason for this is clear from Figure 2 which shows approximate potential energy curves for $O(^1D)$ approaching N_2. Transitions from the initial singlet potential surface to the triplet surfaces leading to quenching are localized at the crossings between the attractive singlet and the three repulsive triplet states. A straight-line trajectory at small impact parameter passes through the crossing region exactly twice, once on the way in and once on the way out. The probability of a singlet - triplet transition at this crossing is governed by spin-orbit coupling, which is quite small in this system. Therefore these models predict cross sections that are too small, as shown in Table I. We expect, of course, that as a consequence of the very deep potential well of the lowest singlet (the stable ground state of N_2O), thermal energy trajectories will exhibit very complicated behavior corresponding to a long-lived collision complex. This is illustrated in

In State-to-State Chemistry; Brooks, P., et al.;
ACS Symposium Series; American Chemical Society: Washington, DC, 1977.

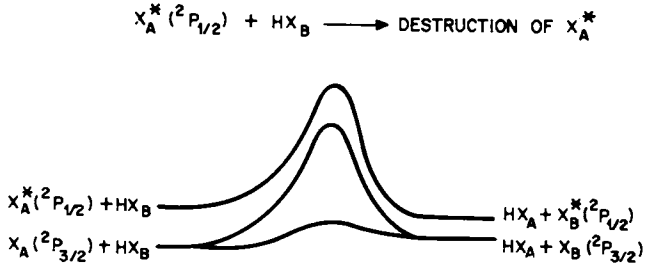

Figure 1. Schematic of X_aHX_b potential curves

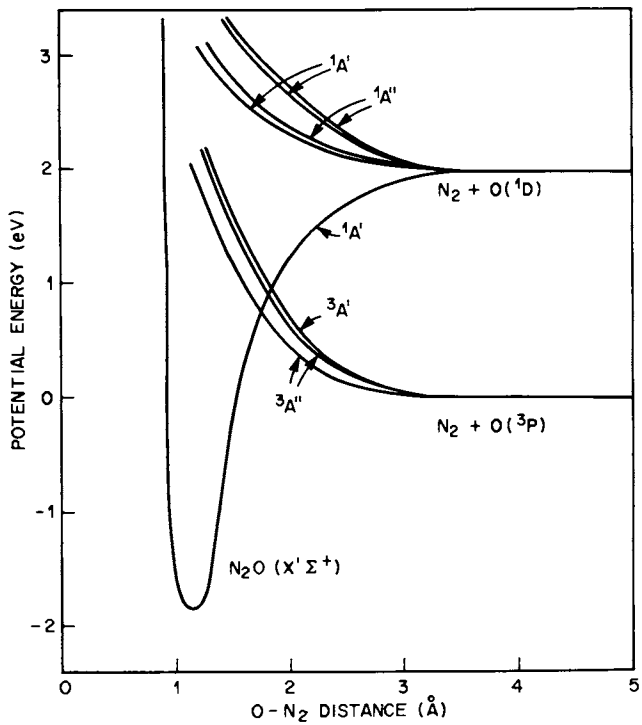

Figure 2. Approximate N_2O potential curves

Figure 3. The singlet-triplet crossing may be traversed a great many times before the complex breaks up. This picture suggests the following statistical model of quenching (9): The quenching cross section is the product of the cross section for formation of a "close collision" complex times the probability that the complex will decay by a singlet-triplet transition. The close collision cross section can be obtained by assuming that a complex is formed whenever the centrifigal barrier determined by the known $O(^1D)$ - N_2 inverse sixth power potential is surmounted, with proper account taken of the five-fold degeneracy of $O(^1D)$. The complex can break up by either of two paths, first by going back over the centrifugal barrier to reform reactants, and second by a singlet-triplet transition. The rate for the first process can be obtained, according to standard RRKM theory of unimolecular decay, from the volume of phase space at the "critical configuration"; i.e., the centrifugal barrier. The rate of the second process can be estimated by postulating a second kind of critical configuration, a curve crossing. The rate of decay of the complex by this route is proportional to the corresponding volume of phase space times an electronic transition probability, which we have approximated using the Landau-Zener formula (9). The underlying assumption of this statistical model is that vibrational, rotational and translational motion are equilibrated in the collision complex, but that electronic transitions occur in a specific way, namely at curve crossings. Predictions of this simple model are in good agreement with experiment (10,11), as shown in Table I. More importantly for the present discussion, it provides a clear illustration of the unsuitability of impact parameter theories for most low-energy inelastic processes.

Table I. Quenching of $O(^1D)$ by N_2 at 300°K

	Rate Constant (10^{-11} cc/sec)	Avg. Product Vibr. Energy (kcal/mole)
Impact P. Theory (7)	0.2	0.
Impact P. Theory (8)	0.1	0.
Statistical Model (9)	7.0 ± 0.8	14 ± 4
Experiment (10)	6.9 ± 0.6	...
Experiment (11)	...	15 ± 2

In State-to-State Chemistry; Brooks, P., et al.;
ACS Symposium Series; American Chemical Society: Washington, DC, 1977.

Multi-Dimensional Treatments

Simple statistical models such as the one outlined above appear to be satisfactory for certain cases. However, most chemically reactive processes do not behave in a statistical manner. This is certainly true for the halogen atom - hydrogen halide systems that we have chosen as our goal. Theoretical descriptions of these processes must take into account the chemical forces that govern the specific paths followed by the interacting nuclei. We must trace out the detailed motion of the nuclei, either quantum mechanically, semiclassically, or classically, as they move along complicated many-dimensional potential energy hypersurfaces. Except for the very simplest systems, classical mechanics has been, and will continue to be for some time, the only practical method for doing this. Classical mechanics is not always adequate, of course. There are inaccuracies due to neglect of tunnelling effects, particularly near threshold. Quantum interference effects are omitted. Direct state-to-state information is not provided. The last deficiency can usually be satisfactorily handled by converting continuous classical distributions into discrete state populations using boxing or moment techniques. In fact, as will be seen below, classical mechanics can provide surprisingly accurate and complete descriptions of reactive collisions, even those involving the most highly quantum mechanical atom, hydrogen. Classical mechanics can be expected to be entirely adequate for most processes that do not involve hydrogen. This is true, at least, if there are no electronic transitions. Electronic transitions are quantum mechanical events - electronic motion is far from classical. It remains to be seen to what extent classical mechanics, with suitable semiclassical extensions to account for electronic transitions, can describe collision processes such as the $X^* + HX$ system.

Any theory of this type must ultimately be a mixture of classical and quantum mechanics. The fundamental inconsistency associated with the mixing of the two mechanics is at the root of most of the difficulties afflicting these theories. Although this inconsistency cannot be removed, short of treating all degrees of freedom quantum mechanically, we can hope to minimize its adverse effects. There are some existing methods that have been highly successful in some situations, and there is promise that these can be extended.

In State-to-State Chemistry; Brooks, P., et al.;
ACS Symposium Series; American Chemical Society: Washington, DC, 1977.

All theories of nonadiabatic molecular collisions invoke a separation of degrees of freedom into two (or more) groups, which we will call internal coordinates ($\underset{\sim}{q}$) and external coordinates ($\underset{\sim}{Q}$). We can categorize the various theories according to how they make this separation, as shown in Figure 4. The most common choice is to describe electronic, vibrational, and rotational motion by $\underset{\sim}{q}$, and only translation by $\underset{\sim}{Q}$. Theories based on this choice can provide direct state-to-state information, they accomodate near-resonant effects in a natural way, and some have been applied very successfully to high energy processes. But separation of translational motion from vibration and rotation is justified at low energies only for very large impact parameters, so, as discussed above, such methods will not be useful toward achieving our goal, description of processes like $X^* + HX$.

A more natural separation of degrees of freedom is to choose $\underset{\sim}{q}$ to be electron coordinates and $\underset{\sim}{Q}$ to be nuclear coordinates. We are then faced with solving for the motion of the nuclei $\underset{\sim}{Q}$ on many-dimensional potential energy hypersurfaces. Complete quantum mechanical procedures for doing this are at present impractical, except for the very simplest systems. Quantum descriptions of collisions involving electronically excited species are usually particularly difficult because the availability of electronic energy can open a huge number of possible vibration-rotation channels. Our only alternative is to attempt a classical or semiclassical description of nuclear motion.

The distinction between classical and semiclassical methods can be somewhat arbitrary. We will not concern ourselves with this here and lump them both together. All classical or semiclassical treatments of nonadiabatic collisions consist of two steps, first, prescription of some trajectory $\underset{\sim}{Q}(t)$ describing nuclear motion, and second, calculation of an electronic transition probability along this trajectory. Pechukas has shown, in a paper that has strongly influenced subsequent work in this area, that these two steps are intertwined (12). The transition probability depends on the trajectory, and the effective potential that governs the trajectory depends on the transition probability. There are a variety of theories that differ mainly in how the effective potential is approximated. For example, various averages of two interacting potential energy surfaces, perhaps weighted by transition probabilities, have been suggested. There is a crucial requirement,

In State-to-State Chemistry; Brooks, P., et al.;
ACS Symposium Series; American Chemical Society: Washington, DC, 1977.

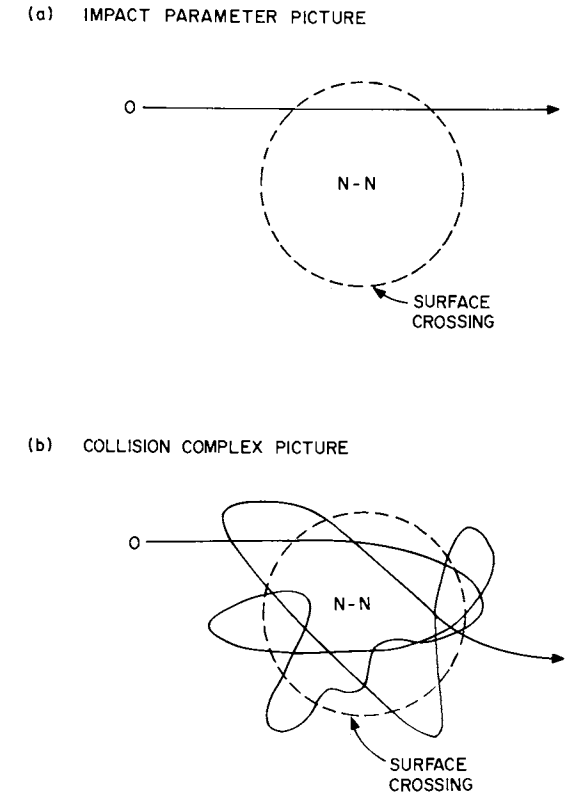

Figure 3. Quenching mechanisms

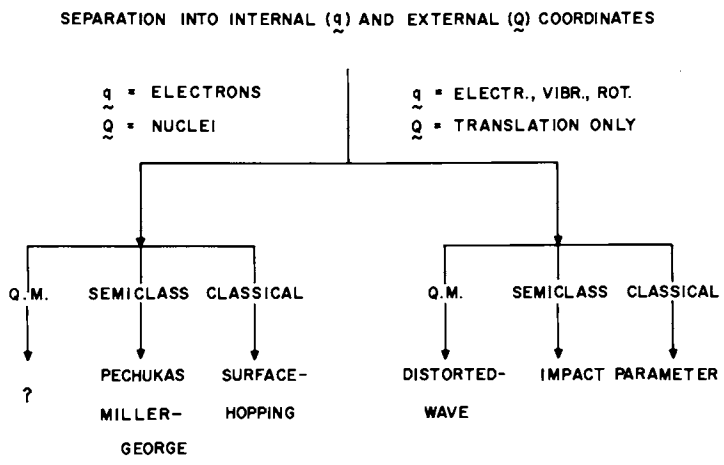

Figure 4. Classification of nonadiabatic molecular collision theories

In State-to-State Chemistry; Brooks, P., et al.;
ACS Symposium Series; American Chemical Society: Washington, DC, 1977.

however, which renders most of these methods unsuitable for low-energy chemically reactive collisions. The requirement is that a single trajectory must be allowed to split into branches, each following its own potential. Forces on two different interacting potential energy surfaces can be very different from each other. Perhaps one surface can lead to chemical reaction and another cannot. No single effective potential can correctly describe all of the different possible types of motion. Trajectories may experience some effective average interaction in regions of strong coupling between the potential surfaces, but at the end of the collision a trajectory must be moving along some individual potential surface. Therefore, unless the electronic transition probability is zero or one, the trajectory must develop branches, each ultimately following a particular potential energy surface.

Whereas this requirement can often be relaxed in atomic collisions, for low-energy atom-molecule or molecule-molecule encounters it is absolutely essential. This eliminates all current existing theoretical approaches except two, the surface-hopping trajectory (SHT) model (13,14) and the complex-valued trajectory theory (MG) of Miller and George (15,16). There are related approaches that have promise (17,18), but it is not yet clear whether they will be accurate or tractable for multi-dimensional situations.

Surface-Hopping

The SHT method is an extension of the ordinary classical trajectory approach to motion on several interacting potential energy surfaces. The underlying assumption of the method is that an accurate effective potential governing nuclear motion can be defined in two limiting regimes. The first are regions where the separation between the potential surfaces is sufficiently large and the interaction between them sufficiently small that electronic transitions do not occur. Motion then evolves along one potential surface or the other. The second regime occurs in strongly interacting regions where the separation between the potential surfaces is small compared to the kinetic energy of nuclear motion, so that trajectories along either surface would be essentially identical in these regions. There are, of course, cases where intermediate regions may be important. This is the major limitation of the SHT method. But there are also many

In State-to-State Chemistry; Brooks, P., et al.;
ACS Symposium Series; American Chemical Society: Washington, DC, 1977.

cases where intermediate regions are unimportant and SHT theory is very accurate. We will present two examples, one where SHT theory appears adequate and one where it does not.

A SHT calculation requires, as input, a potential energy surface as a function of internuclear coordinates for each electronic state active in the collision. It requires, in addition, specification of surface hopping locations - regions of strong nonadiabatic coupling where trajectories will be permitted to branch. These are taken at avoided crossings or, more generally, at maxima of the nonadiabatic interaction. Finally, it requires a transition probability $P(\underset{\sim}{Q},\dot{\underset{\sim}{Q}})$ that electronic transitions will occur. This is obtained by integrating the time-dependent electronic Schrodinger equation along the trajectory $\underset{\sim}{Q}(t)$:

$$i\hbar\dot{a}_k = \sum_j a_j \left(H_{kj} - i\hbar\dot{\underset{\sim}{Q}}\cdot\langle\varphi_k|\underset{\sim}{\nabla}\varphi_j\rangle\right)\exp\left[-\frac{i}{\hbar}\int^t (V_j - V_k)dt'\right] \quad (1)$$

The transition probability $P(\underset{\sim}{Q},\dot{\underset{\sim}{Q}})$ is obtained by squaring the appropriate amplitude a_k. $P(\underset{\sim}{Q},\dot{\underset{\sim}{Q}})$ is evaluated throughout the interaction region. If adiabatic potential energy surfaces are employed, the term H_{kj} will be zero and the transition amplitude will depend only on the nonadiabatic coupling strength $\langle\varphi_k|\underset{\sim}{\nabla}\varphi_j\rangle$. If diabatic potentials are used, H_{kj} will not vanish nor, in general, will $\langle\varphi_k|\underset{\sim}{\nabla}\varphi_j\rangle$. Any correct choice of representation will of course give the same final transition probabilities. There are a variety of approximate evaluations of Eq. (1) for the transition probability which may be useful in some situations; e.g., Magnus expansions, Landau-Zener-Stueckelberg, Demkov, etc.

Once the input information has been prescribed, a SHT calculation proceeds in much the same way as an ordinary classical trajectory calculation. Initial conditions are selected at random from distributions chosen to model a particular experimental situation. The trajectory is then integrated along the initial potential surface until a surface hopping location is reached. At this point the trajectory is split into branches, one branch weighted by $P(\underset{\sim}{Q},\dot{\underset{\sim}{Q}})$ following the new potential surface and a second branch weighted by 1-P following the original surface. Note that whereas branching takes place at a particular point on the trajectory, the transition probability P is obtained by integrating Eq.(1) throughout the entire interac-

In State-to-State Chemistry; Brooks, P., et al.;
ACS Symposium Series; American Chemical Society: Washington, DC, 1977.

tion region. Each branch of the trajectory is traced out individually, with additional branches developing if additional hopping locations are encountered. The final results are treated in the same way as a classical trajectory calculation, with only the slight complication that trajectory branches will have non-unit weights.

If diabatic potential surfaces are employed, trajectories will branch at points where the potentials are degenerate and energy will be conserved automatically. If adiabatic potentials are used, the component of velocity along the nonadiabatic coupling vector is adjusted in order that the branch beginning on the new potential surface remain at the same total energy. This is essentially equivalent to making a local transformation to a diabatic representation in the neighborhood of the transition.

To illustrate the SHT model, we consider collisions of H^+ with H_2; e.g.,

$$\begin{aligned} H^+ + D_2 &\rightarrow D^+ + HD \\ &\rightarrow HD^+ + D \\ &\rightarrow D_2^+ + H \end{aligned}$$

The Diatomics-in-Molecules (DIM) potential energy surfaces employed for this study are in good quantitative agreement with ab initio surfaces known to be accurate for this two-electron system. Thus any serious inaccuracy can be attributed to the SHT theory. This is a difficult test of the theory, first, because the involvement of hydrogen atoms makes the assumption of classical mechanics suspect, and second, because there are a variety of product channels and the competition between these channels is very specific; i.e., not statistical.

The SHT model was applied in a very straightforward way (13). Hopping locations were taken to be the avoided intersections between the two lowest singlet surfaces of H_3^+. Electronic transition probabilities were computed by numerical integration of Eq.(1) along each trajectory, using nonadiabatic coupling computed by DIM. After sufficient statistics on transition probabilities were obtained in this way, hopping probabilities for later trajectories were obtained from a fit of the previous numerical results to a function of the Landau-Zener form.

Agreement between SHT predictions and experiment are excellent, within experimental uncertainty for essentially every computed reaction property. Cross sections are compared in Figure 5. Both the

In State-to-State Chemistry; Brooks, P., et al.;
ACS Symposium Series; American Chemical Society: Washington, DC, 1977.

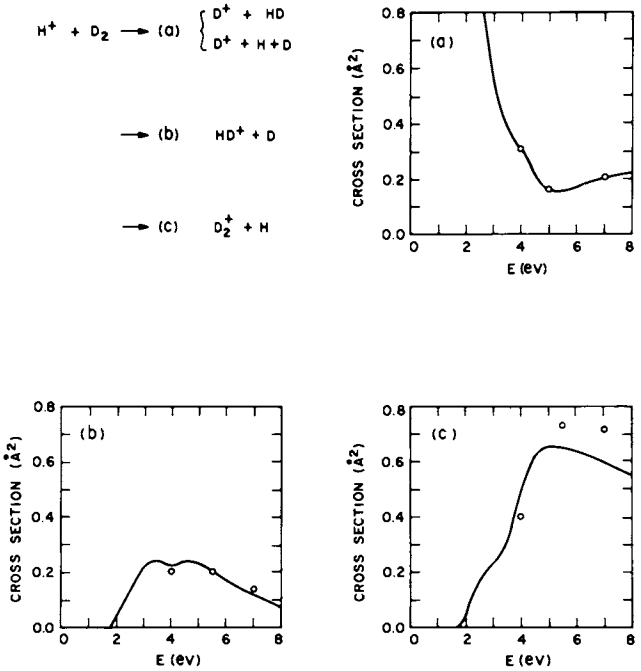

Figure 5. Absolute reaction cross sections for $H^+ + D_2$. Circles: SHT; curves: experiment (20).

theoretical (19) and experimental (20) results are absolute (un-normalized) cross sections, and the theory is completely a priori in that no adjustable parameters of any kind were employed. SHT also appears to provide accurate predictions of details such as translational energy distributions, as shown in Figure 6. Because it is a classical mechanical theory, SHT cannot provide direct state-to-state transition probabilities. Nevertheless, the agreement of Figure 6 suggests that application of standard boxing or moment methods to simulate discrete quantum transition probabilities should be a very satisfactory procedure.

As a second example of the SHT method, we consider the reaction of $F^*(^2P_{1/2})$ with H_2, a process very similar to those we initially chose to represent our goal. There are three important reasons why this reaction is more difficult for the SHT method than the H_3^+ reaction. The first is that nonadiabatic coupling is more delocalized; there is no avoided crossing of potential surfaces, as illustrated by the solid curves

In State-to-State Chemistry; Brooks, P., et al.;
ACS Symposium Series; American Chemical Society: Washington, DC, 1977.

of Figure 7. This, fortunately, does not turn out to be a serious problem, because the nonadiabatic coupling peaks sharply at about 3.8 a_o, as shown by the dashed curve of Figure 7, resulting in a well defined hopping location.

The second difficulty arises from the fact that the splitting between the interacting potential surfaces in the strong coupling region is about the same magnitude as the thermal kinetic energy, so the velocity adjustment is very severe. This problem will be removed by the Miller-George theory discussed below. The final and most serious difficulty is that near-resonant effects are not included properly. This will also be discussed below.

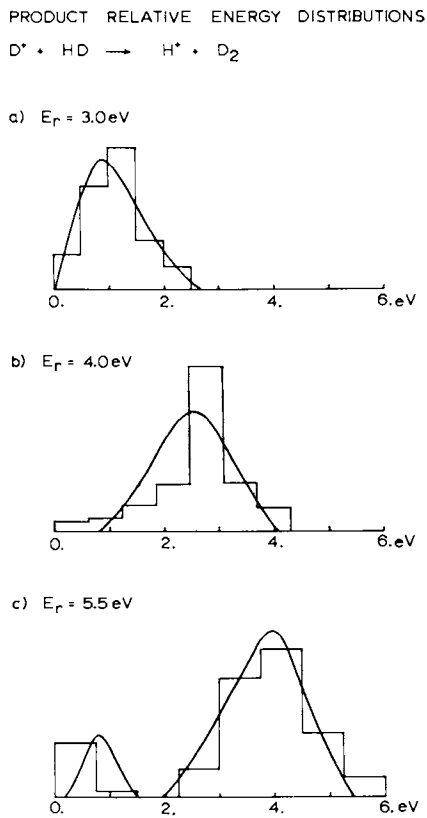

Figure 6. Product translational energy distributions. Histograms: SHT. Curves: experiment (19).

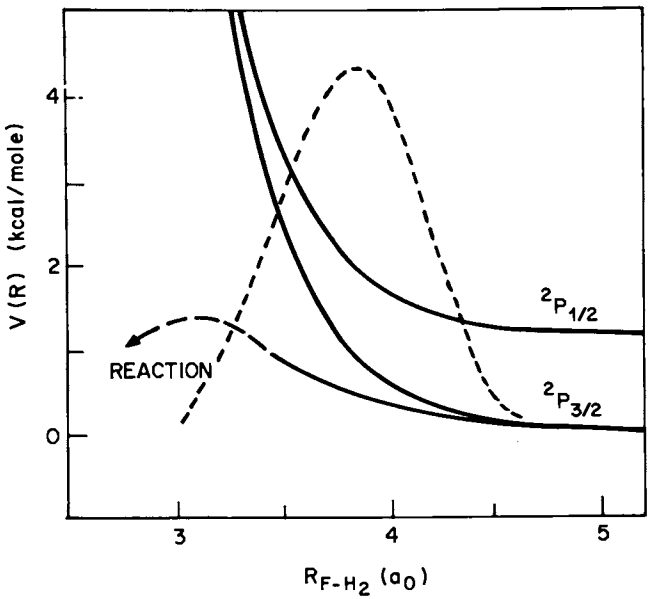

Figure 7. Approximate FH_2 potential curves. Dashed curve is nonadiabatic coupling (arb. units).

Application of SHT theory to this system (21) gives the cross sections shown in Figure 8. $F^*(^2P_{1/2})$ reacts with H_2 with considerably lower probability than does $F(^2P_{3/2})$. Even though its extra energy of 1.1 kcal/mole is very helpful in surmounting the 1 kcal/mole barrier to reaction, $F^*(^2P_{1/2})$ does not easily undergo the required transition to the lowest reactive potential surface. This conclusion is probably qualitatively correct, but it must be considered suspect due to the last two difficulties mentioned above.

Miller-George Theory

Miller and George (15,16) have developed an elegent semiclassical theory of nonadiabatic collisions which removes the SHT problem associated with discontinuous velocity adjustments at surface hops. They exploit the fact that adiabatic potential energy surfaces which interact at, e.g., an avoided crossing (or a curve merging as in the F + H example), will actually cross at some complex value of the internuclear coordinates; i.e., when analytically continued to com-

In State-to-State Chemistry; Brooks, P., et al.;
ACS Symposium Series; American Chemical Society: Washington, DC, 1977.

plex coordinates two potential energy surfaces can exhibit branch points at which they become degenerate. Miller and George integrate classical trajectories with complex coordinates and time along the analytic continuation of an adiabatic potential energy surface until such a branch point is reached. At this point the trajectory can pass continuously from one surface to the other. The probability of transition is related to the magnitude of the excursion away from the real axis required to reach the branch point. The transition amplitude is obtained in the MG theory from the semiclassical Stueckelberg approximation:

$$a_k = \exp\left[-\frac{i}{\hbar}\int_{t_1}^{t^*} V_j\,dt - \frac{i}{\hbar}\int_{t^*}^{t_2} V_k\,dt\right] \qquad (2)$$

where V_k and V_j are the adiabatic potential surfaces for states j and k and t* is the complex time at which the surfaces intersect.

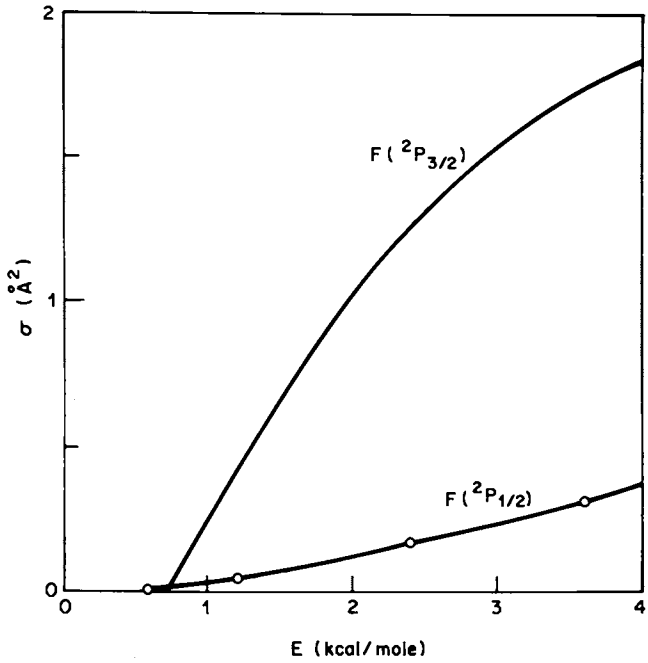

Figure 8. Cross sections for reaction of $F(^2P_{1/2})$ and $F(^2P_{3/2})$ with H_2

As discussed earlier, classical and semiclassical theories of nonadiabatic collisions have two major features, prescription of trajectories and calculation of the electronic transition amplitude. With the SHT theory, trajectories are defined in a more or less *ad hoc* way. Branching is achieved either at intersections of diabatic potential surfaces or at nonadiabatic coupling maxima of adiabatic surfaces, with appropriate velocity adjustments in the latter case. Once the trajectory has been defined, SHT computes the electronic transition probability exactly by integration of Eq.(1). The MG theory is a consistent semiclassical procedure. The electronic transition amplitude, Eq.(1), is is approximated by the semiclassical Stueckelberg relation, Eq.(2), which assumes the electronic transition amplitude to be localized at the complex intersection of the adiabatic potential energy surfaces. The complex valued trajectories are integrated to this intersection on the initial potential surface, at which point they switch to the new surface, exactly as indicated by Eq.(2).

The MG theory has two advantages over SHT. First, trajectories and transition amplitudes are self-consistent, as discussed above. Second, MG avoids the discontinuous velocity adjustment sometimes required by SHT. This makes it appear better suited for situations like our initial goal, reactions of halogen atoms with hydrogen halides, where SHT velocity adjustments might be comparable with nuclear velocities.

MG theory has two serious disadvantages as well. The more obvious one is that it is considerably more difficult to implement than SHT. The second is associated with the fact that MG theory employs the Stueckelberg approximation to the electronic transition amplitude, whereas SHT computes it exactly. The Stueckelberg expression involves no nonadiabatic coupling matrix elements, at least not explicitly. All information about transition probabilities, in MG theory, is contained in the adiabatic potential surfaces and their analytic continuations. This somewhat surprising absence of nonadiabatic coupling terms has been demonstrated by Davis and Pechukas (22) to be rigorously correct in the strict semiclassical limit. In some ways this result is disappointing, however. It is easy to see that there are cases where important effects will be left out. Consider, for example, the unrealistic but illustrative example of two adiabatic potential surfaces which are parallel everywhere, separated by the constant energy 2A.

In State-to-State Chemistry; Brooks, P., et al.;
ACS Symposium Series; American Chemical Society: Washington, DC, 1977.

$$V_1(Q) = -A$$
$$V_2(Q) = A \qquad (3)$$

The analytic continuations of these surfaces will never intersect, so MG theory will predict no transitions between them. These adiabatic surfaces can be thought to arise from diagonalization of a 2X2 symmetric diabatic Hamiltonian matrix defined by the matrix elements H_{11}, H_{22}, and H_{12}. One possible choice of these matrix elements that would produce the adiabatic curves of Eq.(3) is

$$H_{11}(Q) = -A$$
$$H_{22}(Q) = A \qquad (4)$$
$$H_{12}(Q) = 0$$

i.e., there is no off-diagonal coupling between the curves. Then the exact quantum dynamics and the SHT model would both agree with MG that no transitions would occur between the surfaces. However, the same adiabatic surfaces could arise from any unitary transformation of the matrix defined by Eq.(4). Only one particular unitary transformation will correspond to the "true" diabatic representation. The eigenvalues of a matrix (the adiabatic curves) do not carry all information about the original matrix. For example, diagonalization of the diabatic Hamiltonian matrix

$$H_{11}(Q) = -A + f(Q)$$
$$H_{22}(Q) = A - f(Q) \qquad (5)$$
$$H_{12}(Q) = (2Af - f^2)^{1/2}$$

would result in identical adiabatic surfaces, Eq.(3). If the arbitrary function f(Q) were large, the exact quantum dynamics and the SHT theory applied to this model system might predict substantial (and hopefully similar) electronic transition probabilities, whereas MG would again predict no transitions.

It is clear that there will be situations where SHT will be more accurate and others where MG theory will be more accurate. The methods must be applied with care. Two important conclusions to be made about both theories are first, both are capable of very accurate descriptions of wide classes of systems, and second, neither are capable of adequately describing near-resonance effects.

Near-Resonance Effects

There is strong experimental evidence that in our prototype collision process, $X^* + HX$, a near-

In State-to-State Chemistry; Brooks, P., et al.;
ACS Symposium Series; American Chemical Society: Washington, DC, 1977.

degeneracy between a particular vibrational-rotational state of the diatomic and the excited electronic state of the halogen atom X can produce a very large enhancement of the electronic transition probability (1). Model quantum mechanical calculations support the importance of this effect (23,24). To achieve our stated goal we must develop a theory which can incorporate this effect realistically. There are several methods based on the large impact parameter assumption that can describe near-resonance effects easily and accurately. An example is the Sharma-Brau-Ewing model (5,6) which is entirely a near-resonance theory. But we have argued that none of the impact parameter approaches can be generally applicable because they cannot adequately describe complicated nuclear motion that is crucial in most thermal energy molecular collisions. Thus we have been forced to turn to many-dimensional classical and semiclassical treatments. There is some hope, however, that classical mechanical approaches may be extended to incorporate near-resonance effects accurately. We can illustrate the situation with a simple model calculation, an SHT treatment of collisions of $Br^*(^2P_{1/2})$ with HBr. In order to make the calculation simple for illustrative purposes, we restrict the collision to occur in a plane, and artificially force the H end of the diatomic to always point at the colliding Br^* atom, as shown in Figure 9. We also add one more artificial aspect that makes this calculation totally unrelated to to the real Br^* + HBr system; we take the vibrational frequency of HBr to be an adjustable parameter. We can then tune this frequency through resonance with the Br^* excited state.

We perform the calculation for a fairly large impact parameter, 8.5 a_o, so we must be careful to include the correct long-range dipole-quadrupole interaction that dominates this region of the potential surfaces.

We then proceed with the SHT calculation, obtaining a classical trajectory along the initial Br^*-HBr surface and integrating Eq.(1) for the electronic transition amplitude along this trajectory. The potential energy surfaces for this system resemble qualitatively those for F + H_2, shown in Figure 7. In particular, the nonadiabatic coupling peaks around 4 or 5 a_o, far inside the distance of closest approach of our 0.6 kcal/mole trajectory. Thus the trajectory never reaches a hopping location. Similarly, the real part of the location of the complex intersection of the adiabatic surfaces will occur in the same 4-5 a_o re-

In State-to-State Chemistry; Brooks, P., et al.;
ACS Symposium Series; American Chemical Society: Washington, DC, 1977.

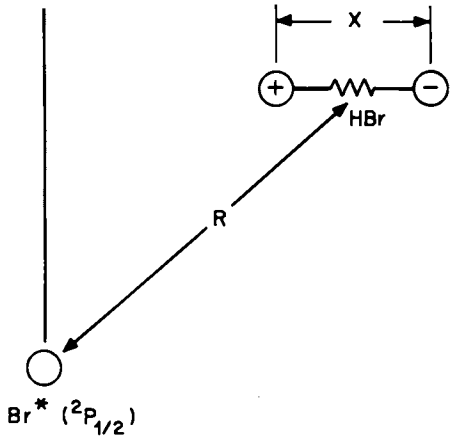

Figure 9. Collisions of Br with HBr*

gion, so MG theory will include no near-resonance effects. However, as we tune the vibrational frequency through resonance, the SHT transition probability from Eq.(1) becomes very large. In fact, as shown in Figure 10, it closely parallels that obtained using the near-resonant theory of Sharma-Brau-Ewing, which is a first-order perturbation theory calculation of the transition probability between two quantum levels connected by, in this case, a time-dependent dipole-quadrupole interaction. The reason why the classical calculation produces this quantum near-resonance effect can be understood by examination of Eq.(1). When two potential surfaces exhibit a large splitting, $V_j - V_k$, the transition amplitude will in general become very small because the exponential term in Eq.(1) will oscillate rapidly. In this case, however, the coupling H_{kj}, via the change in dipole moment with internuclear distance, is oscillating at the vibrational frequency of the diatomic. If this frequency becomes nearly equal to the oscillation frequency of the exponential term, there will be a net buildup of transition amplitude. This is, of course, the resonance criterion.

The above example demonstrates that information about near-resonance transition probabilities is contained in the SHT theory. Unfortunately, the SHT trajectories are not adequate to describe nuclear motion under near-resonance conditions. This deficiency results from the ad hoc procedure for choosing trajectories which is not rigorously consistent with calculation of the transition amplitude. To remove this

In State-to-State Chemistry; Brooks, P., et al.;
ACS Symposium Series; American Chemical Society: Washington, DC, 1977.

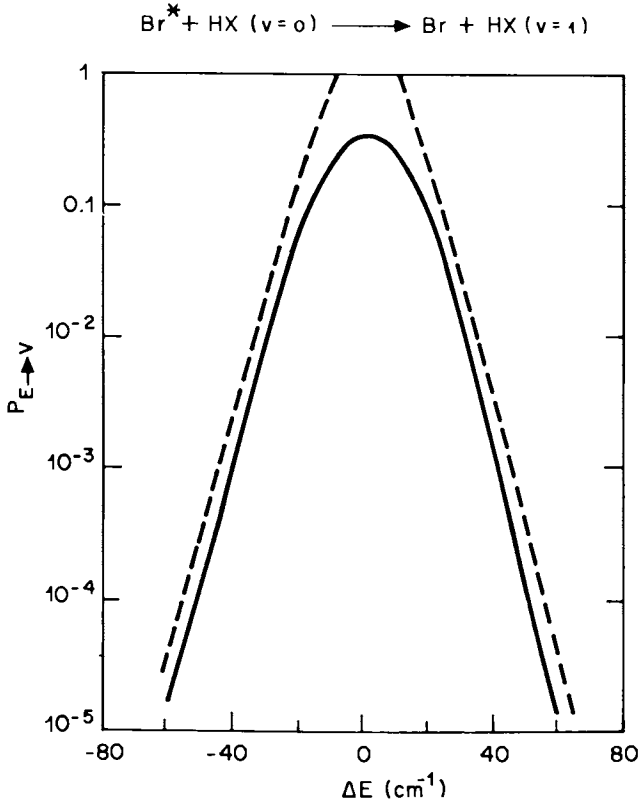

Figure 10. Near-resonant E → V transfer probability. Solid curve: SHT. Dashed curve: Sharma–Brau–Ewing (5, 6).

inconsistency, MG theory invokes the Stueckelberg approximation for the transition probability. This, unfortunately, eliminates near-resonance contributions entirely. Thus neither existing theory is adequate. What is needed is a new semiclassical theory based on a more accurate expression than Eq.(2) with trajectory and transition amplitude computed self-consistently.

Summary

We conclude by repeating what we stated at the outset; there are currently no existing practical methods capable of accurate description of nonadiabatic chemical collisions of the type exemplified by the X* + HX process. Nevertheless, clas-

In State-to-State Chemistry; Brooks, P., et al.;
ACS Symposium Series; American Chemical Society: Washington, DC, 1977.

sical and semiclassical techniques appear promising. There are still serious problems to be worked out, particularly with regard to near-resonance processes. But there is hope that these can be solved, and there are already a large number of important problems that can be addressed accurately and predictively with existing techniques.

Literature Cited

(1) Pritt,A.T.,Coombe,R.D.,J.Chem.Phys.(1976),65, 2096.
(2) Bergmann,K.,Leone,S.R.,Moore,C.B.,J.Chem.Phys. (1975), 63, 5547.
(3) Donovan,R.J.,Fotakis,C.,Golde,M.F.,J.Chem.Soc. Faraday Trans.II(1976), 2055.
(4) Bauer,E.,Fisher,E.R.,Gilmore,F.R.,J.Chem.Phys. (1969),51,4173.
(5) Sharma,R.D.,Brau,C.A.,J.Chem.Phys.(1969),50,924.
(6) Ewing,J.J.,Chem.Phys.Letters (1974),29,50.
(7) Fisher,E.R.,Bauer,E.,J.Chem.Phys.(1972),57,1966.
(8) Delos,J.B.,J.Chem.Phys.(1973),59,2365.
(9) Tully,J.C.,J.Chem.Phys.(1974),61,61.
(10) Heidner,R.F.,Husain,D.,Wiesenfeld,J.R.,J.Chem. Soc.Faraday Trans.II (1973),69,927.
(11) Slanger,T.G.,Black,G.,J.Chem.Phys.(1974),60,468.
(12) Pechukas,P.,Phys.Rev.(1969),181,1974.
(13) Tully,J.C.,Preston,R.K.,J.Chem.Phys.(1971),55, 562.
(14) Tully,J.C.,"Dynamics of Molecular Collisions", Vol.2,W.H.Miller,ed.,p.217,Plenum,N.Y.,1976.
(15) Miller,W.H.,George,T.F.,J.Chem.Phys.(1972), 56,5637.
(16) Miller,W.H.,Advan.Chem.Phys.(1974),25,69.
(17) Pechukas,P.,Davis,J.P.,J.Chem.Phys.(1972), 56,4970.
(18) Laing,J.R.,Freed,K.F.,Phys.Rev.Letters(1975), 34,849.
(19) Krenos,J.R.,Preston,R.K.,Wolfgang,R.,Tully,J., J.Chem.Phys.(1974),60,1634.
(20) Ochs,G.,Teloy,E.,J.Chem.Phys.(1974),61,4930.
(21) Tully,J.C.,J.Chem.Phys.(1974),60,3042.
(22) Davis,J.P.,Pechukas,P.,J.Chem.Phys.(1976), 64,3129.
(23) Zimmerman,I.H.,George,T.F.,J.Chem.Phys.(1974), 61,2468.
(24) Rebentrost,F.,Lester,W.A.,J.Chem.Phys.(1976), 64,4223.

In State-to-State Chemistry; Brooks, P., et al.;
ACS Symposium Series; American Chemical Society: Washington, DC, 1977.

26

The Information-Theoretic Approach: An Interim Progress Report*

R. D. LEVINE

Department of Physical Chemistry, The Hebrew University, Jerusalem, Israel

One of the pleasing outcomes of recent work in molecular reaction dynamics (1) is the recognition that chemical systematics remain even when one is probing the process on a fairly detailed level. As an example, figure 1 (adapted from (2)) shows (not always direct) experimental measurements (3-6) of the effect of HCl vibrational excitation on the reaction rate with F, Br and I atoms. It is evident that there is an exponential enhancement of the reaction rate as long as the reaction endoergicity (indicated by an arrow) exceeds the vibrational energy of HCl and that the enhancement is much more moderate past this point (7-9). The effective 'threshold' in the reaction rate vs. reagent vibrational excitation can be directly traced to the 'exponential-gap' dependence of the 'state-to-state' rates (2,9). This article is a progress report on the information theoretic approach which was used to derive the above (and other) conclusion(s).

The approach is currently undergoing a transition to its third generation of developments, where it is derived as an exact solution for the dynamics of the collision. In this report we briefly review (with a few examples) the techniques of surprisal analysis and of surprisal synthesis. We then comment on the derivation of these techniques as strict implications of the equations of motion (be they quantal or classical).

Surprisal Analysis

One can distinguish two broad aims of the information theoretic approach. The first is analysis. Here one is seeking to find a compact characterization of the result in a manner that will facilitate comparison and correlation both within a family of similar reactions and for different families. An example is provided in figure 2 (adapted from (10)). It shows three experimental vibrational state distributions for CO. The first is the nascent state distribution measured (11) for the

*Work supported by US Air Force, Office of Scientific Research.

In State-to-State Chemistry; Brooks, P., et al.;
ACS Symposium Series; American Chemical Society: Washington, DC, 1977.

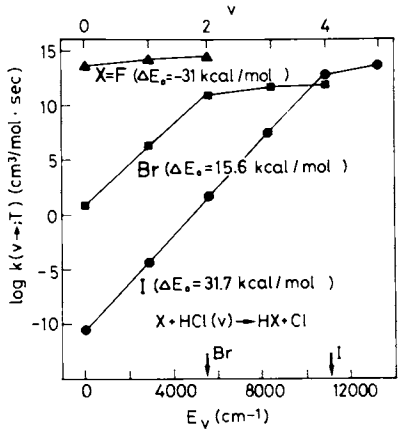

Figure 1. Experimental measurements of the effect of HCl vibrational excitation on the rate of reaction with F, Br, and I atoms (3–6).

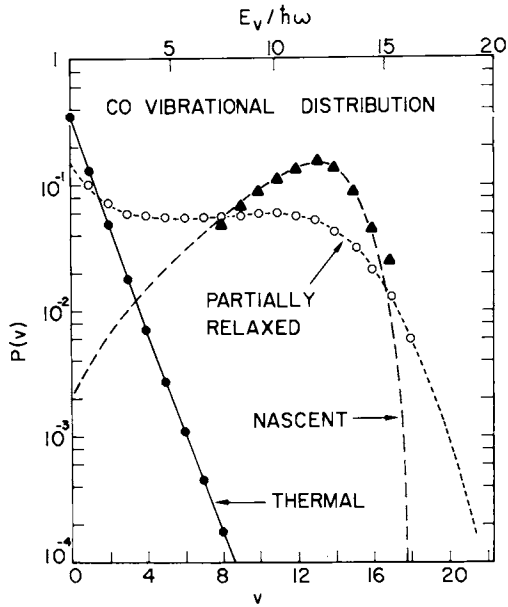

Figure 2. Vibrational state distributions for CO. Experimental results for the nascent state distribution (11): ▲; partially relaxed distribution (14): ○; and thermal distribution: ●. The dashed curves were obtained from Eq. (3).

$$O + CS \rightarrow CO(v) + S \qquad (1)$$

reaction, (see also (12, 13)). The second is a partially relaxed distribution measured (14) for the $CS_2/O_2/He$ system. The final one is the distribution at thermal equilibrium. One knows very well how to characterize the last distribution. The only property of the vibrational state that matters is its energy. Given the mean vibrational energy, the distribution is fully characterized. For an arbitrary distribution P(n), over some index n, one can show that the corresponding property is I(n),

$$I(n) = -\ell n[P(n)/P^o(n)], \qquad (2)$$

where $P^o(n)$ is a fixed reference or 'prior' distribution. It is convenient to refer to I(n) as the 'surprisal'. It is evident that the surprisal is sufficient to describe the distribution P(n). All that is required is to solve (2) for P(n),

$$P(n) = P^o(n)\exp[-I(n)]. \qquad (3)$$

If we know the n-dependence of the surprisal we clearly know P(n). The dashed lines in figure 2 were indeed obtained in this fashion (10).

It is less obvious that the surprisal is not only sufficient but is also necessary to characterize the distribution. It provides everything we have to know about the distribution P(n) in order that it be fully specified. It does not however provide more than we need to know.

The early (first generation) applications were all essentially surprisal analysis, as shown for example in figure 3, (adapted from (10)). The surprisal I(v) of the nascent vibrational state distribution of different highly exoergic chemical reactions is shown vs. f_v,

$$f_v = E_v/E, \qquad (4)$$

the fraction of the available energy in the product vibration. The solid lines are fits to the functional form

$$I(f_v) = \lambda_0 + \lambda_v f_v. \qquad (5)$$

Here λ_0 is not an independent parameter but is determined by the condition that $\Sigma P(v) = 1$ and the magnitude of λ_v, $\lambda_0 \equiv \lambda_0(\lambda_v)$. The advantage of using the reduced variable f_v (15) is evident from the plot. Similar reactions have the same surprisal (and hence the same raw, $P(f_v)$, distribution) when expressed in terms of this variable.

The Cl + HI/DI experimental results (16) were used to draw the first surprisal plot (17). The F + H_2/D_2/HD results (18) provided the first independent verification of the (near) isotopic invariance. These reactions were since studied (19) at several temperatures of the reagents (over the 280 - 1300 K range) and the surprisal analysis (adapted from (20)) is shown in figure 4.

In State-to-State Chemistry; Brooks, P., et al.;
ACS Symposium Series; American Chemical Society: Washington, DC, 1977.

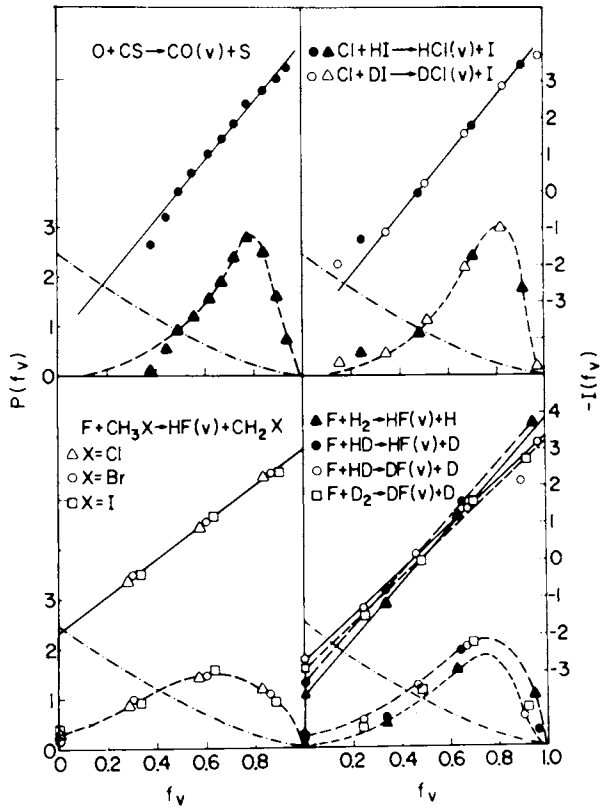

Figure 3. Vibrational surprisal plot (right axis) and probability distribution (left axis) vs. fraction of available energy in product vibration. All points correspond to experimental data. The dashed curves were obtained from Eq. (3). The solid curves for the surprisal were obtained from Eq. (5). The dash-dotted line gives the prior distribution.

Finally, figure 3 shows an analysis (21) for a series of abstraction reactions.

In all these plots the prior distribution ($P^o(v)$, dash-dotted line in figure 3) is computed on the basis of the assumption that all final product (quantum) states are equally probable (17). This is the least informative (or most democratic) distribution. The prior distribution is not meant to agree with experiment but only to serve as a reference for comparison with the experimental (or computational) distribution.

In State-to-State Chemistry; Brooks, P., et al.;
ACS Symposium Series; American Chemical Society: Washington, DC, 1977.

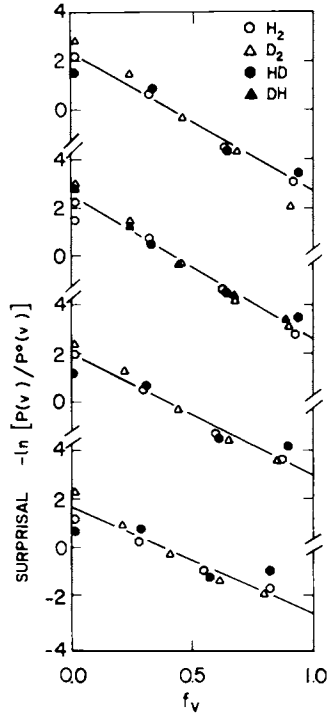

Figure 4. The surprisal of the products vibrational state distribution vs. the fraction of available energy for the $F + H_2$ reaction and its isotopic variants (○: $F + H_2$, △: $F + D_2$, ●: $F + HD$, ▲: $F + DH$). Each plot corresponds to a different set of initial rotational (T_R) and translational (T_T) temperatures. There are slight differences in the temperatures within each set. From top to bottom, and in the order: $F + H_2 \rightarrow FH + H$; $F + D_2 \rightarrow FD + D$; $F + HD \rightarrow FH + D$; and $F + DH \rightarrow FD + H$, the initial experimental temperatures (listed as (T_R, T_T) in K) are: Set I: (279, 281), (279, 283), (279, 282). Set II: all temperatures (including $F + DH$) at 300 K. Set III: (718, 678), (718, 645), (718, 661). Set IV: (1315, 1219), (1315, 1130), (1315, 1187).

Detailed balance implies (8) that the surprisal is the same for the forward and reversed reactions. Thus, if for exoergic reactions the products vibrational energy disposal has a 'linear' surprisal (equation 5) the same is true for vibrational energy consumption in the reversed endothermic reaction. Explicit examples are indeed available (7). What happens however for a reaction that can be either endothermic or exothermic, depending on the reagents or products? As an example consider the

$$Cl + HCl(v) \rightarrow H + Cl_2(v') \qquad (6)$$

reaction which is endoergic (ground state reagents to ground state products). As we change the vibrational energy of HCl, the process will change from endothermic (i.e. one that requires energy from the translation (or rotation)) to exothermic. The point of change (indicated by an arrow in figure 5) does depend on v'. Figure 5 (adapted from (9)) is an explicit illustration of the opposite trends in the surprisal for exothermic and endothermic processes. Extensive documentation of this behaviour is available for energy transfer collisions (22-25). Figure 6 (adapted from (25)) shows such 'exponential gap' behaviour for low energy rotational energy transfer

$$H + CO(J) \rightarrow H + CO(J') \qquad (7)$$

In State-to-State Chemistry; Brooks, P., et al.;
ACS Symposium Series; American Chemical Society: Washington, DC, 1977.

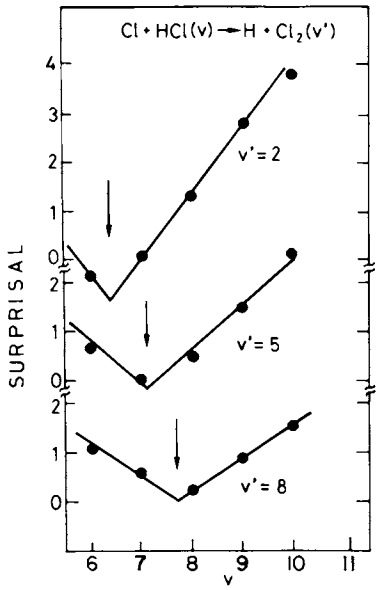

Figure 5. Effect of variation of the endoergicity ($\Delta E_0 + E_{v'}$) of the reaction on the surprisal plot. Shown is (the surprisal) $-ln\ k(v \rightarrow v';T)/k(v \rightarrow v';T)$ vs. v for $v' = 2$, 5, and 8 at $T = 850$ K. The arrows mark the boundary between the endothermic and exothermic behavior.

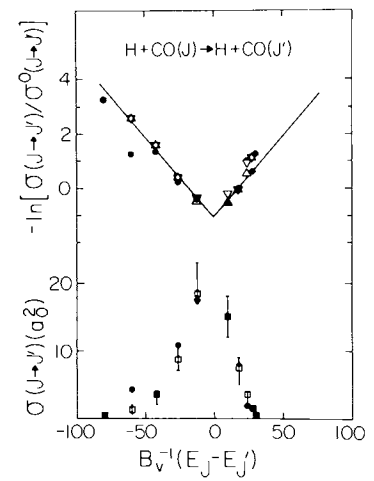

Figure 6. Surprisal synthesis, using a sum rule (25), of both the classical and the quantal state-to-state cross sections for $H + CO(j)$. $E = 0.05$ eV, $j = 5$. Top panel: the synthetic surprisal (line) and the surprisal obtained from quantal (points (26)), classical (triangles (27)), and classical "method I" (wedges (27)) cross sections. The classical method I was carried out on a potential energy surface modified so as to simulate CO as a homonuclear diatomic molecule. Bottom panel: synthetic state-to-state cross sections (squares) vs. quantal (dots (26)) and classical trajectory results (bars, spanning stated (27)) uncertainty limits of the classical computation).

In State-to-State Chemistry; Brooks, P., et al.;
ACS Symposium Series; American Chemical Society: Washington, DC, 1977.

computed by quantum mechanical (26) and classical (27) methods.

Applications of surprisal analysis to processes involving changes in electronic states have also been reported (10,28-31).

Since its very inception the procedure of surprisal analysis has been extensively reviewed (2,10,15,32-35). A discussion of state-to-state processes will be found in (2,10,35). (33) is a general account of the first generation work with (34) providing all the necessary working equations. (35) and, in particular, (10) forge the link to thermodynamics.

Surprisal Synthesis

The second major aim of the information theoretic approach is predictive. The practical argument is obvious. The surprisal, even when non-linear (e.g. (36-38)) is found to have a simple behaviour and to depend on just a few parameters (one, for a linear surprisal). Would it not be simpler to compute directly the parameters of the surprisal. During the second generation of developments there were two types of attempts in this direction. In the first, the functional form of the surprisal was derived from approximate dynamical considerations (see, e.g. (39-43)). In this way the surprisal parameters could be related to features of the potential energy surface (e.g. (40-44)). Alternatively one could compute the surprisal parameters via an exact classical trajectory method and equate these to the corresponding quantal parameters. In this way one obtains a 'quantal' surprisal and hence a discrete probability distribution. Several encouraging results were reported (25,45-47), even for 3-D collisions (25,46). The convergence of the method has been demonstrated (47).

The second methodology relied more heavily on physical intuition and hence is more empirical in nature. The advantage is that it does lead to practical results. Indeed it has been extensively employed to generate a variety of state-to-state rate constants. The worry is that the method has no built-in check of its validity (except of course by comparison with exact computation or with experiment). Figure 6 demonstrates the utility of the procedure. The surprisal line is not a fit but an independent direct computation of the surprisal (25). Once the surprisal is known, the distribution is also available (cf. (3)) and the squares at the bottom of figure 6 were obtained in this fashion.

The essence of the surprisal synthesis is as follows. One expands the surprisal in a set of (linearly independent) properties of the different states

$$I(n) = \lambda_0 + \lambda_1 A_1(n) + \lambda_2 A_2(n) + \ldots \qquad (8)$$

One now requests that the distribution P(n) defined by (3) and (8),

$$P(n) = \exp[-\lambda_0 - \sum_{r=1} \lambda_r A_r(n)], \qquad (9)$$

reproduce the correct expectation values of the A_r's. Explicitly

$$\sum_n Q(n) A_r(n) = \sum_n P(n) A_r(n) = \langle A_r \rangle \qquad (10)$$

In State-to-State Chemistry; Brooks, P., et al.;
ACS Symposium Series; American Chemical Society: Washington, DC, 1977.

where Q(n) is the, thus far unknown, experimental (or computational) distribution. This then serves to fix the magnitude of the λ_r's (and, since $A_0(n)=1$, λ_0 insures that P(n) is normalized). The operators are the 'constraints' and convergence is obtained when enough terms have been included in (8) so that Q(n) = P(n) for all n. (The convergence is monotonic (47,48)). The problem is that one neither knows which constraints are required nor the magnitude of their expectation values. For later reference it is important to note that there are really two 'needs to know'. The first is that we need to know which constraints. If we do, we have an alternative route to surprisal analysis. Rather than determine the constraints by fitting (8) to the data (i.e. to Q(n)) we determine the constraints by obtaining (8) from some theory. The second need only arise if we need to numerically determine the distribution Q(n). Then we need the magnitude of the λ_r's or, equivalently, of the $\langle A_r \rangle$'s.

Surprisal synthesis on the empirical level seeks to identify the constraints on physical grounds and then proceeds to use any available experimental input as a guide (or, better still, an actual determination) for the magnitude of the constraints. Alternatively, one can use models to directly determine the magnitude of the constraints. Applications to vibrational (22,49-51), rotational (25,37,38,52,53) and translational (54-56) state-to-state rate constants have been reported and the details will be found in the original papers.

The Road Ahead

Future work is likely to be very much influenced by the forging of the link between the information theoretic approach and the dynamical point of view. Given an initial state and the Hamiltonian (i.e. the potential energy surface(s)), the equations of motion are sufficient to characterize the final state distribution. Yet, the surprisal was introduced as being necessary and sufficient to characterize the final state distribution. The inevitable conclusion is that it must be possible to derive equation (8) as an exact dynamical result. This has now been done (57), leading to a formalism consisting of two parts. The first is purely algebraic and provides a specification of all the constraints (i.e. all the operators that appear in (8)). The algebraic procedure enables one to easily draw general conclusions (e.g. similar reactions have a common set of dynamic constraints). The second part of the formalism provides explicit (coupled) differential equations for the Lagrange parameters (the λ_r's) or for the mean value of the constraints (the $\langle A_r \rangle$'s, cf. (10)). The number of coupled equations equals the number of dynamic constraints. Under certain (not uncommon) circumstances, these differential equations can be solved analytically. Applications to several (simple) examples have been worked out (57).

In State-to-State Chemistry; Brooks, P., et al.;
ACS Symposium Series; American Chemical Society: Washington, DC, 1977.

In the future it should become possible to perform exact dynamical computations directly for the surprisal. In this way, the equations of motion are employed to generate only necessary information. Converseley, the results of surprisal analysis of experimental data can be used to learn all that there is to learn about the potential.

Literature Cited

1. Levine, R.D. and Bernstein, R.B., "Molecular Reaction Dynamics", Clarendon Press, Oxford, 1974.
2. Levine, R.D. (eds. B. Pullman and R. Parr), "The New Worlds of Quantum Chemistry", p. 103-129, Reidel, Holland, 1976.
3. Kompa, K.L. and Wanner, J., Chem. Phys. Lett., (1972), 17, 560.
4. Kirsch, L.J. and Polanyi, J.C., J. Chem. Phys., (1972), 57, 4498.
5. Bergmann, K. and Moore, C.B., J. Chem. Phys., (1975), 63, 643.
6. Douglas, D.J., Polanyi, J.C. and Sloan, J.J., Chem. Phys., (1976), 13, 15.
7. Levine, R.D. and Manz, J., J. Chem. Phys., (1975), 63, 4280.
8. Kaplan, H., Levine, R.D. and Manz, J., Chem. Phys., (1976), 12, 447.
9. Pollak, E. and Levine, R.D., Chem. Phys. Lett., (1976) 39,199.
10. Levine, R.D. and Ben-Shaul, A. (ed.: C.B. Moore) "Chemical and Biochemical Applications of Lasers" Vol. III, p. 145-197, Academic Press, New York, 1977.
11. Hancock, G., Morley, C. and Smith, I.W.M., Chem. Phys. Lett., (1971), 12, 193.
12. Ben-Shaul, A., Chem. Phys., (1973), 1, 244.
13. Kelley, J.D., Chem. Phys. Lett., (1976), 41, 7.
14. Tsuchiya, S., Nielsen, N. and Bauer, S.H., J. Phys. Chem., (1973), 77, 2455.
15. Levine, R.D. (eds.: E.D. Bergmann and B. Pullman) "Chemical and Biochemical Reactivity", p. 35-50, Reidel, Boston, 1974.
16. Mavlotte, D.H., Polanyi, J.C. and Woodall, K.B., J. Chem. Phys., (1972), 57, 1547.
17. Ben-Shaul, A., Levine, R.D. and Bernstein, R.B., J. Chem. Phys., (1972), 57, 5427.
18. Berry, M.J., J. Chem. Phys., (1973), 59, 6229.
19. Perry, D.S. and Polanyi, J.C., Chem. Phys., (1976), 12, 419.
20. Wassam, W.A. Jr. and Levine, R.D., Mol. Phys., (1977) 33, 689.
21. Bogan, D.J. and Setser, D.W., J. Chem. Phys., (1976), 64, 586.
22. Procaccia, I. and Levine, R.D., J. Chem. Phys.,(1975) 63 4261.
23. Kafri, A. and Levine, R.D., J. Chem. Phys., (1976), 64, 5320.
24. Levine, R.D., Bernstein, R.B., Kahana, P., Procaccia, I., and Upchurch, E.T., J. Chem. Phys., (1976), 64, 796.
25. Procaccia, I. and Levine, R.D., J. Chem. Phys.,(1976) 64, 808.
26. Chu, S.I. and Dalgarno, A., Proc. Roy. Soc. A,(1975) 342, 191.
27. Brumer, P., Chem. Phys. Lett., (1974), 28, 345.

In State-to-State Chemistry; Brooks, P., et al.;
ACS Symposium Series; American Chemical Society: Washington, DC, 1977.

28. Manos, D.M. and Parson, J.M., J. Chem. Phys.,(1975) 63, 3575.
29. Liu, K. and Parson, J.M., J. Chem. Phys.,(1976), 65, 815.
30. Chalek, C.L. and Gole, J.L., Chem. Phys., (1977), 19, 59.
31. Faist, M.B. and Levine, R.D., Chem. Phys. Lett. (1977), 47, 5.
32. Levine, R.D., in "The Physics of Electronic and Atomic Collisions" (eds.: B.C. Lobic and M.V. Kurepa), Institute of Physics, Beograd, 1973.
33. Levine, R.D. and Bernstein, R.B., Accts. Chem. Res., (1974), 7, 393.
34. Bernstein, R.B. and Levine, R.D., Adv. Atom. Mol. Phys., (1975), 11, 215.
35. Levine, R.D. and Bernstein, R.B. (ed.: W.H. Miller) "Dynamics of Molecular Collisions", Vol. B p. 323-364, Plenum, New York, 1976.
36. Kafri, A., Pollak, E., Kosloff, R. and Levine, R.D., Chem. Phys. Lett., (1975), 33, 201.
37. Pattengill, M.D. and Bernstein, R.B., J. Chem. Phys., (1976), 65, 4007.
38. Kosloff, R., Kafri, A. and Levine, R.D., Astrophysical J., (1977), July 15.
39. Hofacker, G.L. and Levine, R.D., Chem. Phys. Lett., (1971), 9, 617.
40. Hofacker, G.L. and Rösch, N., Ber. Bunsenges. physik. Chem., (1973), 77, 661.
41. Berry, M.J., Chem. Phys. Lett., (1974), 27, 73
42. Schatz, G.C. and Ross, J., J. Chem. Phys., (1977), 66, 2943.
43. Heller, D.H., Chem. Phys. Lett., (1977), 45, 64.
44. Goldflam, R. and Kouri, D.J., J. Chem. Phys., (1976), 65, 4218.
45. Truhlar, D.J. and Duff, J.W., Chem. Phys. Lett.,(1975) 36, 551.
46. Gordon, R.J., J. Chem. Phys., (1976), 65, 4945.
47. Halavee, U. and Levine, R.D., Chem. Phys. Lett., (1977) 46, 35.
48. Procaccia, I., Shimoni, Y. and Levine, R.D., J. Chem. Phys., (1976), 65, 3284.
49. Clendening, C., Steinfeld, J.I. and Wilson, L.E., Report AFWL TR-76-144.
50. Nanbu, K., J. Chem. Phys., (1977), 66, 136.
51. Kaplan, H., Levine, R.D. and Manz, J., Mol. Phys., (1976), 31, 1765.
52. Procaccia, I. and Levine, R.D., Phys. Rev., (1976), A14, 1569.
53. Kaplan, H. and Levine, R.D., Chem. Phys., (1976), 13, 161.
54. Kaplan, H. and Levine, R.D., J. Chem. Phys., (1975), 63, 5064.
55. Kaplan, H. and Levine, R.D., Chem. Phys., (1976), 18, 103.
56. Tamir, M. and Levine, R.D., Chem. Phys., (1976), 18, 125.
57. Alhassid, Y. and Levine, R.D., to be published.

In State-to-State Chemistry; Brooks, P., et al.;
ACS Symposium Series; American Chemical Society: Washington, DC, 1977.

27

State-to-State Considerations in Reactions in Interstellar Clouds

R. N. PORTER

Department of Chemistry, State University of New York, Stony Brook, NY 11794

In a symposium on "State-to-State Chemistry" in the late 1970's, it seems appropriate to call attention to a class of reactions for which such detailed knowledge is essential. These are the ion-molecule reactions that are presumed to occur at the extremely low temperatures and pressures of the interstellar clouds. Detailed analyses of interstellar chemistry have been given by Herbst and Klemperer (1,2) and by Watson (3). Since the temperatures range between ~10-50 K, only exothermic and thermoneutral reactions without activation energy can occur; and since molecular densities are of the order of 10^4 cm^{-3}, molecules coupled to the radiation field will have vibration-rotation temperatures close to the 2.7 K blackbody temperature. Since hydrogen is by far the most numerous species, the states of the molecules are generally widely spaced and many of the molecules have ortho-para species that do not interconvert radiatively. Under these conditions one expects classical dynamics to give an inadequate picture. Furthermore, averages and sums over states of molecules with ortho-para modifications must treat nuclear spin statistics properly. A central question is how to extrapolate thermal rates of the reactions, usually measured near room temperature, down to interstellar temperatures.

An important exothermic reaction is

$$H_2 + H_2^+ \rightarrow H_3^+ + H, \qquad (R1)$$

the 40 kcal/mole being released into vibration and rotation of H_3^+ as well as relative translation (4,5). The observation of the radiospectrum of HCO^+ in several clouds (6) suggests that it may be formed by (1,2)

$$H_3^+ + CO \rightarrow HCO^+ + H_2 \ . \qquad (R2)$$

The observation of DCO^+ in concentrations nearly as great as that of HCO^+ (7) when the D/H atomic ratio is on the order of 10^{-5} (8) indicates isotope fractionation by (3,9)

In State-to-State Chemistry; Brooks, P., et al.;
ACS Symposium Series; American Chemical Society: Washington, DC, 1977.

$$H_3^+HD \rightarrow H_2D^+ + H_2 \ . \qquad (R3)$$

The measured forward rate of this reaction is 3×10^{10} cm^3 sec^{-1} (10), a factor of about 6 less than the Langevin rate. This reaction is of particular interest, not only because of its possibly key role in concentrating deuterium in interstellar molecules, but because the structure and spectra of the triatomic species are at this point known exclusively from *ab initio* calculations (3,11-15).

To use Eq. (R3) in a satisfactory model of interstellar chemistry, we need (a) its equilibrium constant K_p, from which we can calculate its backward rate, and (b) the value of its forward rate extrapolated to interstellar temperatures.

We have obtained (a) from sums over the rotation states of the reactant and product molecules, taking due account of ortho-para modifications. The reaction has a $\Delta E_0^o/R \sim 134$ K as measured from the ground vibration states (12, 14), but this result is misleading since H_3^+ has a zero-point *rotational* energy of 91.7 K (13) and a combined nuclear spin-rotational degeneracy of 6 in the ground state. The extent to which the resulting entropy offsets the rotational energy is highly temperature-dependent, of course. The results for K_p of (R3) range from $\sim 10^9$ at 10 K to ~ 10 at 50 K and depend upon assumptions about ortho/para ratios. With H_2D^+ highly favored at low temperature, the observed intensities of DCO^+ formed by the deuterium analogue of (R2) are quite reasonable (9).

Obtaining (b) may be a more formidable task, since the collision complex is the stable ion H_5^+, one might expect the activation energy to be negligible. Then why is the rate only 1/6 the Langevin rate? The critical rotational barriers are at $11a_0$ and $7.4a_0$ in the reactant and product channels, respectively, so large as to indicate applicability of Light's statistical theory (17,18). One must of course use the quantum-mechanical form, as in the calculation of K_p. The hope then is that the factor 1/6 might find its explanation in the detailed statistics of the Pauli-principle dominated rotation states of these molecules (14,15). Since the number of accessible states is manageable, the calculation is easily done, giving the results 502Å^2, 286Å^2, and 234Å^2 for the reaction cross sections at ε/k = 10 K, 30K, and 50 K, respectively. The percent o-H_2 in the product predicted by the theory is 18, 37, and 57 at the three respective energies, and the percent o-H_2D^+ is predicted to be 64, 50, and 68, respectively. The rotational temperatures of nascent H_2D^+ as determined by the relative populations of the two lowest-lying para states (ν = 1361 GHz) are predicted to be 29 K, 173 K, and 571 K at the three energies. These temperatures are expected to relax radiatively to about 2.7 K before a collision occurs. Unfortunately, the total reaction cross sections are within a few percent of the Langevin values. Simple reasoning about

In State-to-State Chemistry; Brooks, P., et al.;
ACS Symposium Series; American Chemical Society: Washington, DC, 1977.

tunneling through rotational barriers does not appear to provide the factor 1/6, although steric arguments help elucidate distinctions between "reactive" and "nonreactive" rotation states. At present it appears that beam-spectroscopy measurements, coupled with a full quantum-dynamical analysis, may be required for a satisfactory solution to problem (b) for use in models of interstellar chemistry -- a challenge the papers at this symposium indicate we may soon be able to accept!

Literature Cited

(1) Herbst, E. and Klemperer, W., Astrophys. J. (1973) 185, 505.
(2) Herbst, E. and Klemperer, W., Physics Today (1976) 29, 32.
(3) Watson, W. D., Rev. Mod. Phys. (1976) 48, 513.
(4) Carney, G. D. and Porter, R. N., J. Chem. Phys. (1974) 60, 4251.
(5) Stine, J. R. and Muckerman, J. T., J. Chem. Phys. (1976) 65, 3975 and private communications.
(6) Hollis, J. M., Snyder, L. E., Lovas, F. J. and Buhl, D., Astrophys. J. (1975) 200, 584.
(7) Hollis, J. M., Snyder, L. E., Lovas, F. J. and Buhl, D., Astrophys. J. (1976) 207, 663.
(8) McKellar, A. R. W., Goetz, W. and Ramsay, D. A., Astrophys. J. (1976) 207, 663.
(9) Solomon, P. M., Porter, R. N. and Jura, M., unpublished results.
(10) Huntress, W. T. and Anicich, V. G., Astrophys. J. (1976) 208, 237.
(11) Salmon, L. and Poshusta, R. D., J. Chem. Phys. (1973) 59, 3497.
(12) Carney, G. D. and Porter, R. N., J. Chem. Phys. (1976) 65, 3547.
(13) Carney, G. D. and Porter, R. N., J. Chem. Phys. (1977) 66, 2756.
(14) Carney, G. D. and Porter, R. N., "Ab initio prediction of the vibration spectra of the deuterated species of H_3^+," Chem. Phys. Lett. (in press).
(15) Carney, G. D. and Porter, R. N., "Rotation states of H_3^+ and its isotopes," unpublished.
(16) Porter, R. N., details to be published elsewhere.
(17) Pechukas, P. and Light, J. C., J. Chem. Phys. (1965) 42, 3281.
(18) Pechukas, P., in "Dynamics of Molecular Collisions, Part B," Ed. by Miller, W. H., Ch. 6, p269, (Plenum, N. Y., 1976).

In State-to-State Chemistry; Brooks, P., et al.;
ACS Symposium Series; American Chemical Society: Washington, DC, 1977.

A New Helicity Representation for Reactive Atom-Diatom Collisions

C. W. McCURDY and W. H. MILLER

Department of Chemistry, University of California, Berkeley, CA 94720

There have recently been several accurate quantum mechanical scattering calculations for the H + H_2 reaction in three dimensions, (1,2) and this provides interesting data to test approximate theoretical models. In particular, we would like to see the extent to which "classical S-matrix" theory (3) provides a good description of the threshold region of this reaction; earlier calculations (4) for the collinear version of the reaction showed the semiclassical model to be quite accurate. Preliminary semiclassical calculations for the three dimensional H + H_2 reaction have been reported, (5) but these were not extensive enough and of too preliminary a nature to allow a very useful comparison with the latest quantum mechanical reactive scattering calculations.

To keep the semiclassical calculation as manageable as possible, we would like to take advantage of the helicity, or "j_z-conserving" approximation (6,7) that has been seen to work well quantum mechanically (8,9). This effectively eliminates one degree of freedom from the problem, and semiclassically this means that the quantizing boundary conditions that must be applied to the classical trajectories require only a two dimensional root search rather than a three dimensional one (5).

The usual j_z-conserving approximation is specifically designed for inelastic collision processes, however, and it is not immediately obvious how such an approximation should be applied to reactive collisions. Thus, if the helicity K, the projection of the total angular momentum $\vec{J}$ along the initial relative translational coordinate $\vec{R}$, $K = \vec{J}\cdot\hat{R}$, is assumed to be conserved along the incoming part of the trajectory, and if the projection K' of J along the translational coordinate $\vec{R}'$ of the final arrangement is assumed to be conserved for the outward part of the trajectory, then at some point during the trajectory one must stop conserving K and start conserving K', since the two are not the same. The particular point at which one switches from conserving the helicity in one arrangement to conserving it in the other, however, is somewhat arbitrary.

In State-to-State Chemistry; Brooks, P., et al.;
ACS Symposium Series; American Chemical Society: Washington, DC, 1977.

To avoid this ill-defined situation, we have considered a new helicity representation: the body-fixed quantization axis we choose is neither $\vec{R}$ nor $\vec{R}'$, but rather the principal axis of the ABC triangle of atoms which corresponds to the smallest principal moment of inertia. This quantization axis becomes the translational coordinate $\vec{R}$ asymptotically when the initial atom A is far from the diatom BC, it becomes the final translational coordinate $\vec{R}'$ when the final atom C is far from AB, and it varies smoothly between them in the intermediate region. If the atoms are collinear, the axis is the collinear axis.

The projection of $\vec{J}$ onto the body-fixed axis of the smallest principal moment of inertia thus becomes the ordinary helicity in the initial and final asymptotic regions, and it varies smoothly between the two during the collision. In this regard the new helicity is somewhat like a "natural collision coordinate" (10) for this variable. By analogy with the well known behavior of rigid asymmetric rotors (11), it is also clear that the projection of $\vec{J}$ onto the axis of the smallest principal moment of inertia is the body-fixed projection that should be most nearly conserved.

The classical Hamiltonian can be written in this new representation by taking the classical limit of the quantum mechanical Hamiltonian worked out by Diehl et al. (12); unlike the usual definition (13), the three Euler angles in this case orient the principal axes of the triangle of atoms with respect to a space-fixed axis. The classical Hamiltonian so obtained can be written as

$$H(\underset{\sim}{p},\underset{\sim}{q}) = \frac{1}{2\mu}(p_R-\Delta p_R)^2 + \frac{1}{2m}(p_r-\Delta p_r)^2 + \left(\frac{1}{2mr^2} + \frac{1}{2\mu R^2}\right)(p_\gamma-\Delta p_\gamma)^2$$

$$+ V(R,r,\gamma) + \frac{J_1^2}{2I_1} + \frac{J_2^2}{2I_2} + \frac{J_3^2}{2I_3} \quad , \tag{1}$$

where the canonical variables are $q = (R,r,\gamma,q_K)$, and $p = p_R,p_r,p_\gamma,K)$; R, r, and γ are the usual translational coordinate, vibrational coordinate, and relative angle ($\cos\gamma \equiv \hat{r}\cdot\hat{R}$), respectively. J_1, J_2, J_3 are the components of total angular momentum along the principal axes of rotation of the triangle of particles, and $\{I_i\}$, i = 1,2,3 are the principal moments of inertia ordered so that $I_1 < I_2 < I_3 \equiv I_1 + I_2$; specifically

$$I_2 - I_1 = [(\mu R^2)^2 + (mr^2)^2 + 2\mu R^2 mr^2 \cos 2\gamma]^{\frac{1}{2}} \tag{2a}$$

$$I_2 + I_1 = \mu R^2 + mr^2 \quad . \tag{2b}$$

The terms Δp_R, Δp_r, and Δp_γ are

In State-to-State Chemistry; Brooks, P., et al.;
ACS Symposium Series; American Chemical Society: Washington, DC, 1977.

$$\Delta p_R = - J_3 \frac{2 \sin\gamma\ \mu R^2 m r^2}{(I_2 - I_1)^2} \frac{\cos\gamma}{R} \tag{3a}$$

$$\Delta p_r = J_3 \frac{2 \sin\gamma\ \mu R^2 m r^2}{(I_2 - I_1)^2} \frac{\cos\gamma}{r} \tag{3b}$$

$$\Delta p_\gamma = - J_3 \frac{2 \sin\gamma\ \mu R^2 m r^2}{(I_2 - I_1)^2} \sin\gamma \frac{\mu R^2 - m r^2}{\mu R^2 + m r^2} \tag{3c}$$

Choosing the quantization axis as we do, i.e., along principal axis 1, the angular momentum projections $\{J_i\}$ are given in terms of the canonical variables by

$$J_1 = K \tag{4a}$$

$$J_2 = \sqrt{J^2 - K^2} \cos q_K \tag{4b}$$

$$J_3 = \sqrt{J^2 - K^2} \sin q_K \quad ,$$

where J is the (fixed) value of the total angular momentum.

A helicity conserving approximation can now be obtained by approximating the Hamiltonian of Eq. (1) to eliminate the dependence on q_K, thus making K a conserved quantity. One way of doing this is to drop the "rotation-vibration" coupling terms Δp_R, Δp_r, and Δp_γ, and to average over q_K, so that

$$J_2^2 = \sqrt{J^2 - K^2} \cos^2 q_K \rightarrow \frac{1}{2} (J^2 - K^2) \tag{5a}$$

$$J_3^2 = \sqrt{J^2 - K^2} \sin^2 q_K \rightarrow \frac{1}{2} (J^2 - K^2) \ . \tag{5b}$$

The resulting approximate, helicity-conserving Hamiltonian is

$$H_{J,K}(p_R, p_r, p_\gamma, R, r, \gamma) = \frac{p_R^2}{2\mu} + \frac{p_r^2}{2m} + \left(\frac{1}{2\mu R^2} + \frac{1}{2m r^2}\right) p_\gamma^2 + V(R, r, \gamma)$$

$$+ \frac{K^2}{2I_1} + (J^2 - K^2) \frac{1}{2}\left(\frac{1}{2I_2} + \frac{1}{2I_3}\right) \ . \tag{6}$$

Preliminary tests of some of these ideas have been carried out. Reactive classical trajectories for the three dimensional $H + H_2$ reaction have been examined, for example, and we see that the "new" helicity, J_1, and the "old" helicity, $\vec{J} \cdot \hat{R}$, are about

In State-to-State Chemistry; Brooks, P., et al.;
ACS Symposium Series; American Chemical Society: Washington, DC, 1977.

equally well conserved for the incoming part of the trajectory. The classical reactive cross section computed (via a trajectory calculation) from the Hamiltonian of Eq. (6), however, is not in as good agreement with the exact classical result as is that obtained from the "old" helicity-conserving Hamiltonian. This seems to be due to the fact that the effective centrifugal potential in Eq. (6) is too small for large R, allowing too much reaction for large J. For small and intermediate values of J the reaction probability given by Eq. (6) is in reasonably good agreement with the exact classical results. Other approximations to the classical Hamiltonian of Eq. (1) are being explored to try to correct this deficiency of Eq. (6).

Literature Cited

1. Elkowitz, A. B., and Wyatt, R. F., J. Chem. Phys. (1975) 62, 2504.
2. Schatz, G. C., and Kuppermann, A., J. Chem. Phys. (1976) 65, 4642, 4668.
3. For reviews, see Miller, W. H., Adv. Chem. Phys. (1974) 25, 69; (1975) 30, 77.
4. George, T. F., and Miller, W. H., J. Chem. Phys. (1972) 56, 5722; (1972) 57, 2458.
5. Doll, J. D., George, T. F., and Miller, W. H., J. Chem. Phys. (1973) 58, 1343.
6. McGuire, P., and Kouri, D. J., J. Chem. Phys. (1974) 60, 2488.
7. Pack, R. T., J. Chem. Phys. (1974) 60, 633.
8. Kuppermann, A., Schatz, G. C., and Dwyer, J. P., Chem. Phys. Lett. (1977) 45, 71.
9. Wyatt, R. E., private communication
10. Marcus, R. A., J. Chem. Phys. (1966) 45, 4493, 4500; (1968) 49, 2610.
11. Townes, C. H., and Schawlow, A. L., Microwave Spectroscopy, McGraw-Hill, New York, 1955, pp. 83-109.
12. Diehl, H., Flugge, S., Schroder, U., Volkel, A., and Weigury, A., Z. Physik. (1961), 162, 1.
13. Miller, W. H., J. Chem. Phys. (1969) 50, 407.

Supported in part by the National Science Foundation under grant GP-41509X.

Monte Carlo Trajectory Study of Ar + H_2 Collisions

Translation to Vibration Energy Transfer from Different Initial States

NORMAND C. BLAIS
University of California, Los Alamos Scientific Laboratory, Los Alamos, NM 87545

DONALD G. TRUHLAR
Chemical Dynamics Laboratory, Department of Chemistry,
University of Minnesota, Minneapolis, MN 55455

We present here rate constants for vibrational state changes induced by collisions of Ar atoms with H_2 molecules with initial vibrational quantum numbers v = 0, 4, 6, 10, and 13. All of the other initial collision conditions were selected from equilibrium distributions at 4500°K. The rates were calculated using quasiclassical trajectory methods and the final vibrational quantum number v' was obtained by the histogram method for $|\Delta v| = 1$ and smooth sampling for $|\Delta v| > 1$ (1). The potential energy surface on which the trajectories were calculated is the full potential as reported elsewhere (1). The rate constants we report here are the most accurate and complete set obtainable from a study of this kind. They were obtained from a total of 2663, 4594, 3351, 2650, and 1976 trajectories for v = 0, 4, 6, 10, and 13 respectively.

The cross sections $\sigma_{b\to n}(v,T\to v')$ presented here are computed by averaging over both the initial relative velocity V_R and the initial bound (b) rotational states and by summing over all nondissociative (n: bound and quasibound) final rotational states. The rate constants are $k_{b\to n}(v,T\to v') = \langle V_R\rangle \sigma_{b\to n}(v,T\to v')$ where $\langle V_R\rangle = (8kT/\pi\mu)^{\frac{1}{2}}$.

Figure 1 shows the cross sections. Statistical errors (associated with Monte Carlo averaging) are smallest (7-10%) for $\Delta v = -1$, but increase for large $|\Delta v|$ to about 100% at the end points where only one trajectory may be contributing to the cross section. The cross sections are 1-5 Å^2 for $\Delta v = \pm 1$ for all $v \geq 4$. Larger Δv occur with smaller cross sections, but the smallest for which we can give a value is only 10^{-4} times that for $\Delta v = \pm 1$. By plotting the same data so as to display the negative of the surprisal (2,3), as we do in Figure 2, better symmetry about $\Delta v = 0$ appears. The disparity between positive and negative Δv insofar as the range over which the cross section varies is reduced, and on either side of $\Delta v = 0$ the size of the average slope is nearly the same, in contrast to Figure 1. There is also a definite trend toward monotonicity (less crossing of lines connecting points of different initial states). However, curvature between line segments connecting individual points is not much improved from Fig. 1.

In State-to-State Chemistry; Brooks, P., et al.;
ACS Symposium Series; American Chemical Society: Washington, DC, 1977.

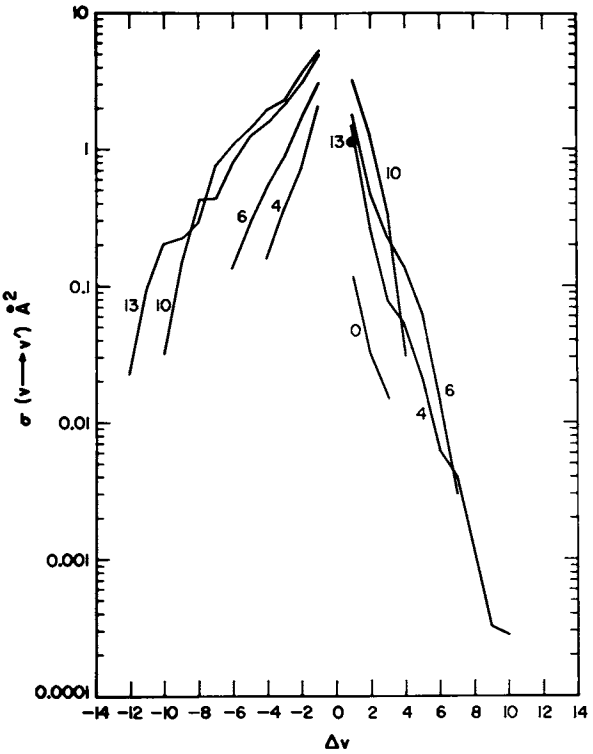

Figure 1. A plot showing how the cross section $\sigma_{v \to v'}(v,T \to v')$ depends on change of vibrational quantum number $\Delta v = v' - v$ for initial $v = 0, 4, 6, 10,$ and 13

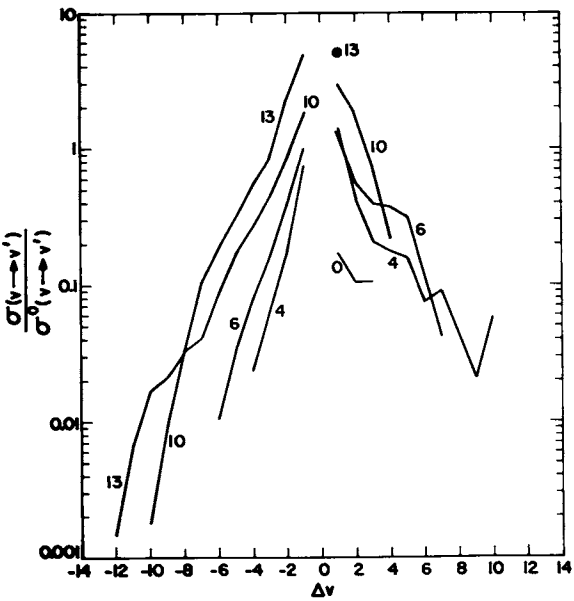

Figure 2. A surprisal plot for Ar + H_2 vibrational energy transfer collisions for the initial states $v = 0, 4, 6, 10,$ and 13 of H_2. The prior expectations $\sigma^0_{v \to v'}(v,T \to v')$ were calculated using the prescription suggested by Ben–Shaul et al. (2) and expressed analytically by Procaccia and Levine (3). The accurate energy states of H_2 were used in the calculations and all nondissociative (bound and quasibound) final states were included. As for the trajectory results, however, averaging over initial states included only bound states.

Table I compares ratios of $\Delta v = \pm 1$ transition rates from our trajectories with those from the Landau-Teller harmonic oscillator (LTHO) model: $k(v \to v+1) = (v+1)k(0 \to 1)$ and $k(v \to v-1) = vk(1 \to 0)$. The agreement is good for $v \to v-1$ but not so good for $v \to v+1$, in which case our rates increase with increasing v more rapidly than does LTHO. This trend changes at v=13 which can be explained by the ease of dissociation from v=13 and the small number of rotational states for v' = 14. We also compare our $\Delta v = \pm 1$ transitions with $k(4 \to 5)$ and $k(4 \to 3)$. This is because $k(0 \to 1)$ is the most uncertain of the rates reported here.

Table I. Comparison of $k_{b \to n}(v, T \to v+1)$ with LTHO model.

v	$k(v \to v+1)/k(0 \to 1)$		$k(v \to v-1)/k(1 \to 0)$	
	present	LTHO	present	LTHO
0	1.00	1.00	--	--
4	13.	5.00	4.9	4.00
6	15.	7.00	7.2	6.00
10	27.	11.00	12.	10.00
13	10.	14.00	13.	13.00

v	$k(v \to v+1)/k(4 \to 5)$		$k(v \to v-1)/k(4 \to 3)$	
	present	LTHO	present	LTHO
0	0.08	0.20	--	--
4	1.00	1.00	1.00	1.00
6	1.19	1.40	1.48	1.50
10	2.09	2.20	2.34	2.50
13	0.77	2.80	2.59	3.25

One of the most important aspects of our results is the ease with which multiquantum transitions occur. Collisions with v = 6 lead to almost all values of v' including dissociation. We present transition probabilities defined as $k_{b \to n}(v, T \to v')$ divided by the collision frequency $Z = \langle v_R \rangle \pi D^2$ where D is the zero-energy turning point of the spherically averaged interaction potential. Table II shows in tabular form what is also evident in Figure 1, that $\Delta v = 7$ is observed with a probability of 0.2% as large as $\Delta v = 1$. For comparison we give results calculated from equations used by McElwain and Pritchard and by Johnston and Birks. McElwain and Pritchard (4) obtained an analytic fit to transition probabilities calculated using the Jackson Mott distorted-wave treatment of collinear collisions. For the results in Table II we substituted accurate energy levels into their equation. Johnston and Birks (5) used an equation based on the vibrational matrix elements alone but renormalized to an experimental relaxation time (6) as extrapolated by the method of Landau and Teller. According to either of these models multiquantum transitions greater than $\Delta v = \pm 2$ would be less important than our trajectories indicate for $\Delta v = 7$. For $\Delta v = \pm 6$ our results differ from these models by 5-15 orders of magnitude. Previous models (4,5,7) of dissociation of H_2 in shock tubes assumed multiquantum transitions are unimpor-

In State-to-State Chemistry; Brooks, P., et al.;
ACS Symposium Series; American Chemical Society: Washington, DC, 1977.

tant. Our results indicate that they should be considered. McElwain and Pritchard and Johnston and Birks used special assumptions for the probability of dissociation. Our dissociation probabilities are smaller than those of Johnston and Birks but much larger than those of McElwain and Pritchard.

Table II. $k_{b\to n}(v = 6, T = 4500°K\to v')/Z$

v	present	McElwain-Pritchard	Johnston-Birks
0	4.29(-3)	5.92(-18)	2.13(-10)
1	9.02(-3)	8.67(-15)	1.07(-8)
2	1.65(-2)	2.45(-11)	2.90(-7)
3	2.67(-2)	1.12(-7)	5.99(-6)
4	5.08(-2)	7.03(-4)	1.17(-4)
5	9.43(-2)	2.71(-2)	3.27(-3)
6	--	--	--
7	5.56(-2)	1.44(-2)	1.57(-3)
8	1.52(-2)	4.68(-4)	3.99(-5)
9	6.89(-3)	1.80(-6)	2.20(-6)
10	4.16(-3)	6.23(-9)	1.86(-7)
11	1.93(-3)	6.03(-11)	2.16(-8)
12	4.28(-4)	1.60(-12)	3.29(-9)
13	9.51(-5)	1.19(-13)	6.45(-10)
14	0.	2.64(-14)	1.63(-10)
diss.	1.82(-3)	1.88(-14)	4.83(-3)

As a test for how well the trajectory results satisfy detailed balance, we examined the ratio of our calculated forward and reverse rates for the six cases for which we had data. We found agreement with the ratios predicted by the prior expectations to within the statistical errors.

Literature Cited

1. Blais, N.C. and Truhlar, D.G., J. Chem. Phys. (1976) 65, 5335.
2. Ben-Shaul, A., Levine, R.D. and Bernstein, R.B., J. Chem. Phys.(1972) 57, 5427.
3. Procaccia, I. and Levine, R.D., J. Chem. Phys. (1975) 63, 4261.
4. McElwain, D.L.S. and Pritchard, H.O., Thirteenth Symposium (Int.) on Combustion (Combustion Inst.,Pittsburgh, 1971) p. 37.
5. Johnston, H. and Birks, J., Accounts of Chem. Res. (1972) 5, 237.
6. Kiefer, J.H. and Lutz, R.W., J. Chem. Phys. (1966) 44, 668.
7. Dove, J.E. and Jones, D.G., J. Chem. Phys. (1971) 55, 1531.

* This work was performed under the auspices of the U.S. Energy Research and Development Agency and supported in part by the National Science Foundation under grant no. CHE75-06416.

Observations on State-Resolved Cross Sections for Long-Range Molecules

WILLIAM C. STWALLEY

Department of Chemistry, University of Iowa, Iowa City, IA 52242

I. Introduction.

Because of the long-range behavior (e.g., $-C_6R^{-6}$) of the interaction potential between two atoms, there are often a number of closely spaced vibrational-rotational levels near dissociation with large vibrational amplitudes and long classical vibrational periods (most of which are spent at large distance). Because properties of such molecules (calculated theoretically or observed spectroscopically) are quite exotic and nonintuitive although simply related to long-range forces, they are referred to as "long-range molecules" (1,2,3). Moreover, such molecules, in the absence of collisions, are metastable in electronic states which correlate only to ground or metastable atoms (4). The purpose of this manuscript is to briefly discuss three aspects of these molecules relevant to "state-to-state chemistry": the problem of defining discrete states as the dissociation limit is approached (II); the relative probabilities for elastic, vibrationally inelastic, and collisionally dissociative processes near the dissociation limit (III); and highly state-selective "Franck-Condon" processes between long range levels in different electronic states (IV). In a sense this is a progress report since there is apparently no direct experimental evidence and since much theoretical work on each topic remains.

II. State Definition Near Dissociation.

In conventional diatomic theory one speaks of a series of discrete vibrational levels in the potential energy curve of a given electronic state, followed by a translational continuum beginning precisely at the dissociation limit. Real "long-range molecules", however, exhibit a number of features which cloud this simple picture, as illustrated in Table I for $A\,^1\Sigma_u^+$ $^6Li_2$. These levels are predicted assuming $V(R) = -C_3R^{-3}$ (5), the interesting complications arising from rotation, fine and hyperfine structure, and retardation being ignored here for simplicity and brevity. Note first that nearly half of the vibrational levels are in the top 1% of the potential well, and that the highest

In State-to-State Chemistry; Brooks, P., et al.;
ACS Symposium Series; American Chemical Society: Washington, DC, 1977.

Table I. Predicted long-range vibrational levels v with binding energy ε_v, outer classical turning point R_{v+} and classical vibrational period τ_v for the A $^1\Sigma_u^+$ state of $^6Li_2$ assuming v_D = 105.5.

v	$\varepsilon_v(cm^{-1})$	$R_{v+}(a_o)$	τ_v(sec)
60	90.	30	3.2(-12)
70	20.	49	1.1(-11)
80	2.8	96	5.8(-11)
90	0.14	260	7.0(-10)
99	7.6(-4)	1,500	5.4(-8)
100	2.8(-4)	2,100	1.3(-7)
101	8.4(-5)	3,100	3.4(-7)
102	1.9(-5)	5,000	1.2(-6)
103	2.5(-6)	9,000	6.4(-6)
104	1.2(-7)	28,000	8.3(-5)
105	1.6(-10)	250,000	2.0(-2)
105.5	0	∞	∞

levels become ridiculously weakly bound and closely spaced. The five highest levels are within their own natural linewidth (1.97x 10^{-4} cm^{-1}) of the dissociation limit, i. e. they form a structured continuum below the nominal onset of the ordinary continuum. In absorption from the ground state, the continuity of oscillator strength across the dissociation limit should be apparent (6). The very large outer turning points R_{v+} (near which most of the classical vibrational period is spent) imply very large pressure broadening cross sections (presumably observable using Doppler-free spectroscopy at very low pressures) and perhaps even the effect of a finite container (e. g. a capillary) could be observed. Finally note that for v>99, the classical vibrational period exceeds the 27 nsec radiative lifetime. Traditional arguments whereby one averages over vibrational motion in calculating electronic transition probabilities are clearly inappropriate and a wave packet or scattering formalism capable of distinguishing between "state" preparation at small versus large distance, for example, is needed.

III. Thermal Energy Inelastic Collisions.

In this section let us consider the collision of a long range molecule AB^∞ with a thermal energy inert gas atom such as He or Ar for which little reaction is expected (though it is energetically possible because of the weak binding of AB^∞). First note that the expectation values of the kinetic energy (7) and also the magnitude of the momentum go to zero as the dissociation limit is approached, and for long-range levels these expectation values are usually much smaller even than for the zero-point level in the same potential. This is because most of the vibrational wavefunction amplitude is in the large distance region near R_{v+} where the total energy is very close to the potential energy. In a

In State-to-State Chemistry; Brooks, P., et al.;
ACS Symposium Series; American Chemical Society: Washington, DC, 1977.

sense, AB^{∞} molecules correspond to A and B atoms at slightly negative temperature. In a collision with a thermal third body (thermal kinetic energy and momentum), the overwhelmingly favorable process is thus expected to be collision-induced dissociation, with vibrationally inelastic collision being much less probable and elastic collision less probable still. (Note that the behavior of an ordinary vibrationally excited molecule $AB^{\dagger}$ is quite different.)

IV. Franck-Condon Processes.

In this section let us consider processes involving electronic change in a long-range molecule AB^{∞} which approximately obeys the Franck-Condon principle (that nuclear kinetic energy is unchanged in an electronic transition), e.g. photoexcitation, Penning ionization, electron or proton impact excitation, photoionization, photodetachment, etc. The point here is that Franck-Condon factors for a transition from a long-range level of one electronic state to a long-range level of another electronic state should be very large. One can think of this as a result of the fact that only the long-range molecules and the lowest energy portion of the continuum have sufficiently small kinetic energies to obey the Franck-Condon principle in a transition from a long-range level (4,7). For example, in realistic model calculations of the $A\ ^1\Sigma^+(0 \leq v' \leq 26) \rightarrow X\ ^1\Sigma^+(0 \leq v'' \leq 23)$ bands of ^7LiH (4,8), by far the largest Franck-Condon factor was for the transition $^7LiH^{*\infty}$ $(v' = 26) \rightarrow {}^7LiH^{\infty}$ $(v'' = 23)$ (the upper and lower vibrational wavefunctions having an overlap of 75%!). Thus given a source of AB^{∞} in some electronic state, highly selective interconversions to other electronic (and charge) states should be possible.

Support of this work by the National Science Foundation is gratefully acknolwedged.

V. Literature Cited.

(1) Stwalley, W. C. in D. W. Smith and W. B. McRae, Editors, "Energy, Structure and Reactivity", p. 259 (Wiley, N.Y. 1973).
(2) Le Roy, R. J. in R. F. Barrow, D. A. Long, and D. J. Millin, Editors, "Molecular Spectroscopy 1", p. 113 (Chem. Soc. Spec. Periodical, London 1973).
(3) Stwalley, W. C., Contemp. Phys. (1977), 18, xxxx.
(4) Stwalley, W. C. and Zemke, W. T., Intl. J. Quantum Chem. (1976), 10S, 223.
(5) Stwalley, W. C., Chem. Phys. Letters (1970), 6, 241.
(6) Allison, A. C. and Stwalley, W. C., J. Chem. Phys. (1973), 58, 5187.
(7) Stwalley, W. C., J. Chem. Phys. (1973), 58, 3867.
(8) Stwalley, W. C., Zemke, W. T., Way, K. R., Li, K. C. and Proctor, T. R., J. Chem. Phys. (1977), 66, xxxx.

31

Molecular Vibration States: CH_2 Asymmetric Stretch

CHRISTOPHER A. PARR and JAMES L. ROOKSTOOL

The University of Texas at Dallas, Box 688, Richardson, TX 75080

State-to-state chemistry can be modelled theoretically given molecular potential-energies and dynamics calculations. Proper simulation and analysis requires that initial and final molecular states be quantized modes of motion. Even for classical or quasi-classical dynamics, wherein molecular reactants and/or products are not necessarily quantized, the creation of reactants and the analysis of products requires a proper decomposition of molecular energies into vibrational/rotational components. In this paper, we ignore the contribution of rotation to the molecular motion problem. We concentrate instead on the establishment of the classical vibration states of a realistic model of ground state methylene $^3B_1$ CH_2. We seek the natural vibration modes into which the vibrational Hamiltonian is "most nearly" separable; we wish to reduce the (3N-6)-dimensional problem to 3N-6 quasi-one-dimensional problems. Without such a reduction, exact state-to-state calculations are not possible. We report here the successful isolation of the natural asymmetric stretch mode at energies from near zero point to near atomization.

The natural vibration modes are asymptotically equivalent to the normal vibration modes (1) in the limit of infinitesimal vibra-amplitude. The dynamics of normal vibration are characterized by invariant periodicity, invariant energy, and a one-dimensional trajectory in coordinate space. These properties are destroyed in finite vibration amplitude dynamics (2). The same properties may be retained by the natural vibration modes through the ergodic limit (3, 4) beyond which vibration dynamics need not be "regular" and "quasi-periodic". We use classical trajectory methods (2) to identify the natural vibration modes, hereinafter called regular modes. An iterative search strategy is developed wherein the initial conditions of a trajectory are perturbed until the resultant trajectory is a closed, self-tracing, one-dimensional curve in coordinate space. The solution is a pure regular mode, and its energy conservation and periodicity requirements are satisfied *a fortiori*. The family of such solutions, each member at a different energy, complete the chacterization of the regular mode.

Asymmetric stretch vibrations for a methylene model potential

In State-to-State Chemistry; Brooks, P., et al.;
ACS Symposium Series; American Chemical Society: Washington, DC, 1977.

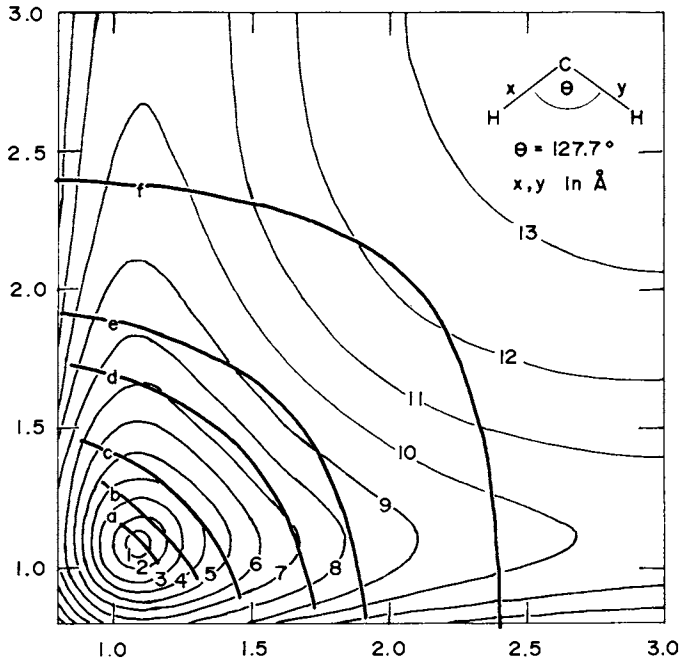

Figure 1. Potential-energy contours and selected asymmetric vibration trajectories for $^3B_1$ methylene. Insert shows relevant geometry parameters and defines the axes. Numbered contours are curves of constant potential energy. The energies themselves (in kcal mol^{-1} relative to zero at equilibrium) are the squares *of the identifying numbers. While the contours are thus unevenly spaced in energy, quadratic potentials would yield such contours evenly spaced in the co-ordinates. The observed uneven spacing in coordinates reflects the degree of anharmonicity in the potential. (This choice of contouring reduces the severe crowding observed in most potential maps.) Lettered curves represent regular asymmetric vibrations. Parameters for those vibrations are given in Table I.*

(5) are shown as lettered curves in Figure 1. The search strategy consisted of variation of asymmetric kinetic energy and initial bond angle at a given symmetric stretch coordinate. This strategy was successful because symmetric and bend contributions to regular asymmetric stretch are at extrema for C_{2v} geometries. These contributions do not destroy the purity of the regular asymmetric mode because they occur at the asymmetric stretch frequency. That symmetric motions contribute to "asymmetric stretch"

is obvious from both the curvature of the asymmetric trajectorjes and the deviation of their midpoints from the equilibrium geometry. The bend contribution cannot be seen in Figure 1 as it has been projected out; however, Table I indicates the extent of its contribution. As the asymmetric stretch energy is increased, the regular motion involves a decreasing bond angle. The oscillation of this bond angle during the asymmetric stretch vibration is minimal (about one degree at the highest energy studied, trajectory f). Because each asymmetric stretch shown in Figure 1 occurs at a different bond angle, the Figure is something of a cheat; the numbered potential-energy contours were drawn for the equilibrium bond angle, θ =127.7°. However, due to the weak bending force constant ($F_{\theta\theta}$ = 0.234 mdyn $Å^{-1}$ rad^{-2}), there is less than a 4 kcal/mol difference in the energy contours between the extremes of the asymmetric trajectories depicted. Further, the trajectories are satisfyingly normal to the contour levels at their endpoints; hence the spirit of comparison between the trajectory and its potential bounds is preserved.

The energy of the asymmetric stretch vibration is a good classical constant of the motion; hence it is associated with a good quantum number of a quantum mechanical dynamics (2). The asymmetric stretch action is the total classical action in these trajectories; thus one may obtain JWKB vibrational quantum numbers from the trajectories in a straightforward manner (6). These quantum numbers are presented in Table I. The attributes of the

Table I. Methylene Asymmetric Stretch

Label	v_{JWKB}	ν (cm^{-1})	E ($kJ\ mol^{-1}$)	$(x=y)_m$ (Å)	θ_m (degrees)	$\delta\theta_t$
n	-0.5	3361	0	1.08192	127.705	0.0
a	0.02	3311	20.54	1.09411	127.05	0.01
b	2.55	3082	117.53	1.15666	124.08	0.07
c	6.07	2780	240.87	1.25000	120.51	0.17
d	12.88	2268	445.39	1.45000	114.87	0.40
e	17.52	1937	555.64	1.60000	111.71	0.61
f	25.89	1249	720.69	2.02000	106.52	1.23

a-f) Calculated trajectories
m) Midpoint geometry for asymmetric vibration
n) Normal mode results at the equilibrium geometry
t) $\delta\theta$ is the difference in θ between turning and midpoint

In State-to-State Chemistry; Brooks, P., et al.;
ACS Symposium Series; American Chemical Society: Washington, DC, 1977.

asymmetric stretch vary so smoothly with JWKB quantum number that one can interpolate their values at integral quantum numbers confidently with Lagrange interpolation (7). The term values presented in the table represent an easily-obtained, first approximation route to pure asymmetric stretch spectral information from the potential model.

The successful extraction of this pure regular vibration mode raises the possibility of the establishment of regular vibration modes for arbitrary bound molecular potentials. These modes and their combinatorial dynamics will be ofgreat utility in the creation and analysis of representative vibration states in theoretical dynamical studies.

Literature Cited

(1) Wilson, E. B., Decius, J. C., and Cross, P. C., "Molecular Vibrations", McGraw Hill Book Company, Inc., New York, 1955.
(2) Parr, C. A., Kuppermann, A., and Porter, R. N., J. Chem. Phys. (1977) 66 (7) 2914-31
(3) Moser, J., "Stable and Random Motions in Dynamical Systems", Princeton University Press, New Jersey, 1973.
(4) Brumer, P. and Duff, J. W., J. Chem. Phys. (1976) 65 (9) 3566-74.
(5) Eaker, C. W. and Parr, C. A., J. Chem. Phys. (1976) 64 (4) 1322-32.
(6) Messiah, A., "Quantum Mechanics", vol. 1, 239-41, North-Holland Publishing Co., Amsterdam, 1970.
(7) Margenau, H. and Murphy, G. M., "The Mathematics of Physics and Chemistry", 2nd edition, 470-1, D. Van Nostrand Co., Inc., Princeton, 1956.

In State-to-State Chemistry; Brooks, P., et al.;
ACS Symposium Series; American Chemical Society: Washington, DC, 1977.

32

Thermochemical Properties for Atoms and Molecules in Specific Quantum States

W. C. GARDINER, JR.
University of Texas, Austin, TX 78712

R. D. LEVINE
The Hebrew University, Jerusalem, Israel

Our knowledge and understanding of state-to-state chemistry spans a wide spectrum of level of detail. At the ultimate end of this spectrum there is the state-to-state differential cross section for an elementary process in which all reactants and products are in specified quantum states at a well defined total energy. At the other end of the spectrum would be an elementary chemical reaction with no state selection whatever; here all species would be characterized by a (Boltzmann) thermal distribution of quantum states. Most experimental and many theoretical studies are somewhere in the middle of this spectrum, where some state specification is combined with some thermal averaging. In particular, it is quite common to have a thermal distribution of the kinetic energy. In such studies one may find it useful to have the thermochemical properties of species that have some degree of state selection. Indeed there are problems such as computer modeling of chemical lasers where knowledge of these thermochemical properties is an absolute prerequisite for setting up the solution. In such situations a chemist may experience some doubt about the validity of combining state specification with thermodynamics, probably due to a concern about inadvertently generating a model for a perpetual motion machine. The purpose of our study was to set up the correct formalism and working equations for finding the thermochemical properties of species in specified quantum states, or groups of quantum states. More particularly, we present formulas for modifying standard tabulations of thermochemical properties (1) to get the thermochemical properties for atoms and molecules in specified internal quantum states.

The line of reasoning which justifies, on the basis of detailed-balance arguments, the combination of thermodynamics with state specification has been presented elsewhere (2). A brief overview is given by considering the production of a species in state i, $AB^{(i)}$, in an elementary process that is otherwise described by thermal distributions.

†The Hebrew University, Jerusalem, Israel

In State-to-State Chemistry; Brooks, P., et al.;
ACS Symposium Series; American Chemical Society: Washington, DC, 1977.

$$A + BC \rightarrow AB^{(i)} + C \qquad (1)$$

as a kind of Hess' Law problem combining the purely thermal process

$$A + BC \rightarrow AB + C \qquad (2)$$

with the excitation process

$$AB \rightarrow AB^{(i)}. \qquad (3)$$

The equilibrium constant for process (2) is clearly described by ordinary thermodynamics, while that for process (3) is described by the Boltzmann distribution

$$\frac{[AB^{(i)}]}{[AB]} = \frac{g_i \exp(-E_i/kT)}{q_{\neq}} \qquad (4)$$

where g_i and E_i are the degeneracy and energy of quantum state i and $q_{\neq}$ is the sum-over-states for the unequilibrated degree(s) of freedom from which i is selected. Since (1) is the sum of (2) and (3), its equilibrium constant K_c' is the product of the equilibrium constants

$$K_c' = K_c \times \frac{g_i \exp(-E_i/kT)}{q_{\neq}} \qquad (5)$$

Contact with thermochemical properties is then made by noting that $K_c = \exp(-\Delta A°/RT)$, such that the standard Helmholtz function for the state-selected species $AB^{(i)}$ must be related to the ordinary standard Helmholtz function of AB by

$$A°_i = A° - RT \ln g_i + E_i + RT \ln q_{\neq} \qquad (6)$$

Equation (6) shows the basic ingredients of the link between ordinary and state-specific thermochemical properties: the energy and degeneracy of the specified state are required, and the ordinary partition function for the degree(s) of freedom from which the state was selected.

The rest of the thermochemical properties are readily found by simple manipulations of (6); in particular, we find for the modifications required for the common thermochemical properties

$$\Delta H°_{f0}(i) = \Delta H°_{f0} + E_i \qquad (7)$$

$$S°(i) = S° + R \ln g_i - S°_{\neq} \qquad (8)$$

In State-to-State Chemistry; Brooks, P., et al.;
ACS Symposium Series; American Chemical Society: Washington, DC, 1977.

$$C_p^\circ(i) = C_p^\circ - C_{p\neq}^\circ \qquad (9)$$

In our complete paper (3), modification formulas to all JANAF (1) entries are included, both for the single-state situation described here and the situation where a group of states in some distribution over an energy range is specified.

As an illustration of the application of equations like (7) - (9) we take the v = 2, J = 6 state of HF at T = 400 K. Since E_i is 24.593 kcal for this state, (7) gives -40.535 kcal for ΔH_{f0}° (i) in place of -65.128 kcal for ordinary HF ideal gas. $S_{\neq}^\circ$ for the rotational and vibrational degrees of freedom of HF at 400 K is found to be 7.162 cal/K by standard statistical thermodynamics formulas (4), and g_i = 13; S_i° is then given from (8) as 41.490 cal/K in place of 43.555 cal/K for ordinary HF at 400 K. Subtracting the heat capacity of rotation and vibration leaves only the translational contribution 5/2 R = 4.968 cal/K for $C_p^\circ(i)$ in (9).

Literature Cited

1. Stull, D.R. and Prophet, H., "JANAF Thermochemical Tables," Second Edition, NSRDS-NBS 37, National Bureau of Standards, Washington, 1971.
2. Levine, R.D., Chem. Phys. Lett., (1976) 39, 205.
3. Levine, R.D. and Gardiner, W.C., Jr., J. Chem. Phys., to be published, 1977.
4. Ref. 1, pp. 9-10.

In State-to-State Chemistry; Brooks, P., et al.;
ACS Symposium Series; American Chemical Society: Washington, DC, 1977.

INDEX

In State-to-State Chemistry; Brooks, P., et al.;
ACS Symposium Series; American Chemical Society: Washington, DC, 1977.

In State-to-State Chemistry; Brooks, P., et al.;
ACS Symposium Series; American Chemical Society: Washington, DC, 1977.

In State-to-State Chemistry; Brooks, P., et al.;
ACS Symposium Series; American Chemical Society: Washington, DC, 1977.